BEHAVIOUR OF CONTINUOUS REINFORCED CONCRETE BEAMS DURING THE PATCH REPAIR PROCESS

Eoin Coakley

Thesis submitted for the degree of
Doctor of Philosophy to the
School of the Built Environment,
Heriot Watt University,
Edinburgh.

March 2009

Copyright Statement

Abstract

The main cause of deterioration of reinforced concrete is chloride-induced corrosion of reinforcement. Repairs may require that contaminated concrete around the reinforcement be broken out and replaced. The pattern of strains will change when bond is lost and if the beam carries load during the repair process, the pattern of strains will differ from those in the "as new" condition. This study aims to develop analytical procedures to represent structural behaviour and to assess the circumstances in which changes in behaviour are significant.

The testing programme embraced a range of parameters including the length and position of breakout and the load carried by the structure during casting of the repair. Various top and bottom reinforcement areas were chosen to investigate the influence of the exposed steel area and the difference between the elastic and plastic bending moment diagrams for the "fully bonded" specimen.

In a statically indeterminate structure, breakout of concrete over a portion of a span causes loss of section stiffness in that region and a consequent transfer of moment to other parts of the structure. However, test and numerical data show that the flexural strength of a member with exposed reinforcement was primarily influenced by the increase in stress at the breakout location. Flexural strength and ductility of the repaired member are more likely to be reduced if the member carries load during repair as this increase in stress remains "locked into" the member.

Acknowledgements

The author is deeply grateful to his research supervisor Dr. John Cairns for the guidance, help and encouragement received throughout the research. His thorough feedback was received promptly during preparation of this thesis and was very much appreciated. Dr. Omar Laghrouche also deserves a special mention for his assistance with the numerical modelling that was carried out.

Thanks are extended to the technical staff of the Concrete and Structures Laboratory for their help throughout the experimental investigation. Their willingness to help did not go unnoticed and their experience proved invaluable. A sincere gratitude is also due the School of the Built Environment's administrative staff and the I.T. department for their assistance.

The author wishes to express his thanks to the suppliers of materials for the test specimens. A special mention is due to Fosroc Ltd. who supplied the repair concrete premix.

Finally, the support and encouragement of the author's friends and family was deeply appreciated. Their help and understanding did not go unnoticed.

ACADEMIC REGISTRY
Research Thesis Submission

Name:	Eoin Coakley		
School/PGI:	School of the Built Environment		
Version: *(i.e. First, Resubmission, Final)*	Final	Degree Sought (Award **and** Subject area)	PhD. In Civil Engineering

Declaration

In accordance with the appropriate regulations I hereby submit my thesis and I declare that:

1) the thesis embodies the results of my own work and has been composed by myself
2) where appropriate, I have made acknowledgement of the work of others and have made reference to work carried out in collaboration with other persons
3) the thesis is the correct version of the thesis for submission and is the same version as any electronic versions submitted*.
4) my thesis for the award referred to, deposited in the Heriot-Watt University Library, should be made available for loan or photocopying and be available via the Institutional Repository, subject to such conditions as the Librarian may require
5) I understand that as a student of the University I am required to abide by the Regulations of the University and to conform to its discipline.

* *Please note that it is the responsibility of the candidate to ensure that the correct version of the thesis is submitted.*

Signature of Candidate:	Eoin Coakley	Date:	12-03-2009

Submission

Submitted By *(name in capitals):*	EOIN COAKLEY
Signature of Individual Submitting:	Eoin Coakley
Date Submitted:	12-03-2009

For Completion in Academic Registry

Received in the Academic Registry by *(name in capitals):*			
Method of Submission *(Handed in to Academic Registry; posted through internal/external mail):*			
*E-thesis Submitted (**mandatory from January 2009**)*			
Signature:		Date:	

Please note this form should bound into the submitted thesis.

Updated February 2008, November 2008, February 2009

Contents

List of tables

List of figures

Notation

a	distance from roller support to arbitrary point "a"
$A_{average}$	average cross-sectional area of bar
A_s	area of tension reinforcement
$A_{s\ bottom}$	area of bottom reinforcement
$A_{s\ hog}$	area of tension reinforcement within hogging moment region
$A_{s\ sag}$	area of tension reinforcement within sagging moment region
$A_{s\ top}$	area of top reinforcement
A_{sv}	total cross-sectional area of a shear link at the neutral axis
a_v	shear span
b	width of cross-section
d	effective depth of tension reinforcement
E_c	elastic modulus of the concrete
E_{rm}	elastic modulus of the repair material
E_{st}	elastic modulus of the steel
E_{sub}	elastic modulus of the substrate
EI	flexural stiffness
f_c	compressive stress in the concrete
f_{cu}	concrete cube compressive strength
f_{st}	stress in the tension reinforcement
$f_{st\ exp}$	stress in the exposed tension reinforcement
f_t	concrete tensile strength
f_y	yield strength of the reinforcement
$f_{y\ average}$	average yield strength of a reinforcement bundle
$f_{y\ hog}$	yield strength of tension reinforcement within hogging region
$f_{y\ sag}$	yield strength of tension reinforcement within sagging region
f_{yv}	yield strength of links
K_{12}	stiffness matrix at node 1 due to displacement at node 2
K_{22}	stiffness matrix at node 2 due to displacement at node 2
K^n	represents the stiffness matrix, tangential to the plot at the point (P^{n-1}, a^{n-1})
K^{n+1}	represents the stiffness matrix, tangential to the plot at the point (P^n, a^n)

L	span length
L_{crush}	length over which limiting compression strain is reached
L_{exp}	exposed length of bar
L_{hog}	length of hogging moment region (distance between points of contraflexure)
l_t	crack transmission length
ΔL_{bonded}	elongation of the bonded reinforcement at ultimate load
$\Delta L_{unbonded}$	elongation of the unbonded reinforcement at ultimate load
M	bending moment
M_a	moment about an arbitrary point "a"
M_{cap}	moment capacity of a given section
M_{cr}	moment at which flexural cracking occurs
$M_{E\ hog}$	maximum hogging moment from elastic bending moment diagram
$M_{E\ sag}$	maximum sagging moment from elastic bending moment diagram
$M_{P\ hog}$	maximum hogging moment from plastic bending moment diagram
$M_{P\ sag}$	maximum sagging moment from plastic bending moment diagram
M_{hog}	maximum hogging moment over the internal support
$M_{hog\ (predicted)}$	maximum hogging moment from predicted failure bending moment diagram
M_{sag}	maximum sagging moment within the spans
$M_{sag\ (predicted)}$	maximum sagging moment from predicted failure bending moment diagram
m_2	moment at node 2
ΔM	change in moment at the midspan during moment transfer
$\%\Delta M_{breakout}$	percentage change in breakout moment during breakout
$\%\Delta M_{non\text{-}breakout}$	percentage change in non-breakout moment during breakout
δm	virtual applied moment
P	total applied load
P_{bonded}	ultimate load of fully bonded specimen
P_{calc}	calculated ultimate load of fully bonded specimen
$P_{exposed}$	ultimate load of specimen with exposed reinforcement
$P_{repaired}$	ultimate load of repaired specimen
P_{test}	ultimate load observed during testing
P_L	left point load

P_R	right point load
P_i	specified load interval
P_{ult}	ultimate load
P^n	load value corresponding to the displacement value a^n
P^{n+1}	load value corresponding to the displacement value a^{n+1}
p_1	total solution at node 1
p_2	total solution at node 2
p_1^{comp}	complementary solution at node 1
p_2^{comp}	complementary solution at node 2
p_1^{part}	particular solution at node 1
p_2^{part}	particular solution at node 2
q_2	vertical load at node 2
r	distance between point load and nearest support
R	radius of curvature
1/R	section curvature
$1/R_{1cr}$	curvature during initial loading as flexural cracking begins
$\%\Delta(1/R)$	percentage change in section curvature during breakout
R_C	vertical reaction at the central support
R_L	vertical reaction at the left support
R_R	vertical reaction at the right support
R_{Total}	sum of the support reactions
s	spacing of point loads
s_{cr}	crack spacing
s_v	spacing of links along the member
UTS	ultimate tensile strength of the steel
u_2	displacement matrix at node 2
v	design shear stress
V_a	shear force at arbitrary point “a”
v_c	design concrete shear stress
V_{cap}	shear capacity of a given section
V_{max}	maximum shear force in the member
x	compression zone depth
y	height within section being considered
z	lever arm

z_{hog}	lever arm within hogging region
z_{sag}	lever arm within sagging region
α_L	rotation at left side of central support
α_R	rotation at right side of central support
α_m	ratio of maximum hogging moment over the internal support to the maximum sagging moment within the spans
α_r	ratio of tension reinforcement area over the internal support to the tension reinforcement area within the spans
$\%\Delta\alpha_m$	percentage change in hogging : sagging moment ratio
β_b	(moment at a section after redistribution) / (moment at a section before redistribution)
β_t	integration factor for the steel strain along the transmission length
γ_m	load factor
γ_ψ	residual force norm
δ	displacement
δ^n	displacement for the iteration being considered
δ^{n+1}	displacement for the following iteration
δ_L	left midspan displacement
δ_R	right midspan displacement
δ_L`	displacement beneath left-most load
δ_R`	displacement beneath right-most load
δ_2	vertical displacement at node 2
ε	strain
$\varepsilon_{c\ comp}$	compression strain in the concrete
$\varepsilon_{c\ tens}$	tensile strain in the concrete
ε_{cp}	concrete strain at peak compressive stress
ε_{st}	tensile strain in the steel
$\varepsilon_{st\ crack}$	the strain in the reinforcement at a crack
$\varepsilon_{st\ exp}$	exposed steel strain
$\varepsilon_{st\ mean}$	mean steel tensile strain
ε_{t0}	concrete strain at end of tension softening curve
ε_y	yield strain of the reinforcement
$\Delta\varepsilon_{c\ comp}$	change in compression strain in the concrete
$\Delta\varepsilon_{st\ cs}$	increase in the steel strain in the cracking state

θ	rotation
θ_L	rotation at left pinned support
θ_R	rotation at right pinned support
θ_{ult}	rotation at ultimate load
θ_y	rotation at reinforcement yield
θ_2	rotation at node 2
λ_{dt}	incremental displacement norm
μ	ductility
σ_c	compressive stress
σ_t	tensile stress
$0.2\%\sigma$	0.2% proof stress (taken as yield stress, f_y)
ν	Poisson's ratio
$\int^l \varepsilon_c \, dl$	elongation of substrate throughout exposed length l
$\int^l \varepsilon_s \, dl$	elongation of steel throughout exposed length l
$Ø_{average}$	average bar diameter

Chapter 1: Introduction

Deterioration of concrete structures has become a major problem in recent years. Reports suggest that approximately £500 million is spent annually on the repair of reinforced concrete structures within the UK **[1]**. Deterioration may be caused by electrochemical processes, physical processes, chemical processes or mechanical damage. The principal cause of degradation is chloride induced corrosion of reinforcement. Corrosion causes delaminating and cracking along reinforcing bars and in severe cases, loss of reinforcement cross-section can occur.

There are various remedial procedures that may be used to counteract the adverse effects of corrosion. To carry out an effective repair, the chloride contaminated concrete surrounding the reinforcement should be removed and replaced with a suitable repair material. Composite action between the reinforcement and the concrete is lost when the bars are exposed. The beam loses stiffness during breakout and the pattern of strains after completion of the repair will have changed, particularly if load is carried during the process.

Research has already been carried out on both stages of the patch repair process – on beams in the "weakened" condition during breakout of concrete **[2, 3]**, and on repaired beams, when load is reapplied **[4, 5]**. Numerous parameters have been investigated including load arrangement, location of breakout / repair, length and depth of breakout / repair, area of exposed reinforcement and various properties of the repair material.

In practice, in-situ concrete construction benefits from structural continuity. When a member is being cast, reinforcement projects beyond the pour to enable lapping of the reinforcement with that in the next member. Once the next member is cast, the joint behaves monolithically. Most previous work has concentrated on repairs to simply supported beams, but there is also a need for investigation of repairs to indeterminate structures. Research on patch repairs of continuous reinforced concrete beams is limited to a few numerical analyses **[6]** and should be investigated in greater detail.

In a statically determinate structure, equilibrium alone controls the bending moment. Unlike simply supported beams, however, continuous structures are statically

indeterminate. The distribution of moment in such structures is influenced by variations in flexural stiffness throughout the length of the member. Consider the effect of the concrete breakout process for repairs to a statically indeterminate structure, such as a two-span beam. Breakout of soffit concrete from around the tension reinforcement within one of the spans would cause a loss of section stiffness in that region. The bending moment within the "weakened" span reduces with the stiffness and moment transfers towards the internal support. Breakout of concrete at one location might therefore cause overstressing of the structure at another location. Thus, the distribution of moment within continuous members subject to repair requires additional investigation. The rate at which this moment transfer takes place and the parameters that affect it should be examined.

If a specimen carries load during casting and curing of the repair material, the change in stress pattern resulting from breakout remains "locked into" the member. Previous work **[4]** on simply supported beams shows ultimate strength of a beam need not be adversely affected by carrying load during the repair. The patch repair performs efficiently under subsequent loading as the repair material is relatively unstrained at service load. However, due to moment transfer that would take place during concrete breakout, increases in stress elsewhere within the member may prove detrimental.

Temporary propping of the structure during placement of the repair material has the benefit of ensuring serviceability limit states are not exceeded. If the member is completely relieved of load during the repair, behaviour should be similar to that of an equivalent "as new" specimen. Complete relief of stress from a structure is impossible in practice so assuming similarity of behaviour of repaired and "as new" specimens is flawed. Propping can also be expensive and it may be difficult to locate props without obstructing the repair process.

Investigation of the two main stages of the patch repair of continuous beams is required. Since the transfer of moment during the breakout process is of paramount importance to this investigation, parameters should be chosen to influence the moment transfer within a member. Changes in the stress patterns should be monitored throughout the breakout process. The influence of the altered stress pattern during subsequent loading of the repaired specimen is also of interest. This is dictated by the proportion of the service load carried by the specimen during the repair process. Therefore, the relative merits of propped and unpropped repair should also be examined.

1.1 Aims and objectives

The aim of the investigation is to extend existing guidance for structural aspects of patch repairs to simply supported beams, for application to continuous beams. The investigation will primarily consist of results from an experimental analysis and will be supported by a finite element analysis. The primary objectives of the investigation are to:

1. Investigate the parameters that influence moment transfer in "as new" control specimens during loading to failure.
2. Determine the influence of these parameters on moment transfer induced by progressive breakout of concrete at different locations within the member.
3. Examine behaviour of specimens during breakout of concrete and establish the margin of safety against failure.
4. Monitor the change in stress patterns within a member due to concrete breakout and investigate the influence on post-repair behaviour.
5. Evaluate ultimate limit state behaviour of repaired specimens by comparison with corresponding "as new" specimens.
6. Examine the effect of different propping conditions on the performance of the patch repaired member.
7. Draw parallels between results from continuous beams and conclusions from existing literature on simply supported beams.

Chapter 2: Review of literature

2.1 Deterioration of structural members

The deterioration and repair of concrete structures has become an issue of increasing importance, particularly in recent years. Reinforcement corrosion is the primary cause of structural deterioration and it is important to understand the processes that lead to corrosion and its effect on structural performance.

Certain chemical and physical reactions cause structural concrete to deteriorate over time. Exposure to the atmosphere, chlorides and other environmental corrosives contribute to an electrochemical reaction on the reinforcing steel. The high alkaline environment (the pH of concrete) and a naturally occurring passivating film on steel, work to prohibit formation of anodic and cathodic sites needed to initiate the corrosion cycle.

Carbonation describes the general breakdown of passivity by neutralization of the alkaline concrete. This is predominantly caused by reaction with atmospheric carbon dioxide. Large amounts of carbon dioxide are produced from burning of fossil fuels and from industrial plants. This acidic gas can penetrate porous concrete, neutralizing the alkalinity of concrete and making the steel susceptible to normal atmospheric corrosion.

Chloride induced corrosion of reinforcement is the localized breakdown of the passive film on steel by chloride ions. Chlorides from marine exposure, acid rain, and de-icing salt run-off may all contribute to corrosion of embedded steel reinforcement. In the past, chlorides were introduced to a concrete mix in the form of calcium chloride (a cure-accelerating admixture). Contaminated aggregates have also been a common cause of chloride induced corrosion in some parts of the world. Chlorides, like carbonation, break down steel's passive oxide coating.

A range of measures can be used to prevent corrosion of reinforcement. Corrosion resistant alloys such as stainless steel may be used instead of mild steel. Epoxy coating of reinforcement can prevent chlorides from getting to the steel surface. High-range water reducer admixtures permit the use of low water-cement ratio

concretes that have lower permeability to corrosive agents, resulting in slower corrosion initiation of the reinforcement. Cathodic protection may be provided by connecting the steel to a sacrificial anode or making the steel a cathode by passing a direct current through it. Many combinations of these methods can be used to increase the service life of reinforced concrete structures. However, the focus of this study is not corrosion prevention but the remedial measures taken once corrosion is deemed excessive.

The severity of corrosion can be quantified by examining the chloride content of the concrete cover. Mangat and Molloy **[7]** used a modified version of Fick's second law of diffusion to predict long-term chloride concentration in concrete. Analysis of short-term and long-term powder samples was used to validate their expression. This enables powder samples from an existing structure to be used to predict future chloride concentrations and to assess when remedial measures may be required.

The effect of corrosion on loss of bond and ultimate strength must be examined to establish conditions for which repair is deemed necessary. Al-Sulaimani et al **[8]** found the cover : bar diameter ratio is a significant corrosion protection parameter (longitudinal cracking occurred at lower levels of corrosion in specimens with smaller cover : bar diameter ratios). Confinement from shear reinforcement is also considered to influence the reduction in bond strength due to corrosion. Cairns et al **[9]** observed slight increases in strength of beams with corroded reinforcement (relative to control specimens), which was partly attributable to confinement from the links. Conversely, appreciable reductions in flexural strength were observed by Mangat and Elgarf **[10]** as links were excluded from most of their test specimens (similar degrees of corrosion to **[9]**).

Mangat and Elgart **[10]** observed that the reduction in residual strength due to corrosion is primarily due to the loss of bond between corroded reinforcement and the surrounding concrete. The effect of loss of reinforcement cross-section due to corrosion is much less significant. Eyre and Nokhasteh **[11]** present a mathematical model to quantify the loss of flexural strength due to corrosion in under-reinforced specimens (complete debond of reinforcement was assumed throughout the corroded length, loss of reinforcement cross-section was neglected). Flexural strength was unaffected if the reinforcement reached yield before concrete crushing began. Therefore, reductions in flexural strength were less likely to occur in lightly reinforced sections. For a given length of debond, the load arrangement was also

found to influence the loss of flexural strength. Greater reductions in strength were anticipated for concentrated loads than for distributed loads. Such mathematical models can be used to assess the effect of corrosion on ultimate strength and establish if remedial measures are required.

2.2 Repair methods

2.2.1 Epoxy resin injection

When a deteriorated member has been structurally assessed and it is decided that repair measures are necessary, a range of alternative methods are available. Resin injection is commonly employed to prevent further downgrading of a structure. Cracks or voids that have formed are filled with a resin with suitable physical properties. A low viscosity is desirable to allow penetration into fine cracks but the resin should also possess adequate shear strength to remain in position once injected **[12]**. Abu-Tair et al **[13]** describe the resin injection process. Acrylic sealant is applied over the length of the crack leaving gaps at suitable intervals for resin injection. The resin is injected at the lowest injection point along the crack until resin escapes from the next injection point. The first injection point is then sealed and the process is repeated at subsequent injection points until the crack is filled. Experimental investigations **[14, 15]** show that repaired cracks generally remain sealed and new cracks form during loading to failure of repaired specimens. Testing of severely damaged beams repaired by epoxy resin injection (while unloaded) showed the flexural strength of the repaired specimens was not less than the original strength.

If corrosion is caused by chloride contamination of concrete, effective repairs will not be achieved unless all of the contaminated concrete is removed. Therefore, the above procedure will only postpone the failure of a beam deteriorated by corrosion. Patch repair is the most effective solution as the deteriorated concrete is removed and replaced with a suitable repair material. A comprehensive insight into the behaviour of patch repaired members is the main focus of this thesis. The patch repair process is described in detail in Section 2.2.2.

2.2.2 The patch repair process

Emmons and Vaysburd **[16, 17]** discuss a systematic approach to carrying out a patch repair. To ensure the long term performance of a repair, due consideration must be

given to the design and specification of the repair, the demands of the environment and choice of repair material. The structural behaviour of the repair is primarily influenced by the load relief strategy during casting of the repair and the compatibility of the repair material with the substrate. However, prevention of further corrosion and durability of the patch repair must also be ensured.

The first step of a patch repair is the breakout of deteriorated concrete. For chloride induced corrosion, all the chloride contaminated concrete must be removed (not just the areas which have spalled or delaminated) to prevent an incipient anode effect **[18, 19]**. To ensure that the aggregate of the repair material can be compacted behind the reinforcement, the depth of breakout should be at least 20mm beyond the steel. In some cases, smaller aggregate sizes may be used in the repair concrete for convenience. It is also suggested that the length of the exposed reinforcement should extend at least 50mm beyond the corroded length **[6]**. Removal techniques include diamond saw cutting, high-pressure water jetting, and mechanical methods such as light breakers. Obviously, high pressure water jetting is the most desirable method as it is least likely to damage the reinforcement or cause cracks in the substrate. However, diamond saw cutting and mechanical breakers remain the most commonly used methods. Cross saw-cuts or axial saw-cuts through the cover to the reinforcement make the breaking out process less laborious. In any case, saw-cuts should be made at either end of the exposed length to prevent feather edging.

Surface preparation of the substrate has a huge influence on the bond between the repair material and the substrate. Studies **[20, 21]** of various surface preparation techniques found that the greatest adhesion strengths were achieved with sand blasting or shotblasting. Methods such as hand milling and mechanical milling produce more cracks and therefore lower pull-off strengths. It is vital to wash the substrate thoroughly to remove any chlorides. The exposed reinforcing bars should ideally be grit-blasted to remove any rust deposits. If severe corrosion has occurred, loss of reinforcement cross-section may require lapping with supplementary reinforcement. Bonding agents are sometimes applied to the substrate but the repair material must be applied while the bonding agent is still wet. Otherwise, the bonding agent can have a debonding effect. If no bonding agent is used, the surface of the substrate must be in a saturated – surface dry condition to reduce suction. A dry substrate sucks water from the repair material near the interface, causing poor hydration of the cement and reducing the shear strength at the interface.

Canisius and Waleed **[6]** describe the three main techniques for applying patch repair materials: hand applied, flowing repairs and sprayed concrete. Hand applied techniques are carried out by using a trowel to apply the repair material. The material must have good cohesion properties and is usually applied in thin layers when repairing slab and beam soffits. The suggested thickness of the layers and associated setting time between applications is usually recommended by the manufacturer of the repair material.

Flowing repairs involve positioning of formwork to completely surround the repair area. After adequate soaking and subsequent drying of the substrate surface, the formwork is filled with a suitable repair concrete of slurry consistency. For example, when repairing the soffit of a beam, channel shaped formwork is constructed (Fig. 2.1). It is propped to the underside of the beam and clamped to the beam sides. Access points are left in the channel sides for pumping of the repair material. Bleed points must also be left in the channel to ensure the repair patch is completely filled and to prevent air voids from forming. Note: Bleed points should be at the opposite end of the patch repair formwork to the access point to completely fill the repair area. The protrusions in the repair at the access points and bleed points may be removed after curing as they do not contribute to the structural behaviour of the repair.

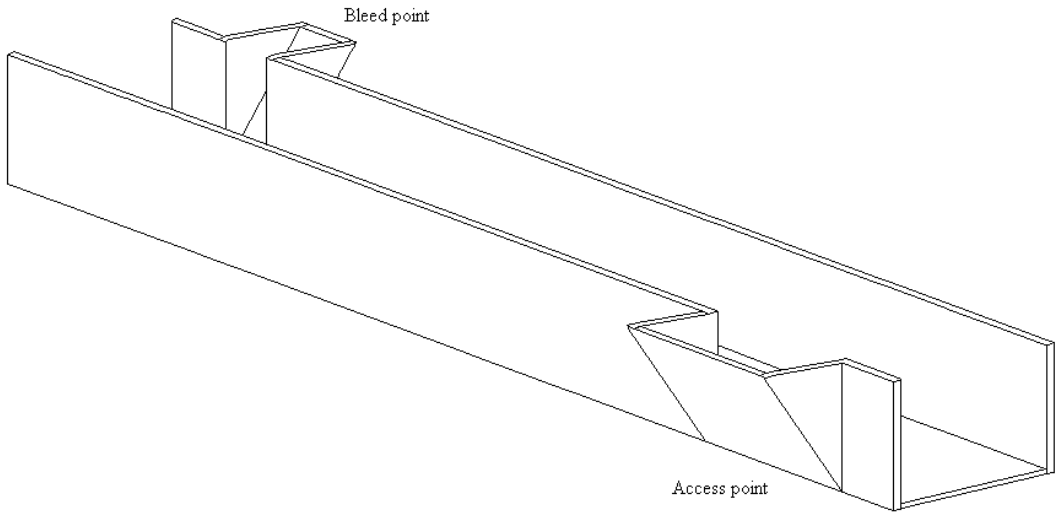

Fig. 2.1: Channel formwork for flowing repair to beam soffit

Sprayed concrete is the most commonly used repair technique on site. Once concrete has been broken out and the surface cleaned, a bonding coat is applied and the surface of the substrate is kept moist. The application technique may be carried out in one of two ways. In the dry process, the cement, aggregate and additives are batched and mixed. If the contractor is of the opinion that the mix is oven-dry, it may be damped with water. The mixture is delivered to the hopper and conveyed to the nozzle where the water and liquid additives are injected. The wet process is similar but water is added to the original mix. The initial layer of material is sprayed and this is allowed to stiffen before subsequent layers are applied. Once sufficient layers have been applied, the repair surface may be finished with a trowel. Ideally, the concrete should then be kept moist for a curing period of about 7 days.

2.3 Behaviour after breakout of contaminated concrete

2.3.1 Parameters affecting behaviour of beams with exposed reinforcement

The structural behaviour of reinforced concrete members must be assessed throughout the patch repair process. The two stages of the repair process should be considered separately: while the concrete is broken out, when load restrictions may be imposed, and after completion of repair, when the member must again be capable of carrying the full design load. When concrete is broken out and the bond between the steel and the concrete is lost, conventional section analysis can no longer be applied. The pattern of strains in the repaired member is altered if the member carries load when the repair is cast.

Initially, investigation of beam behaviour with a portion of the reinforcement exposed is carried out. Several parameters are reported **[2, 22]** to affect the change in behaviour of a simply supported reinforced concrete beam when reinforcement is exposed. These include:

- loading arrangement and positioning
- extent of loss of concrete-steel bond
- percentage of tension reinforcement
- position of damaged section within the span
- depth of removal of concrete
- inclusion of compression reinforcement
- concrete cube strength

Work by Cairns and Zhao **[2]** mainly focussed on simply supported beams subjected to symmetric two-point loading. It was evident that for a given value of moment at the midspan, the change in elongation of the steel on exposure was greater when the loads were positioned closer together. To maintain compatibility, the curvature of the concrete section was also greater. Therefore, the potential reduction in ultimate bending moment is greater for a single point load than for a symmetrical two-point load arrangement (for a given value of maximum moment).

The loading position also has a significant influence on the structural performance of a member with exposed reinforcement. Raoof and Lin **[23]** investigated the loss of strength for a short length of exposed reinforcement near the support with varying position of a single point load along the span while maintaining all other parameters constant. They found the greatest reduction in strength occurred with $0.3 < a_v / L < 0.4$, where (a_v) is the distance of the load from the left hand support and (L) is the span length. Thus, an asymmetrical point load was more severe than a central point load. However, these results could have been influenced by the position of breakout, which was also asymmetrical.

Logic tells us that the greater the extent of loss of bond, the greater the change in behaviour from a fully bonded specimen. A simple numerical model **[2]** showed that an increase in the length of exposure causes an increase in the maximum compression strain of the concrete at midspan and a reduction in bending strength, Fig. 2.2. Note: The loading and reinforcement exposure were symmetrical about the midspan in this programme. The effect of this increase in compression strain on the ultimate strength of the beam depends on how heavily reinforced the beam is (whether reinforcement yields before concrete crushing begins).

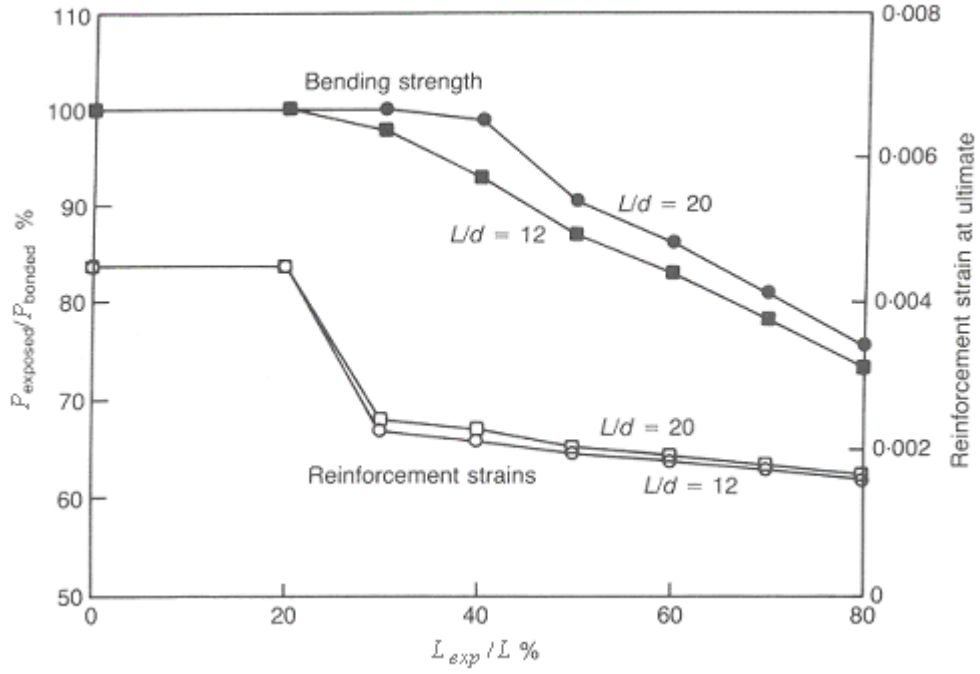

Fig. 2.2: Loss of strength with increasing bar exposure **[2]**

If the section is initially designed for a balanced failure (i.e. concrete crushing and reinforcement yielding designed to take place simultaneously), it would effectively become over-reinforced with a short length of bar exposed within the shear span due to the increase in concrete strain making concrete crushing the more likely failure mode. However, if the section is designed to be under-reinforced, the reinforcement could still yield before the concrete starts to crush, even if the concrete is subjected to a relatively large increase in strain. Therefore, for a given length of exposure, the flexural strength is more likely to be reduced in a heavily reinforced section.

Cairns and Zhao **[2]** carried out experiments investigating the reduction in strength with increasing reinforcement percentages. The tests were carried out on beams of width 150-230mm, overall height of 230-410mm and over a span of 2.7m. Two-point loading, symmetrical about the midspan was applied to the members. The results for a range of L_{exp}/d values are plotted in Fig. 2.3.

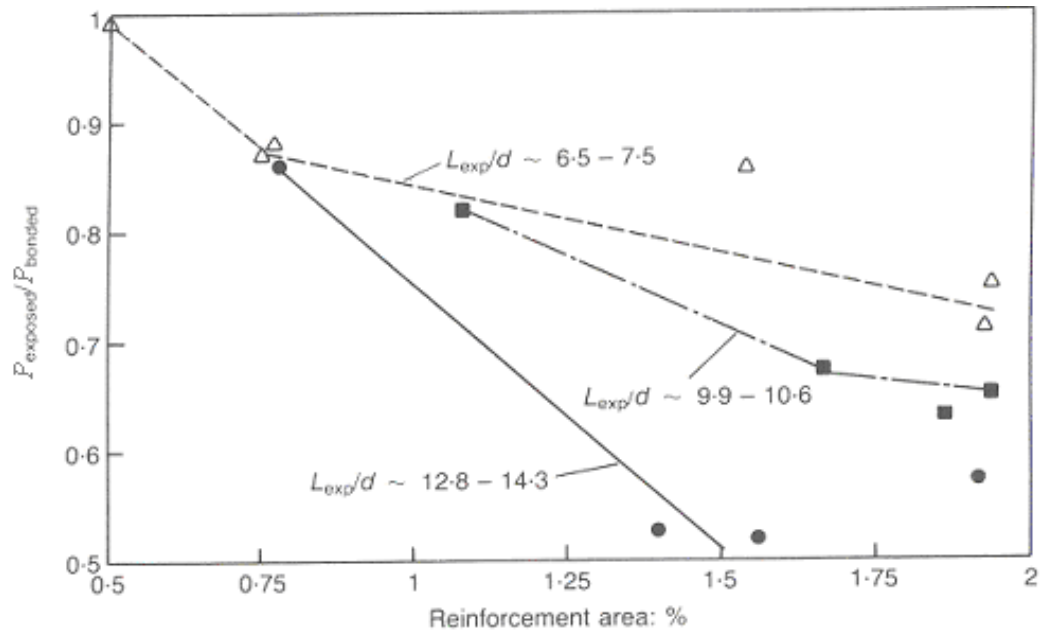

Fig. 2.3: Loss of strength vs. steel percentages for various lengths of exposure **[2]**

Raoof and Lin **[3]** carried out tests on 150×300mm beams tested over a span of 3m (Note: Tests specimens of similar scale to Cairns and Zhao **[2]**). Fig. 2.4 shows a plot of strength reduction against reinforcement percentages for various lengths of exposure. Single point loading was applied at a_v / L = 0.3 from the support. The position of the damaged section was found to significantly affect the ultimate strength of the beam. Experimental results **[3]** show that, while maintaining all other

parameters constant, the closer the region of exposed reinforcement to the support, the higher the loss of strength. The specimen with its breakout region closest to the support exhibited a top face crack, which caused a significant loss of strength (many of the specimens tested by Raoof and Lin had no top reinforcement). On the other hand, the beam with its damaged region furthest from the support experienced a ductile failure.

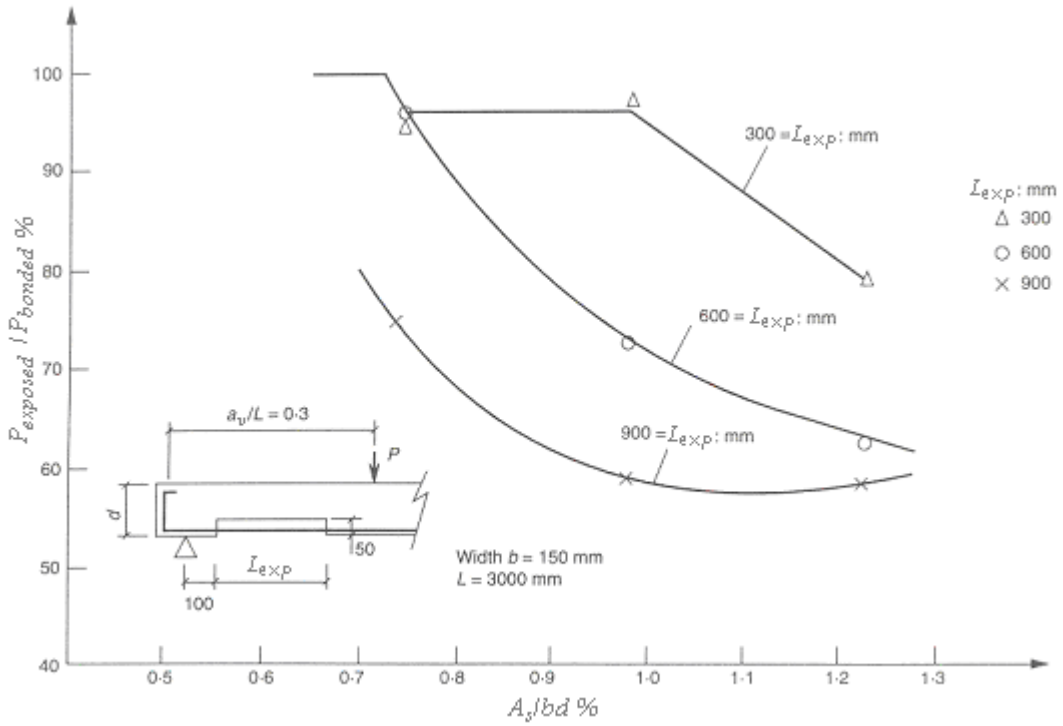

Fig. 2.4: Loss of strength vs. steel percentages for various lengths of exposure **[3]**

Results from Cairns and Zhao **[2]** can be compared with Raoof and Lin **[3]** to examine the loss of ultimate strength for various reinforcement percentages. To assist the comparison, the lengths of exposure used by Raoof and Lin **[3]** are converted to L_{exp} / d values (Table 2.1).

L_{exp} (mm)	300	600	900
L_{exp} / d	1.08	2.15	3.22

Table 2.1: Conversion of breakout lengths for comparison between studies

Cairns and Zhao tested much larger L_{exp} / d values but the observed loss in strength was generally less. For example, consider a reinforcement ratio of $1.00<A_s/bd<1.25$ for both studies. Cairns and Zhao recorded a strength reduction between 60% and 70% for an exposed length of L_{exp} / d = 12.8 – 14.3. However, for the same steel percentages, Raoof and Lin found a similar reduction in strength for an exposed length as short as L_{exp} / d = 2.15. The primary cause for this discrepancy was the position of the breakout. Cairns and Zhao tested specimens with exposed lengths that were symmetrical about the mid-span, whereas Raoof and Lin tested specimens with the exposed length positioned 100mm away from the support. Raoof and Lin observed severe tension cracking over the supports due to a short breakout length within the shear span and recorded significant reductions in strength as top reinforcement was not included in the test specimens **[3, 24]**. The position of loading may have also contributed to the discrepancy.

On site, removing all the contaminated concrete generally requires breakout to at least 20mm beyond the reinforcement. Raoof and Lin **[3]** investigated the effect of varying the depth of removal of concrete, while maintaining all other parameters constant. When the concrete was broken out just beyond the reinforcement, a negligible loss of ultimate strength was recorded. They concluded that reductions in ultimate strength only occurred when the depth of removal exceeded 13% of the effective depth.

The inclusion of top steel can assist the performance of specimens with exposed tension reinforcement. Tests by Cairns and Zhao **[2]** showed some minor cracking from the top face near the ends of the exposed length, but the cause of failure was concrete crushing within the constant moment zone. By contrast, some of the specimens tested by Raoof and Lin **[3]** had only main tension steel. These specimens were clearly more vulnerable to top face cracking near the supports. Below a certain threshold of exposed length, no tension strains are predicted to occur at the top face of the beam. The inclusion of nominal top steel as normally used in conjunction with shear links, has little effect on the ultimate strength of the beam unless this threshold is exceeded. Numerical results from Zhang and Raoof **[22]** also showed that top steel is more beneficial for larger exposed lengths (Fig. 2.5).

The reduction in flexural strength with breakout for a range of concrete cube strengths was predicted by Zhang and Raoof **[22]** and is plotted in Fig. 2.5. For f_{cu} = 20N/mm^2, loss of ultimate strength occurred for lengths of exposure as low as 30% of the span. The difference in behaviour between f_{cu} = 30N/mm^2 and f_{cu} = 40N/mm^2 was not

significant, with lengths of exposure as high as 70% of the span for f_{cu} = 40N/mm^2 before any loss of ultimate strength was observed.

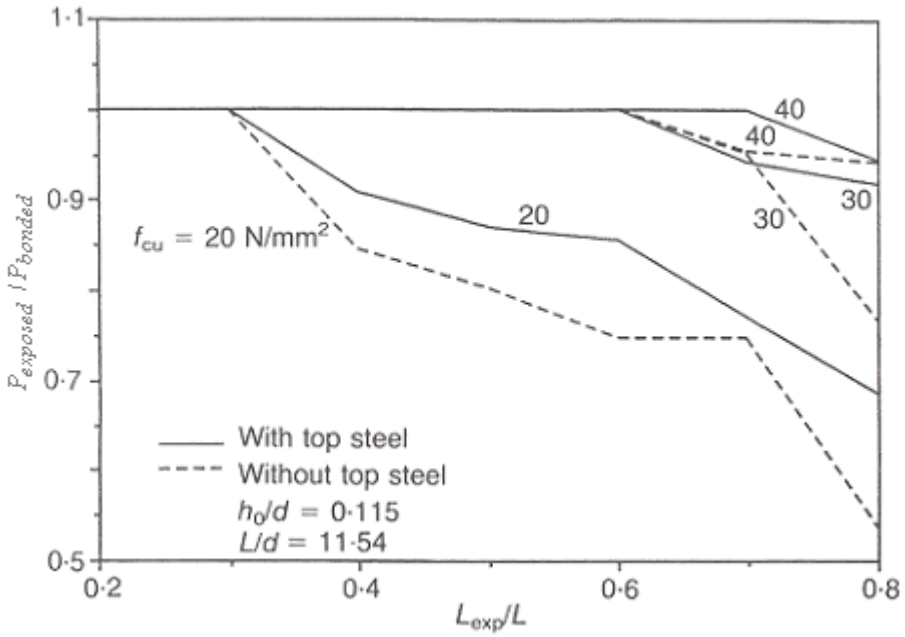

Fig. 2.5: Loss of strength with breakout for several concrete cube strength values **[22]**

Numerical modelling carried out by Cairns and Zhao **[2]** suggests the variation of loss of member strength with concrete cube strength is described by Fig. 2.6. Note: Nominal top steel was included in the model. The overall loss of strength for 80% reinforcement exposure is similar to that for Fig. 2.5 but the initial strength reduction for f_{cu} = 30N/mm^2 and f_{cu} = 40N/mm^2 occurred for smaller proportions of exposed length. As identical beam dimensions, steel percentages and loading arrangements were used in both studies, any discrepancies are attributed to differences in the numerical modelling packages used.

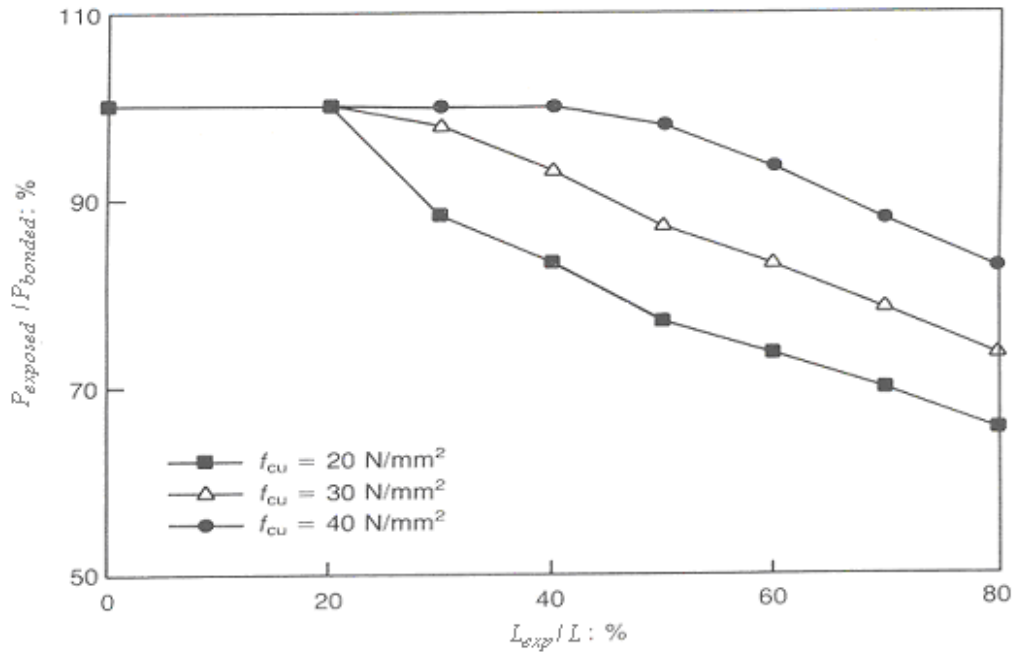

Fig. 2.6: Loss of strength with breakout for several concrete cube strength values **[2]**

2.3.2 Models for behaviour of beams with exposed reinforcement in flexure

Cairns and Zhao **[2]** use the following explanation to describe the behaviour of a simply supported member with exposed tension reinforcement. When reinforcement is exposed during the repair process, it can no longer act compositely with the concrete and the strain distribution through the section is altered. In describing the structural behaviour of beams with exposed reinforcement, it is convenient to initially assume linear elastic behaviour and to neglect the tensile strength of concrete. It is also assumed that plane section behaviour holds true for the concrete section. Equilibrium requires the net horizontal force at any given section to be zero and the internal forces to balance the applied moment. Compatibility of deformations between the steel and the concrete must also be maintained.

$$A_s f_{st} + f_c b(x/2) = 0 \qquad 2.1$$

$$A_s f_{st} z = M \qquad 2.2$$

$$\int^l \varepsilon_s \, dl = \int^l \varepsilon_c \, dl \qquad 2.3$$

where A_s = area of tension reinforcement

f_{st} = stress in the tension reinforcement

f_c = compressive stress in the concrete

b = width of the section

x = depth to the neutral axis

z = lever arm

M = bending moment

$\int^l \varepsilon_s \, dl$ = elongation of steel throughout exposed length l

$\int^l \varepsilon_c \, dl$ = elongation of substrate throughout exposed length l

Consider a beam subjected to two-point loads (both equidistant from the midspan) and assume initially that the reinforcement is fully bonded, Fig. 2.7(a). The depth of the neutral axis (x) is constant throughout the span. Thus, the lever arm (z) from the centroid of the concrete compression zone to the steel reinforcement remains constant. Assuming the cross-sectional area of the tension reinforcement (A_s) remains constant throughout the span, Equation 2.2 shows that the tensile stress in the steel (f_{st}) varies in proportion to the applied moment (M). If section breadth (b) is also constant, it follows that maximum compressive stress in the concrete (f_c) also varies with the applied moment to maintain horizontal force equilibrium (Equation 2.1). As reinforcement is assumed to be bonded to the concrete, the reinforcement will therefore be subjected to the same strain as the concrete at that depth, satisfying Equation 2.3.

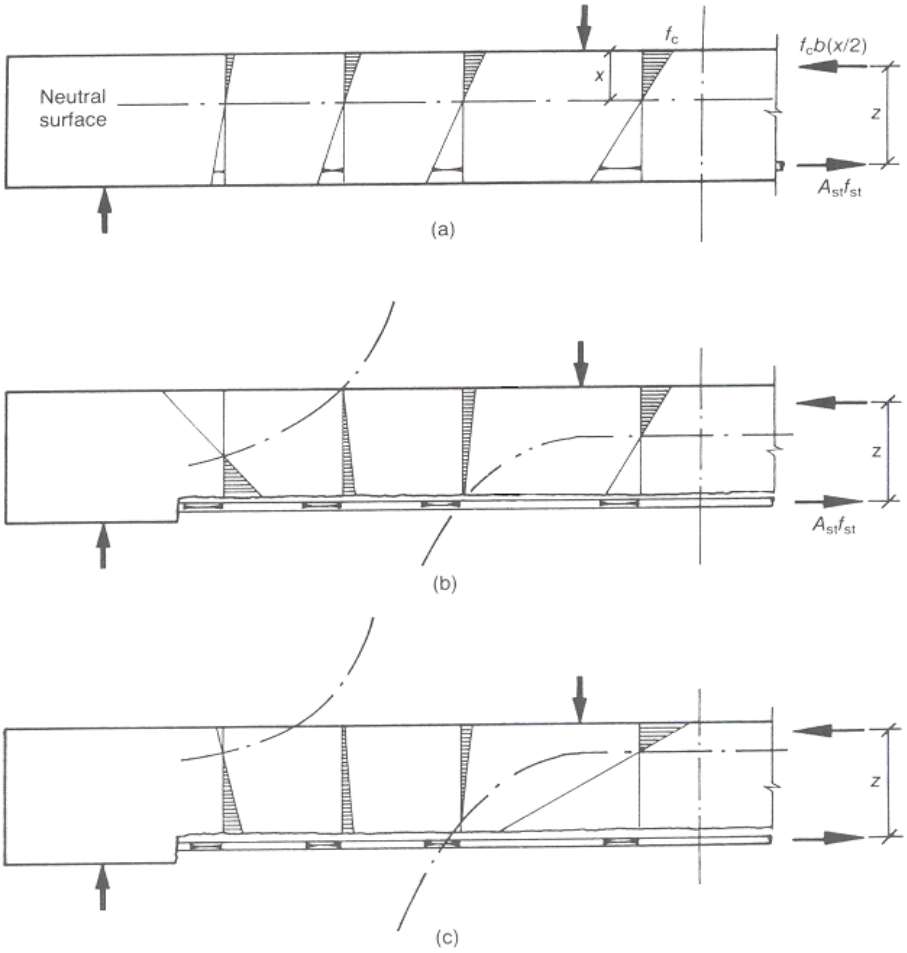

Fig. 2.7: Neutral axis variations for a member with exposed reinforcement **[2]**

(a) Stress pattern for fully bonded member

(b) Initial assumed stress pattern for exposed reinforcement

(c) Final stress pattern to maintain compatibility

Now consider a member where the reinforcement is exposed over a portion of the span and try to satisfy the equilibrium conditions. The depth of the neutral axis at midspan is initially taken to be identical to that in the bonded beam, with an illustration of stress patterns shown in Fig. 2.7(b). The stress in the reinforcement must remain constant throughout the exposed length due to the absence of bond with the concrete. Therefore, to satisfy Equation 2.2, the lever arm (z) must vary with the applied moment.

Outside the constant moment zone, the lever arm must initially reduce as the bending moment reduces towards the support, so the depth to the neutral axis increases to maintain moment equilibrium. As the tensile stress in the steel remains constant and

the neutral axis depth (x) increases, the maximum stress in the concrete decreases in inverse proportion to satisfy Equation 2.1. Further towards the support, a point is reached where the concrete is stressed in compression throughout its full depth. If a section closer to the support is considered, the neutral axis appears from above the beam and moves down into the section. However, the concrete is in tension above the neutral axis at this location and in compression below it.

Although the pattern of stress shown in Fig. 2.7(b) has been demonstrated to satisfy equilibrium requirements, it is clear that deformations in the concrete and the steel will not be compatible. The overall elongation of the exposed bar exceeds that of the bonded bar. Equation 2.3 cannot be satisfied unless the bottom face of the substrate elongates. This can be achieved by considering a smaller neutral axis depth at midspan (Fig. 2.7(c)), than the value initially assumed equal to that for the bonded steel. This is confirmed experimentally **[2]** by observing the greater crack heights within the constant moment zone upon exposure of reinforcement. This reduction in neutral axis depth leads to an increase in section curvature. The associated increase in the lever arm causes a slight reduction in the reinforcement stress, to maintain internal/external moment equilibrium. For Equation 2.1 to remain satisfied, the maximum stress in the concrete must increase. The increased curvature of the section near the midspan provides the main contribution to balancing Equation 2.3.

The following simplified analysis was used by Cairns **[25]** to quantify the loss of moment capacity with increasing length of breakout. The following assumptions were made in the analysis.

- The bending strength is relatively unaffected if reinforcement yields before concrete starts to crush.
- If the reinforcement yields, the pattern of stress in the concrete at ultimate load is relatively unaffected by the loss of bond.
- For a two-point load arrangement at the breakout location, concrete strains at ultimate load within the shear span are small relative to those within the constant moment zone.
- Sufficient reinforcement anchorage is provided at the ends of the exposed length to prevent a bond failure.
- Failure is attributable to crushing of concrete near midspan

Consider initially, the strain distribution graph at ultimate load shown in Fig. 2.8. The strain in the concrete at the depth of the tension reinforcement, and therefore the strain in the bonded tension steel at ultimate load can be calculated.

$$\varepsilon_{st} = 0.0035 ((d - x) / x) \qquad 2.4$$

where x = the depth of the neutral axis at ultimate load

d = the effective depth of the tension reinforcement

The depth of the neutral axis was calculated from

$$x = (A_s f_y) / (0.9 (0.67) f_{cu} b) \qquad 2.5$$

where A_s = the area of tension reinforcement

f_y = the yield strength of the reinforcement

f_{cu} = the concrete cube strength

b = the width of the section

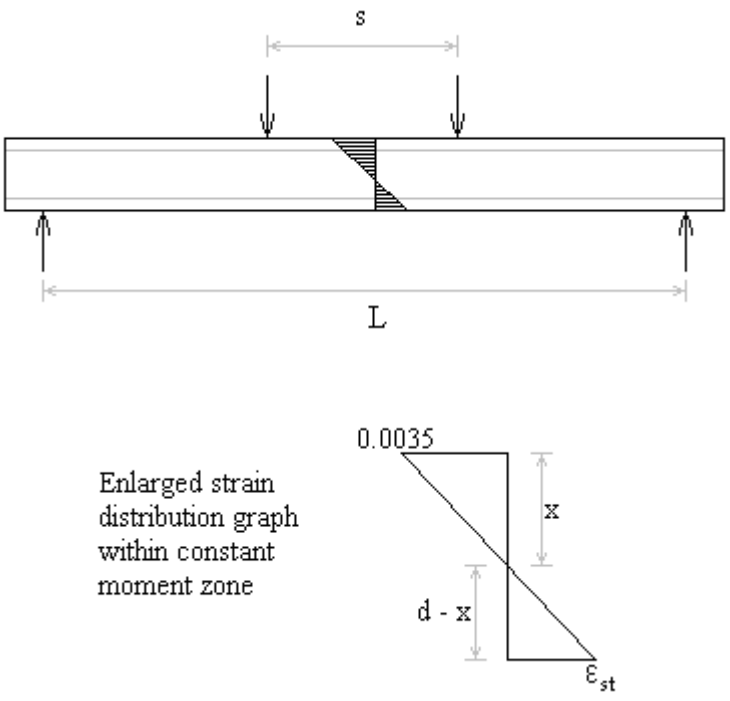

Fig. 2.8: Strain distribution within "fully bonded" member at ultimate load

The elongation of the bonded reinforcement at ultimate load was calculated from

$$\Delta L_{bonded} = L_{crush}\, 0.0035\, ((d - x) / x) \qquad 2.6$$

where L_{crush} = the length over which concrete crushing occurs

For a single point load arrangement, the length L_{crush} was taken as the length over which the limiting concrete compression strain is reached, calculated from the following expression derived by Phipps **[26]**.

$$L_{crush} = 3.5x - 0.0075x^2 \qquad 2.7$$

For a two-point load arrangement, it was assumed that the limiting compression strain of the concrete is reached at ultimate load throughout the length of the constant moment zone and the concrete compression strains within the shear spans are negligible. Consequently, L_{crush} for a two-point load arrangement was taken as

$$L_{crush} = \max\, \{(3.5x - 0.0075x^2), s\} \qquad 2.8$$

where s = the spacing of the point loads

Now consider ultimate limit state behaviour of the same specimen with a portion of the tension reinforcement exposed (Fig. 2.9). The strain in the unbonded reinforcement is constant throughout the exposed length. For reinforcement yield at ultimate load, the elongation of the reinforcement over the exposed length is

$$\Delta L_{unbonded} = L_{exp}\, \varepsilon_y = L_{exp}\, f_y / E_{st} \qquad 2.9$$

where L_{exp} = the exposed length of reinforcement
ε_y = the yield strain of the steel
f_y = the yield stress of the steel
E_{st} = the elastic modulus of the steel

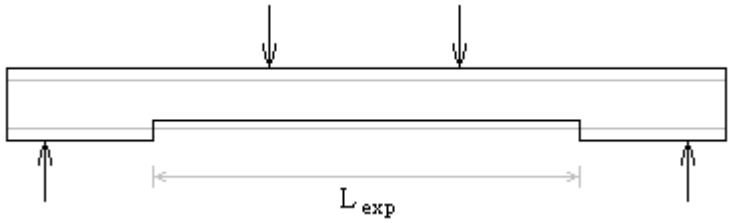

Fig. 2.9: Simply supported member with exposed length, L_{exp}

To ensure yielding of reinforcement occurs before concrete crushing in the specimen with exposed reinforcement, the elongation in the steel at ultimate load in the bonded section must not be less than the elongation of the exposed reinforcement at ultimate load.

$$\Delta L_{bonded} / \Delta L_{unbonded} \geq 1 \qquad 2.10$$

Equations 2.6, 2.9 & 2.10 can be rearranged to establish the maximum allowable breakout length without a significant loss of moment capacity.

$$L_{exp} \leq (L_{crush}) (E_{st} / f_y) 0.0035 ((d - x) / x) \qquad 2.11$$

The permissible length of exposure is primarily dependent on the x / d ratio at the breakout cross-section. Larger areas of tension reinforcement, and therefore larger x / d, reduce the maximum allowable breakout length (consistent with greater observed reductions in strength in more heavily reinforced specimens **[2, 3]**). The load arrangement and the material properties also affect the permissible breakout length.

Non-prestressed external reinforcing bars can be retro-fitted to a deteriorated concrete beam (anchored at the supports at the level of the bonded tension reinforcement) to increase ultimate strength. The achievable increase in flexural strength primarily depends on the relative area of bonded reinforcement. A section initially designed for a balanced failure essentially becomes over-reinforced due to installation of external reinforcement. Consequently, increases in flexural strength are greater in specimens with smaller percentages of bonded reinforcement **[27]**. The increase in strength cannot equate to that for the equivalent area of bonded reinforcement unless the unbonded reinforcement yields i.e. achieves an under-reinforced failure **[28]**. Load

arrangement and the use of deflectors (to prevent a reduction in the effective depth of the external reinforcement as the beam deflects) also influence the attainable increase in flexural strength **[29, 30]**. Increases in shear strength were also observed due to the change in stress pattern from purely flexural to a combination of flexural and tied-arch behaviour **[31]**. Ideally, the area of external reinforcement should be chosen to give the maximum increase in flexural strength while ensuring a shear failure does not occur.

2.3.3 Behaviour of beams with exposed reinforcement in shear

The shear strength of reinforced concrete beams is conventionally regarded as the sum of contributions from the following sources: concrete in the compression zone, aggregate interlock, dowel action of the tension reinforcement and resistance provided by shear links **[32]**. If the concrete around the longitudinal reinforcement is removed, the effect of dowel resistance is lost. The ability of a link to contribute to shear resistance will also be impaired if corner anchorage is lost. Thus, a reduction in shear strength of a simply supported beam with exposed reinforcement might be expected. However, this is contradicted by test results **[33]**.

For shear strength analysis of beams with exposed reinforcement, it is common practice to ignore the contribution from the exposed bars. This assumption clearly errs on the side of caution. Provided that exposed tension bars are adequately anchored and that no lap joints exist within the exposed length, the preceding section shows exposed bars may develop an appreciable portion of their design strength.

As discussed in Section 2.3.2, stress in the steel is uniform throughout the exposed length as it no longer acts compositely with the concrete. This leads to a reduction in the lever arm as sections further from midspan are considered, and a consequent "arching" of the neutral axis. The resulting beam action changes from purely flexural to a combination of flexural and tied-arch action. Cairns **[33]** carried out tests on simply supported beams (with nominal top steel and links) designed to fail in shear. Observed increases in shear strength were attributed to the above-mentioned arching action.

The change in shear strength on exposure of reinforcement is not simply a function of the exposed length. The position of exposure (either wholly within the shear span or

within both shear and flexure spans) has been shown to influence the increase in strength **[33, 34]**. The load arrangement (i.e. shear span ratio, a_v / d) and the area of tension reinforcement are also influential. Cairns **[33]** predicted a greater increase in shear strength due to arching action for smaller areas of exposed reinforcement. As reductions in shear strength do not occur due to reinforcement exposure, the parameters that affect the reductions in flexural strength are of primary concern.

2.4 Post-repair behaviour

2.4.1 Load relief during patch repairs to reinforced concrete beams

Post-repair behaviour is obviously influenced by the properties of the repair material but the load carried by the structure during casting of the repair also has a significant effect. Obviously, no load relief strategy will be the best suited option in all cases. Propping should be avoided if possible as props can be difficult to position without causing severe obstruction to the repair process. Omission of propping also represents the least expensive strategy but can only be carried out if an adequate margin of safety is ensured and serviceability limit state criteria are not exceeded **[35]**. Propping may serve two distinct functions: to provide an alternative load path or to relieve the structure of stress. An alternative load path may not be required if the member possesses adequate reserves of strength or if imposed loads on the member can be reduced throughout the repair process. Results from experimental work **[4]** demonstrate that ultimate strength of a beam need not be adversely affected by omission of load relief, provided an adequate margin of safety is maintained while the beam is being repaired. However, serviceability performance may deteriorate, with deflections and crack widths both increasing. To provide an alternative load path, props should be positioned in contact with the underside of the member, so as not to relieve stress. In this case, the temporary propping only takes up load when further deflection occurs.

Relieving the structure of load aims to ensure the stress pattern in the repaired beam is similar to that in an equivalent "as new" beam. This involves complete load relief from the structure during the repair process by propping to actively impose forces, to counteract the applied loading. In reality, it is impossible to remove all stress from a member. For example, cracks that become filled with dust would not be able to close when the member is relieved of load. Also, reinforcement crossing such wedged cracks would be unable to completely relieve itself of tensile stress. Even if a member can be completely unstressed by propping, it cannot be unstrained due to the non-linearity of concrete. Therefore, behaviour of a structure relieved of stress during casting should not be assumed to be consistent with that of the original structure.

Cairns **[4, 36]** investigated casting repairs under various amounts of load relief. For specimens repaired while under service load, the height of the flexural cracks in the constant moment zone increased when reinforcement was exposed. This coincided with the change in stress pattern described by Cairns and Zhao **[2]**. However, shear cracking did not increase with concrete breakout due to the increase in shear strength associated with "arching" action **[33]**. For beams fully relieved of load during repair, cracks in the original concrete reopened during loading to service load, unless they were injected with an epoxy resin sealer prior to reloading. This caused appreciable cracking in the repair material up to service load. Service load cracking within the patch repair was less severe for specimens propped to prevent excessive deflection. Shear stresses at the repair substrate interface are less severe in specimens repaired while under load and consequently, horizontal interface cracking develops at a lower load in members relieved of load during repair.

Cairns **[4]** carried out numerical modelling to compare behaviour of a repaired beam relieved of 50% of the service load during repair, with that of a similar "as new" beam. The stiffness of the repaired beam was found to be appreciably larger than that of the "as new" beam. Ali and Ambalavanan **[37]** carried out an experimental investigation of repairs to specimens under 50% of the service load and observed similar increases in stiffness to Cairns **[4]**. This enhanced stiffness is attributed to the greater contribution to tension stiffening of the less highly strained repair concrete. As large areas of tension steel do not allow significant tension stiffening to develop in the repair concrete, this increase in stiffness is more noticeable in lightly reinforced sections.

Mangat and O'Flaherty **[5]** carried out full scale bridge repairs under propped and unpropped conditions. By examining strain measurements within the patch repair, they concluded that the structural efficiency of the propped repairs was inferior as the contribution of the repair material to tension stiffening was less than for unpropped repairs. Results **[4, 36]** also show that the flexural stiffness of temporarily supported beams was greater than for beams fully relieved of load. However, reductions in member ductility occurred in specimens repaired under load.

2.4.2 Properties of concrete repair materials for effective structural application

Along with choosing the method of repair, an appropriate repair material must also be selected. Emberson and Mays **[38]** suggest structural performance of a repair may depend on a number of material properties such as:

- strength
- modulus of elasticity
- Poisson's ratio
- coefficient of thermal expansion
- tensile adhesion
- early curing shrinkage
- long term creep and shrinkage

Tests **[38]** were carried out on a selection of repair materials including: resinous materials (epoxy mortars, acrylic mortars), polymer modified cementitious materials, and cementitious materials (OPC/sand mortar, flowing concrete). Strength assessment showed that all materials provide adequate compressive strength for the vast majority of applications. Each product was found to possess a tensile strength matching or exceeding that associated with most conventional concretes, with the highest values exhibited by the resinous materials. The resinous materials also showed the largest flexural strength of the tested repair materials. Mai and Cotterell **[39]** tested a series of epoxy resin modified mortars to investigate the influence of resin content. They observed increases in flexural strength with increasing resin content. However, the change in flexural strength was negligible beyond 10% resin content by weight.

Compression modulus test results **[38]** ranged from 18kN/mm^2 to 50kN/mm^2 with the resinous materials tending to the lower end of the range. Values of tension modulus exhibited a similar range of values. Poisson's ratio was found to be 0.2 for most materials.

Some materials displayed two values for the coefficient of thermal expansion, one for below cure temperature and one for above. This is due to a contraction associated with post-curing of resinous materials. In general, the resinous materials had

significantly higher coefficients of thermal expansion than non-resinous materials. Thermal expansion can induce significant stresses in a repaired member subjected to appreciable temperature variations if the repair material chosen has a high thermal coefficient.

Pull-off test results showed the resinous materials had tensile adhesion strengths sufficient to cause failure in the substrate concrete. In contrast, the non-resinous materials predominantly failed at the interface. The flowing concrete was the exception, having one of the largest tensile adhesion values.

The resin mortars had small and relatively stable shrinkage values beyond the age of one month. Most of the other materials showed an increase in shrinkage with time, presumably due to continued drying.

Emberson and Mays **[40]** emphasized that interaction between individual properties should also be considered. For example, a material prone to high shrinkage requires sufficient adhesion strength to remain bonded to the substrate. Also, relaxation due to creep may offset stresses due to shrinkage restraint.

The structural performance of the repaired specimen is of utmost importance but the durability of the repair material must also be considered. The environmental conditions, to which the repaired specimen is exposed, can have a significant influence on repair material properties. Plum **[41]** investigated the influence of temperature and relative humidity on the properties of polymer modified concretes. Reductions in compressive and flexural strength were observed for high relative humidity conditions during the curing period. Mangat and Limbachiya **[42]** observed greater shrinkage during the curing period for lower values of relative humidity, particularly in polymer modified cementitious mortars. Therefore, curing conditions should be chosen to suit the selected repair material.

Mangat and Elgarf **[43]** investigated loss of flexural strength due to subsequent corrosion of repaired specimens and highlighted the importance of chemical passivation of the embedded steel by the repair concrete. Rizzo and Sobelman **[44]** discussed desirable characteristics of a repair material and methods of testing. Polarisation techniques or accelerated corrosion tests were used to establish the chemical passivation provided by repair concretes. Repair materials of low permeability are desirable to prevent moisture and oxygen from reaching the steel.

Workmanship of a repair can have a huge influence on the structural performance and aesthetics of the repaired specimen **[35, 45]**. It is essential that repair materials are

easy to mix in the correct proportions and that the mix is of suitable workability. Ease of application is a desirable characteristic of a repair material and the placement technique should allow casting of a repair with specified results.

2.4.3 Effect of adhesion and restrained concrete shrinkage in repaired concrete beams

Xiong et al **[46]** investigated bond between the repair material and the substrate on the flexural strength of a repaired member. "Unbonded repair" specimens had a layer of PVC membrane between the repair and the substrate. A corresponding set of "bonded repair" specimens were also tested. Extreme fibre compression strains were appreciably higher in the "unbonded repair" members as the lack of bond at the repair-substrate interface caused more significant increases in curvature during loading to failure. Therefore, interface slip caused an undesirable shift towards over-reinforced behaviour.

Adequate adhesion of the repair material to the substrate is vital to the success of a patch repair. Drying shrinkage will occur in the repair material and this is restrained by the reinforcement and the substrate concrete. The adhesion strength at the interface must be sufficient for strain transfer between the repair material and the substrate to take place.

Cleland et al **[47, 48]** described a pull-off test devised to quantify adhesion of a repair material to a substrate. When bonding agents were not used, adhesion was influenced by surface roughness and moisture condition, curing conditions and position of the repair. Surface preparation techniques and their influence on bond are well documented **[20, 49]**. Cleland **[47]** tested a range of substrate moisture conditions and found lower pull-off bond strengths for both "oven-dry" and "saturated surface-wet" conditions. When casting a repair, the substrate should be in a "saturated surface-dry" condition. If the repair material is cast to the underside of a beam / slab, gravitational effects will inhibit bond to the substrate. However, measures can be taken when casting the repair to improve the bond. For example, when carrying out a flowing repair on a beam, adequate head of repair material can be provided through the access points to ensure sufficient hydrostatic pressure at the interface.

Much of the longitudinal shrinkage strain in the repair material will be restrained by the reinforcing bars and the substrate. A mismatch between the elastic moduli of the substrate and repair materials may cause an increase in concrete internal stresses due to restrained concrete shrinkage. Research by Mangat and O'Flaherty **[5, 50]** showed that high stiffness repairs were more effective in redistributing shrinkage strain to the substrate. They suggested the optimum relationship between the elastic modulus of the repair material (E_{rm}) and the elastic modulus of the substrate (E_{sub}) was $E_{rm}>1.3E_{sub}$. However, Emberson and Mays **[51]** recommend that repair material properties should not differ significantly from the substrate properties and suggest $E_{rm}= E_{sub} \pm 10$ kN/mm^2. Higher modulus values were found to attract load away from the substrate and place higher demands on interfacial adhesion.

Investigations by Mangat and O'Flaherty were carried out on full scale repairs to bridge soffits. High stiffness repair materials ($E_{rm}>E_{sub}$) were used in the patch repair of Lawns Lane Bridge near Wakefield on the M1 **[52]**. Conversely, repair materials of lower elastic moduli than the substrate ($E_{rm}<E_{sub}$) were used during repairs to Gunthorpe Bridge spanning the River Trent in Nottinghamshire **[50]**. Comparison between these studies is used here to highlight the influence of the elastic modulus on structural behaviour of a patch repair.

Fig. 2.10 shows the variation of strain within the repair patch with time for ($E_{rm}>E_{sub}$). The plot denoted "subs" represents the change in strain at the interface, "steel" represents the change in strain in the previously exposed steel and "emb" represents the strain in the repair material at the level of the tension reinforcement.

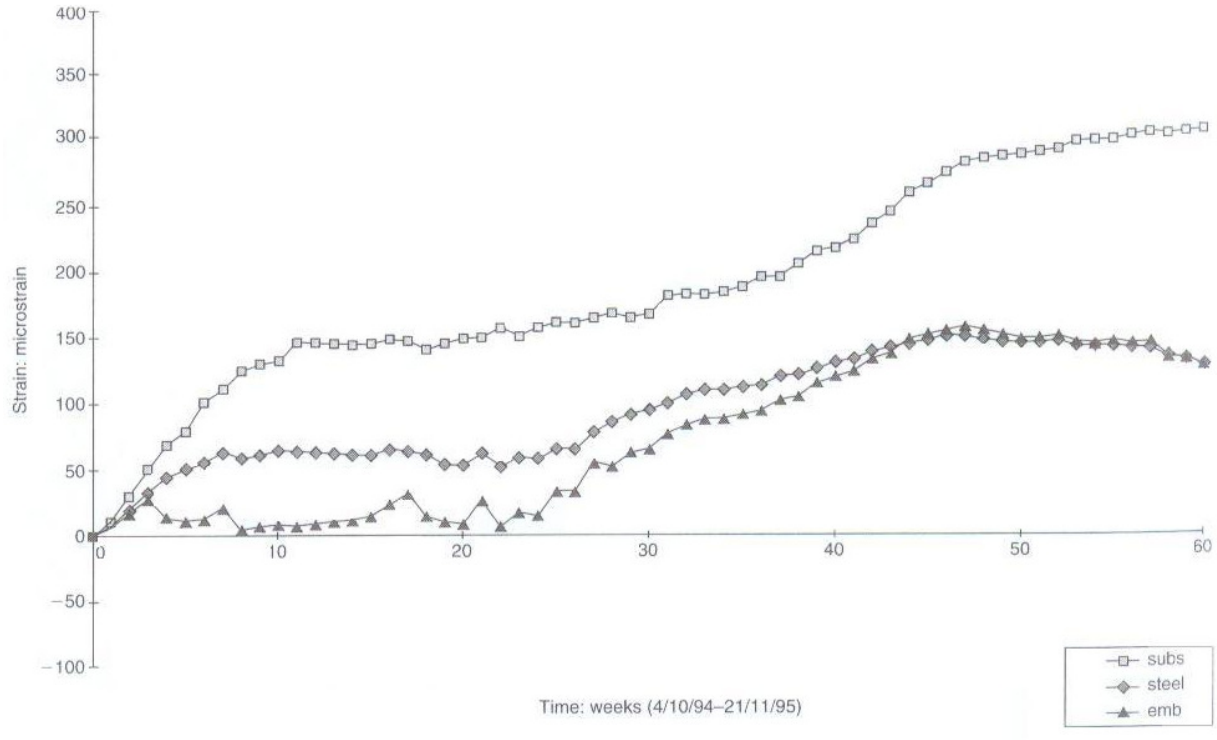

Fig. 2.10: Variation in strain with time, Lawns Lane Bridge (E_{rm}>E_{sub}) **[52]**

Mangat and O'Flaherty **[52]** described the variation in strain with time using the schematic diagram, Fig. 2.11. Zone 1 illustrates the shrinkage transfer stage, which is said to occur in the first 11 weeks. Rapid free shrinkage of repair materials generally occurs during the first 28 days with subsequent increases in shrinkage strain being relatively small **[53]**. During Zone 1, the stiffer repair material gradually transferred some of its steadily increasing shrinkage strain to the substrate concrete. Therefore, the shrinkage restraint provided by the substrate reduces as it is itself strained to accommodate the repair material. As a result, the tension strain in the repair material was reduced. This substrate restraint decreases with increasing distance from the interface, thereby permitting greater free shrinkage near the extreme fibre, and therefore higher compression strain. The strain in the steel reinforcement (steel, Fig. 2.11) and the repair material at the level of the steel reinforcement (emb, Fig. 2.11) also increased linearly with time as a similar strain transfer took place to the reinforcement. However, the strain was much lower than the free shrinkage strain of the repair material due to the restraint provided by the steel reinforcement. The shrinkage restraint provided by the steel was larger than that provided by the substrate as the steel is stiffer than the substrate.

During Zone 2 (11-25 weeks), the increase in the free shrinkage of the repair material became negligible and no transfer of shrinkage strain occurs to the substrate. During Zone 3, the externally applied load gradually redistributed to the repair patch. After week 47, no further redistribution of strain seemed to take place. A repair material which is prone to a moderate degree of creep may allow some relaxation of tensile stress within the patch repair.

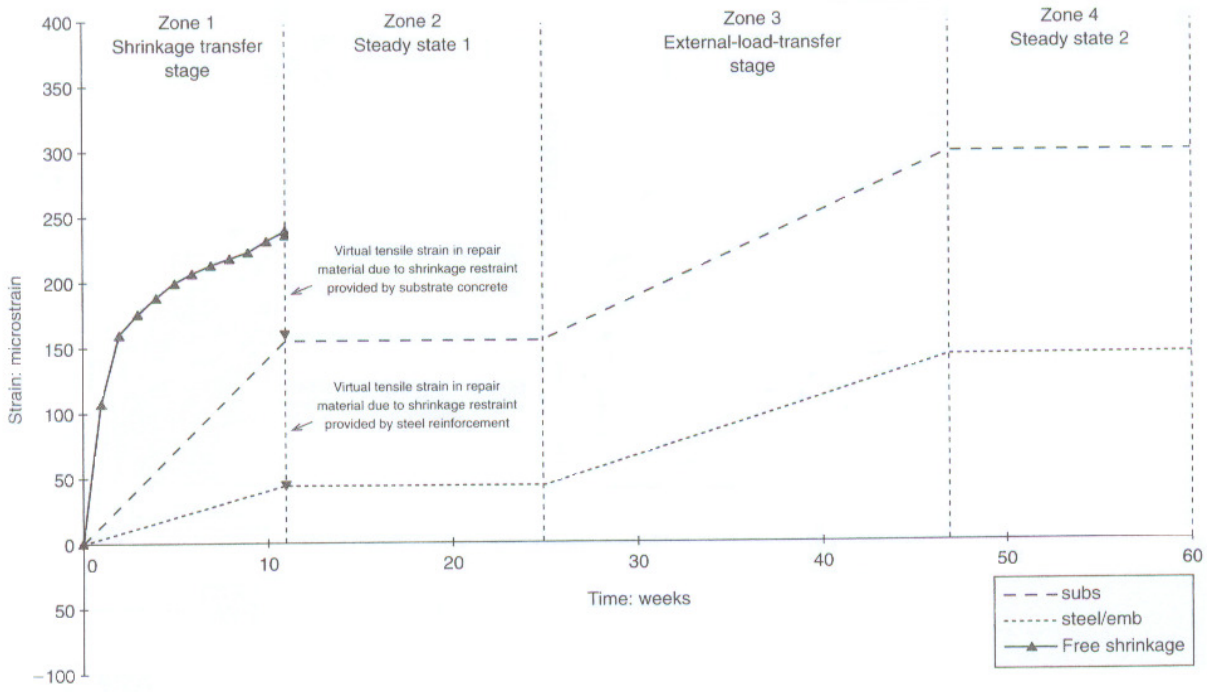

Fig. 2.11: Schematic representation of strain redistribution with time ($E_{rm}>E_{sub}$) **[52]**

The development of strain with time for repair materials with elastic moduli ($E_{rm}<E_{sub}$) is illustrated in Fig. 2.12. Significant differences in the strain redistribution are apparent (when compared with Fig. 2.10). For example, the repair material seems unable to transfer any shrinkage strain to the stiffer substrate during the previously defined Zone 1. The difference between the strain in the reinforcement (steel, Fig. 2.12) and the repair material at the same level as the reinforcement (emb, Fig. 2.12) is negligible, despite the high free shrinkage of the material. This is due to the steel effectively restraining the repair material from shrinking. During the external load transfer stage (25-47 weeks), insignificant changes in the tensile strain distribution occur. This implies that lower stiffness repair materials are unable to attract external applied load from the substrate. While the repair material can still accommodate

varying steel stress along the previously exposed bars, it is less effective at restoring section stiffness than a material of greater elastic modulus.

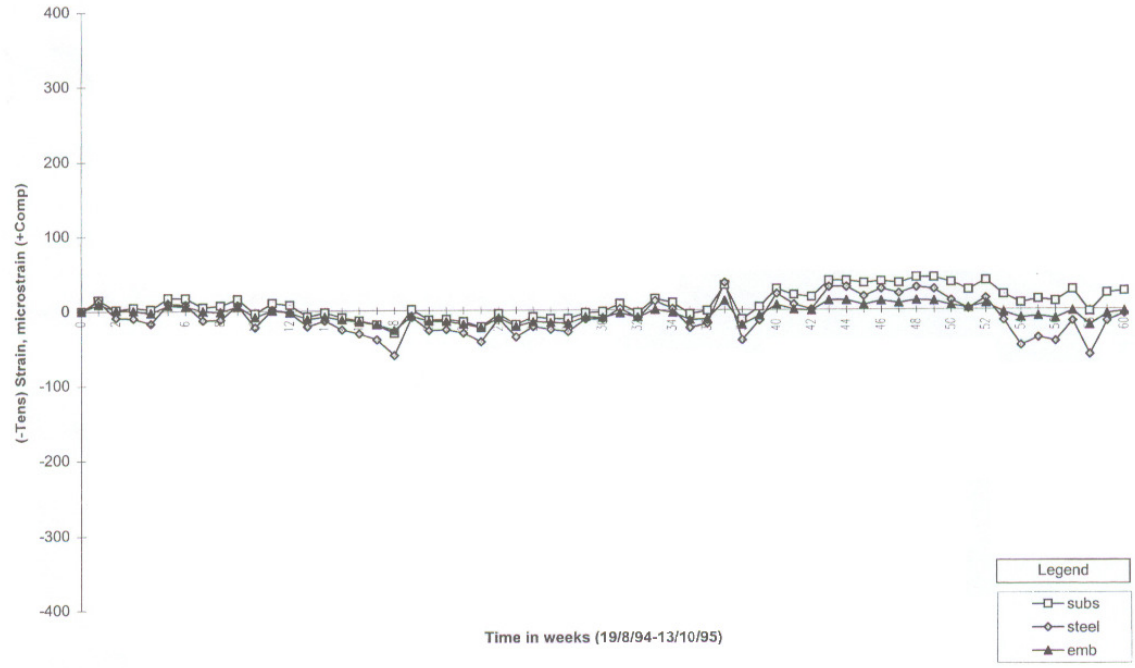

Fig. 2.12: Variation in strain with time, Gunthorpe Bridge (E_{rm}<E_{sub}) **[50]**

More recent work by Mangat and O'Flaherty **[54, 55]** discusses a simplified mathematical model to assess the depth of the substrate affected by shrinkage transfer. The model also enables calculation of the stresses in the substrate and repair material at the interface if the modular ratio (E_{rm} / E_{sub}) is known. This allows a repair material of suitable elastic modulus to be chosen to ensure interface stresses are not excessive and the adhesion strength of the repair material to the substrate is sufficient to prevent bond failure.

2.5 Moment redistribution effects in beams

The effect of shifts in the pattern of moment during a patch repair is of primary concern in this study. Canisius & Waleed **[6]** carried out numerical simulations of patch repair of continuous two-span beams subjected to uniformly distributed loading. Their analysis included both unpropped and propped repair within one of the spans. Significantly higher tension strains were observed during loading of the unpropped repaired specimens, at both the repair region and the internal support. This increase in strain at the internal support is attributed to the transfer of moment during breakout of concrete within one of the spans.

Loss of stiffness due to breakout of concrete at one location causes moment transfer to other parts of the structure. This effect may be more severe if design of the "fully bonded" specimen incorporates moment redistribution, should an increase in concrete compression strains lead to concrete crushing before reinforcement yields at all plastic hinge locations. Moment redistribution is traditionally considered to occur close to the ultimate limit state as it is linked to reinforcement ductility. However, tests **[56, 57]** have shown that a significant portion of the total moment redistribution can occur at the serviceability limit state. The parameters that affect moment redistribution have implications for unpropped patch repair of continuous reinforced concrete members and require investigation.

The flexural stiffness (EI) for ultimate limit state bending moments is usually based on the entire concrete cross-section (ignoring the reinforcement) and this method is sufficient for design purposes. Design codes permit a linear elastic analysis at ultimate limit state but acknowledge non-linear behaviour by allowing a limited amount of moment redistribution to occur. The permissible redistribution from a given section is primarily influenced by the x / d ratio, but also the ductility of the steel at the ultimate limit state **[58]**. Moment redistribution is generally employed by designers to transfer moment away from high moment locations. This produces a smaller bending moment envelope for a set of loadcases, which still satisfies equilibrium. Therefore, a more economic design can be achieved.

For initial loading of a specimen, the bending moment diagram is similar to the elastic bending moment diagram (calculated on the basis of uniform flexural stiffness throughout the member). As loading increases, the presence of reinforcement and the formation of cracks cause the actual flexural stiffness to differ from that derived with

the gross concrete cross-section approach. Scott and Whittle **[59]** suggest the total redistribution is made up of two components, "elastic redistribution" (or crack induced redistribution) and "plastic redistribution" (which occurs when the reinforcement yields). "Elastic redistribution" is primarily influenced by the reinforcement areas at relevant sections within the member. However, load arrangements also influence crack patterns and therefore moment balance (i.e. the ratio between maximum hogging and sagging moments) within a member.

Testing by Scott and Whittle **[59]** was carried out on two-span beams with point loads at each midspan. An elastic analysis shows the bending moment at the central support to be 3PL / 16, where P is the value of each applied point load and L is the span. The corresponding moment at the midspans is 5PL / 32. Therefore, the maximum hogging moment at the central support is 1.2 times greater than the maximum sagging moment within the spans. A range of parameters were investigated including the percentage of tension steel above the central support and within the spans. Practical design would choose to reduce the maximum moment at the central support by selecting a greater tension reinforcement area within the spans than at the support. Specimens designed for various amounts of redistribution to the spans were tested and the required redistribution was generally achieved at the ultimate limit state. However, a significant portion of the required redistribution had already occurred at service load. To investigate this point further, several specimens were reinforced so that 0% redistribution was expected (the area of tension steel above the central support was chosen to be 20% greater than within the spans as the elastic bending moment over the support was 20% larger than that within the spans). An "elastic redistribution" occurred up to service load caused by the internal supports being more heavily reinforced than the spans. The only way the assumed ultimate limit state bending moment diagram could be achieved was through plastic hinge development at the support. Therefore, "plastic redistribution" occurred to offset the "elastic redistribution".

Scott and Whittle **[59]** also carried out numerical modelling to investigate the influence of load arrangement on "elastic redistribution". Fig. 2.13 compares the "elastic redistribution" for various load arrangements and support conditions. Note: Positive redistribution represents redistribution from the fixed support to the span. Comparison between a central point load and a uniformly distributed load applied to a propped cantilever are of particular interest here. For all values of design moment

redistribution, “elastic redistribution” from the support to the span was greater for the central point load. This trend is attributed to the crack patterns induced by different load arrangements affecting tension stiffening within the member.

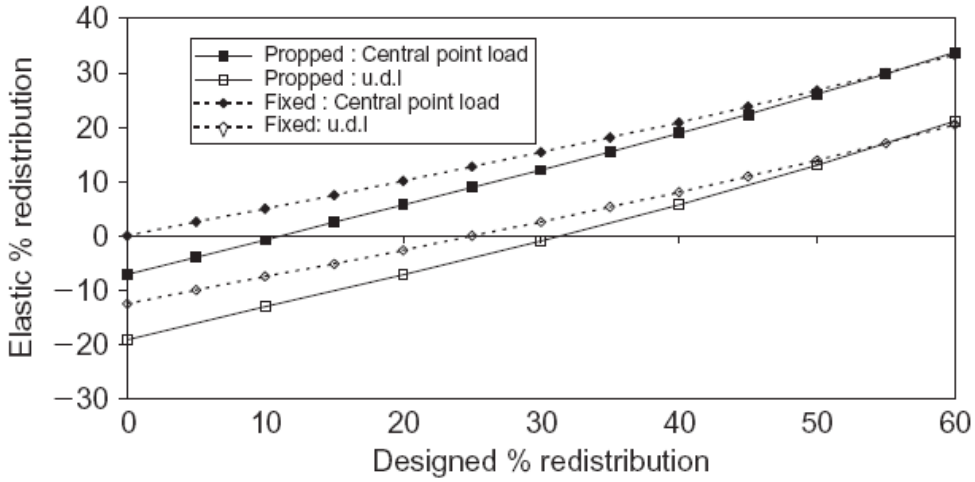

Fig. 2.13: Plot of “elastic redistribution” vs. total design redistribution for various load arrangements and support conditions **[59]**

2.6 Summary of review

Previous research on the structural behaviour of patch repairs has concentrated on the analysis of simply supported beams. Results from repaired continuous structures are limited **[49, 60]** and the effect of moment transfer during the repair process was not discussed. Canisius and Waleed **[6]** carried out numerical simulations on continuous beams but only briefly mentioned high stress concentrations that occurred at the internal support due to repair within one of the spans. Investigation is required to quantify the moment transfer that occurs during concrete breakout and to evaluate its effect on structural performance at serviceability and ultimate limit states, both during and following completion of a repair. Parameters should be chosen to correspond to the most influential parameters established for repairs to simply supported beams and also to vary the design moment redistribution.

The change in specimen behaviour with increasing length of reinforcement exposure (for simply supported beams) is well documented **[2, 3, 33]**. In practice, it is usually desirable to carry out all necessary breakout in one stage. However, increasing the breakout length increases the change in behaviour from "fully bonded" behaviour. Therefore, establishing a limit to the tolerable breakout length within multi-span beams is required. This will be investigated by increasing the length of breakout progressively. Progressive breakout also allows monitoring of the moment transfer away from the breakout location as loss of section stiffness in that region increases.

The area of exposed steel significantly influences the loss of ultimate strength during breakout and repair of simply supported beams. Flexural strength is more likely to be reduced in heavily reinforced sections as the increase in concrete compression strain during breakout can cause concrete crushing before reinforcement yields **[2]**. This increase in compression strain remains "locked into" the repaired member if the structure carries load during casting of the repair. Investigation of this effect in multi-span beams is warranted.

Moment transfer during the repair process is of primary importance in this study. Parameters that influence moment redistribution in "fully bonded" members should be examined. Their influence on "elastic redistribution" that occurs up to service load **[57, 59]** may add to the severity of the moment transfer during concrete breakout. The reinforcement areas at relevant sections within a member can be used to vary the amount of "elastic redistribution".

In a two-point load arrangement, the change in elongation of the exposed steel, and therefore the increase in curvature at the breakout location, was more severe when the point loads were positioned closer together **[2]**. Therefore, load arrangement influences the loss of section stiffness during breakout, and thus moment transfer from the breakout location. The influence of load arrangement on moment transfer during concrete breakout requires examination.

The position of breakout / repair within a multi-span beam is also of interest. Breakout of concrete at a support would cause moment transfer to the adjacent spans and vice versa. A range of specimens designed for varying degrees of moment redistribution should be analysed for both breakout at an internal support and within a span.

Chapter 3: Specimen design

3.1 Introduction

Previous work has investigated the post-breakout and post-repair behaviour of simply supported beams and the influence of a wide range of parameters is well documented. This study investigates such behaviour but extends previous work on statically determinate beams to statically indeterminate beams. Parameters that influence moment redistribution within continuous members are included, together with parameters found to affect behaviour of simply supported beams during the repair process. Literature on temporary propping during the repair process shows omission of load relief is acceptable, provided the margin of safety (while the beam is in the "weakened" condition) is sufficient. This hypothesis is extended to continuous beams. This chapter discusses the conceptual stages of specimen design and the parameters chosen for investigation.

The investigation comprises of two main phases. Firstly, changes in bending moment and residual strength are examined during exposure of reinforcement. Secondly, the influence of the load carried during the repair on the structural performance of the repaired member is assessed. A small number of reference specimens with "fully bonded" reinforcement are also tested.

3.2 Analytical investigation

An analytical study of the influence of load arrangement on behaviour during breakout of concrete is conducted to help determine parameters for investigation. Section 2.3.1 suggests that for a two-point load arrangement on a simply supported beam, the rate of increase in curvature with breakout length is greater when the point loads are positioned closer together (for a given value of maximum moment). Therefore, the reduction in flexural stiffness at the breakout location is greater for more closely spaced point loads. Consequently, the load arrangement at the breakout location may influence moment transfer due to concrete breakout. This section presents a simplified analysis to investigate this phenomenon.

Consider initially a single point load arrangement at the breakout location. The red lines in Fig. 3.1 represent the shape of the bending moment diagram near the breakout region. A constant area of tension reinforcement is assumed. While the specimen is "fully bonded", the compression zone depth remains approximately constant. If the bending moment is divided by the area of reinforcement and the "constant" lever arm, the red lines in Fig. 3.1 are an approximate representation of the stress in the tension reinforcement in the "fully bonded" specimen.

Tension stiffening provided by the concrete between flexural cracks is lost when the concrete cover is removed. The shaded region in Fig. 3.1(a) represents the integral of the increase in average stress due to loss of tension stiffening within the exposed length. Once the reinforcement is exposed, the tensile stress in the steel is uniform throughout the breakout length as it can no longer act compositely with the concrete. To maintain the same bending moment at the centre of the breakout (and initially assuming no increase in lever arm), the stress in the exposed reinforcement must equal that below the point load in the "fully bonded" member. The shaded area in Fig. 3.1(b) represents the increase in stress in the exposed steel due to loss of composite action between the steel and the concrete. In continuous structures, loss of section stiffness causes a reduction in moment at the breakout location. The shaded area in Fig. 3.1(c) represents the reduction in stress due to the decrease in moment. Note: The increase in lever arm that occurs during breakout to maintain compatibility between the exposed steel and the substrate also contributes to this reduction in stress. Fig 3.1(a - c) can be superimposed to give the stress in the exposed steel, Fig. 3.1(d).

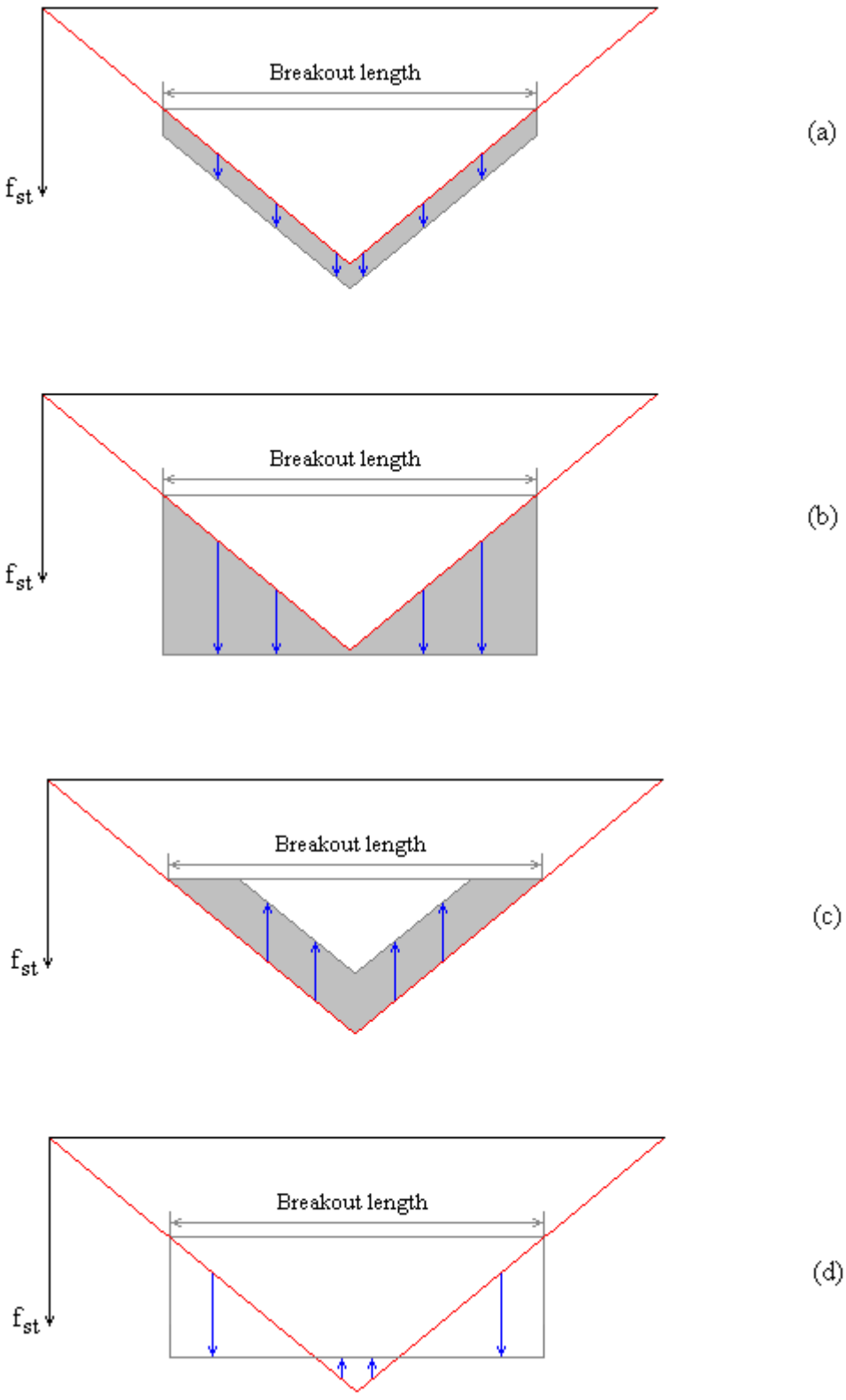

Fig. 3.1: Schematic diagram of variation in reinforcement tensile stress near breakout region (single point load arrangement)

Fig. 3.2 shows the corresponding representation of reinforcement stress for a two-point load arrangement. The shaded area in Fig. 3.2(a) represents the increase in average stress due to the loss of tension stiffening within the breakout length. Fig. 3.2(b) shows the increase in stress due to loss of concrete-reinforcement bond. In this case, most of the breakout takes place within the constant moment zone between the point loads so the change in behaviour is less severe than for a one-point load arrangement (as both pre-breakout and post-breakout steel stresses were uniform within the constant moment zone). Appreciable increases in stress only occur where the exposed length extends into the shear spans. The shaded area in Fig. 3.2(c) represents the reduction in exposed steel stress due to moment transfer from the breakout location. The increase in the lever arm is negligible until the breakout length extends into the shear spans so its contribution to the change in stress is small. Fig. 3.2(d) shows the exposed steel stress from superposition of Fig. 3.2(a-c).

The increase in exposed steel elongation during breakout (due to loss of composite action between the steel and the concrete), and therefore the loss of section stiffness is greater for a single point load arrangement than for breakout predominantly within the constant moment zone of a two-point load arrangement. Consequently, greater transfer of moment from the breakout location is expected for a single point load arrangement.

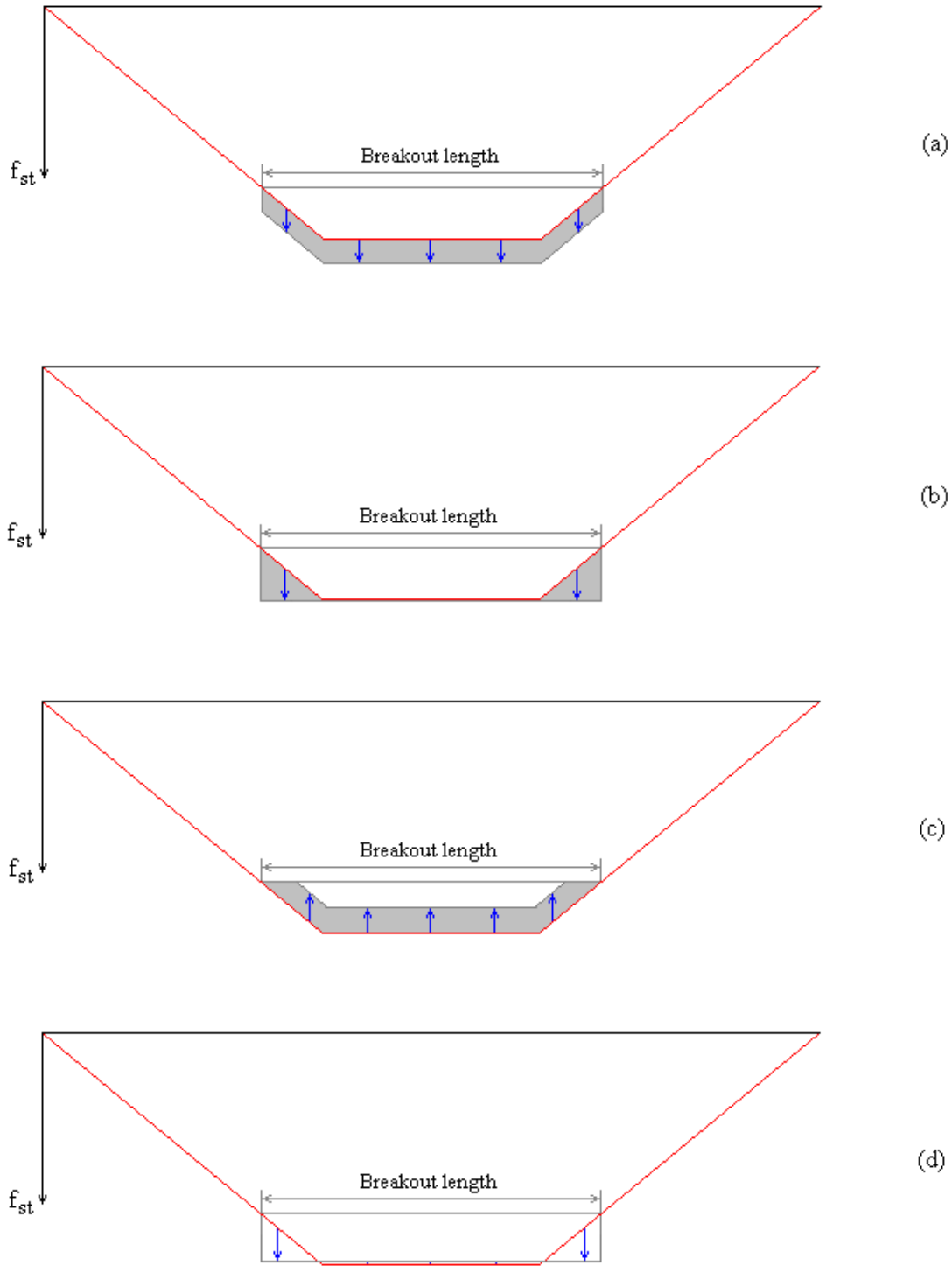

Fig. 3.2: Schematic diagram of variation in reinforcement tensile stress near breakout region (two-point load arrangement)

3.3 Limits to scope of investigation

It was decided to confine physical testing to two-span beams continuous over an internal support and simply supported at either end. Testing of a greater number of spans would unnecessarily complicate the testing rig. Pinned supports were chosen as rotational restraint associated with fixed supports is difficult to achieve in practice. Two spans of equal length were chosen to limit the number of parameters being investigated. For example, breakout within the shorter of the two spans would cause a different rate of moment transfer to the internal support than for breakout within the longer span. Such an investigation would undesirably broaden the scope of the experimental programme.

The overall length of the test specimens was limited by practical considerations. A maximum length of 4.3m was chosen for ease of construction and manoeuvrability in the structures lab. This allowed for 2 × 2m long spans with 150mm overhang beyond both outer pinned supports.

BS 8110 **[61]** limits the span to effective depth ratio (L / d) to prevent excessive deflections at service load. The allowable L / d ratio of a span that is simply supported at one end and continuous at the other end is 23 (neglecting modification factors for tension and compression reinforcement). If the effective depth was chosen to give the limiting L / d ratio (Note: L = 2000mm), extra displacement caused by unpropped breakout would be excessive. An effective depth of approximately 168mm was chosen to give an L / d ratio of 11.9. This allowed for a reasonable increase in displacement due to breakout of concrete.

The width of the cross-section was chosen to be 150mm. This allowed sufficient spacing between the reinforcing bars so as not to inhibit breakout of concrete or casting of a repair.

All test specimens were of uniform rectangular cross-section. The increase in concrete compressive stress near the breakout region was of concern. T-sections were therefore avoided as the narrow web of the T would be more susceptible to concrete crushing.

It was decided to concentrate on breakout and repair within the tension zone as the test specimens were quite small scale and concrete breakout from around the compression reinforcement would remove a significant portion of the concrete compression zone depth. This would significantly reduce the load carrying capacity

of the test specimens. Also, compression zone breakout would lead to difficulties during the testing procedure. For example, breakout and repair beneath the point loads would involve complete removal of the loading apparatus during testing.

3.4 Parameters for investigation

3.4.1 Location and length of breakout

Fig. 3.3 shows a schematic diagram of the chosen breakout locations: hogging breakout centred on the maximum hogging moment cross-section above the central support, and sagging breakout centred on the left midspan. Hogging breakout would instigate moment transfer from the central support to the spans while sagging breakout would cause moment transfer from the spans to the central support. Sagging breakout was centred on the left midspan to avoid an unbalanced portion of the breakout being within the shear span near the left support, which has been shown to severely reduce the load carrying capacity of the beam **[2, 3]**.

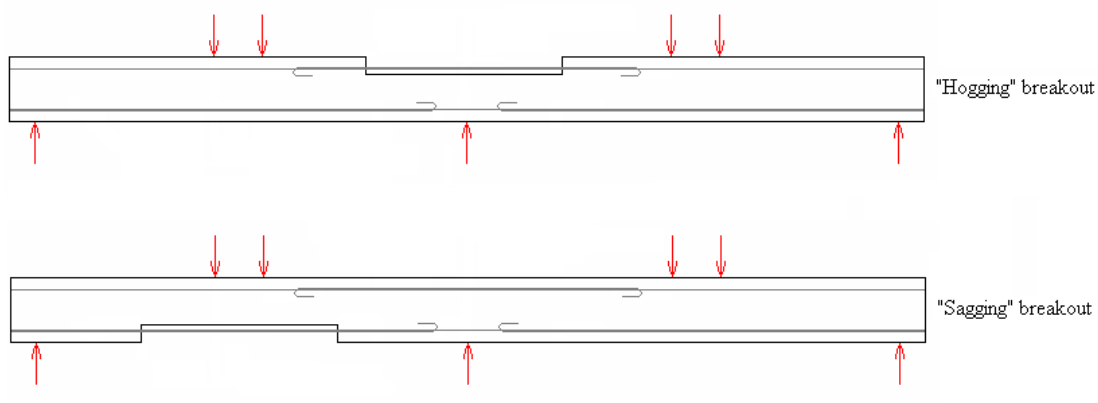

Fig. 3.3: Schematic diagram of breakout locations

Testing **[2]** identified that departure from "fully bonded" behaviour increases with the length of breakout. In the first set of specimens, successive increments of breakout allowed the influence of the breakout length on the pattern of moments within the structure to be assessed. Monitoring of structural behaviour up to service load was desirable to examine the most critical case (i.e. no load relief during breakout process). After completion of breakout, these specimens were tested to failure to assess their residual strength.

Progressive breakout of concrete allows maximum limits of breakout length (for no significant loss of strength) to be established. Although the benefits of breakout over as long a length as possible are recognised, it was considered impractical to extend

breakout far beyond points of contraflexure. Breakout extending significantly into compression zones would markedly reduce the tensile stress the exposed bar could develop. Points of contraflexure are not fixed within the structure as moment transfer is anticipated during testing. Predicted ranges of contraflexure points were established and the maximum breakout lengths chosen accordingly. Maximum breakout lengths of 50% of the span length were chosen for both hogging and sagging locations for ease of comparison between the two locations.

In the second part of the study, a corresponding set of specimens were repaired under various load relief conditions and then tested to failure. Their structural performance was compared to that of "as new" control specimens also included in the test programme. Casting of the repair was carried out for the maximum breakout lengths (50% of the span length) in all specimens to establish behaviour of the longest "advisable" repair length. The effect of load relief during casting of the repair was investigated. Tests were conducted for repair at both hogging and sagging locations, carried out while the specimen was completely unloaded and also while the specimen was under notional service load. Unloaded repair represents "propped" repair whereby props actively impose forces to counteract the applied loads and relieve the structure of stress. Casting the repair under service load represents repair without temporary propping or relief of live load from the structure. Examinations of repair under no load and under service load represent either end of the load relief range. This allows repaired specimen behaviour for any proportion of load relief to be postulated.

3.4.2 Load arrangement

Load arrangement has been found to influence the increase in curvature at the breakout location. Literature **[2]** shows that for a two-point load arrangement, a greater increase in curvature occurs when the point loads are positioned closer together (for a given value of maximum moment). Section 3.2 illustrates this effect and discusses how load arrangement may also influence moment transfer from the breakout location to other parts of the structure. A single point load arrangement is expected to cause greater moment transfer during concrete breakout and this arrangement is represented by breakout of concrete over the "one-point" central

support reaction. To highlight the effect of load arrangement, a two-point load arrangement (symmetrical about each midspan) was chosen. Comparison between the two breakout locations demonstrates the influence of load arrangement on the moment transfer due to concrete breakout.

The total load on the specimen was divided into four loads of equal magnitude to benefit from the simplicity of a bending moment diagram symmetrical about the central support. The distance between the point loads relative to the span length was chosen to give a large shear span to effective depth ratio. The chosen load arrangement is shown in Fig. 3.4.

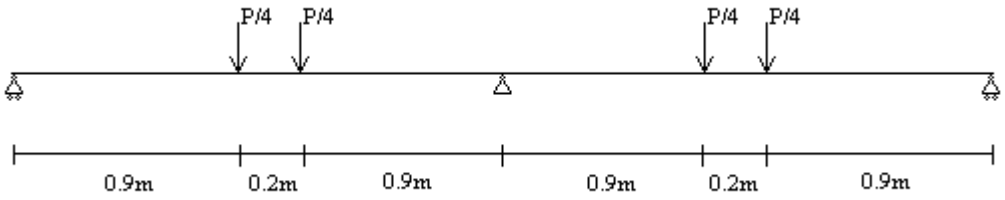

Fig. 3.4: Two-span load arrangement

3.4.3 Neutral axis depth

For "fully bonded" sections, there are well established code rules governed by the compression zone depth ratio to ensure a section has sufficient ductility to achieve its target redistribution of moment. A range of x / d ratios was desirable to vary the amount of redistribution permitted in "fully bonded" beam design. BS 8110 **[61]** suggests the x / d ratio is related to the allowable redistribution away from a section as follows.

$$x / d \leq (\beta_b - 0.4) \text{ for } \beta_b \leq 1.0 \qquad 3.1$$

where x = the compression zone depth

d = the effective depth of the tension reinforcement

β_b = (moment at a section after redistribution) /
(moment at a section before redistribution)

The allowable redistribution is then given by the change in moment during redistribution (moment before – moment after), relative to the moment before redistribution. This can be simplified as follows.

$$\text{Allowable redistribution} = (1 - \beta_b) \times 100\% \qquad 3.2$$

Therefore, the larger the compression zone depth ratio at a given section (maximum limit taken as 0.6), the lower the allowable redistribution away from the section being considered. The x / d ratio at a given section is influenced by numerous parameters including concrete and steel material properties, concrete cross-section geometry, and the areas of tension and compression reinforcement. A singly reinforced section has a greater x / d ratio than a doubly reinforced section as the compression zone is not assisted by the stress in the compression steel. The area of compression reinforcement should be minimised in order to push the x / d ratio towards the limit of the values for permissible redistribution. Following the procedures of BS8110 **[61]**, the compression zone depth ratio for a singly reinforced specimen is given by

$$x / d = (A_s f_y) / (0.9\ (0.67)\ f_{cu}\ b\ d) \qquad 3.3$$

where A_s = the area of tension reinforcement

f_y = the yield strength of the reinforcement

f_{cu} = the concrete cube strength

b = the width of the section

d = the effective depth of the tension reinforcement

As material properties and concrete cross-section dimensions were approximately constant throughout the test programme, the x / d ratio was primarily influenced by the area of tension reinforcement. For specimens of a given design moment redistribution, varying the reinforcement areas throughout the member varies the permitted redistribution.

3.4.4 Hogging : sagging reinforcement ratio

In a “fully bonded” specimen, the area of tension reinforcement over the internal support relative to that within adjacent spans defines the balance of bending moment within the structure at ultimate load (provided the section can tolerate the necessary redistribution). A range of hogging : sagging reinforcement area ratios were chosen to vary the moment redistribution demand. Designing for 0% redistribution meant choosing a hogging : sagging reinforcement area ratio equal to the ratio of maximum hogging : sagging moments from the elastic bending moment diagram. Moment transfer from a breakout location may be more critical if reinforcement layout encourages “elastic redistribution” away from the breakout location. By designing specimens for substantial moment redistribution away from the central support and varying section capacity to redistribute, the intention was to establish criteria to limit permissible breakout lengths while still exploiting redistribution. Designing for moment redistribution from the spans to the central support is impractical (as it increases the maximum moment in the structure) and was not included for analysis.

Moment redistribution requires that the most highly strained section deforms in a ductile manner until the full collapse load is reached. Work on simply supported sections has shown a loss of ductility when the reinforcement is exposed (even if the ultimate strength was not affected). In indeterminate structures designed using redistribution, such loss of ductility could lead to substantial loss of strength. The test programme was therefore designed to assess such loss of strength by varying the hogging : sagging reinforcement ratio (to vary the difference between elastic and ultimate moments) and x / d (to vary the ductility and hence the capacity of a section to redistribute).

3.5 Calculation of ultimate load

3.5.1 Flexural failure load

The process used for detailed design of test specimens is currently discussed. This section describes the steps taken to determine the ultimate load for a given tension reinforcement layout in a test specimen. Specimen design was based on "fully bonded" behaviour in accordance with BS 8110 **[61]**. Any partial safety factors were ignored in the calculation procedure. When calculating the failure load, the amount of redistribution expected in the member and the expected mode of failure have to be considered. A mixture of elastic and plastic approaches was used in the design.

The flexural failure load of a specimen was calculated as follows. The elastic bending moment diagram (assuming a constant flexural stiffness throughout the member) for the loading arrangement used during testing was first calculated (Appendix A). Fig. 3.5 shows the elastic bending moment diagram in terms of the total applied load, P.

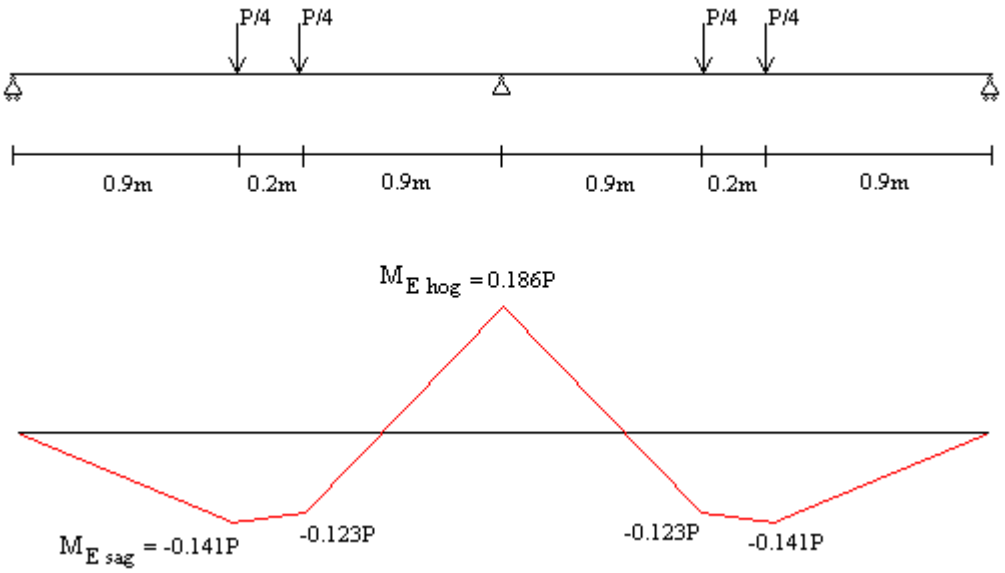

Fig. 3.5: Test load arrangement and elastic bending moment diagram

To assess the amount of redistribution required to achieve a "fully plastic" failure, the plastic bending moment diagram must be determined for the reinforcement layout being considered. Fig. 3.6 shows a sample plastic bending moment diagram. The

ratio of the plastic moment over the central support to the plastic moment within the spans is represented by α_m. α_m was set equal to the ratio of reinforcement area over the central support to the reinforcement area within the spans, α_r.

$$\alpha_r = A_{s\,hog} / A_{s\,sag} \qquad 3.4$$

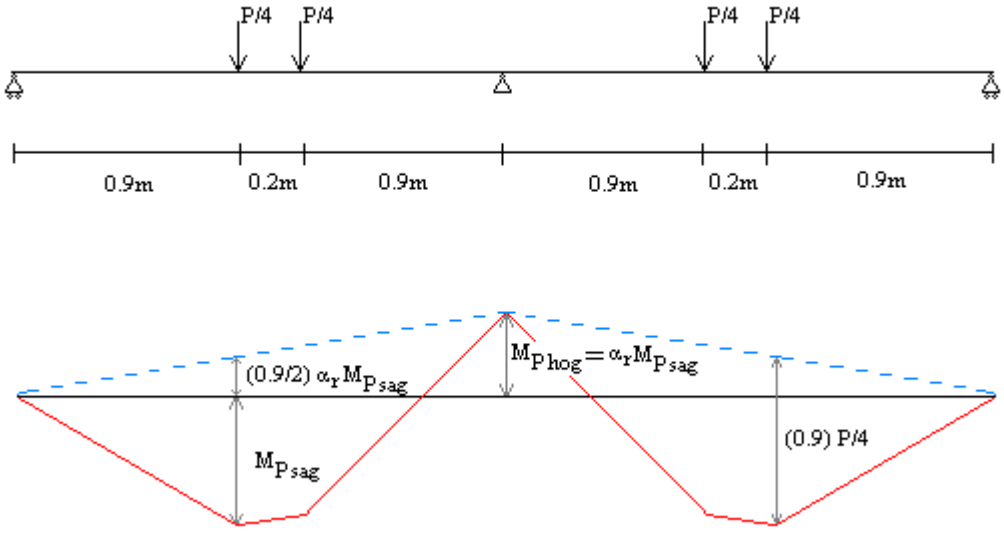

Fig. 3.6: Test load arrangement and plastic bending moment diagram

From Fig. 3.6, the plastic sagging moment can be related to the applied load.

$$M_{P\,sag} + (0.9/2)\,\alpha_r\,M_{P\,sag} = (0.9)\,P/4 \qquad 3.5$$

Rearranging Equation 3.5 gives

$$M_{P\,sag} = 0.225\,P / (1 + 0.45\alpha_r) \qquad 3.6$$

The hogging plastic moment is then found from

$$M_{P\,hog} = \alpha_r\,M_{P\,sag} = 0.225\,P\,\alpha_r / (1 + 0.45\alpha_r) \qquad 3.7$$

The required hogging redistribution from the central support was found by comparing $M_{P\,hog}$ from Equation 3.7 with the corresponding bending moment value from the elastic bending moment diagram, Fig. 3.5 ($M_{E\,hog}$ =0.186P).

Required redistribution from central support = $(M_{E\,hog} - M_{P\,hog}) / M_{E\,hog} \times 100\%$ 3.8

A positive result to Equation 3.8 indicates moment redistribution away from the central support. All specimens were designed for varying amounts of moment redistribution from the central support to reduce the maximum moment within the structure.

The allowable redistribution from a given section was calculated (as described in Section 3.4.3) from the compression zone depth ratio, x / d. x / d was calculated on the assumption of a singly reinforced specimen from Equation 3.3. From this, the value of β_b was established and the allowable redistribution calculated from Equation 3.2.

The predicted failure bending moment diagram was constructed by using the required or allowable moment redistributions to establish the expected redistribution from the elastic bending moment diagram. The required redistribution value was used unless the allowable redistribution was less than the required redistribution, in which case, the allowable redistribution value was used. For example, if a 10% reduction of moment was required at the central support, the maximum hogging moment became $0.186P \times 0.9 = 0.1674P$. However, if the allowable redistribution for the same section was only 5%, the hogging moment was taken as $0.186P \times 0.95 = 0.1767P$. The predicted maximum sagging moment within the spans was then calculated from a modified form of Equation 3.5.

$$M_{sag\,(predicted)} = (0.9)\,P/4 - (0.9/2)\,M_{hog\,(predicted)} \qquad 3.9$$

The moment capacities of the sections at the left load in the left span and at the central support were calculated from BS 8110 **[61]**. Certain assumptions were made to simplify the calculation. The effect of the nominal hanger bars as compression reinforcement was neglected. Partial safety factors were taken as 1.0 throughout. The compression zone depth ratio, x / d was calculated from Equation 3.3. The lever arm (z) was then calculated from

$$z = d\,(1 - 0.45\,x / d) \qquad 3.10$$

The moment capacity of the section was then calculated from

$$M_{cap} = A_s f_y z \qquad 3.11$$

where A_s = the area of tension reinforcement at the cross-section being considered
f_y = the yield strength of the steel
z = the lever arm

From the predicted failure bending moment diagram, values of maximum hogging and sagging moments were known in terms of the failure load. For a flexural failure over the central support, the predicted hogging moment was set equal to the moment capacity at that cross-section. Similarly, a failure load was determined for a flexural failure beneath the loading within the spans. The lower of these two failure loads was taken as the flexural failure load for the member.

For a given reinforcement layout, the required and allowable redistribution from the central support can be determined. The influence of the hogging : sagging reinforcement ratio and the reinforcement percentages on the required and allowable redistribution can be illustrated as follows. Fig. 3.7 shows a sample plot of required and allowable redistribution from the central support vs. hogging : sagging reinforcement ratio. For a given reinforcement ratio, the required redistribution was calculated using Equations 3.7 & 3.8. The x / d ratio was calculated from Equation 3.3 using the following geometric and material properties: b = 150mm, d = 170mm, f_y = 520N/mm^2 & f_{cu} = 35N/mm^2. The reinforcement area within the spans was set equal to 257mm^2 and x / d at the central support was calculated for a range of hogging : sagging reinforcement area ratios. The allowable redistribution was then calculated from Equations 3.1 & 3.2. When $\alpha_r = 0$, the central support cross-section is unable to carry moment and 100% redistribution is required. 0% redistribution was required for a value of $\alpha_r = 0.186 / 0.141 = 1.32$ (from the elastic bending moment diagram, Fig. 3.5). The required redistribution from the central support was greater than the allowable for values of $\alpha_r \leq 0.58$.

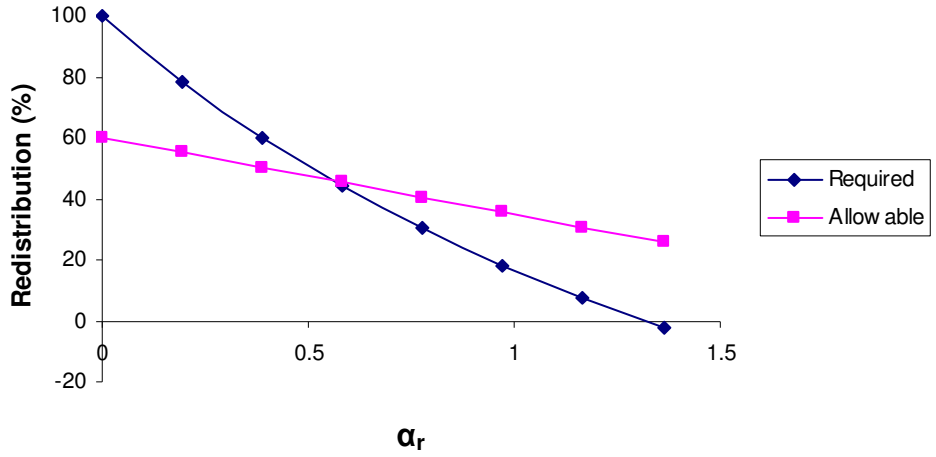

Fig. 3.7: Sample plot of required and allowable redistribution vs. hogging : sagging reinforcement ratio ($A_{s\ sag}$ = 257mm^2)

Fig. 3.8 shows the equivalent moment redistribution plot when the reinforcement area within the spans is set equal to 502mm^2. The plot of required redistribution vs. α_r was unaffected by the quantities of reinforcement within the specimen. However, for a given hogging : sagging reinforcement ratio, the area of reinforcement at the central support was greater than for Fig. 3.7. This caused a significant reduction in the allowable redistribution from the central support. The required redistribution is greater than the allowable for all values of reinforcement ratio due to the large quantities of reinforcement within the specimen.

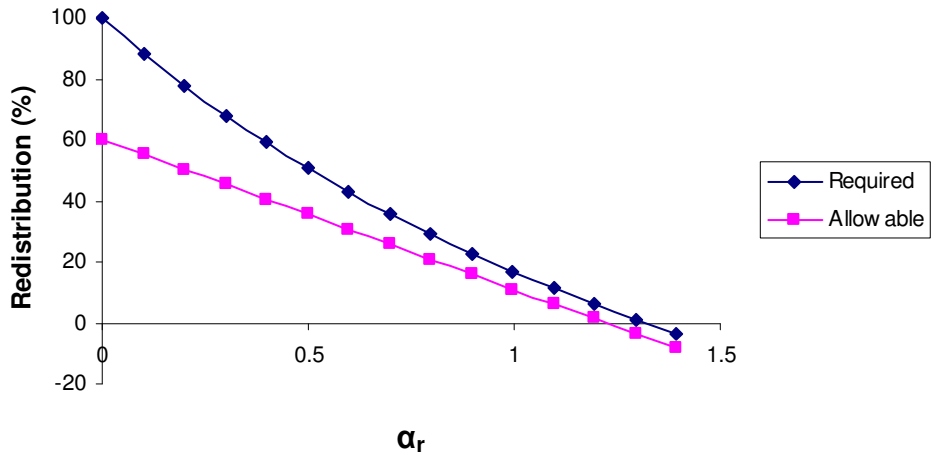

Fig. 3.8: Sample plot of required and allowable redistribution vs. hogging : sagging reinforcement ratio ($A_{s\ sag}$ = 502mm^2)

3.5.2 Shear failure load

A shear failure check was also carried out to establish whether a shear failure was likely (again assuming "fully bonded" behaviour in accordance with BS 8110 **[61]**). The maximum shear force in the member was calculated according to the predicted failure bending moment diagram. Fig. 3.9 shows the shear force diagram for the test load arrangement. The left reaction was calculated from the following equation.

$$0.9\ R_L = M_{sag\ (predicted)} \qquad 3.12$$

The predicted failure sagging moment was calculated as described in Section 3.5.1. The maximum shear force in the member is $(P/2 - R_L)$. Due to the symmetry of the loading, the magnitude of the maximum shear force is also equal to $(R_R - P/2)$.

$$V_{max} = P/2 - R_L \qquad 3.13$$

where V_{max} = the maximum shear force in the member

P = the total applied load

R_L = the vertical reaction at the left support

As $M_{sag\ (predicted)}$ is known in terms of the applied load, the maximum shear force in the member can be calculated by substituting R_L from Equation 3.12 into Equation 3.13.

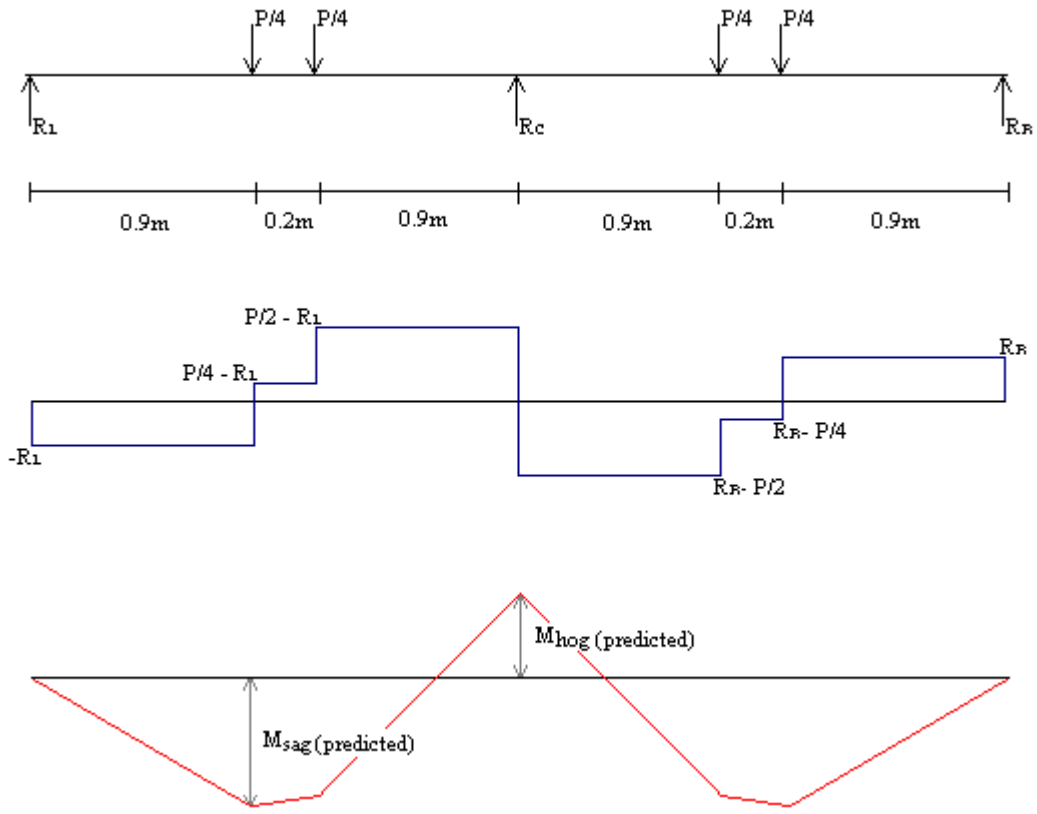

Fig. 3.9: Loading arrangement, shear force diagram and corresponding "predicted" bending moment diagram

The shear capacity of the section was calculated from BS 8110 **[61]**. The design concrete shear stress is calculated from

$$v_c = 0.79 \{100A_s / (b\,d)\}^{1/3} (400/d)^{1/4} (f_{cu}/25)^{1/3} \qquad 3.14$$

where A_s = the area of tension steel at the section being considered

b = the width of the cross-section

d = the effective depth of the tension reinforcement

f_{cu} = the concrete cube strength

Note: The lesser of the top and bottom reinforcement areas gave the more critical concrete shear stress.

The design shear stress was then calculated from

$$v = \{(A_{sv} f_{yv})/(b s_v)\} + v_c \quad 3.15$$

where A_{sv} = the total cross-section of a link at the neutral axis

f_{yv} = the yield strength of the links

s_v = the spacing of the links along the member

The shear capacity of the member was determined from

$$V_{cap} = v b d \quad 3.16$$

The shear capacity was set equal to the maximum shear force in the member from Equation 3.13 and the ultimate load for a shear failure was determined. If this shear failure load was less than the flexural failure load for a particular specimen, then a shear failure was deemed the likely failure mode. A complete example of a failure load calculation is included in Appendix B.

Assessment of specimen behaviour at service load is desirable (particularly for specimens with exposed reinforcement) to ensure serviceability limit state criteria are not exceeded. The service load of a given specimen is established from the ultimate load. BS 8110 **[61]** suggests a load factor of 1.4 for dead load and 1.6 for live load so an average load factor of 1.5 is assumed. A steel material properties factor of 1.15 is also included in limit state design. The total load factor used is therefore $1.5 \times 1.15 = 1.725$. Therefore, the service load should be $(1 / 1.725) = 0.58$ times the ultimate load. A conservative proportion of ultimate load (0.55) was chosen for testing as significant portions of tension reinforcement would be exposed in some test specimens.

Note: Flexural failures were desirable for all "fully bonded" specimens to allow the full plastic capacity to be achieved. However, shear checks carried out during initial specimen design were inaccurate. Consequently, shear reinforcement provided was not sufficient to ensure a flexural failure in all test specimens as will be discussed later.

3.6 Summary

Initial test specimen design and the choice of parameters for investigation were discussed in this chapter. Reinforcement layouts were chosen to vary the design moment redistribution and the allowable redistribution from the central support. The length of exposed reinforcement and the position of breakout / repair were investigated and analysis of repaired specimen behaviour under various load relief conditions during casting of the repair was also carried out.

The degree of variation of certain parameters was limited by practical considerations. For example, tension reinforcement areas were chosen to represent the typical range of reinforcement percentages used in practice ($0.89\% \leq A_s / bd \leq 2.92$). Also, maximum breakout lengths were chosen to avoid a significant length of exposed bar extending beyond contraflexure points, which would increase the likelihood of an over-reinforced failure. The scale of the test specimens was chosen for ease of construction and manoeuvrability in the laboratory and facilitate set-up of the testing rig. Test specimen dimensions were constant throughout the test programme to limit the scope of the investigation. Also, a load arrangement symmetric about the internal support was chosen to limit the number of parameters being investigated. A numerical analysis was carried out to establish suitable degrees of variation of the proposed parameters and results from the initial investigation are discussed in Chapter 4.

Chapter 4: Numerical modelling

4.1 Introduction

Chapter 3 discussed the choice of parameters for investigation in the experimental programme. LUSAS finite element software was used to carry out a preliminary investigation to assess the influence of the proposed parameters. The numerical analysis helped to eliminate any parameters that were less influential on specimen behaviour. LUSAS was also used to choose the degree of variation of certain parameters. In some cases, parameters were limited by the values used in practice. Parameters were usually varied throughout their entire range (within the practical limits) so a noticeable change in behaviour occurred.

For a given specimen, three main stages of the repair process were analysed. Firstly, analysis of "as new" specimens was carried out. These control specimens would be used as reference against equivalent specimens after breakout of concrete or completion of a repair. Secondly, specimens were analysed after a portion of the tension reinforcement had been exposed. Finally, specimens were analysed after completion of the repair. Measurements of structural performance were taken at notional service load and also at 90% of the "fully bonded" ultimate load. Typical measures of behaviour included bending moment, midspan displacements and strain distributions at critical cross-sections.

The preliminary analysis used to assist the design of the test specimens was carried out using assumed material properties. The analysis was subsequently re-run using measured material properties and the results are reported in Chapter 8.

4.2 Model verification

Before numerical investigation of proposed specimens was carried out, LUSAS modelling of reinforced concrete members had to be verified. Experimental and numerical results from Cairns and Zhao **[2]** were used to verify the behaviour of simply supported beams, for both "fully bonded" members and members with a portion of the tension reinforcement exposed. Failure loads, midspan displacements and concrete and steel strains at critical cross-sections were used as verification criteria.

Certain analysis parameters were analysed individually to assess their influence on the results. For example, the magnitudes of the load steps in the solution strategy were varied for a given member. The effect on the strain pattern within the member at a given load was negligible. In most cases, the effect on the ultimate load was not significant as LUSAS employs an automatic step reduction procedure to assist convergence. The solution strategy is discussed in greater detail in Section 4.3.3.

The fineness of the mesh influences the accuracy of results. A fine mesh is expected to give more accurate results but is more expensive on computational time. A simple investigation on mesh fineness was carried out to determine the least dense mesh to give sufficiently accurate results. The analysis was carried out on a 2m long simply supported beam subjected to a central point load. The midspan displacement under a given applied load was monitored with increasing mesh density. The midspan displacement provided a more stable measure than the ultimate load as complications associated with convergence criteria were avoided.

Fig. 4.1 shows a plot of midspan displacement against mesh density. The mesh density was quantified in terms of the number of mesh divisions per metre length of bar. The number of mesh divisions in the vertical direction was adjusted throughout, to maintain an approximately constant mesh shape. The "true value" was taken as the displacement for the finest mesh modelled. Very coarse meshes gave displacements up to 70% lower than the "true value". Beyond a mesh density of 3 divisions per metre, the displacement value remained within 3.5% of the "true value". A mesh density of 3 divisions per metre was considered a reasonable lower threshold.

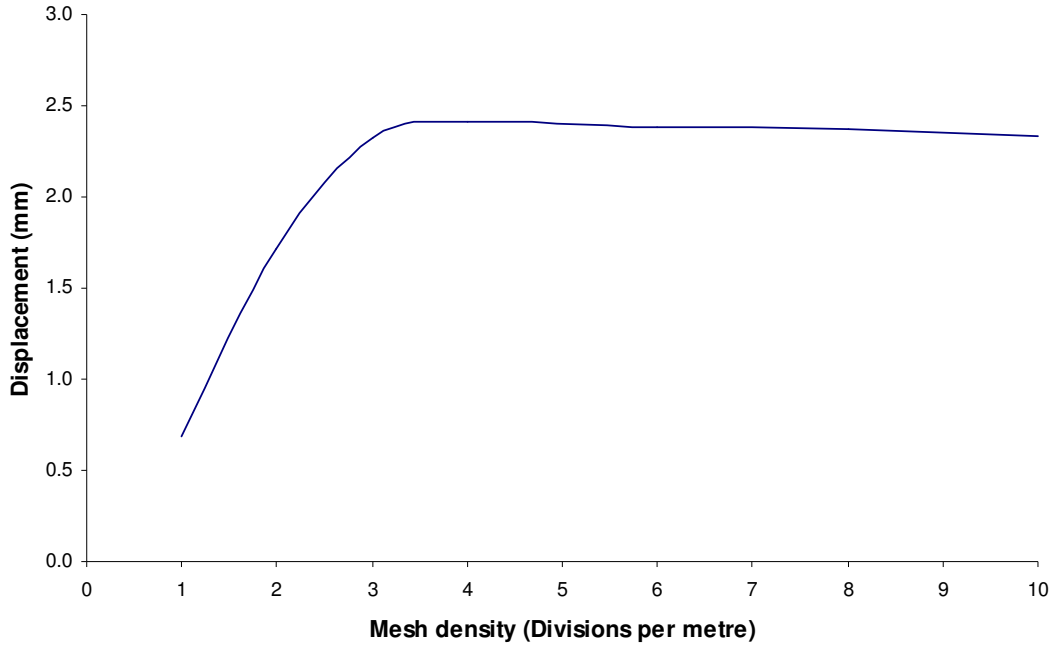

Fig. 4.1: Plot of midspan displacement vs. mesh density for a simply supported reinforced concrete beam

4.3 Modelling of "as new" specimens

4.3.1 Representation of concrete

A 2-dimensional analysis was chosen to model the test specimens as the out-of-plane stresses could be neglected. The concrete was modelled as a series of surfaces. If the node for one surface was positioned along the edge line of an adjacent surface, the node did not remain bonded to the line once deformation took place. Therefore, when defining the surfaces within the monolithic concrete, corner nodes of neighbouring surfaces had to coincide.

A "plane stress" generic element type was used to describe the concrete as no force was applied and thus, no stress was induced out-of-plane. A quadrilateral mesh was used to describe the concrete, so all surfaces used to model the concrete were quadrilaterals. A quadratic interpolation order was chosen so that a linear variation of strain could take place along a given element. The number of mesh divisions for a given surface was chosen according to the size of the surface. For two adjoining surfaces, the number of divisions along the common border had to be the same for both surfaces. The width of the cross-section was also input.

LUSAS has a built-in concrete model (model 94) which allows various parameters to be input by the user. The uniaxial compressive strength of concrete would be found from cube tests on the concrete mix. For the preliminary analysis, the compressive strength was taken as $35N/mm^2$. The elastic modulus of concrete varies with the compressive strength of concrete. BS 8110 **[61]** describes the relationship between the two parameters as follows

$$E_c\ (kN/mm^2) = 5.5\ \sqrt{(f_{cu}/\gamma_m)} \qquad 4.1$$

where f_{cu} = concrete cube strength in N/mm^2.

γ_m = the load factor (taken as 1.0 here)

The uniaxial tensile strength would be determined from results of split cylinder tests but was initially taken as 3N/mm^2. Poisson's ratio of concrete was taken as 0.2. The self-weight of the structure was considered negligible relative to the applied loads so the mass density of the concrete was set to zero.

Fig. 4.2 describes model behaviour of concrete in compression. The maximum compressive stress and the elastic modulus are input when defining the material properties. The strain at peak compressive stress (ε_{cp}) can also be specified. The LUSAS manual **[62]** suggests Equation 4.2 to describe ε_{cp} in terms of the cube compressive strength.

$$\varepsilon_{cp} = 0.002 + 0.001((f_{cu} - 15) / 45) \qquad 4.2$$

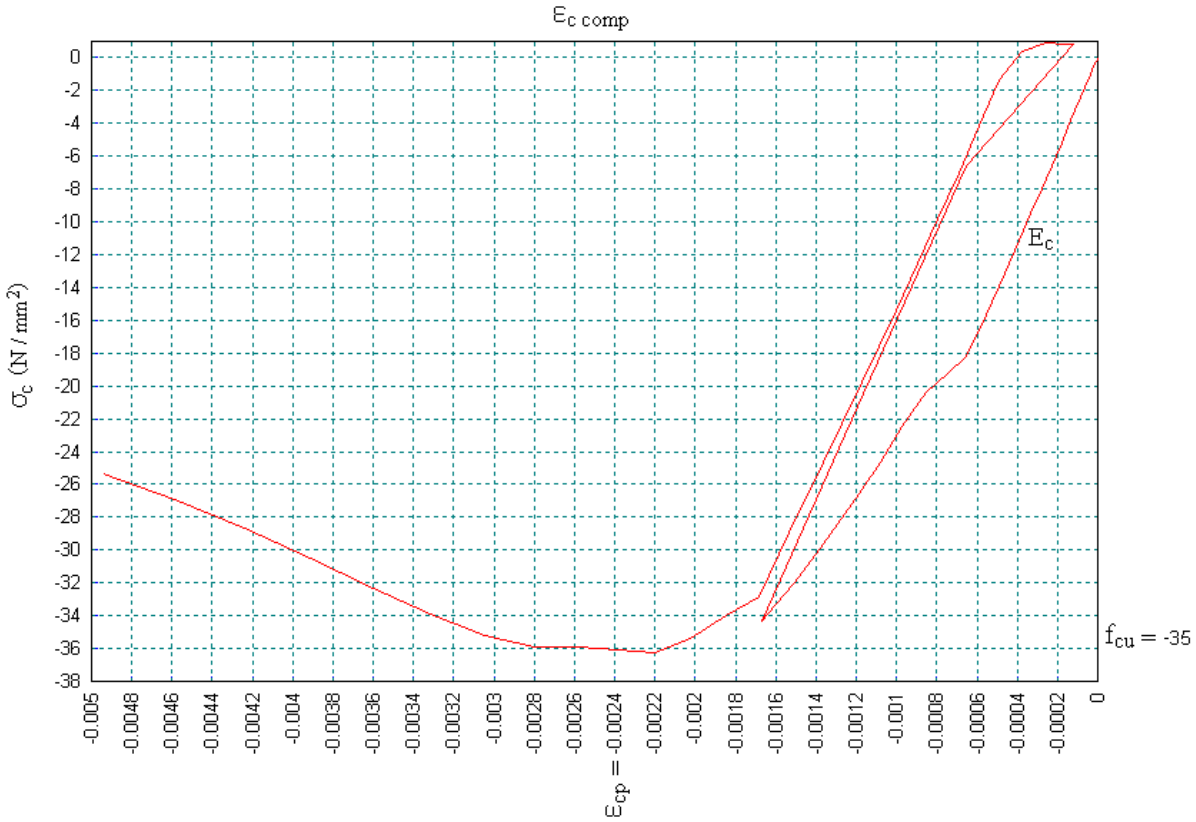

Fig. 4.2: Non-linear behaviour of concrete in compression

Fig. 4.3 describes the model representation of non-linear concrete in tension. LUSAS assumes the elastic modulus of concrete in tension is equal to the elastic modulus in compression. The strain at the end of the softening curve (ε_{t0}) is specified when

defining material properties. Exponential decay of the stress in the concrete occurs between the strain at peak tensile stress and the strain at the end of the softening curve.

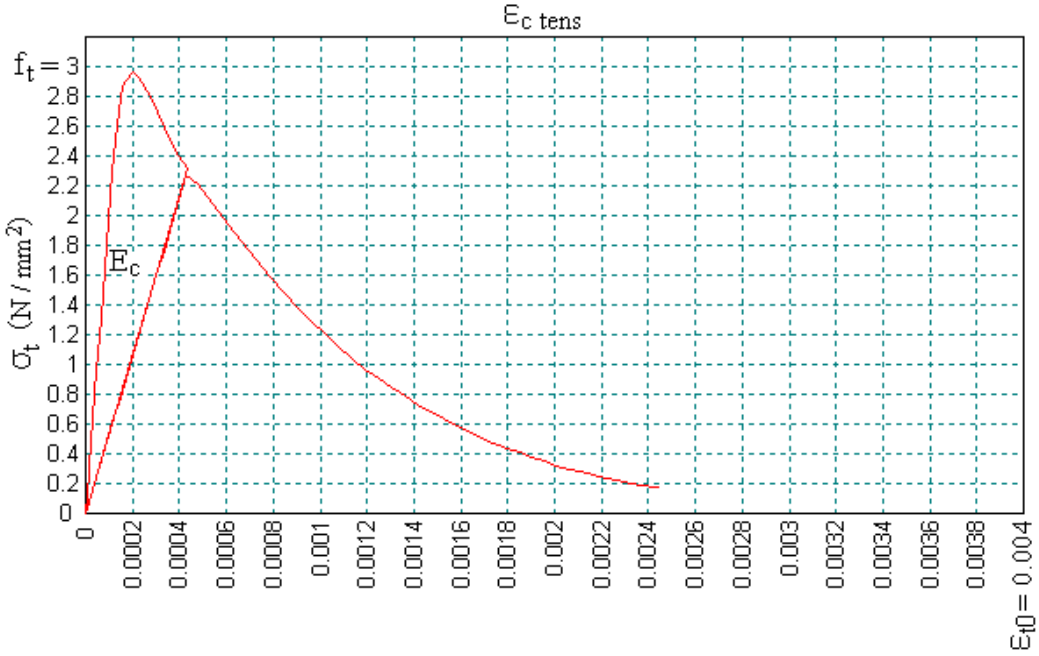

Fig. 4.3: Non-linear behaviour of concrete in tension

The contribution of the concrete between flexural cracks effectively increases the stiffness of the tension reinforcement and this is known as the tension stiffening effect. Consider a reinforced concrete section with a stabilized crack pattern. At a cracked cross-section, all tensile forces are balanced by the steel only. However, between adjacent cracks, the bond between the steel and the surrounding concrete allows transmission of the tensile stress from the steel to the concrete. The stress distribution along a bar embedded in cracked concrete resembles a periodic function with maximum values at the cracks and minima midway between the cracks.

Tension stiffening is influenced by a range of parameters including the tensile strength of the concrete, the area of reinforcement, the applied stress, the spacing of flexural cracks and the strain behaviour of the steel and the concrete between cracks. Fig. 4.4 shows the strain distribution pattern between flexural cracks from the CEB–FIP Model Code 90 **[63]**. The mean steel strain over the total member is calculated from the following expression.

$$\varepsilon_{st\ mean} = \varepsilon_{st\ crack} - \beta_t(\Delta\varepsilon_{st\ cs}) \qquad 4.3$$

where $\varepsilon_{st\ mean}$ = the mean strain in the reinforcement

$\varepsilon_{st\ crack}$ = the strain in the reinforcement at the crack

β_t = integration factor for the steel strain along the transmission length

$\Delta\varepsilon_{st\ cs}$ = the increase in steel strain in the cracking state

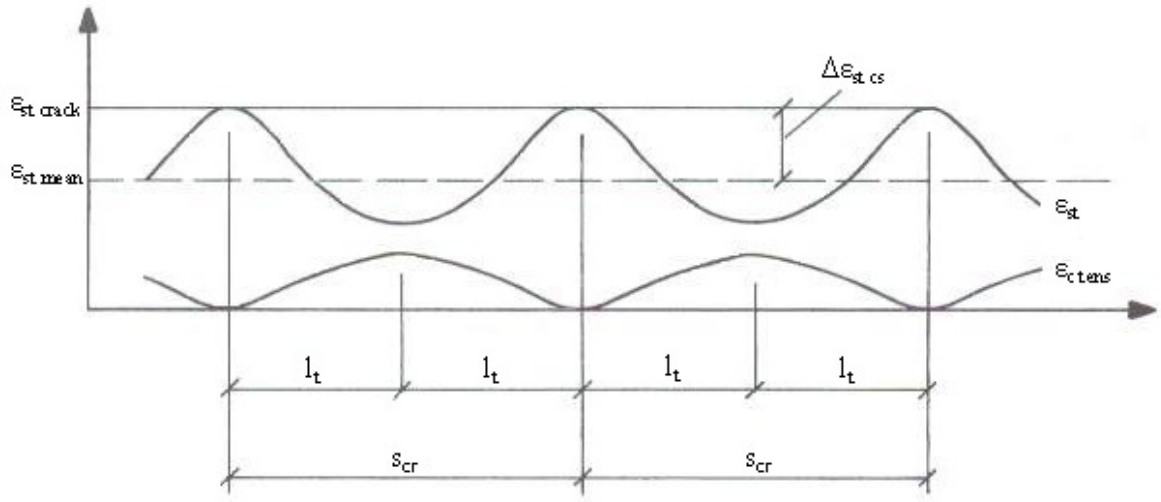

Fig. 4.4: Strain distribution for stabilized crack pattern **[63]**

The tension stiffening effect is of particular interest in this investigation as tension stiffening is lost when the reinforcement is exposed. The strain softening model in LUSAS may be used to account for the effect of tension stiffening. CEB–FIP Model Code 90 **[63]** describes strain softening in terms of the fracture energy per unit area but LUSAS assumes exponential decay to a specified value of strain at the end of the softening curve. Investigation of the influence of ε_{t0} on the "tension stiffening" effect was required. A low value of ε_{t0} causes a rapid loss of concrete tensile strength once initial cracking occurs. Therefore, the "tension stiffening" effect would be small. If a greater value of ε_{t0} is specified, strain softening occurs more slowly and the "tension stiffening" effect is greater.

To investigate the influence of the strain softening parameter (ε_{t0}) on "tension stiffening", a specifically designed reinforced concrete model subjected to pure tension was analysed. The cross-section of the specimen was 100mm×100mm and it was 1m long. The reinforcement was positioned along the axis of the specimen over its full length. The analysis was initially carried out for an area of reinforcement of

326mm^2. A non-linear analysis was carried out and the displacement of the free end was recorded for a prescribed load of 97.8kN. The prescribed load was chosen to give a reinforcement stress of 300N/mm^2 (approximation of service load stress). The displacement represented the elongation of the specimen. The elongation was then divided by the original length of the specimen (1m) to give the mean strain throughout the specimen. The analysis was repeated for a selection of ε_{t0} values and the mean strain (relative to the strain in the bare bar for an applied stress of 300N/mm^2) is shown in Fig. 4.5. For values of $\varepsilon_{t0} \leq 0.25$ (which represent a rapid reduction in concrete tensile strength once cracking occurs), the tensile strength of the concrete prior to cracking contributes to a reduction in the mean strain relative to the strain in the bare bar. As expected, the mean strain in the steel reduced for larger values of ε_{t0}. LUSAS theory manual **[62]** suggests a value of $\varepsilon_{t0} = 0.004$ is suitable for most concretes and this value was used for modelling of the test specimens.

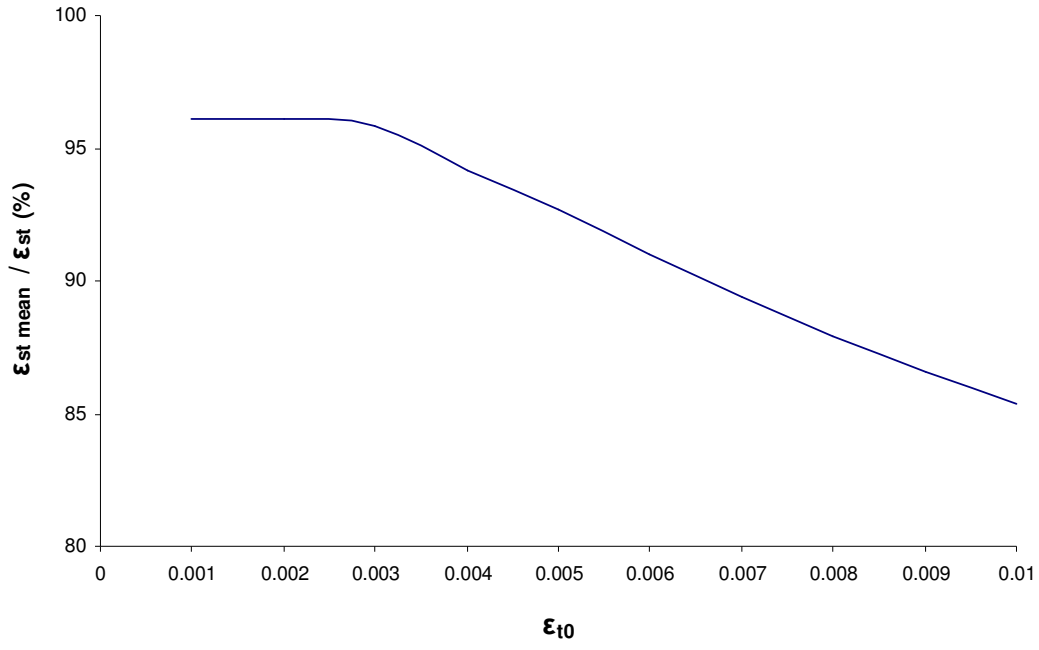

Fig. 4.5: Plot of mean strain (relative to the strain in a bare bar) vs. strain at end of softening curve (A_s = 326mm^2)

The results shown in Fig. 4.5 quantify "tension stiffening" for a reinforcement area of 326mm^2. LUSAS treatment of "tension stiffening" for a range of reinforcement areas is also of interest. Fig. 4.6 shows a plot of the mean strain (relative to the strain for

the bare bar for a value of $\varepsilon_{t0} = 0.004$). As expected, the reduction in mean steel strain due to "tension stiffening" was greater for smaller areas of reinforcement.

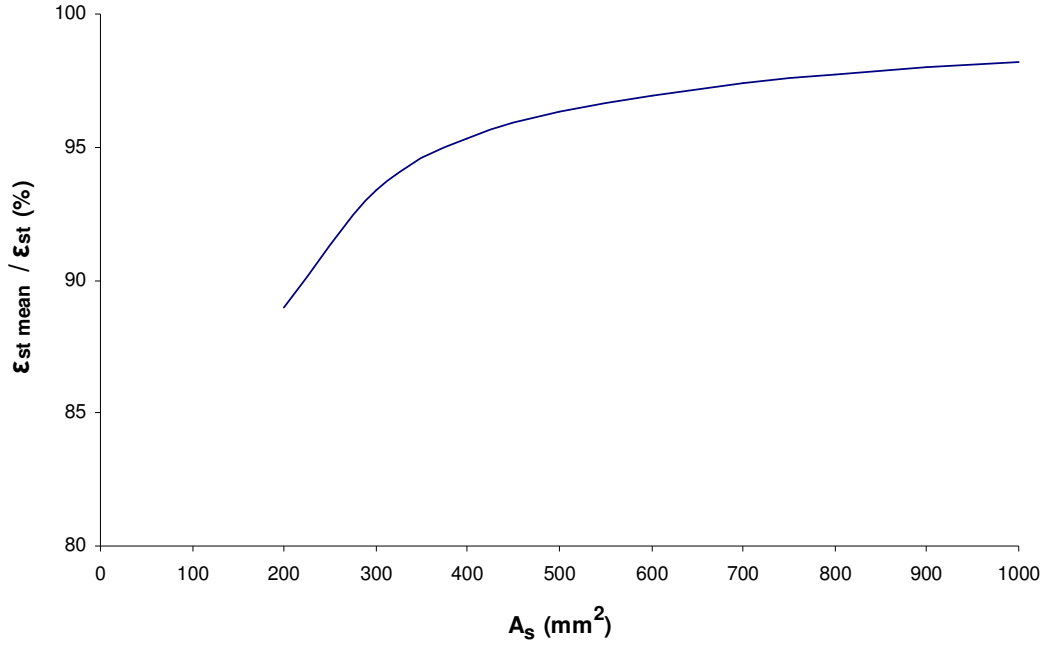

Fig. 4.6: Plot of mean strain (relative to the strain in a bare bar) vs. area of reinforcement ($\varepsilon_{t0} = 0.004$)

4.3.2 Representation of reinforcement

The bonded reinforcement was modelled by linear plane stress elements within the concrete. In order to maintain the bond between the steel and the concrete, the elements defining the steel had to coincide with the edges of concrete surfaces. Shear reinforcement was represented in a similar manner. Fig. 4.7(a) shows an annoted sketch of the reinforcement layout for an "as new" specimen. Horizontal surface edges were positioned within the model at levels of top and bottom reinforcement. Vertical edges were positioned at regular longitudinal intervals to describe the shear reinforcement. Vertical surface edges were positioned to coincide with load or support points, as both concentrated loads and reactions had to be assigned to nodes. As discussed in Section 3.4.3, curtailment of reinforcement in compression zones was desirable. Nodes were required at curtailment points to enable assignment of different

steel areas to either side of the node. The beam was extended by 150mm beyond the outer supports to provide sufficient anchorage to the main reinforcement.

Fig. 4.7(b) illustrates the concrete mesh for the "as new" model. The mesh divisions along the bar type element had to coincide with the divisions in the adjacent surfaces. Again, a quadratic interpolation order was chosen for compatibility of strains between the bonded bar and the surrounding concrete.

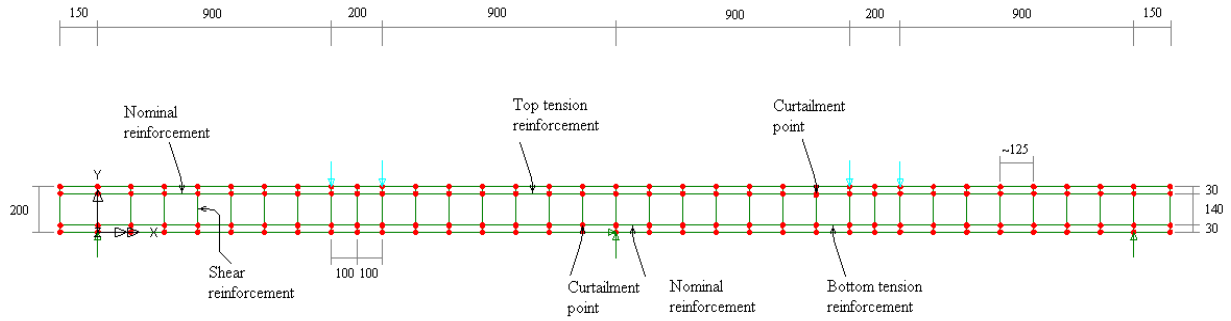

(a)

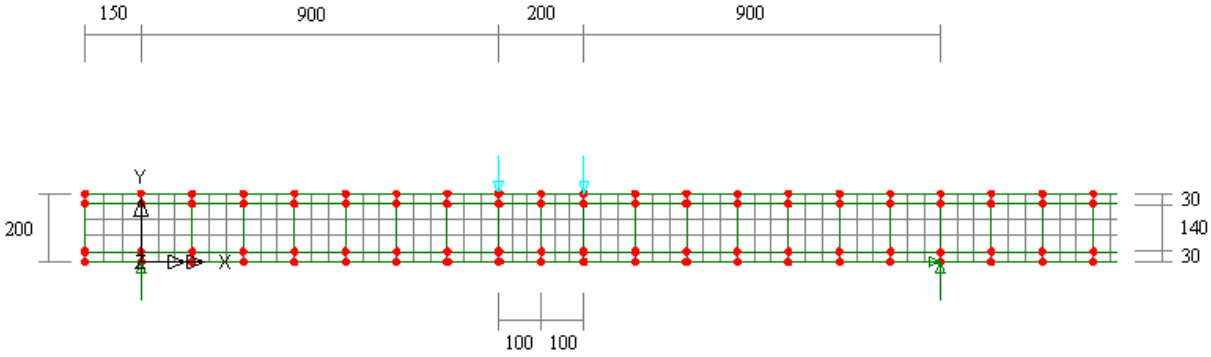

(b)

Fig. 4.7: Typical model layout for "as new" specimen

The only geometric property of relevance for the chosen "bar" type element was its cross-sectional area. The steel was represented by a Von Mises stress potential type. The steel was adequately described by its modulus of elasticity, Poisson's ratio and the initial uniaxial yield stress. Young's Modulus of steel was taken as E_{st} = 200kN/mm^2, ν = 0.25, and the yield stress, f_y, was initially taken as 520N/mm^2. Strain hardening was not thought to significantly affect results and was not included.

4.3.3 Analysis procedure

Due to the non-linear nature of the material properties, the problem was analysed using a load-stepping procedure. Values of -250N were assigned to each of the 4 point loads to give a total downward force of 1kN. The load factor on the structure increased in pre-defined steps. For a given load step, an iteration procedure was used to find the displacement for that load value with sufficient accuracy. Various convergence criteria were set to control the required accuracy. Fig. 4.8 illustrates the iteration process of the Newton-Raphson method for a one degree of freedom response. An improved approximation of the displacement (δ^n) at the specified load interval (P_i) is found from

$$\delta^{n+1} = \delta^n + (P_i - P^n)/K^{n+1} \qquad 4.4$$

where δ^n = the displacement for the iteration being considered

δ^{n+1} = the displacement for the following iteration

P^n = load value corresponding to the displacement value δ^n

K^{n+1} represents the stiffness matrix, tangential to the plot at the point (P^n, δ^n)

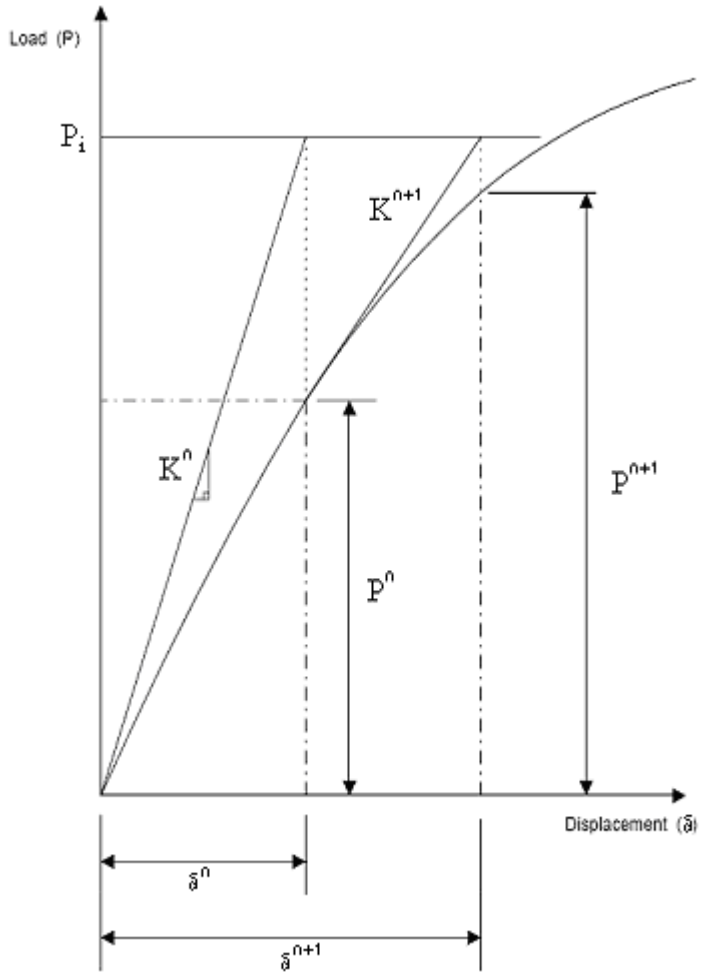

Fig. 4.8: Illustration of Newton-Raphson iteration **[62]**

Although the Newton-Raphson method converges quadratically, its efficiency is questionable as each iteration requires a new tangent stiffness matrix. A modified form of the Newton-Raphson iteration method was used, where the tangent stiffness matrix from the beginning of the increment was used throughout that increment. This method requires more iterations to converge to the same accuracy as the Newton Raphson method but computational time is reduced as the number of tangent stiffness matrix formations is reduced.

Certain convergence criteria were specified in the solution strategy to control the tolerance of the result achieved, before iteration began on the next load increment. A slack tolerance may return inaccurate results but if the tolerance is too restricted, valuable computer time may be wasted. LUSAS allows the user to specify certain criteria which allow the solution to progress to the next load increment when satisfied. The maximum number of iterations in any one load increment may also be specified.

The most influential convergence criteria are the "Residual Force Norm" and "Incremental Displacement Norm". A residual force is the force which remains when the stresses integrated throughout the structure will not satisfy equilibrium with the external forces due to a significant degree of non-linearity occurring during a load step. The "Residual Force Norm" is the sum of the squares of all the residual forces as a percentage of the sum of the squares of all the external forces. A value of γ_ψ = 0.1 was thought to provide sufficient accuracy of convergence. The "Incremental Displacement Norm" is defined as the norm of the iterative displacements expressed as a percentage of the norm of the displacements for that increment. A value of λ_{dt} = 1.0 was considered reasonable. If either of these convergence criteria is satisfied, iteration on the next increment begins.

A constant load level incrementation is the most commonly used incrementation procedure and it is calibrated by specifying the initial load factor and the maximum load increment. The increment size automatically reduces if the solution fails to converge within the specified maximum number of iterations and convergence is sought at the new load level. The step reduction factor had a default value of 0.5. If significant non-linearity only occurs for a specific load (possibly due to severe cracking), the step reduction is overridden beyond that load and the increment returns to the initially specified maximum value. If convergence fails to occur after a specified maximum number of step reductions, the solution is terminated.

4.4 Modelling of breakout and repair

4.4.1 Modelling of specimens after breakout of concrete

Modelling of specimens with various lengths of exposed steel was carried out to establish suitable breakout intervals for an appreciable change in behaviour. To reflect reality, the "fully bonded" specimen should initially carry its service load. The specimen may then be unloaded and the required length of concrete cover removed. If an "unpropped" repair is to be carried out, behaviour of the specimen with exposed reinforcement under service load is of particular interest. This modelling process requires a portion of the concrete within the model to "disappear" after initial loading of the specimen and the forces in that part of the structure to transfer to the remaining elements.

LUSAS "birth and death" feature allows the stiffness of a material to be activated or deactivated between different loadcases during the analysis. The geometry of the breakout region was specified as a series of surfaces (separate to the substrate concrete) before analysis began. The geometric and material properties within the breakout region were set equal to those for the substrate. These surfaces were then selected independently and deactivated when appropriate. The deactivation was assigned to the concrete surfaces only (if the selected lines were included, the "exposed" reinforcement would essentially be removed). Fig. 4.9 illustrates a breakout region within the left span. Separate models were used to analyse each breakout length for a given breakout location.

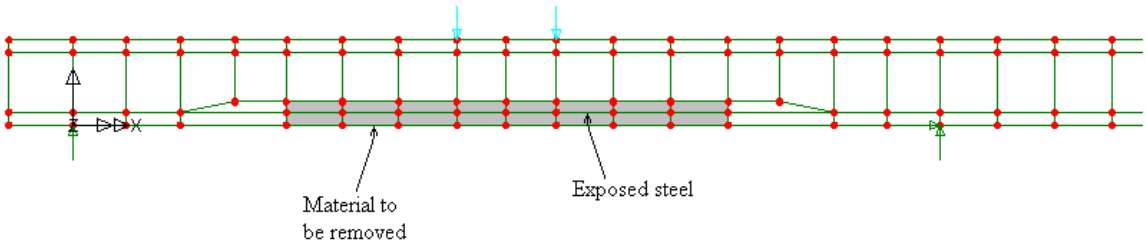

Fig. 4.9: Model layout for a breakout length of 1.0m within the span

To represent exposed steel behaviour, the strain in the steel should be uniform throughout the exposed length. Also, the exposed steel bar should remain approximately straight (slight deflection may occur in practice due to ties to the shear links). The "exposed" steel was defined as the edges of concrete surfaces within the breakout region so that while activated, the breakout material was bonded to the steel. When the breakout material was deactivated, the strain in the "exposed" steel was not affected by the surrounding breakout material of zero stiffness. Consequently, the "exposed" steel strain was uniform throughout the breakout length. While the steel was exposed, it deflected with the breakout material as if it was bonded because it was attached to the deactivated breakout material at the nodes. However, this effect was not significant as displacements were small.

To examine the effect of breakout on the specimen under service load, the "fully bonded" specimen was first loaded and unloaded. An initial loadcase was defined to load the "fully bonded" specimen to service load. When specifying the incrementation criteria for loading to service load, the "maximum total load factor" was set equal to the service load. The load increased in increments as usual but loading in that loadcase ceased once the "maximum total load factor" was reached. A second loadcase was defined to unload the specimen. The breakout region was deactivated for a third loadcase, specified to describe behaviour during loading to failure of the specimen with "exposed" reinforcement.

Fig. 4.10 shows an output plot of the load-displacement history of a specimen before and after exposure of reinforcement. Loadcase 1 continued only as far as service load (120kN). The slope of this portion of the graph reduced at approximately 60kN when flexural cracking became significant. Loadcase 2 reduced the applied load to ~0kN and Loadcase 3 described subsequent loading of the specimen with exposed reinforcement to failure. The midspan displacement at service load (120kN) for Loadcase 3 was almost 40% greater than for Loadcase 1. This increase was predominantly caused by the exposure of reinforcement during Loadcase 3 but the non-linearity of the concrete material also contributed.

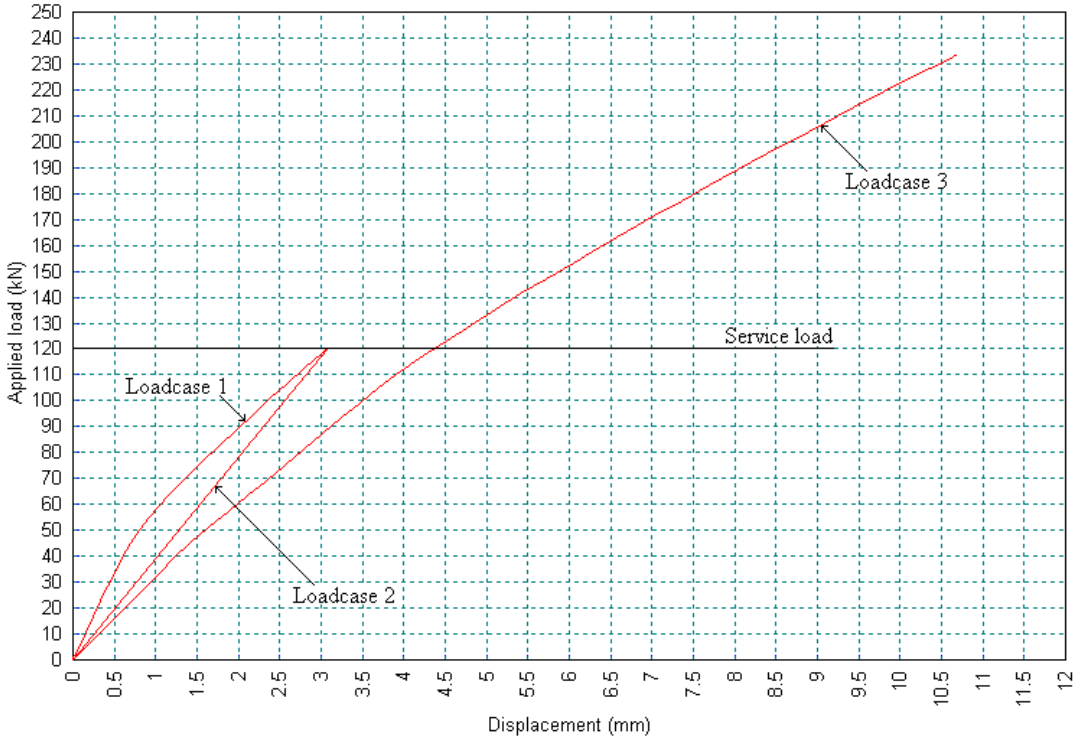

Fig. 4.10: Sample plot of load vs. midspan displacement for a specimen with exposed reinforcement over the central support

Modelling of specimens with exposed reinforcement assisted several design decisions for the experimental investigation. Breakout increments of 200mm were chosen for the test specimens as appreciable moment transfer from the breakout location occurred between breakout increments. Also, exposed steel stresses were monitored until failure of each proposed specimen. This allowed the minimum required anchorage lengths to be established and assisted in the design of the anchorage hooks in the main steel at the ends of the exposed length.

4.4.2 Breakout length investigation

Breakout increments were chosen to produce a noticeable change in the appropriate measures of structural performance. The maximum breakout length also had to be chosen so breakout lengths were initially extended into compression zones to investigate the effect on behaviour. The numerical investigation was carried out for breakout over the central support of a two-span beam with the proposed test load arrangement. The geometric and material properties were set equal to those initially

assumed for the test specimens. The reinforcement areas over the central support and within the spans were chosen to be 326mm^2 and 257mm^2 respectively, to correspond to one of the proposed control specimens.

Fig. 4.11 plots the reduction in exposed steel stress at service load (relative to the corresponding "fully bonded" steel stress) vs. exposed length, relative to the length of the hogging region (L_{hog} was calculated from the bending moment diagram for each breakout interval). Moment transfer away from the central support increased with the length of breakout. Therefore, the distance between points of contraflexure (length of hogging region, L_{hog}) reduced as the breakout length increased. For breakout into the compression zones (L_{exp} / L_{hog} > 1), significant reductions in exposed steel stress occurred. The ultimate load reduced significantly with increasing breakout length due to the reduction in stress in the exposed bars at ultimate load, caused by concrete crushing before reinforcement yield. As moment transfer was anticipated throughout the experimental investigation, the exact length of tension zones could not be established. Maximum breakout lengths of 1m were considered practical for both breakout locations as extension of the breakout lengths into compression zones would not be excessive.

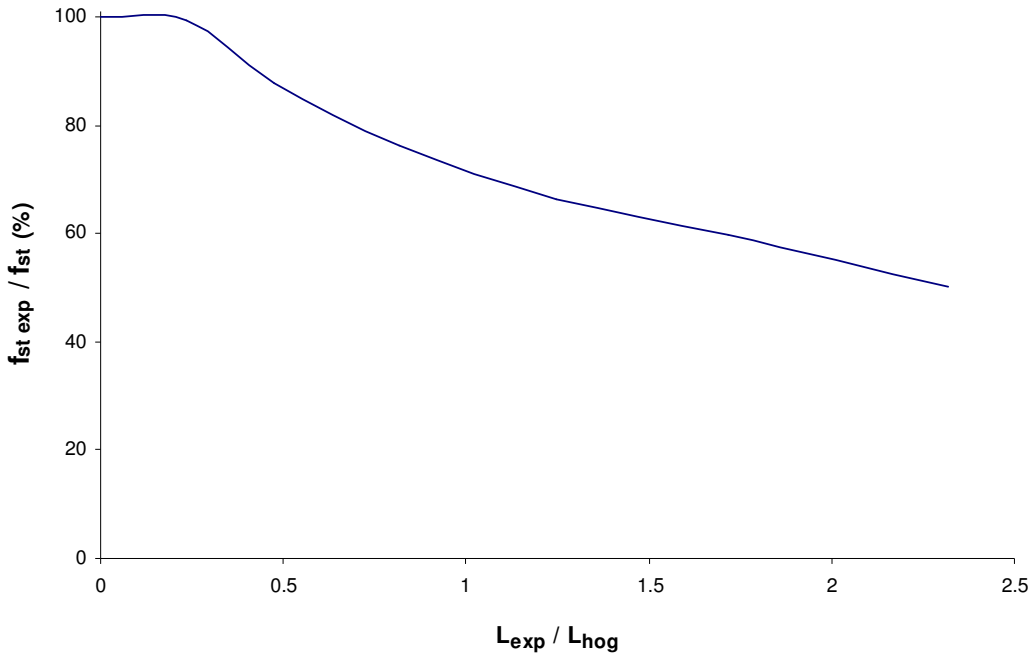

Fig. 4.11: Plot of the reduction in exposed steel stress as the breakout length increased beyond points of contraflexure

4.4.3 Modelling of repaired specimens

Modelling repaired specimens was an extension of the procedure for specimens with exposed reinforcement. The same models were used for the specimens of maximum breakout length and the specimens to be repaired. However, the repair material properties must be assigned to the breakout / repair region before analysis began, as material properties may not be changed between loadcases. This meant that if repair material properties differed from those of the substrate concrete, a portion of the initially "fully bonded" beam had different material properties. By comparing service load measurements from pre-repair specimens (to be repaired under service load) with those for specimens (loaded to failure) with exposed reinforcement, the initial inconsistency in material properties in the repair region was found to have a negligible effect on behaviour. In any case, the test repair material was chosen so that its properties did not differ significantly from the substrate material properties.

Consider initially a specimen to be repaired while under service load. Loadcases 1 & 2 were identical to those for specimens with exposed reinforcement. Loadcase 3 reloaded the pre-repair specimen to service load. Loadcase 4 was added for loading of the repaired specimen to failure. The load sequence for specimens repaired under service load was thus similar to that in Fig. 4.10 but included a separate loadcase to activate the repair material at service load.

Now consider a specimen to be repaired while unloaded. Loadcases 1, 2 & 3 were identical to that for a specimen repaired while under service load. Loadcase 4 was added to unload the specimen before casting of the repair. Loadcase 5 was then used to activate the repair material and load the repaired specimen to failure.

Fig. 4.12 shows a plot of the load-displacement history for a specimen repaired while unloaded. The initial stiffness of the repaired specimen was less than that for the "fully bonded" specimen as flexural cracking was established during previous load cycles. The displacement of the repaired specimen at service load was 8% greater than that for the "fully bonded" specimen. As expected, the initial stiffness of the repaired specimen was greater than for the specimen with exposed reinforcement due to composite action between the steel and the repair material (and also the contribution to tension stiffening of the initially unstrained repair material). The increase in stiffness due to placement of the repair material caused a significant

decrease in the service load displacement (relative to that of the specimen with exposed reinforcement).

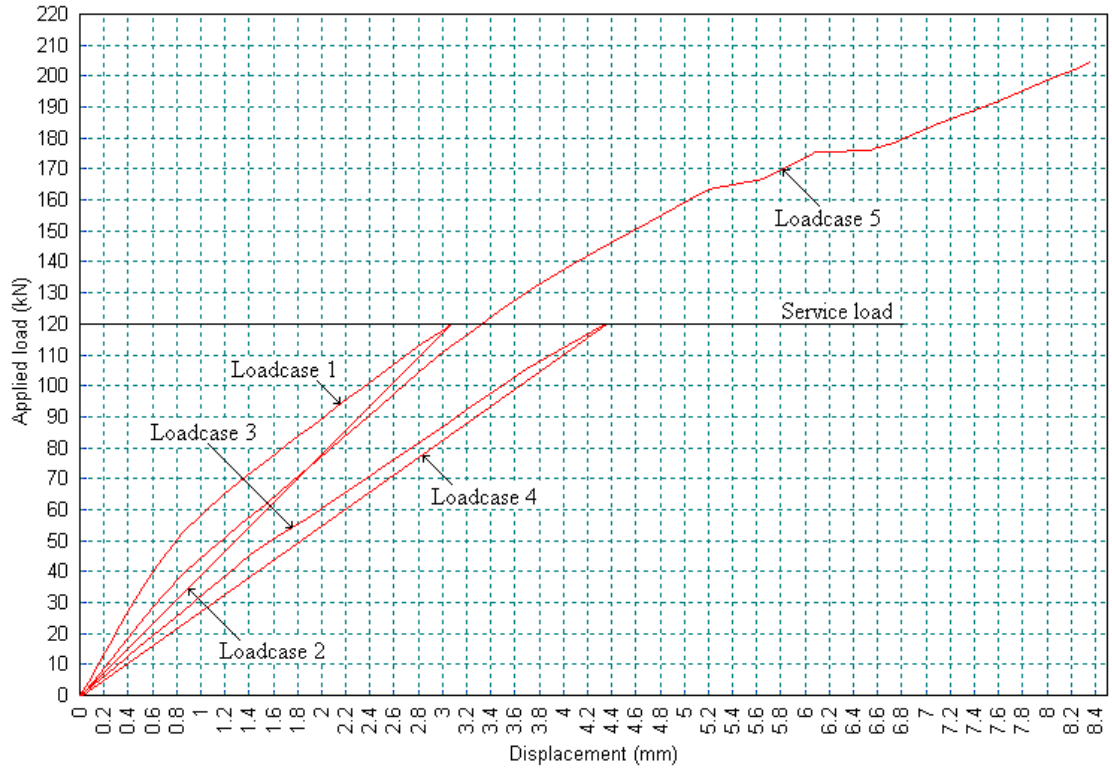

Fig. 4.12: Sample plot of load vs. midspan displacement for a specimen repaired over the central support while unloaded

The numerical model was used to investigate various proportions of load relief. Comparison was made between repaired specimens at 90% of the predicted "fully bonded" failure load (comparison at service load was not practical if specimens repaired at service load were to be included). Investigation of the two extremities of load relief was chosen for testing.

4.5 Load arrangement investigations

4.5.1 Load dispersion

Numerical simulations were carried out to evaluate the effect of load dispersion on stresses near peak moment locations. Fig. 4.13 shows a plot of bending moment (calculated from the loads and support reactions) and tension steel stress near the central support at 90% of the ultimate load of an "as new" model. The area of tension reinforcement is constant and the depth of the neutral axis is approximately constant within the portion of the beam being considered. Therefore, the stress in the steel at a given section should be proportional to the bending moment. Fig. 4.13 shows that near the peak moment, the stress in the steel is about 20% less than that calculated from the bending moment. This is attributed to the effect of load dispersion near concentrated load / reaction points.

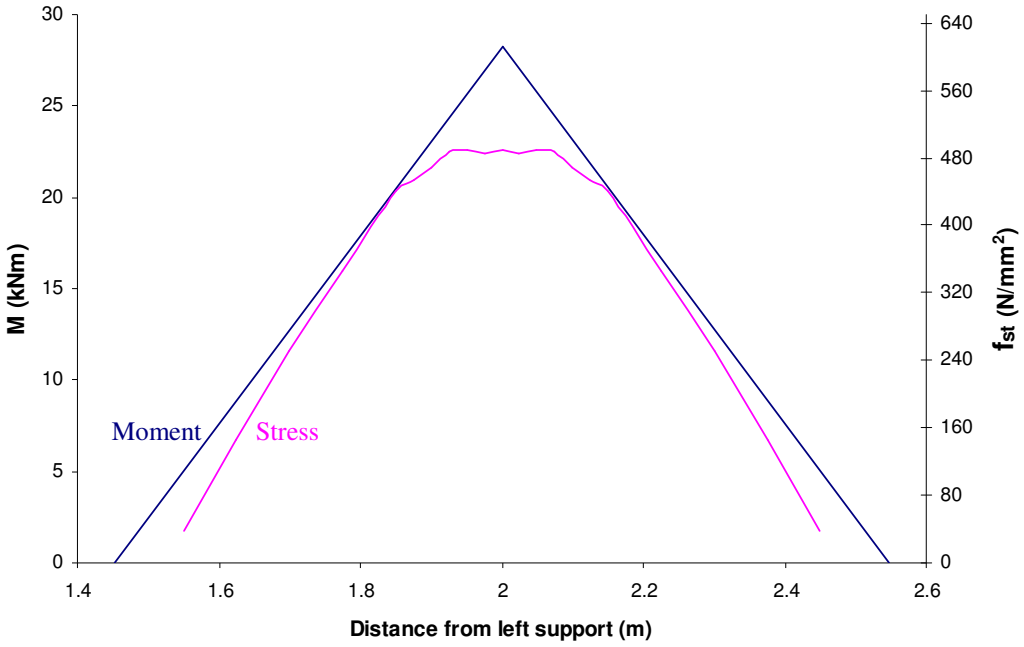

Fig. 4.13: Plot of bending moment and tension steel stress near the central support

Fig. 4.14 shows the corresponding plot of moment and steel stress in the sagging moment region within the left span. In this case, the steel stress is approximately proportional to the moment (calculated from the support reactions) near the peak sagging moment. The effect of load dispersion on the stresses near peak moment was less significant for the two-point load arrangement within the spans as the load was "less concentrated" than for a single point load arrangement.

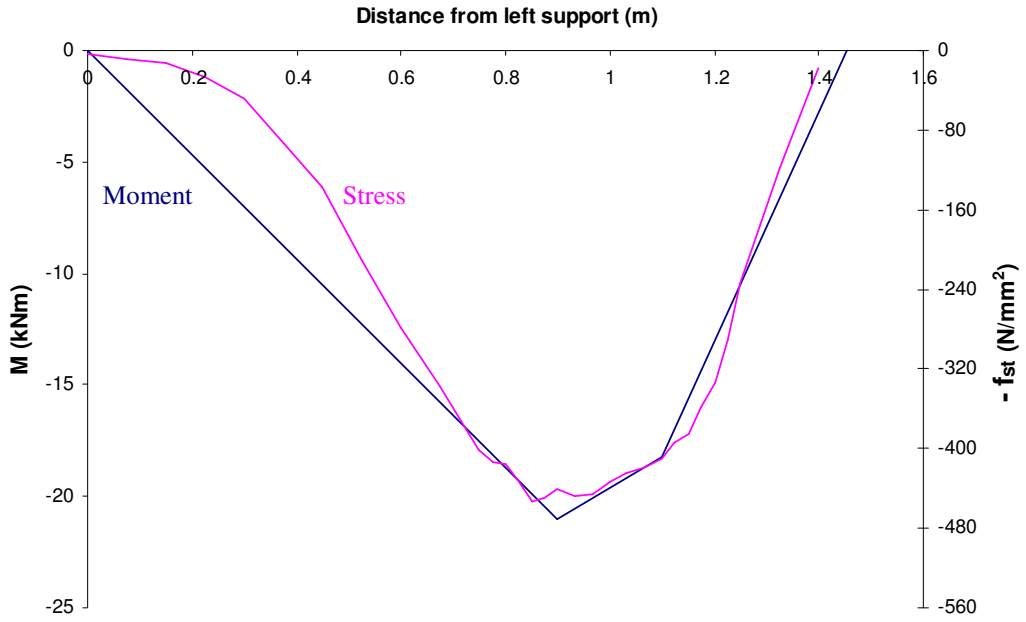

Fig. 4.14: Plot of bending moment and tension steel stress within the left span

4.5.2 Influence of load arrangement on moment balance

Section 2.5 discussed a numerical investigation carried out by Scott and Whittle **[59]** on the effect of load arrangement on moment balance (i.e. the ratio of maximum hogging : sagging moments) within continuous reinforced concrete beams. It was concluded that for a given design moment redistribution, the proportion of moment at the fixed support of a propped cantilever was less for a central point load than for a uniformly distributed load. An extensive experimental investigation of various load arrangements for patch repaired continuous beams was considered beyond the scope

of this study. However, an insight into the influence of load arrangement on moment balance within "fully bonded" reinforced concrete members would prove useful.

The aim of the current investigation is to establish whether load arrangement influences the moment balance (up to service load) within a propped cantilever, for a given design moment redistribution from the fixed support. A two-span model, symmetrical about the internal support was designed to investigate the influence of load arrangement. A two-span beam was used (instead of a propped cantilever model) to avoid complications associated with applying rotational restraint to surface edges. Nominal shear reinforcement was provided and the main reinforcement was curtailed in compression zones (similarly to the "as new" specimen model, Fig. 4.7). The area of tension reinforcement over the central support was maintained constant throughout the analysis. The area of tension reinforcement within the spans was varied according to the design bending moment redistribution. The calculation of the span reinforcement area for a given design redistribution from the central support is described in Appendix C.

Assessment of the moment balance at service load was required. Therefore, a load factor to represent service load for the specimens had to be established. A constant load level throughout the analysis was desirable for comparison between load arrangements. The elastic moment at the central support was greater than within the spans for all load arrangements. The hogging moment would remain the largest moment within the structure unless the specimen was designed for significant moment redistribution from the central support. The moment capacity of the central support cross-section was calculated (Note: The reinforcement at the central support remained constant throughout the analysis). From this, a load factor was deduced for ultimate load of the specimen. The load factor to represent service load was taken as 55% of the load factor for ultimate load and the moment balance at this load factor was assessed throughout the analysis.

As a two-point load arrangement was proposed for testing, two-point load arrangements at a range of distances from the midspan were chosen for investigation. A centrally applied point load was also modelled to relate to the investigation by Scott and Whittle **[59]**. Fig. 4.15 shows diagrams of the three load arrangements chosen for investigation and their corresponding elastic bending moment diagrams. The specified magnitudes of load represent the applied load for a load factor of 1.

It was desirable to maintain a consistent means of quantifying the hogging : sagging moment ratio throughout the investigation. The maximum hogging moment always occurred at the fixed support. However, for a two-point load arrangement, the location of maximum sagging moment depends on the relative magnitudes of the point loads. For a given spacing between the point loads, the ratio of the left point load to the right point load was chosen to give a constant "elastic" moment between the point loads. The sagging moment at midspan was used for calculation of the hogging : sagging moment ratio and thus, the required reinforcement ratios. It was recognized that the maximum sagging moment occurs at the left point load in the two-point load arrangements if the proportion of moment at the fixed support reduces. However, the sagging moment at midspan was used throughout the investigation so values of hogging : sagging moment ratio were compatible with moment ratios for the propped cantilever with a central point load (Load arrangement A).

The variation in bending moment at the fixed support was of particular interest in this investigation. Magnitudes of the point loads (for a load factor of 1) were chosen to give the same "elastic" bending moment at the fixed support for all load arrangements. If no change in moment balance occurred up to service load, the moment at the fixed support would be the same for the three load arrangements (for a given load factor). For example, a load factor of 50 would give a fixed support bending moment of $50 \times 375 \times 10^{-3} = 18.75$kNm for all load arrangements (if no change in moment balance occurred). Also, for a given design redistribution from the fixed support, the same reduction in fixed support moment was required for all load arrangements. Therefore, the observed reductions in fixed support moment were comparable between load arrangements. The virtual work method used to acquire the elastic bending moment diagrams in Fig. 4.15 is described in Appendix C.

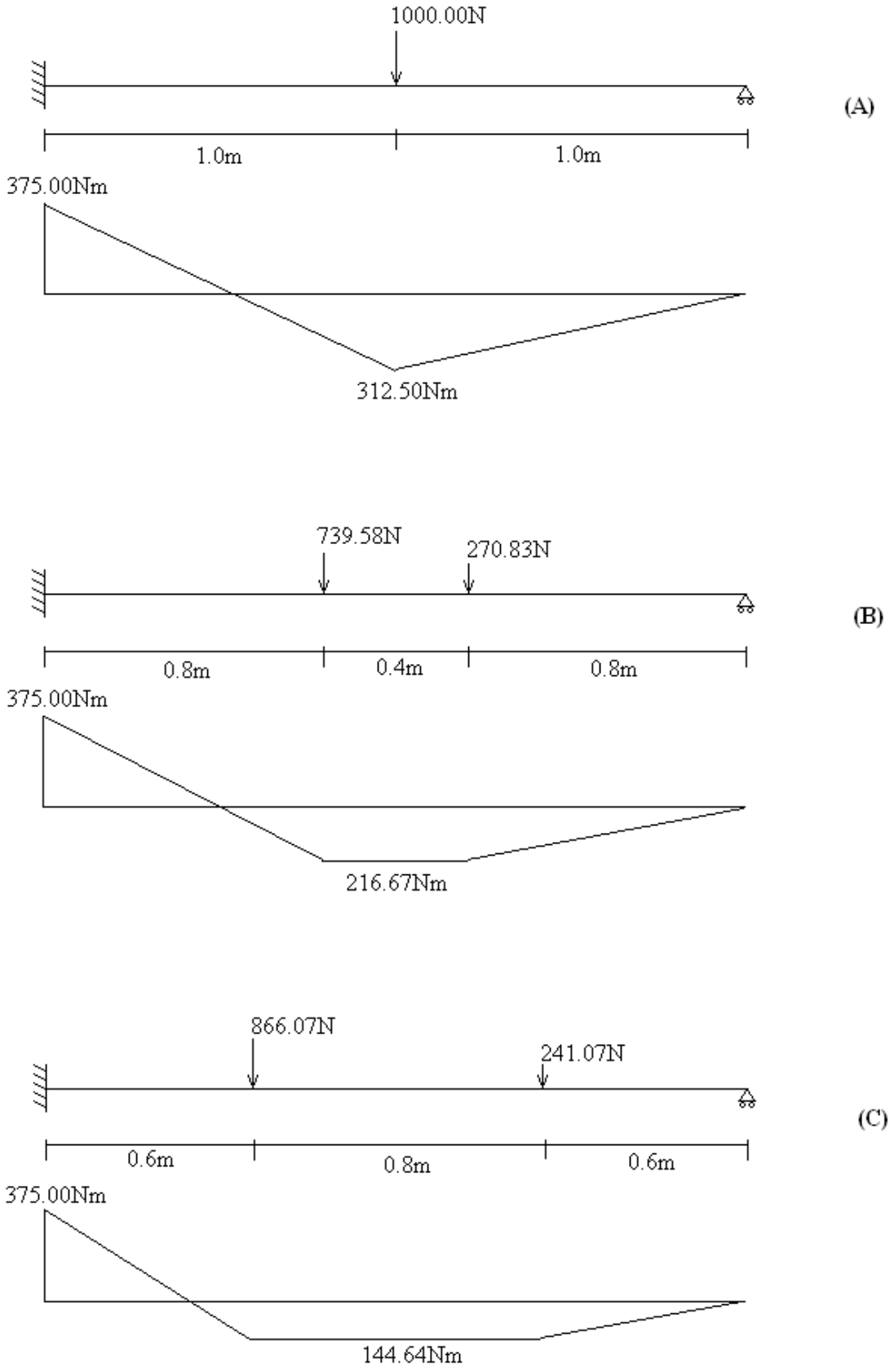

Fig. 4.15: Load arrangements under investigation and corresponding elastic bending moment diagrams

Fig. 4.16 shows a plot of "elastic redistribution" (as defined by Scott and Whittle **[59])** vs. design redistribution for the three load arrangements illustrated in Fig. 4.15. The "elastic redistribution" was calculated by relating the hogging moment at the fixed support to the equivalent hogging moment from the elastic bending moment diagram. Therefore, negative "elastic redistribution" represents an increase in the proportion of moment at the central support during loading to service load. The moment balance for a propped cantilever with a central point load was similar to that for Scott and Whittle **[59]**, Fig. 2.13. Slight variations in magnitude can be attributed to the model properties chosen e.g. reinforcement percentages. Sufficient model detail was not included by Scott and Whittle to replicate their analysis.

A two-point load arrangement allowed less "elastic redistribution" from the fixed support to the span for all design redistributions modelled. This trend was similar to that observed by Scott and Whittle **[59]** for a propped cantilever with a uniformly distributed load. A two-point load arrangement would cause flexural cracking over a greater length than for a central point load. This difference in crack patterns caused less "elastic redistribution" to the spans for a two-point load arrangement due to reductions in flexural stiffness once cracking developed on the bottom face between the point loads. "Elastic redistribution" from the central support was generally greater when the point loads were positioned closer together. However, the distance between the point loads appeared to have a minute effect on the "elastic redistribution" that occurred up to service load.

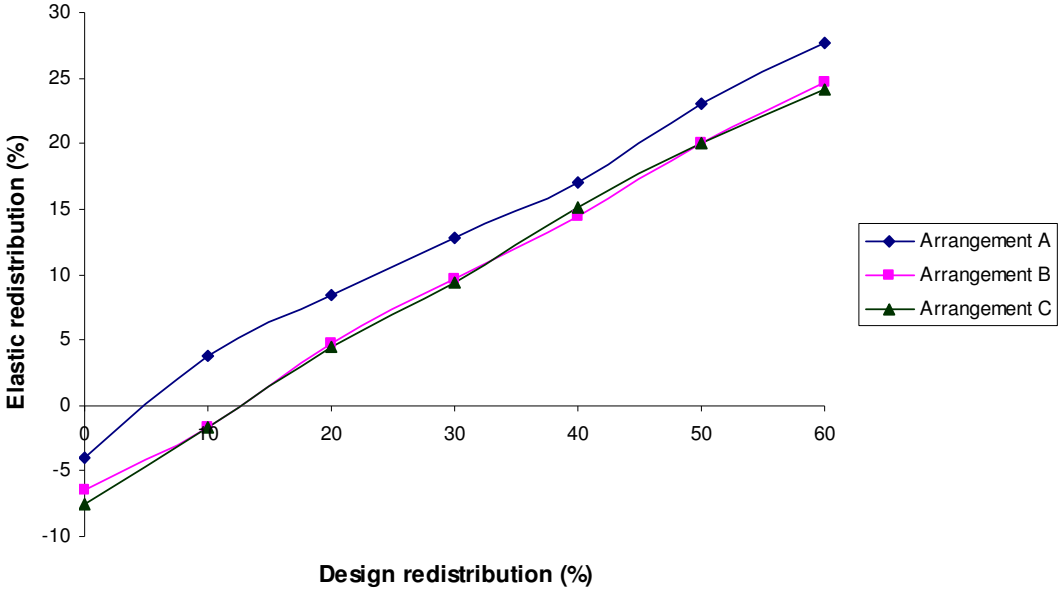

Fig. 4.16: Plot of "elastic redistribution" vs. total design redistribution for various load arrangements

4.6 Summary

This chapter discussed the numerical modelling procedure used to represent behaviour of specimens with a portion of reinforcement exposed and specimens repaired under various load relief conditions. LUSAS concrete model (model 94) was used to represent the concrete and the steel material behaviour was described by a Von Mises stress potential. A non-linear analysis was carried out using a modified Newton-Raphson load stepping procedure. LUSAS "birth and death" feature was used to deactivate the stiffness of the material within the breakout region and subsequently activate the repair material at the appropriate load. Moment transfer from the breakout region as the length of breakout increased was of particular relevance in this study and was assessed by examining changes in support reactions. The effect of breakout and repair on ultimate limit state behaviour was assessed from the maximum load attained and the strains in the steel and the concrete (at sections of maximum moment) at ultimate load.

The numerical model was used to investigate aspects of structural behaviour associated with the chosen test load arrangement. The effect of load dispersion near point loads and support reactions causes reinforcement strains near peak moment locations to be less than those predicted from the conventional bending moment diagram. The distribution of strain within individual elements in the model illustrated this effect. Load dispersion was more prevalent at the central support reaction as loading was "less concentrated" near the two-point load arrangement within the spans. The model was also used to investigate the effect of load arrangement on the moment balance within a member. For a given design moment redistribution, the proportion of moment at the support was less for a single point load arrangement than for a two-point load arrangement within the spans. Scott and Whittle **[59]** observed similar trends when comparing single point load arrangements and uniformly distributed loads. This effect was attributed to the greater extent of cracking for distributed load patterns causing greater loss of section stiffness as flexural cracking occurs.

Numerical model results were used to assist the design of the test specimens and gave an insight into predicted test specimen behaviour (e.g. ultimate loads calculated according to BS 8110 **[61]** were verified using LUSAS). The experimental programme and testing procedure are discussed in Chapter 5.

Chapter 5: Description of experimental work

5.1 Introduction

Chapter 3 discusses preliminary specimen design and outlines the parameters that require investigation during the experimental work. The proposed specimens were modelled using LUSAS finite element software and this process is described in Chapter 4. This allowed appropriate increments and limits of the chosen parameters to be established. The experimental programme was run with a pilot study followed by the main investigation. Once design of the experimental programme was complete, construction of the specimens began.

Before testing commenced, appropriate measures of structural performance were selected and instrumentation was chosen accordingly. Shifts in the balance of hogging and sagging moments throughout the repair process were of particular interest. Reductions in flexural stiffness during the breakout process and subsequent increases due to placement of the repair material were recorded. For repaired specimens, service load midspan displacements and crack widths at maximum moment locations were of interest. At the ultimate limit state, failure load and failure mode were of obvious importance. The plastic behaviour of specimens and the ductility of failure were also examined. Attaining these measures of performance from instrumentation data is discussed in Chapter 6. The current chapter focuses on specimen construction and the testing procedure.

5.2 Test specimen design

5.2.1 Experimental programme

The specimen code defines the condition of the specimen in the repair process, the reinforcement areas in hogging and sagging moment zones and the location of the breakout / repair zones.

Specimen genre

AN → ***"As new"*** control specimen

AB → Specimens tested to failure ***"after breakout"*** of concrete

UR → Specimens tested to failure after ***"unpropped repair"***

PR → Specimens tested to failure after ***"propped repair"***

Reinforcement combination

1 → 2 T8's +2 T10's

2 → 2 T8's +2 T12's

3 → 2 T8's +2 T16's

4 → 2 T8's +2 T20's

Note: First number denotes top reinforcement over the central support
Second number denotes bottom reinforcement within the spans

Breakout / repair location

H → ***Hogging*** breakout / repair over the central support

S → ***Sagging*** breakout / repair within the left span

For example AB23S refers to a specimen tested to failure after breakout of concrete from around the tension steel in the left span, with top steel of 2 T8's + 2 T12's over the central support and bottom steel of 2 T8's + 2 T16's within the spans.

Redistribution of moment towards the central support would increase the largest moment within the member and was considered impractical. Therefore, all test specimens were designed for varying amounts of moment redistribution away from the central support. Table 5.1 shows the reinforcement combinations tested, along with the required and allowable redistributions from the central support, based on "fully bonded" cross-sections. The required moment redistribution from the central support (to achieve the fully plastic bending moments) was calculated from Equation 3.8 after inputting the hogging : sagging reinforcement ratio to Equation 3.7.

The allowable redistribution from a given section was calculated from Equations 3.1, 3.2 & 3.3. To calculate the x / d ratio at a given section at ultimate load, preliminary material properties and concrete cross-section dimensions were chosen. Initial values taken were as follows: f_y = 520N/mm^2, f_{cu} = 35N/mm^2, b = 150mm and d = 170mm. The effect of the nominal hanger bar reinforcement in the compression zones was ignored as curtailment of compression reinforcement was carried out in the main experimental programme. Sample calculation of the required redistribution (to achieve the fully plastic bending moments) and allowable redistribution (according to BS 8110 **[61]**) is included in the failure load calculation, Appendix B.

Reinforcement combination	Required redistribution	Allowable redistribution
11	16.6%	38.2%
21	2.4%	28.5%
22	16.6%	28.5%
12	29.6%	35.2%
23	39.2%	28.5%
34	36.3%	11.5%

Table 5.1: Reinforcement combinations required and allowable moment redistribution

Table 5.2 shows the chosen reinforcement combinations arranged in terms of their hogging : sagging reinforcement ratios and their reinforcement percentages. Reinforcement combination 21 had a hogging : sagging reinforcement ratio of 1.27. As the hogging : sagging moment ratio from the elastic bending moment diagram was 1.32, reinforcement combination 21 was designed for only 2.4% redistribution.

Practical design would commonly attempt to reduce the magnitude of the maximum moment in the structure. For the chosen load arrangement, moment redistribution away from the central support is desirable and is achieved by using a hogging : sagging reinforcement ratio less than the "elastic" hogging : sagging moment ratio. Ultimate strength of specimens with exposed reinforcement is more likely to be reduced in members designed for significant moment redistribution, due to loss of section ductility at the breakout location. Therefore, a greater number of specimens with low reinforcement ratios (i.e. specimens designed for greater moment redistribution from the central support) were tested.

Flexural strength is more likely to be reduced in over-reinforced specimens due to the increase in the concrete compressive strain during breakout of concrete. Thus, for a given hogging : sagging reinforcement ratio, specimens with higher reinforcement percentages have a greater tendency to lose strength during concrete breakout.

		Hogging : sagging reinforcement ratio (α_r)		
		Low (0.65–0.79)	Medium (1)	High (1.27)
Reinforcement percentages (A_s / bd)	Low (0.89%–1.28%)	12	11	21
	Medium (1.29%–1.99%)	23	22	-
	High (2.01%–2.92%)	34	-	-

Table 5.2: Reinforcement combination matrix

AN series

Three "as new" control beams were chosen to provide a reference for post-breakout and post-repair behaviour. AN21, AN11 and AN23 were chosen as they represent the full range of design moment redistributions being tested. AN23 was chosen (instead of AN34) as full plastic moments were more likely to be achieved.

AB series

Reinforcement combinations 21, 11, 23 & 34 were chosen for progressive breakout at both hogging and sagging breakout locations. Again, the full range of hogging : sagging reinforcement ratios was covered by these specimens. Reinforcement combination 34 was included in this test series to assess the extent to which ultimate load would be affected where rotation demand exceeded the anticipated rotation capacity of the section.

For post-breakout analysis of specimens, progressive breakout of concrete was deemed unnecessary for all reinforcement combinations. To reduce labour, some specimens were cast with the reinforcement exposed over the full breakout length. Reinforcement combinations 12 & 22 were chosen for casting with the maximum length of steel exposed (over the central support only) as the design moment redistributions of reinforcement combinations 12 & 22 were mid-range, relative to the design moment redistributions being examined. As hogging breakout was expected to cause a more significant change in behaviour than sagging breakout (Section 3.2), a more extensive investigation of breakout over the support was warranted.

UR series

A set of duplicate beams was designed to be repaired under service load for both repair locations. This test series included reinforcement combinations from either end of the design moment redistribution range, namely: 21, 23 & 34. Sufficient information on the behaviour of these specimens with exposed reinforcement was collected from specimens tested to failure after breakout of concrete (AB series). Therefore, the duplicate specimens were cast with the maximum length of reinforcement exposed.

PR series

Two beams of reinforcement combination 23 (one for each repair location) were also included in the test programme to be repaired while the beams were unloaded. The benefits of "propped" repair are investigated by comparing these specimens with UR23H and UR23S.

5.2.2 Reinforcement detailing

As mentioned in Section 3.4.3, minimising the compression reinforcement throughout the members was desirable to increase the x / d ratio. Therefore, curtailment of tension reinforcement beyond points of contraflexure was required. To enable tying of the steel cages, minimum steel (8mm diameter) was used within the compression zones. To avoid bar lapping, the 8mm bars were designed to run throughout the length of the beam. Anchorage failure of the "main" tension reinforcing bars at the

ends of maximum proposed exposed lengths was undesirable. The available anchorage length was limited by the distance between the ends of the exposed lengths and the nearest point loads / supports. Anchorage hooks were provided to prevent an anchorage failure while a portion of the tension reinforcement was exposed. Sufficient anchorage for all bar diameters was provided by standard 180° anchorage hooks bent according to the minimum required by BS 4466 **[64]**. Bottom reinforcement was allowed to extend over the outer supports without a significant effect on the behaviour of the beam.

Fig. 5.1 shows a sample reinforcement layout for specimen AN23. The shaded regions represent the maximum extent of the two alternative concrete breakout locations. The associated bar schedule is included in Appendix D (Table D.1). Reinforcement detailing was similar for all specimens. Table D.2 displays the top reinforcement bar mark (to replace T12's in Fig. 5.1) and the bottom reinforcement bar mark (to replace B16's in Fig. 5.1) for each individual specimen.

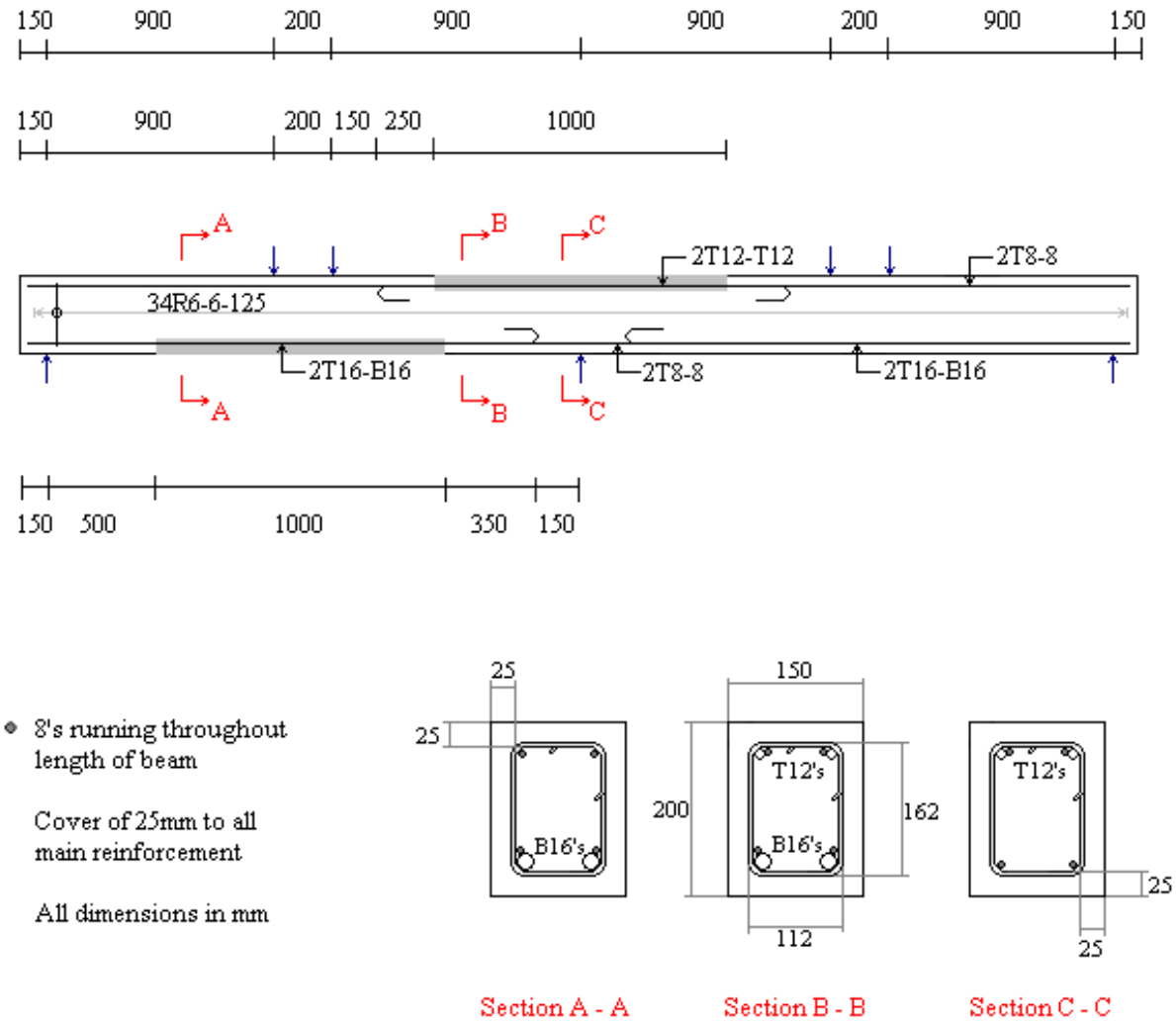

Fig. 5.1: Reinforcement layout for AN23

Details of test specimen dimensions and reinforcement areas are presented in Table 5.3. Note: For a given specimen, the effective depth was taken as the average of the values at the central support and within the spans.

Beam	Condition	b (mm)	d (mm)	A_s / bd (%)		α_r	A_{sv} (mm^2)	s_v (mm)
				Support	Spans			
AN11	Control	150	170	0.89	0.89	1.00	57	125
AN21	Control	150	170	1.28	1.01	1.27	57	125
AN23	Control	150	168	1.29	1.99	0.65	57	125
AB11H	Bars exposed (support)	150	170	0.89	0.89	1.00	57	125
AB11S	Bars exposed (span)	150	170	0.89	0.89	1.00	57	125
AB21H	Bars exposed (support)	150	170	1.28	1.01	1.27	57	125
AB21S	Bars exposed (span)	150	170	1.28	1.01	1.27	57	125
AB23H	Bars exposed (support)	150	168	1.29	1.99	0.65	57	125
AB23S	Bars exposed (span)	150	168	1.29	1.99	0.65	57	125
AB34H	Bars exposed (support)	150	166	2.01	2.92	0.69	57	125
AB34S	Bars exposed (span)	150	166	2.01	2.92	0.69	57	125
AB12H	Bars exposed (support)	150	170	1.01	1.28	0.79	57	125
AB22H	Bars exposed (support)	150	169	1.29	1.29	1.00	57	125
UR21H	Unpropped repair (support)	150	170	1.28	1.01	1.27	57	125
UR21S	Unpropped repair (span)	150	170	1.28	1.01	1.27	57	125
UR23H	Unpropped repair (support)	150	168	1.29	1.99	0.65	57	125
UR23S	Unpropped repair (span)	150	168	1.29	1.99	0.65	57	125
UR34H	Unpropped repair (support)	150	166	2.01	2.92	0.69	57	125
UR34S	Unpropped repair (span)	150	166	2.01	2.92	0.69	57	125
PR23H	Propped repair (support)	150	168	1.29	1.99	0.65	57	125
PR23S	Propped repair (span)	150	168	1.29	1.99	0.65	57	125

Table 5.3: Test specimen geometric details

Note: Curtailment of reinforcement within compression zones was not included in the design of AN11, AB11H & AB11S (tested in the preliminary investigation) and main reinforcement ran throughout the length of the beam. The reinforcement combination was referred to as 11 for ease of specimen coding even though the area of 2T12's is slightly less than that for 2T8's + 2T10's.

5.3 Specimen construction

5.3.1 Casting specimens

25mm plastic spacers were clipped onto the bottom "main" steel to provide the required cover. 20mm spacers were also attached to the sides of the links, to maintain an even spacing between the steel cage and the sides of the shutter. 25mm thick internal quality plywood was used for construction of the shutters. Mould oil was applied to the internal surfaces of the formwork and the cages were placed in the shutters.

Several test specimens required a portion of the tension reinforcement to remain exposed after completion of the casting. For exposure of the top reinforcement, 50mm deep stop-ends were cut to fit through the reinforcement and screwed into position (outside edges 1000mm apart). The concrete was then poured to a lower level (~50mm below the top of the shutter) between these stop-ends (Fig. 5.2).

Fig. 5.2: Photograph of shutter positioned for top reinforcement exposure

Where exposure of the bottom reinforcement was required, 50mm thick polystyrene foam (150mm strip, 1000mm long) was placed in the bottom of the shutter. Longitudinal and cross grooves were cut in the foam to allow for the main steel and the links respectively (Fig. 5.3).

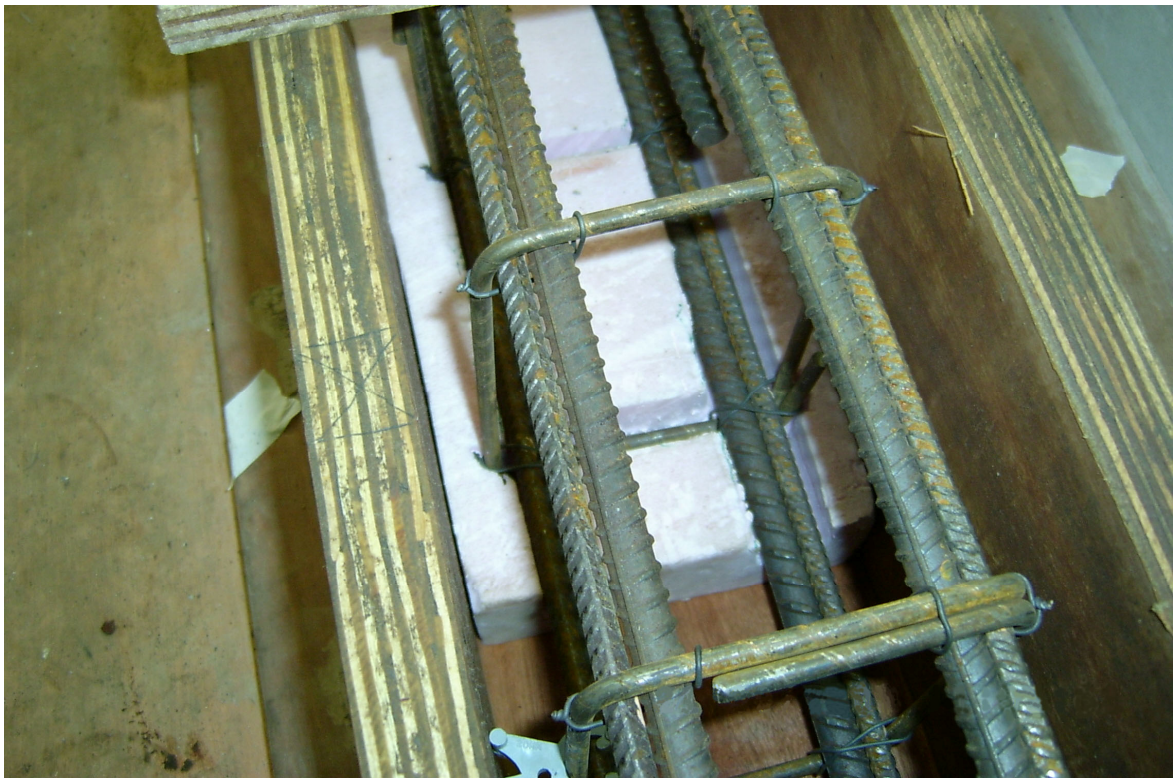

Fig. 5.3: Photograph of polystyrene foam positioned for bottom reinforcement exposure

Concrete was supplied by a local readymix contractor. C28/35 concrete with a maximum aggregate size of 10mm and a slump of 50mm – 90mm was specified. Concrete was poured into the moulds with as small a drop as possible from the chute, to prevent air being absorbed into the mix. A poker vibrator was used to compact the fluid concrete. 100mm concrete cubes and 300mm×150mm concrete cylinders were cast using a vibrating table. The beams, cubes and cylinders were then covered in damp hessian and polythene to cure the concrete. The beams, cubes and cylinders were removed from their moulds two days after pouring and allowed to air cure in the lab. Concrete cubes were not saturated in accordance with BS 1881-116 **[65]** as it was desirable to cure the cubes in the same conditions as the test specimens.

5.3.2 Casting repairs

A proprietary micro-concrete repair material, Renderoc LA was supplied by Fosroc Ltd. Its 7 day compressive strength was similar to that of the substrate concrete and its aggregate size and flow properties were suitable for the scale of the repair. 3.3 litres of water was to be added to the pre-mix bag to yield 12 litres of micro-concrete. Mixing was carried out in a small scale paddle mixer in accordance with the manufacturer specification **[66]**.

Shutters were constructed to contain the flowing micro-concrete repair material (Fig. 5.4). Grooves were cut in the shutters to allow clamping to the beam sides without obstruction from the Demec buttons. A bead of silicon sealant was applied around the edges of the substrate concrete and the formwork was clamped in position.

Fig. 5.4: Photograph of repair shutters for beam soffit (left) and top of beam (right)

For repair above the central support, the shutters were clamped to the sides of the beam and a reinforcing rail was clamped behind each shutter to prevent bulging. The repair area was filled with water, to soak the substrate. After an hour, any excess water that had not leaked through the cracks in the beam was soaked up with paper

towels to leave the substrate in a saturated surface-dry condition. The material was transferred to the repair area using a scoop and no compaction or troweling of the surface was required as the mix was self-levelling. Once the area was filled, the remaining material was used to make concrete cubes. The repair area and the cubes were covered with damp hessian and polythene. After 24 hours, the shutters were removed and the cubes were removed from the moulds. The damp hessian and polythene was then repositioned for 5 days.

For repairs to the beam soffit, channel shaped formwork was used (Fig. 5.4). The formwork was clamped to the underside of the beam (from the top face of the beam) and also clamped to the beam sides. The form was filled with water through the access point to soak the substrate. After an hour, the water was released by loosening the clamps. Any excess water was removed from the substrate using paper towels and the formwork was subsequently repositioned. The repair material was placed through the access point in the channel using a scoop. The access point was filled until the micro-concrete rose above the level of the breakout at the bleed point. The formwork was tapped briefly with the poker vibrator to assist the movement of the material through the reinforcement. Note: The formwork was not filled through both sides as this could have led to trapped air voids. The access point was then overfilled so an upward pressure was applied by the repair material on the substrate. This helped ensure a good bond between the patch repair and the substrate. Again after 24 hours, the shutters were removed and damp hessian and polythene were taped to the sides of the beam around the repair patch for 5 subsequent days.

5.4 Material testing

Offcuts from test specimen reinforcement were used to conduct steel tension tests. Ten steel samples were tested for each bar diameter. The initial length and the weight of the steel specimens were measured. The average cross-sectional area of each steel specimen was then calculated using an assumed density of steel of 7850kg/m^3. Steel was tested in the Denison material tester. Values of 0.2% proof stress (0.2%σ) were representative of the yield stress of the steel. The elastic modulus (E_{st}) was also noted and any unusual values of E_{st} were disregarded due to extensometer slippage. The average values of 0.2%σ, E_{st} and ultimate tensile strength "UTS" were calculated for each reinforcement diameter and are displayed in Table 5.4.

Bar type	$A_{average}$ (mm^2)	$Ø_{average}$ (mm)	E_{st} (kN/mm^2)	0.2%σ (N/mm^2)	UTS (N/mm^2)
R6	26.96	5.86	200	439	512
T8	50.29	8.00	192	518	601
T10	77.71	9.95	197	559	658
T12	110.55	11.86	201	593	686
T16	195.65	15.78	198	569	679
T20	306.70	19.76	203	555	662

Table 5.4: Steel reinforcement properties

The yield stress for a reinforcement bundle was calculated as the average yield stress by area.

$$f_{y\ average} = \sum (A_s\ f_y) / \sum (A_s) \qquad 5.1$$

For example, the yield stress of T8's + T12's was calculated as {(518×50.29) + (593×110.55)} / (50.29 + 110.55) = 570 N/mm^2.

6 concrete cubes and 6 cylinder samples were taken from the main concrete pours. Cube tests were carried out to determine the compressive strength of the concrete **[65]**. Split cylinder tests carried out in accordance with BS 1881-117 **[67]** were used to determine the strength of the concrete in tension. Some cylinders were also used to determine the elastic modulus of the concrete in accordance with BS 1881-121 **[68]**. Relevant concrete and steel material properties are displayed in Table 5.5.

Beam	f_{cu} specimen (N/mm^2)	f_t specimen (N/mm^2)	E_c specimen (kN/mm^2)	f_{cu} repair (N/mm^2)	f_y (N/mm^2)		f_{yv} (N/mm^2)
					Support	Spans	
AN11	19.6 *	-	-	-	593	593	439
AN21	42.6	3.0	21.2	-	570	543	439
AN23	42.6	3.0	21.2	-	570	559	439
AB11H	14.0	-	-	-	593	593	439
AB11S	14.0	-	-	-	593	593	439
AB21H	42.6	3.0	21.2	-	570	543	439
AB21S	42.6	3.0	21.2	-	570	543	439
AB23H	42.6	3.0	21.2	-	570	559	439
AB23S	42.6	3.0	21.2	-	570	559	439
AB34H	42.6	3.0	21.2	-	559	550	439
AB34S	42.6	3.0	21.2	-	559	550	439
AB12H	42.6	3.0	21.2	-	543	570	439
AB22H	42.6	3.0	21.2	-	570	570	439
UR21H	53.0	3.9	21.9	57.5	570	543	439
UR21S	53.0	3.9	21.9	50.6	570	543	439
UR23H	53.0	3.9	21.9	55.5	570	559	439
UR23S	53.0	3.9	21.9	51.3	570	559	439
UR34H	37.4	-	-	53.4	559	550	439
UR34S	53.0	3.9	21.9	55.8	559	550	439
PR23H	53.0	3.9	21.9	51.3	570	559	439
PR23S	53.0	3.9	21.9	52.2	570	559	439

Table 5.5: Concrete and steel material properties

It is recognised that the concrete used for the preliminary investigation (specimens AN11, AB11H & AB11S) was not a structural grade of concrete. Although results from these specimens are included in this thesis, they will be used only with caution in deriving conclusions.

* Specimen AN11 was tested approximately 500 days after casting so allowance was made for the long term strength gain of concrete (relative to the compressive strength of concrete in AB11H & AB11S). Croney and Croney **[69]** suggest a strength increase factor of approximately 1.6 over 500 days for a 28 day strength of $20N/mm^2$. Other sources **[70, 71]** suggest a strength factor between 1.2 and 1.4 over the same

time period. A strength increase factor of 1.4 was chosen and the compressive strength of concrete in AN11 at the time of testing was calculated accordingly.

It is also worth noting that measured elastic modulus values were appreciably lower than those suggested by BS 8110 **[61]** (Equation 4.1). Alexander **[72]** found elastic modulus is significantly influenced by the aggregate stiffness. Cairns and Zhao **[2]** suggest an expression of E_c (kN/mm^2) = 3.2 $\sqrt{}$ f_{cu} (N/mm^2) to account for the lower stiffness traditionally found with Scottish aggregates. Results measured here are consistent with this expression.

5.5 Test preparation

5.5.1 Specimen preparation

All specimens were painted with white matt emulsion so that cracks would be clearly visible and could be marked easily. The positions of the load and support points were also marked along the beam and breakout intervals were measured out.

As mentioned previously, several specimens were constructed with a portion of the reinforcement exposed before testing. The polystyrene foam was removed from around the bottom steel and any excess concrete was broken out. For specimens to be repaired, surfaces were roughened with a hammer and chisel to ensure a good key for the repair material. The substrate surfaces were then power-hosed to remove any loose material and clean the area.

5.5.2 Test set-up

Fig. 5.5 & 5.6 show a photograph and a schematic diagram of the complete test set-up. Heights of the supports were chosen to facilitate breakout or repair on the underside of a beam. Supports were placed 2m apart with the central support aligned with holes in the strong floor. The reaction load cells were positioned and steel plates placed on top, stabilised with temporary timber wedges (50mm thick steel plates were used to adequately distribute load from the load cells). The supports were levelled and the beam was set on plaster to avoid residual stresses in the specimen due to uneven support.

Small 12mm thick plates were placed between the specimen and the "point load" rollers to avoid a local bearing failure under one of the point loads. The spreader beams and hydraulic jack were then positioned. A 50 tonne jack with a threaded piston and locking collar was used to enable locking of piston displacement. The "applied load" load cell was then placed on the fully retracted piston of the jack. Two 30mm diameter threaded steel rods were used to clamp the apparatus to the strong floor.

Fig. 5.5: Photograph of test set-up

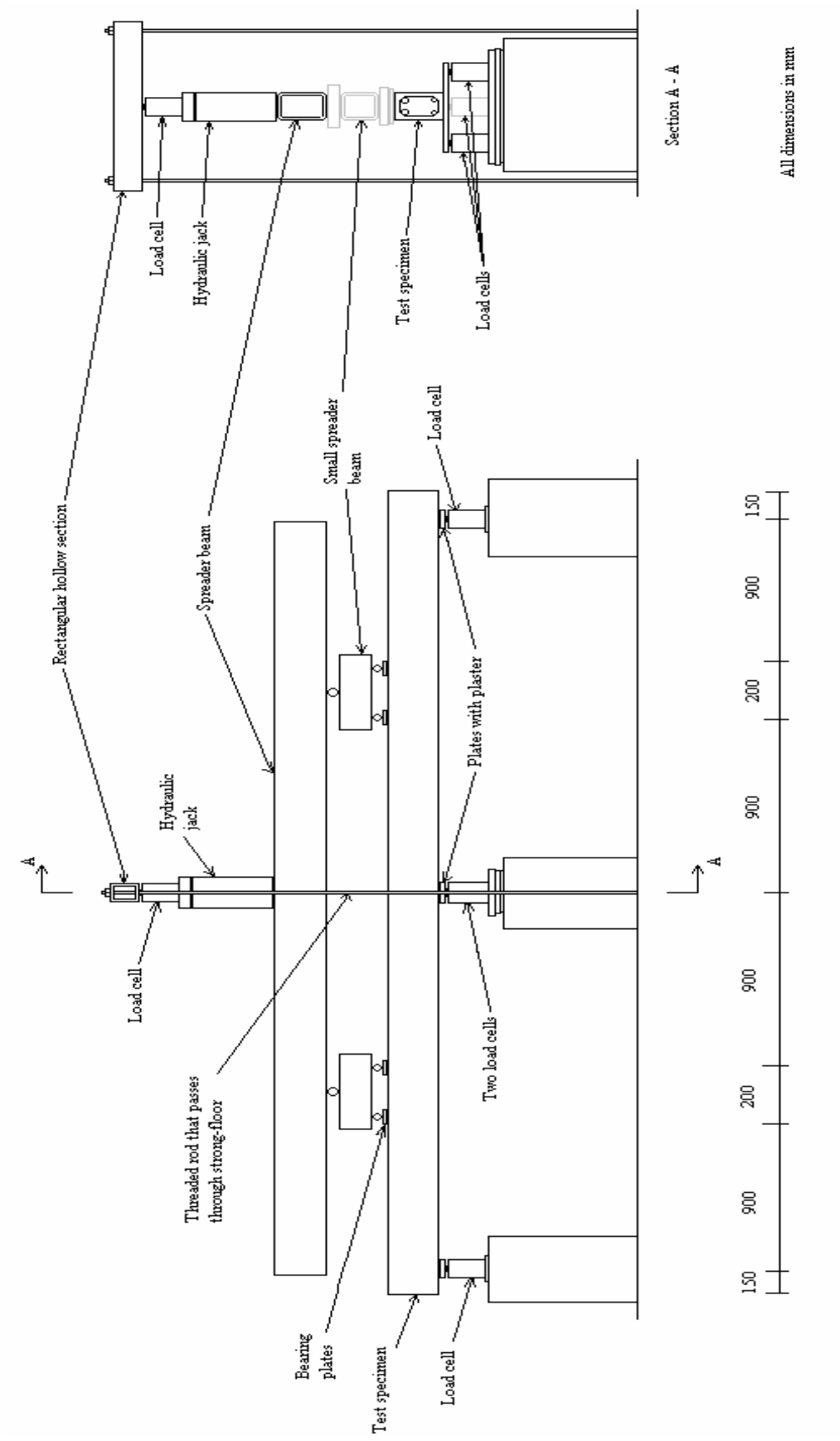

Fig. 5.6: Diagram of apparatus

Displacement transducers were generally clamped with the plunger in contact with the underside of the beam. Where breakout or repair to the beam soffit was required, the transducer was positioned so the plunger extended to the underside of a timber lath glued to the top of the beam and overhanging the beam edge. Readings were zeroed after completion of the apparatus set-up but before loading began (the displacement due to the self-weight of the apparatus was deemed negligible).

The reaction load cells were zeroed immediately after positioning of the test specimen to neglect self-weight of the beam. The spreader beams and hydraulic jack were then positioned. The "applied load" load cell was zeroed when it was placed on the hydraulic jack. Therefore, the weight of the spreader beams and the hydraulic jack applied a load to the specimen that was not included in this load cell reading. The weight of the spreader beams and the hydraulic jack were determined and the total force they contributed was 2.16kN. This value was validated by recording the readings from all the reaction load cells before and after the placement of the spreader beams and the hydraulic jack. This zero error was added to the "applied load" load cell output at the results analysis stage.

5.5.3 Instrumentation

Demountable mechanical (Demec) buttons were glued to the sides of the beam for measurement of strain at sections of maximum hogging and sagging moment. A 150mm gauge length was chosen to approximately coincide with the spacing between flexural cracks, which generally occurred in the vertical plane of the links at 125mm spacing. The Demec buttons were fixed at 75mm to either side of the relevant cross-sections. Strains were measured at 4 heights within the depth of the beam.

Fig. 5.7 shows the Demec positions for breakout within the left span and over the central support. Ideally, the four sets of Demecs would be evenly spaced, with one near the top and one near the bottom of the beam. However, this was not possible at cross-sections where removal of concrete would take place. 15mm clearance beyond the depth of breakout was provided to the centre of the first Demec, to reduce the risk of buttons being chipped off during the breakout process.

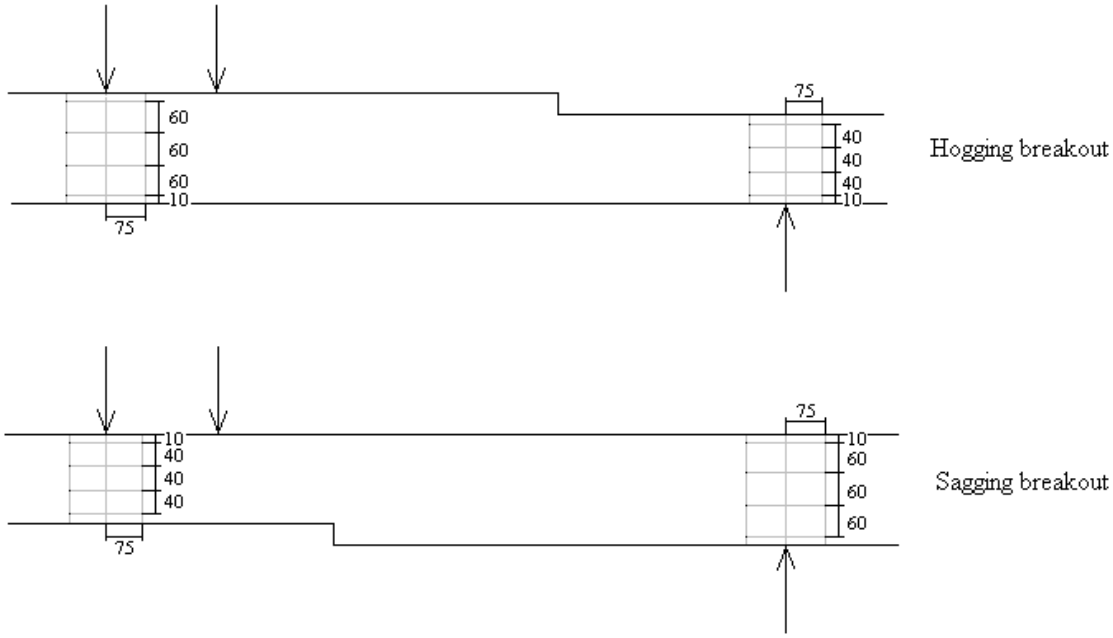

Fig. 5.7: Position of Demecs at breakout and non-breakout locations

Strain measurement within the patch repairs was also desirable. Demec positions at patch repair locations are illustrated in Fig. 5.8. The average depth of a patch repair was 55mm so two sets of Demecs were sufficient for a strain distribution graph through the depth of the repair.

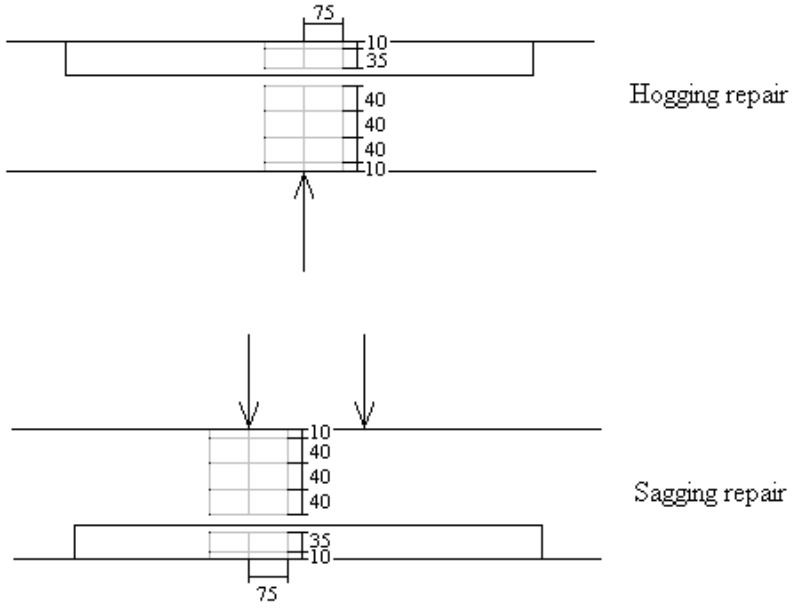

Fig. 5.8: Position of Demecs at repair locations

Demec buttons were fixed to both sides of the beam in the corresponding positions. Placing Demecs on both sides allowed a certain redundancy, enabling measurement of the strain at a specific level, even if a Demec was lost during breakout of concrete. The strain was measured from both sides of the beam and the average of the two values was calculated. Averaging the strain eliminated any torsional effects, possibly due to off-centre loading or supports.

A 50 tonne load cell monitored the total load applied to the beam and 30 tonne load cells measured the three reactions. To ensure stability of the beam set-up, two load cells were provided at the central support, placed on an axis perpendicular to the span of the beam and were spanned by a 50mm thick plate. The sum of the readings from these load cells gave the central support reaction. Single load cells were used for both left and right reactions. Each load cell was calibrated with its associated readout box using the Denison material tester. Repeat calibration checks were carried out throughout the test programme.

Readings from load cells were logged to a Squirrel data logger throughout testing. The logging mode chosen was average time logging and the logging interval was set to 2 seconds. This meant that a reading was taken from each channel every second, and every 2 seconds the average of the two previous readings was calculated and logged.

Two redundancies existed in the load measurement system and were used to verify the load cell readings. Firstly, left and right reactions should be equal due to the symmetry of the loading. Secondly, equilibrium of vertical forces should be maintained (the total applied load should equal the sum of the reactions).

Fig. 5.9 plots left and right reactions as loading increased to failure on AN23. Throughout the test programme, deviation from the average of the left and right reaction rarely exceeded 3.5% and never exceeded 5%. The average of the left and right reactions was used for calculation of “measured” bending moments.

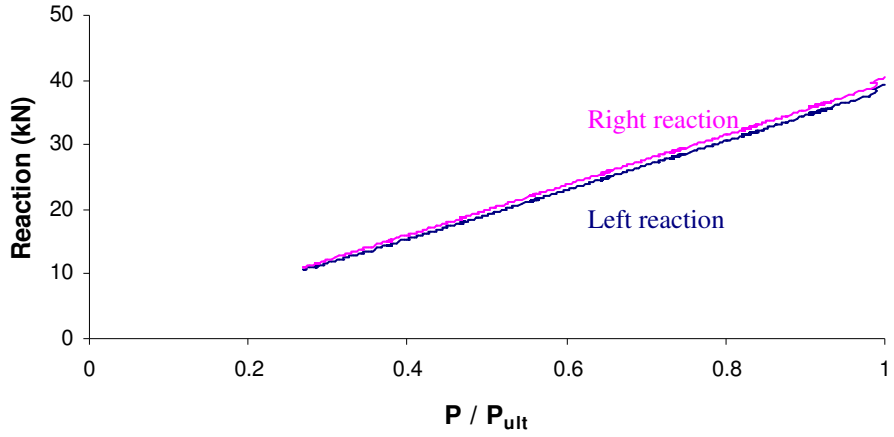

Fig. 5.9: Typical plot of left and right reactions vs. proportion of ultimate load

Fig. 5.10 plots applied load and the sum of the reactions as loading increased to failure on AN23. The "true" applied load was taken as the average of the applied load reading and the sum of the support reactions. Throughout testing, deviation of the applied load value and the sum of the reactions from the "true" applied load never exceeded 2.5%.

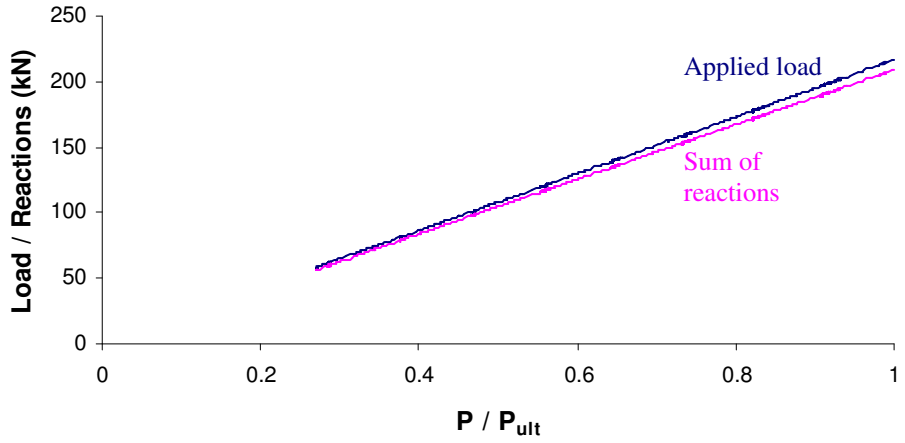

Fig. 5.10: Typical plot of applied load and sum of support reactions vs. proportion of ultimate load

Two displacement transducers measured midspan displacement in both spans. The transducers were calibrated in a micrometer gauge calibration apparatus and calibration graphs of output voltage vs. displacement were produced. Transducer output was also continually logged throughout testing.

5.6 Test procedure

5.6.1 Reference specimens

The failure load for "as new" specimens was previously calculated and the beam service load was determined (approximately 55% of the failure load). Load was increased in standard increments of 16.67% of the beam service load. After initial readings, the first load step was applied and the collar of the piston was screwed down to lock the displacements, in case of loss of hydraulic pressure. Demec readings were taken and any cracks were marked and labelled. The load was increased in increments to full service load with Demec readings recorded for each load increment. Cracks were marked and labelled for each load step. Maximum crack widths at service load were measured above the central support and within the spans.

Once readings were taken at service load, the load was released and the readings again taken for zero load. To try to replicate a period of service, the beam was loaded to service load and unloaded over 10 cycles. 50% of the service load was then maintained on the beam overnight while the displacement of the jack was locked.

The following morning, loading was resumed. The load was increased back to 50% of the service load and the jack collar locked (the sustained load dropped due to overnight straining of the beam), and another complete set of readings was recorded. The load was increased in increments and Demec readings recorded for each increment. Any extra cracks that formed were marked. Loading was increased to failure, considered to occur when a marked drop in load occurred while displacement increased. The peak load and failure mode were noted. The beam was then completely relieved of load and the logger run stopped.

Note: The test procedure for AB12H and AB22H was identical to that for the control specimens.

5.6.2 Progressive breakout specimens

The initial load cycles to service load were identical to that for the control specimens. Again, 50% of the service load was maintained on the specimens overnight. The next morning, loading was increased in increments as explained previously, but only as far as service load. The beam was then completely unloaded and reloaded to 50% of the service load. Demec readings were recorded at this point and the logger run stopped.

Displacement transducers were removed to prevent damage during breakout of concrete. The edges of the breakout area were first defined using a bolster chisel, to confine the breakout and attempt to retain all the Demec buttons. The depth of breakout was taken to 10mm beyond the main steel. Concrete was broken out using a hammer and chisel as a kango hammer would have caused excess damage to the specimen. Breakout was carried out in 200mm increments. Note: "hogging" breakout was always centred on the central support and "sagging" breakout was always centred on the left midspan (breakout progressed symmetrically outwards in both directions).

Demec buttons were glued to the newly exposed steel bars so the average change in strain in the exposed steel could be determined. The positioning of the Demecs along the exposed bar was irrelevant as the strain was uniform throughout the exposed length.

For convenience, the same displacement datum was used throughout the test to attempt to measure the total beam deflection. When replacing the transducer, it was clamped so that the output voltage reading was the same as the reading taken just before the concrete was broken out. This assumed that the beam did not deflect during the breakout process. Obviously, a certain deflection would occur, but was impossible to measure.

Load was then restored to 50% of service load (as straining of the beam during concrete breakout caused the load to drop) and Demec readings were taken. The load was then increased in steps to service load with Demec readings recorded for each load step. Again, any further crack propagation was marked and labelled. The beam was then fully relieved of load and reloaded to 50% of the service load. Again, Demec readings were taken at this load step.

Breakout intervals of 400mm, 600mm, 800mm and 1000mm were subsequently tested in the exact same manner, after which the beam was tested to failure. The failure load and failure mode were noted

5.6.3 Repaired specimens

The initial loading sequence to service load was carried out in the same manner as for the control specimens. The only variation was that Demec readings were also taken from the initially exposed steel. The next morning, the load was increased in the appropriate increments from 50% of the service load to full service load.

For "unpropped" repair, the collar of the jack was locked when service load was reached and this load was maintained throughout casting of the repair. For "propped" repair, however, specimens were completely unloaded (after readings for service load were taken), and remained unloaded during casting of the repair.

The patch repairs were cast as described in Section 5.3.2. 6 days after casting, the repair patches were painted white to assist the observation of crack formation. Two sets of Demecs were glued to either side of the patch repair to measure the strain at the same cross-section as the existing Demecs (Fig. 5.8). The repaired specimens were tested to failure 7 days after casting of the repair. For "unpropped" repaired specimens, the load dropped below service load during curing of the repair as the strain pattern in the beam changed. Initial post-repair Demec readings were taken at the existing load on the beam to establish readings for the Demecs on the patch repair for "zero strain". For "propped" repaired specimens, initial post-repair Demec readings were taken for zero load.

The logger was then initiated and the load increased in the pre-defined load increments to failure. Demec readings were taken and crack patterns noted for each load step. Particular attention was paid to bond cracking at the repair interface and composite cracking (cracks in the substrate extending into the repair patch). The failure load and failure mode were noted.

Chapter 6: Presentation of test results

6.1 Introduction

This chapter describes the reduction of Demec gauge readings and logged data to obtain useful measures of behaviour. Firstly, the instrumentation calibration graphs were used to attain values such as strain, load / reaction, and midspan displacement. Further measures of particular interest for this experimental investigation were bending moment, section curvature, flexural stiffness and section rotation. The processes involved in calculating these values are explained.

Results are presented for the relevant measures of performance for each specimen. Results from specimens subjected to progressive breakout of concrete are compared with those from control specimens under notional service load, to assess the change in behaviour as the breakout length increased. Analysing specimens under service load represents the most critical loadcase during breakout (no load relief during the breakout process). Failure loads for the final breakout interval are also analysed. Results of beams tested to failure after completion of repairs are also presented. The effect of repair under "propped" and "unpropped" conditions on ultimate limit state behaviour is assessed by comparing with equivalent control specimens.

Note: Measurements of strain were taken and bending moments were considered at two cross-sections in each test specimen – at the left load in the left span and at the central support. The breakout location refers to the cross-section within the breakout being considered e.g. the section at the left load in the left span for sagging breakout. The non-breakout location refers to the other cross-section at which measurements were taken within the same specimen e.g. the central support cross-section for breakout within the left span.

6.2 Observation of cracking and failure mode

Flexural cracking in "fully bonded" specimens near maximum moment locations usually began at 33% - 50% of the service load. Flexural cracks generally formed at cross-sections coinciding with the shear links (~125mm spacing). Diagonal cracking near the central support occurred close to service load.

Crack widths should not exceed 0.3mm at the serviceability limit state (BS 8110 **[61]**). Crack widths were measured at maximum hogging and sagging moment locations under service load. For "fully bonded" specimens, typical flexural crack widths were 0.2mm over the central support and 0.1mm within the spans. Crack widths over the support were larger as the bending moment at the support was generally greater than within the spans (elastic bending moment diagram, Fig. 3.5).

In progressive breakout specimens, flexural crack widths within the breakout length increased with the length of breakout and crack widths under service load significantly exceeded the 0.3mm limit. In some cases, cracks at the breakout location reached 1.0mm (Fig. 6.1). However, it is common practice to inject epoxy resin into substrate cracks during the patch repair process.

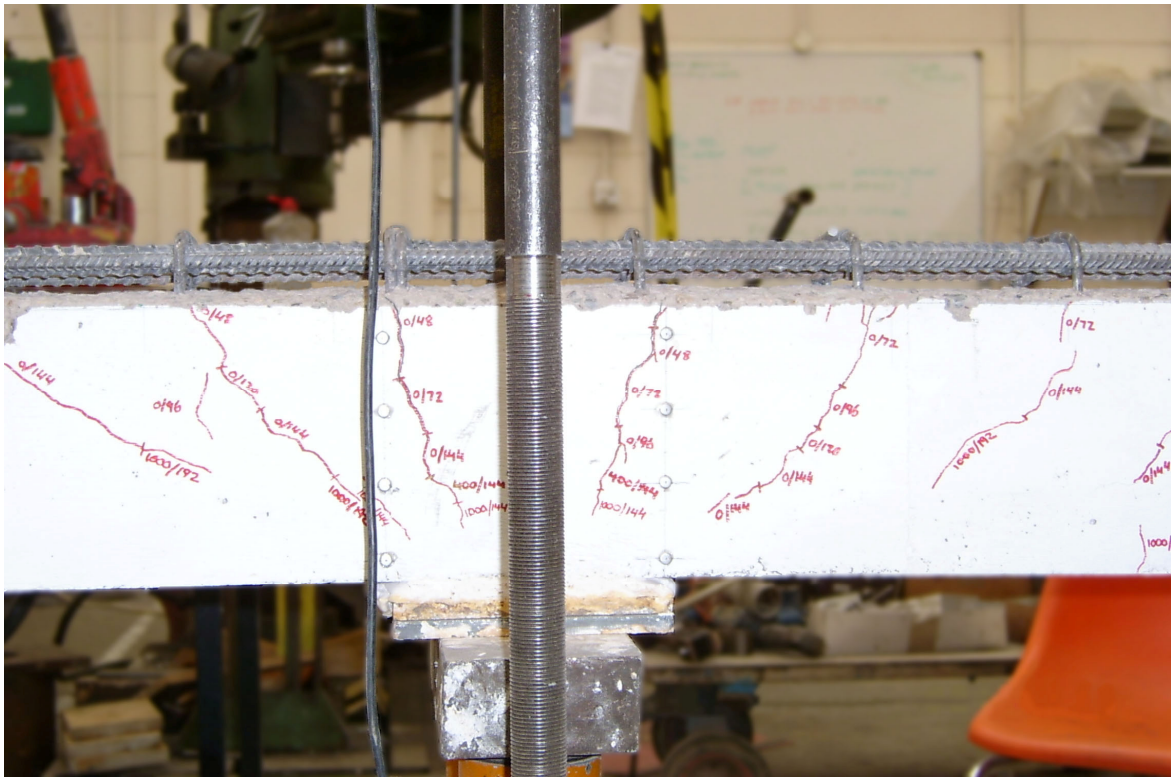

Fig. 6.1: Typical flexural crack pattern for breakout over the central support

Crack widths at non-breakout locations also increased during the breakout process due to moment transfer from the breakout region. Non-breakout crack widths usually reached the 0.3mm limit for the maximum breakout length under service load.

Specimens to be repaired were cast with the relevant portions of reinforcement exposed. The crack pattern that occurred during initial loading to service load differed from that for the progressive breakout specimens (for the maximum breakout length) as a portion of the tension reinforcement was exposed before loading began. Pre-repair loading caused a significant widening of the first crack within the breakout length. Due to the lack of bond between the steel and the concrete, further crack formation within the exposed length was suppressed. This crack pattern was not representative of cracking that would occur after breakout of concrete from an "initially fully bonded" specimen. Thus, progressive breakout specimens gave a more realistic representation of the pre-repair crack pattern that would occur in practice.

The influence of the breakout / repair procedure on the test failure modes was of interest in this study. Flexural failures were identified by concrete crushing or significant crack widening associated with reinforcement yielding at maximum hogging and sagging moment locations. Moment redistribution close to ultimate load was assessed by examining the output from the reaction load cells. Shear failures occurred quite suddenly and were identified by severe diagonal cracking. Shear failures occurred between the central support and the inner point load within one of the spans (where the shear force was largest, Fig. 3.9).

Calculated failure loads (assuming reinforcement was fully bonded) and measured failure loads of all test specimens are displayed in Table 6.1. The expected and actual failure modes are also included. The expected failure load of each specimen (for a fully bonded section) was calculated as described in Section 3.5 using actual material properties from Table 5.5. The measured failure load of a test specimen was taken as the maximum applied load recorded for that specimen.

Member	Calc flexural failure load (kN)	Calc shear failure load (kN)	Calc failure mode	Test failure load (kN)	Test failure mode	Failure location	P_{test} / P_{calc}
AN11	115.7	187.9	Flexural	128.4	Flexural	CS & LS	1.11
AN21	149.7	184.8	Flexural	162.4	Shear	RS	1.08
AN23	212.0	206.2	Shear	225.8	Shear	LS	1.09
AB11H	85.8	178.8	Flexural	81.7	Shear	RS	0.95
AB11S	85.8	178.8	Flexural	88.9	Flexural	LS	1.04
AB21H	149.7	184.8	Flexural	178.8	Flexural	RS	1.19
AB21S	149.7	184.8	Flexural	176.1	Shear	RS	1.18
AB23H	212.0	206.2	Shear	212.6	Shear	RS	1.03
AB23S	212.0	206.2	Shear	225.4	Shear	RS	1.09
AB34H	238.7	210.7	Shear	256.3	Shear	RS	1.22
AB34S	238.7	210.7	Shear	256.6	Flexural	LS	1.22
AB12H	163.8	199.7	Flexural	200.3	Flexural	RS	1.22
AB22H	177.5	199.7	Flexural	193.0	Flexural	LS	1.09
PR23H	230.7	210.1	Shear	273.9	Shear	LS	1.30
PR23S	230.7	210.1	Shear	232.5	Shear	RS	1.11
UR21H	152.8	184.8	Flexural	198.5	Flexural	RS	1.30
UR21S	152.8	184.8	Flexural	199.4	Flexural	CS &RS	1.30
UR23H	230.7	210.1	Shear	279.6	Flexural	RS	1.33
UR23S	230.7	210.1	Shear	219.2	Shear	RS	1.04
UR34H	214.8	207.1	Shear	279.4	Shear	LS	1.35
UR34S	279.0	216.0	Shear	316.2	Flexural	CS & LS	1.46

Table 6.1: "Fully bonded" calculated and experimental failure loads of all test specimens

Note: The location of failure is denoted by the abbreviations LS, CS & RS representing failures within the left span, at the central support and within the right span respectively. Two failure locations are quoted for some flexural failures as concrete crushing was observed at the central support and within one of the spans simultaneously.

Before the influence of breakout or repair on the ultimate load of a specimen can be assessed, the "as new" failure loads must first be validated (relative to those predicted by BS 8110 **[61]**). The experimental flexural failure load of AN11 was 11% greater

than the calculated value. The flexural strength of AN21 was greater than the calculated value (with a shear failure occurring during testing). The experimental failure load of AN23 exceeded the predicted flexural failure load by 7% before also failing in shear. Thus, the flexural strength was greater than predicted by BS 8110 **[61]** for all control specimens. This can be attributed to a number of assumptions made during the calculation process. The beneficial effect of strain hardening of tension reinforcement was ignored. Section 4.5.1 discusses the effect of load dispersion near point loads and supports and shows the stress in the reinforcement at the central support was approximately 80% of that predicted by the conventional bending moment diagram. The moment capacity of the central support cross-section could effectively be 25% greater than predicted. Even though the bending moment diagram within the spans is an accurate representation of the steel stress, the effect of load dispersion at the central support could increase the predicted failure load by approximately 12.5%. Discrepancies in ultimate load may also occur if the distribution of moment within the members does not match the moment balance predicted from the required redistribution or BS 8110 **[61]** rules on allowable redistribution.

The predicted shear failure load of AN21 was 12% less than the measured failure load. However, the shear failure load of AN23 was 9% greater than the calculated value. Note: As stated in Section 3.5.2, insufficient shear reinforcement was included to ensure a flexural failure in all specimens (a shear failure was expected in AN23). As the maximum shear force in the member was calculated according to the predicted bending moment diagram at ultimate load, the shear failure load was also affected by the actual bending moment diagram achieved during testing.

6.3 Analysis of Demec gauge readings

6.3.1 Strain distribution graphs

Surface strains were measured at sections of peak / trough moment, i.e. at the left-most point load and at the central support, using a Demec gauge. The Demec gauge calibration factor was provided by the manufacturer. As mentioned in Section 5.5.3, Demec readings were taken from both sides of a member. The average of the readings from corresponding pairs of Demecs (on either side of the beam) was calculated and used to plot the strain profile throughout the section depth. Linear regression analysis was used to obtain the equation of the best fit line to the strain profile at a given section. This equation enabled calculation of the strain at any depth within the section, the section curvature, and the neutral axis depth for each load increment.

Before loading began on a given specimen, Demec readings were taken to provide a datum for "zero" strain. These datum readings were usually taken after completion of the apparatus set-up. At this stage however, the beam was under load from the self-weight of the apparatus. To examine the effect of this load on the maximum strains within a specimen, Demec readings were taken just after placement of the specimen on the reaction load cells and also after completion of the apparatus set-up, during the set-up of AN21. Both sets of readings were compared and the maximum recorded strain in the specimen was 30×10^{-6} (over the central support). The strain on the beam due to the self-weight of the apparatus was therefore considered negligible and was ignored in subsequent analyses.

Fig. 6.2 shows a sample strain distribution graph beneath the left-most load of AN23. Manipulation of the best fit line equation enabled calculation the strain at any depth.

$$\varepsilon = (114.25 - y) \times 1.08 \times 10^{-5} \qquad 6.1$$

Note: y is measured from the bottom face of the beam. The maximum concrete compression strain just below the left point load is given by setting "y" in the best fit line equation equal to 200. Thus, the extreme fibre concrete compression strain was $\varepsilon = (114.25 - 200) \times 1.08 \times 10^{-5} = -0.00093$.

To calculate the strain in the tension steel, the height of the reinforcement in the section is taken as the sum of the cover to the outside of the steel plus the radius of the larger reinforcement bar. Within the span of AN23, the height of the tension reinforcement was taken as 25 + 8 = 33mm. Thus, the strain in the bonded tension reinforcement was $\varepsilon = (114.25 - 33) \times 1.08 \times 10^{-5} = +0.00088$.

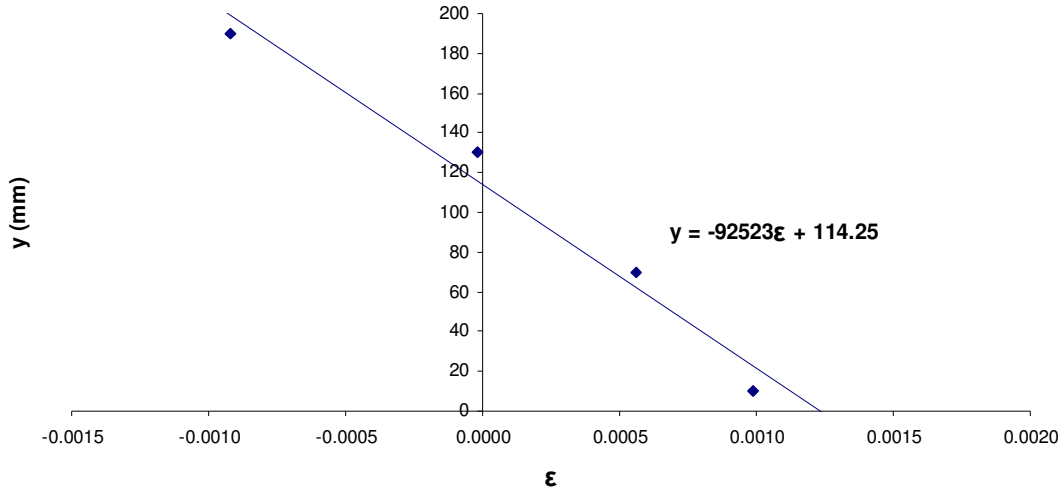

Fig. 6.2: Strain distribution beneath the left load in the left span of AN23 under service load

The height of the neutral axis is calculated by setting ε in the best fit line equation equal to zero. From Equation 6.1, the distance from the bottom of the beam to the neutral axis was y = 114.25mm. The compression zone depth for the section beneath the left load was then x = 200 – 114.25 = 85.75mm. As the effective depth at this cross-section was 167mm, the compression zone depth ratio was x / d = 85.75 / 167 = 0.51. A similar calculation is used for the compression zone depth ratio at the central support, although "y" was measured from the compression face.

The radius of curvature at a given cross-section was equal to the slope of the strain distribution graph. From Fig. 6.2, the radius of curvature of AN23 beneath the left load (under service load) was R = 92523mm = 92.523m. The section curvature was then calculated from $1/R = 1 / 92.523 = 0.011 m^{-1}$.

The pre-repair behaviour of specimens cast with a portion of the reinforcement exposed should be similar to specimens subjected to progressive breakout, at the maximum breakout length. However, as mentioned in Section 6.2, the pre-repair

crack patterns near the breakout region were affected by the reinforcement being exposed before loading began. Due to the wider crack spacing, measured strains were strongly affected by whether cracks formed within the gauge length or not. Consequently, the unrealistic crack patterns of specimens cast with a portion of the reinforcement exposed caused inaccurate pre-repair strain measurements in these specimens.

Adjustment of the strain readings from specimens repaired under service load was carried out at the data analysis stage to reflect the more realistic pre-repair strains of specimens subjected to progressive breakout. Since the magnitude of the pre-repair strains in unloaded repair specimens was small (and relatively unaffected by the position of cracks within the substrate), adjustment of the strain measurements in these specimens was not considered necessary.

The strain datum adjustment for specimens repaired under service load was carried out as follows. Firstly, the service load strain values for progressive breakout specimens (for the maximum breakout length) were calculated for each set of Demecs. These strains were then subtracted from the pre-repair service load strain readings from the corresponding repair specimens (cast with a portion of reinforcement exposed). The resulting values represented "zero datum" strain readings for the repair specimens to ensure the service load strain for the repair specimens was the same as for the corresponding progressive breakout specimens (for the maximum breakout length). The datum readings for the repair specimens were then replaced accordingly. This datum adjustment rendered any strain readings prior to placing of the repair material useless, but these strain patterns were already examined from the progressive breakout specimens. Post-repair strain readings from specimens repaired under service load (during loading to failure) represented the strains that would have occurred if specimens subjected to progressive breakout were repaired under service load.

6.3.2 Extreme fibre compression strains

If a repair is cast while the specimen carries load, the altered stress pattern within the member remain "locked in". Increases in concrete compression strain that occur during the breakout process may cause a reduction in the flexural capacity (and / or

ductility) of the repaired specimen. Previous research **[2]** has shown that the concrete compression strain at the breakout location increases with the breakout length to maintain compatibility between the exposed steel and the substrate. As moment transfers away from the breakout location during breakout, increases in the compression strain may also occur elsewhere. Therefore, variations in the concrete compression strains at both breakout and non-breakout locations were investigated.

Section 6.3.1 describes the calculation of the strain at any depth from the measured strain distribution. Fig. 6.3 plots the extreme fibre concrete compression strain throughout breakout on AB23H and AB23S at both breakout and non-breakout locations. Each dataset is identified by the specimen name and the cross-section being considered. For example, "AB23H – non breakout" refers to the compression strain variation at the left load in the left span as the breakout length increased over the central support of AB23H. Tables 6.2 & 6.3 display the changes in compression strain throughout breakout for all progressive breakout specimens at breakout and non-breakout locations respectively.

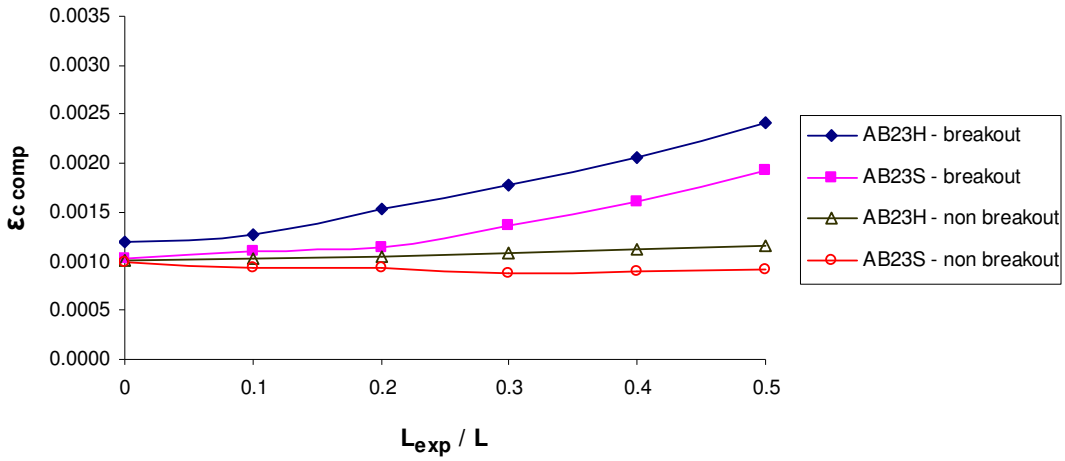

Fig. 6.3: Plot of maximum concrete compression strains as breakout increased on AB23H and AB23S

Specimen	Initial	Final	Difference	% diff
AB11H	0.0018	0.0042	+0.0024	+132%
AB21H	0.0011	0.0021	+0.0010	+90%
AB23H	0.0012	0.0024	+0.0012	+102%
AB34H	0.0013	0.0026	+0.0013	+95%
AB11S	0.0009	0.0018	+0.0009	+102%
AB21S	0.0008	0.0016	+0.0008	+98%
AB23S	0.0010	0.0019	+0.0009	+87%
AB34S	0.0013	0.0024	+0.0012	+91%

Table 6.2: Service load compression strains at breakout location before and after breakout

Specimen	Initial	Final	Difference	% diff
AB11H	0.0012	0.0013	+0.0001	+9%
AB21H	0.0007	0.0008	+0.0001	+18%
AB23H	0.0010	0.0012	+0.0002	+16%
AB34H	0.0011	0.0013	+0.0002	+17%
AB11S	0.0017	0.0018	+0.0001	+6%
AB21S	0.0009	0.0008	-0.0001	-11%
AB23S	0.0010	0.0009	-0.0001	-10%
AB34S	0.0012	0.0012	0.0000	0%

Table 6.3: Service load compression strains at non-breakout location before and after breakout

Table 6.2 shows the extreme fibre compression strain at the breakout location generally doubled during concrete breakout. Increases in compression strains at non-breakout locations due to transfer of moment are modest in comparison (Table 6.3). This suggests initial concerns that the transfer of moment from the breakout location could cause overstressing in other parts of the structure are largely unfounded. The increase in compression strain at the breakout location is far more critical to the flexural strength of the member.

The rate of increase of extreme fibre compression strains during loading of the repaired specimen to failure was also of interest, particularly at the repair location. Compression strains were calculated at service load (55% of the ultimate load) and

also at 90% of the ultimate load. Increases in compression strain were observed only as far as 90% of the ultimate load as plastic hinge formation beyond this load would severely influence the observed increases. Table 6.4 displays the observed increases in compression strain during loading to failure of the repaired specimens at the repair cross-section. The corresponding increases in compression strain in the control specimens are also included (e.g. AN21 – H represents the strains at the maximum hogging moment location of AN21).

Specimen	55%	90%	Increase	% incr
AN21 - H	0.0015	0.0019	+0.0004	+26%
UR21H	0.0022	0.0028	+0.0006	+27%
AN21 - S	0.0008	0.0014	+0.0006	+75%
UR21S	0.0018	0.0022	+0.0004	+22%
AN23 - H	0.0009	0.0016	+0.0007	+78%
PR23H	0.0009	0.0017	+0.0008	+88%
UR23H	0.0027	0.0032	+0.0005	+19%
AN23 - S	0.0009	0.0016	+0.0007	+78%
PR23S	0.0011	0.0019	+0.0008	+73%
UR23S	0.0022	0.0028	+0.0006	+27%
UR34H	0.0023	0.0030	+0.0007	+30%
UR34S	0.0026	0.0034	+0.0008	+31%

Table 6.4: Compression strain at repair location at 55% & 90% of ultimate load

6.3.3 Exposed steel strains

Before progressive breakout began on a given specimen, the strain in the bonded tension steel was assumed equal to the concrete surface strain at the same level as the steel (calculated as described in Section 6.3.1). Demec gauge readings were taken from buttons glued onto the exposed steel once initial concrete breakout had taken place. Initial readings were taken from the steel for an exposed length of 200mm, before any further loading was applied after concrete breakout. These readings acted as a "temporary" datum to calculate the change in strain in the exposed steel. To approximate the strain in the exposed reinforcement, the increase in strain measured

directly from the reinforcement after breakout was added to the concrete surface strain at the depth of the reinforcement, immediately prior to breakout. This assumed the strain in the bonded steel just before breakout was equal to the strain in the newly exposed steel. The actual change in strain upon initial exposure was difficult to quantify as different strain datums were used for the bonded and unbonded steel.

Fig. 6.4 shows a plot of exposed steel strains of AB23H and AB23S as breakout increased. The change in steel strain due to the initial breakout could not be measured so it is not plotted. Between the initial and final breakout intervals, the strain reduced by 9% - 10% for both specimens. This reduction was caused by the transfer of moment from the breakout location at the length of breakout increased. The increase in the lever arm to maintain compatibility between the exposed steel and the substrate also contributed to the reduction in reinforcement strain. Numerical analysis results are used to assess the overall change in exposed reinforcement strain throughout breakout (Section 8.3.3).

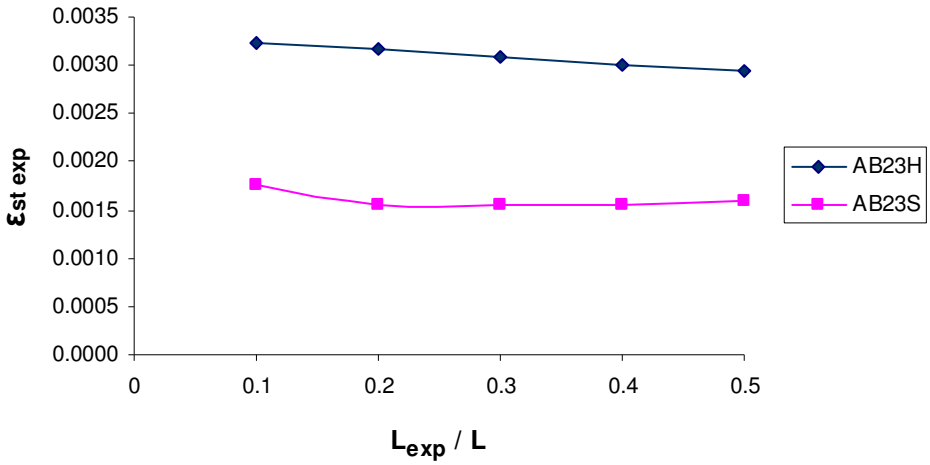

Fig. 6.4: Plot of exposed steel strains as breakout increased on AB23H and AB23S

The exposed steel strains from Fig. 6.4 are excessive (particularly the strain in the exposed steel of AB23H, which is greater than the yield strain of the steel). Due to the calculation procedure used, the magnitudes of the exposed steel strains were primarily influenced by the "fully bonded" strains before breakout commenced. Strain measurements from the surface of the concrete were significantly affected by the location of cracks in relation to the Demecs. Fig. 6.5 shows a typical crack pattern near the central support of a "fully bonded" test specimen. Cracks generally

coincided with the positions of the shear reinforcement (i.e. crack spacing ≈ 125mm). As the gauge length (150mm) was similar to the spacing of the flexural cracks, an accurate representation of the mean strain in the steel is calculated when one crack occurs within the gauge length. However, due to the positioning of the shear links within the test specimens (in relation to the central support), two cracks generally occurred within the gauge length. Consequently, "measured" bonded steel strains were appreciably greater than the mean strain in the steel.

Fig. 6.5: Typical crack pattern above the central support

For all specimens to be repaired, a portion of the reinforcement was exposed before initial loading began on the member. Demec gauge readings taken from the exposed steel before loading commenced were used as a zero datum. The repair was cast around the "previously exposed" steel so direct measurement of strain from the steel was no longer possible. Strain readings from Demecs on the repair material were used in a separate linear regression analysis to measure the change in the previously exposed steel strain. This strain was added to the strain value measured immediately prior to placing of the repair material. This assumed that the tensile strain in the steel remained constant during the repair curing period. A slight reduction was expected to

occur as the steel attempted to reduce the shrinkage of the repair material but this could not be measured and has been neglected.

6.3.4 Section curvature

Fig. 6.6 is a plot of section curvatures for AB23H and AB23S at sections of maximum hogging and sagging moment under service load. Curvatures at a particular location should be equal for a given reinforcement combination before breakout commenced. For example, the initial curvature of "AB23H – breakout" should equal that for "AB23S – non breakout" and vice versa. The initial curvature at the central support was greater than that within the spans for all progressive breakout specimens. This was primarily caused by the service load moment at the central support generally exceeding that within the spans. Note: The position of cracks in relation to the Demecs also influenced the "measured" curvature. Significant increases in curvature were observed at the breakout locations due to the loss of bond between the steel and the concrete. The changes in curvature at breakout and non-breakout locations throughout breakout are displayed in Table 6.5 & 6.6 respectively.

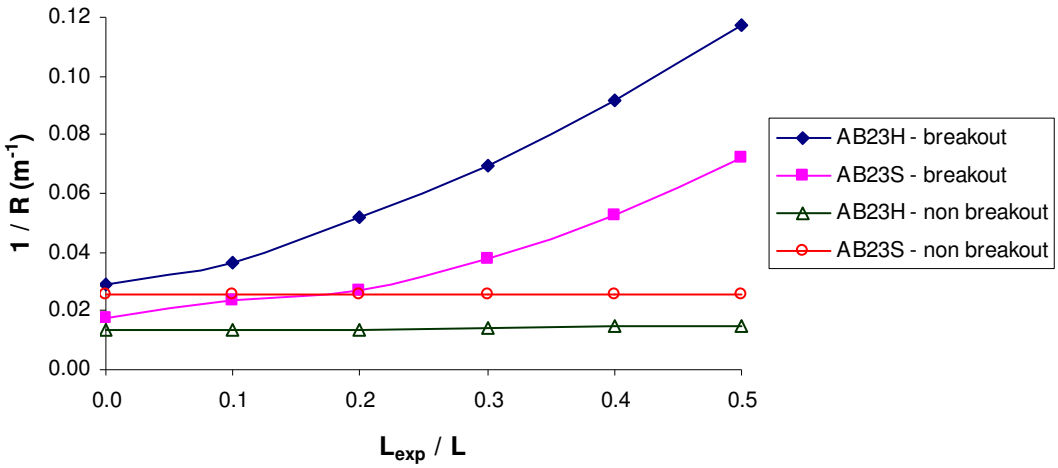

Fig. 6.6: Plot of maximum section curvatures as breakout increased on AB23H and AB23S

Specimen	Initial	Final	Difference	% diff
AB11H	0.025	0.138	+0.113	+462%
AB21H	0.025	0.099	+0.075	+302%
AB23H	0.029	0.117	+0.088	+302%
AB34H	0.026	0.103	+0.078	+301%
AB11S	0.012	0.044	+0.032	+272%
AB21S	0.015	0.076	+0.061	+406%
AB23S	0.017	0.072	+0.055	+314%
AB34S	0.015	0.069	+0.053	+345%

Table 6.5: Service load curvatures at breakout location before and after breakout

Specimen	Initial	Final	Difference	% diff
AB11H	0.013	0.015	+0.002	+15%
AB21H	0.011	0.013	+0.002	+21%
AB23H	0.013	0.015	+0.002	+14%
AB34H	0.015	0.018	+0.002	+14%
AB11S	0.022	0.024	+0.002	+8%
AB21S	0.019	0.020	+0.001	+4%
AB23S	0.026	0.026	0.000	0%
AB34S	0.021	0.021	0.000	0%

Table 6.6: Service load curvatures at non-breakout location before and after breakout

Consider the schematic diagrams illustrating the change in strain distribution due to concrete breakout (Fig. 6.7). The section curvature can be related to the extreme fibre compression strain and the neutral axis depth, x. Table 6.2 shows a general increase in extreme fibre compression strain of approximately 100% occurred during breakout. Assuming linear elastic behaviour of concrete in the compression zone and neglecting the tensile strength of concrete, doubling the compression strain reduces the neutral axis depth by 50% as the shaded area must remain constant to maintain the same compression force. This in turn causes the section curvature to increase by a factor of 4 (or a 300% increase). This is broadly reflected in the observed curvature increases at the breakout location (Table 6.5).

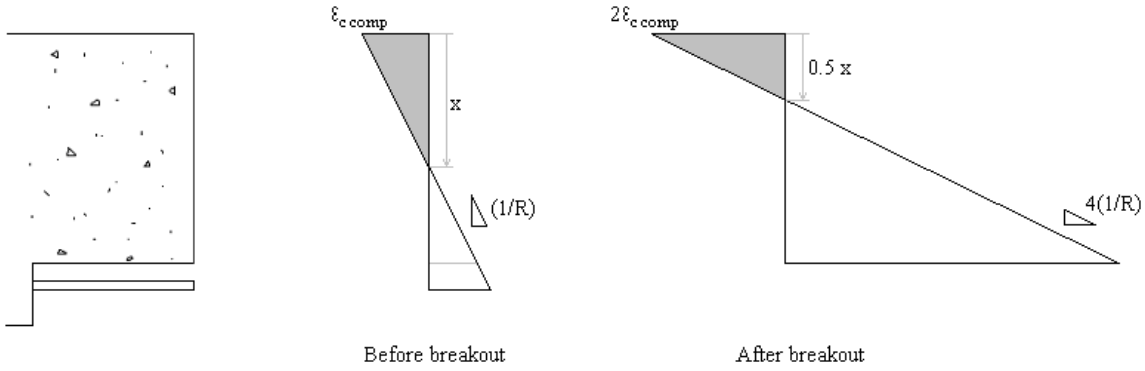

Fig. 6.7: Schematic diagram of change in strain distribution during breakout

Section curvatures of specimens repaired under service load, prior to placing of the repair material, were identical to those for specimens subjected to progressive breakout for the maximum breakout length (due to the adjustment of the strain datum). For all load relief conditions, the post-repair curvature at the repair cross-section was calculated using only Demec readings from the substrate in the linear regression analysis. Curvatures were calculated for each load increment during loading to failure of the repaired specimens. This enabled calculation of the flexural stiffness of the repaired members.

6.3.5 Flexural stiffness

The bending moment and corresponding curvature were calculated for each load step. This enabled plotting of moment vs. curvature for sections of maximum hogging and sagging moment. The slope of the resulting plot gives the flexural stiffness of the member. The flexural stiffness at any particular section reduced throughout loading. Early flexural cracking caused an initial reduction in stiffness and significant reductions occurred near ultimate load if yielding of reinforcement occurred. To obtain a comparable measure of flexural stiffness between specimens, the secant slope of the moment-curvature plot was determined between 55% & 90% of the ultimate load of the "fully bonded" specimen. This range of moment-curvature values was chosen because flexural cracking was well established at service load (55% of the ultimate) and reductions in flexural stiffness due to plastic hinge formation usually occurred beyond 90% of the "fully bonded" ultimate load.

Fig. 6.8 shows a plot of moment against curvature as load increased to failure on AN23. The moment and curvature measurements were taken at the section of maximum sagging moment beneath the left load in the left span and at the section of maximum hogging moment at the central support. The flexural stiffness at the section being considered was represented by the slope of the relevant best fit line. Significant flexural cracking was established at service load by previous load cycles. Therefore, the area of reinforcement at a particular section influenced the flexural stiffness. The stiffness of AN23 within the spans was greater than at the support as the area of tension reinforcement within the spans was greater.

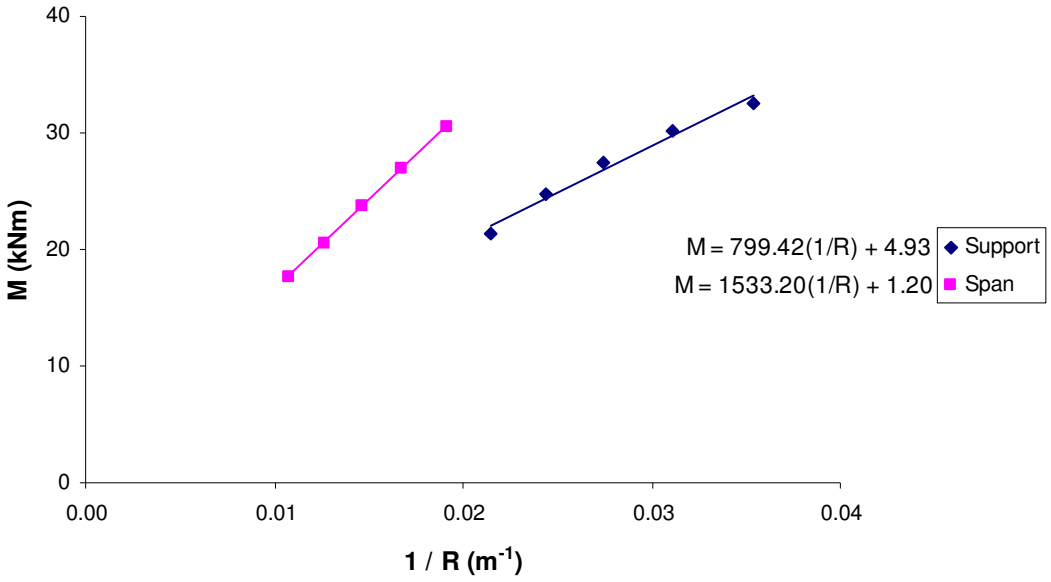

Fig. 6.8: Plot of moment vs. curvature as loading increased to failure on AN23

Fig. 6.9 shows plots of moment vs. curvature for UR23H and UR23S at both repair and non-repair locations. The curvatures at the repair locations were significantly greater than at non-repair locations due to the increase in curvature during concrete breakout, particularly for breakout over the central support (Fig. 6.6). In some cases, increases in stiffness occurred (relative to the corresponding "as new" specimen) due to a greater tension stiffening effect within the patch repair. Thus, although accumulated deformations are greater after "unpropped" repair, stiffness under increased loading tended to increase. Table 6.7 displays the flexural stiffness values

(in kNm^2) recorded for all repaired specimens. The corresponding stiffness values from the control specimens are also included.

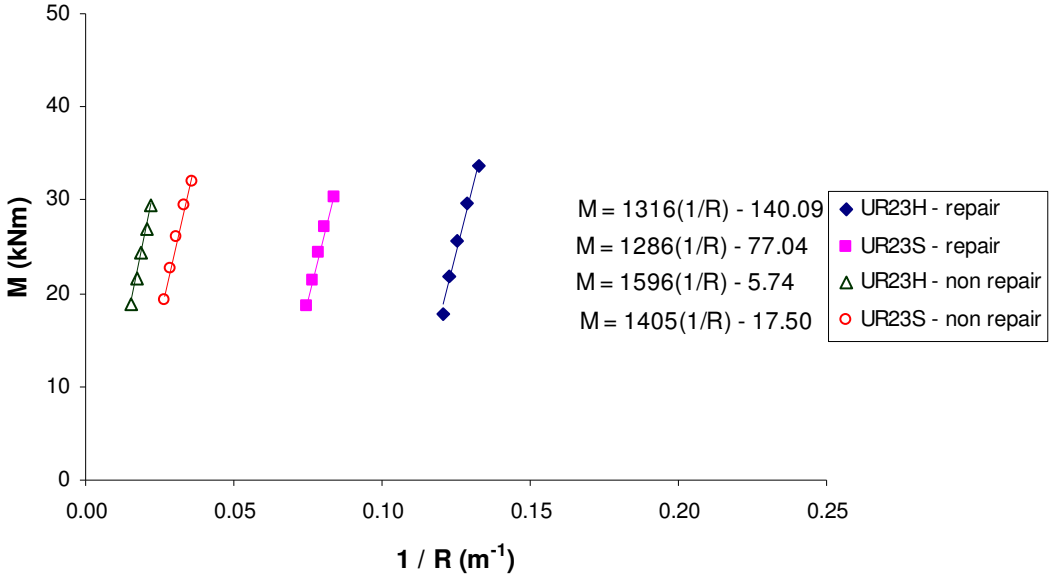

Fig. 6.9: Flexural stiffness at maximum hogging and sagging moment locations during loading to failure of repaired specimens

	AN	UR H	UR S	PR H	PR S
21 "support"	834	1133	1151	-	-
21 "span"	724	813	1362	-	-
23 "support"	799	1316	1405	748	816
23 "span"	1533	1596	1286	1329	899
34 "support"	-	1518	1602	-	-
34 "span"	-	2025	1488	-	-

Table 6.7: Flexural stiffness at maximum hogging and sagging moment locations during loading to failure of "as new" and repaired specimens (kNm^2)

6.4 Analysis of load cell output

6.4.1 Calculation of bending moment

The test load arrangement is shown in Fig. 3.4. The bending moment was calculated from measured values of applied load and reactions. The effect of load dispersion at point loads was neglected. The maximum sagging moment in a specimen was taken as the average of that under the outer point loads in the two spans and was calculated from

$$M_{sag} = (0.9)\ (R_L + R_R)/2 \qquad 6.2$$

where R_L = left support reaction
R_R = right support reaction

The hogging moment at the central support was calculated as the mean of the values calculated by considering equilibrium in both the left and right spans.

$$M_{hog} = (1.1 + 0.9)\ (0.25(P + R_{Total})/2) - (2.0)\ ((R_L + R_R)/2) \qquad 6.3$$

where P = total applied load
R_{Total} = sum of the support reactions

Note: Although P should equal R_{Total}, slight differences were observed (Fig. 5.10). When calculating the hogging moment over the support, the applied load was taken as the average of the "applied load" load cell reading and the sum of the reaction load cells readings.

When simplified, this equation becomes

$$M_{hog} = 0.25(P + R_{Total}) - (R_L + R_R) \qquad 6.4$$

The moment ratio was defined as the maximum hogging moment in the specimen (above the central support) divided by the maximum sagging moment (beneath the outer point loads). Comparing values of moment ratio gave a convenient measure of the moment balance within a member, irrespective of the applied load.

$$\alpha_m = M_{hog} / M_{sag} \qquad 6.5$$

6.4.2 Bending moment transfer during concrete breakout

A reduction in flexural stiffness was observed at breakout locations due to loss of bond between the steel and the concrete. This caused moment transfer from the breakout location as the length of breakout increased. The moment ratio (defined in Section 6.4.1) is used to observe the transfer of moment throughout breakout. Fig. 6.10 shows a plot of moment ratio under service load as the breakout length increased above the central support of AB23H and within the left span of AB23S. Before breakout began, specimens of a given reinforcement combination were essentially identical. The balance of moment within corresponding "fully bonded" members was similar and this was reflected in their initial hogging : sagging moment ratios.

The maximum breakout length for all specimens was half the span length. As the breakout length over the central support increased, loss of section stiffness caused moment transfer from the central support to the spans. This resulted in a decrease in moment ratio with breakout. For breakout within the left span, moment transfer from the spans to the central support occurred. This caused the observed increase in moment ratio as the breakout length increased. In general, moment transfer due to concrete breakout was greater for breakout over the central support. The total changes in moment ratios and the service load hogging and sagging moments (due to progressive breakout on test specimens) are displayed in Table 6.8.

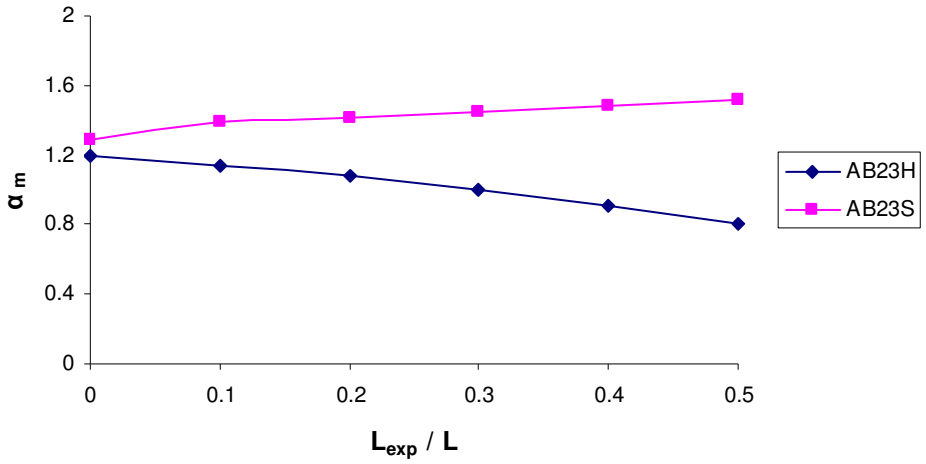

Fig. 6.10: Plot of hogging : sagging moment ratio as the breakout length increased on AB23H and AB23S

Specimen	Initial M_{hog}	Final M_{hog}	% diff M_{hog}	Initial M_{sag}	Final M_{sag}	% diff M_{sag}	Initial α_m	Final α_m	% diff α_m
AB11H	10.65	7.28	-32%	8.73	10.26	+18%	1.22	0.71	-42%
AB21H	22.09	18.17	-18%	10.32	12.08	+17%	2.14	1.50	-30%
AB23H	20.99	16.04	-24%	17.62	19.80	+12%	1.19	0.81	-32%
AB34H	26.02	20.57	-21%	20.68	23.09	+12%	1.26	0.89	-29%
AB11S	10.50	12.40	+18%	8.78	7.92	-10%	1.20	1.57	+31%
AB21S	20.47	22.67	+11%	11.21	10.24	-9%	1.83	2.21	+21%
AB23S	22.00	24.29	+10%	17.10	16.02	-6%	1.29	1.52	+18%
AB34S	23.37	26.93	+15%	21.83	20.18	-8%	1.07	1.33	+25%

Table 6.8: Maximum hogging and sagging moments at service load before and after breakout

Note: Initial "fully bonded" values of moment ratio under service load are appreciably greater than the corresponding values of hogging : sagging reinforcement ratio (α_r in Table 5.3) for all progressive breakout specimens. This is attributed to the influence of load arrangement on tension stiffening and thus, the balance of moments within "fully bonded" specimens as described in Section 4.5.2.

6.4.3 Bending moment variation during loading to failure

The change in moment balance for a repaired specimen can be compared with that for the equivalent "as new" specimen to assess the influence of the repair process on the moment balance within a member. Fig. 6.11 shows a sample plot of the hogging : sagging moment ratio as AN23 was loaded to failure. Note: The final load cycle to failure began at ~27.5% of the ultimate load (the load maintained on the member overnight). Previous load cycles had continued to 55% of the ultimate load so flexural cracking was well established. Before flexural cracks reopened, the bending moment was similar to the elastic bending moment (α_m = 1.32, from Fig. 3.5) as the stiffness was dependant on the gross section properties. As loading increased, the greater tension reinforcement area within the spans caused the balance of moments to shift from the central support to the spans. The moment balance remained constant up to approximately 55% of the ultimate load as previous load cycles continued to this point. Beyond 55%, the rate of change of moment balance increased. Yielding of reinforcement initiated over the central support at approximately 65% of the ultimate load and moment redistribution to the spans took place. Since the allowable redistribution in AN23 was less than the required redistribution, the fully plastic bending moment diagram of AN23 was not achieved. Hinge formation over the central support was evident before the observed shear failure occurred.

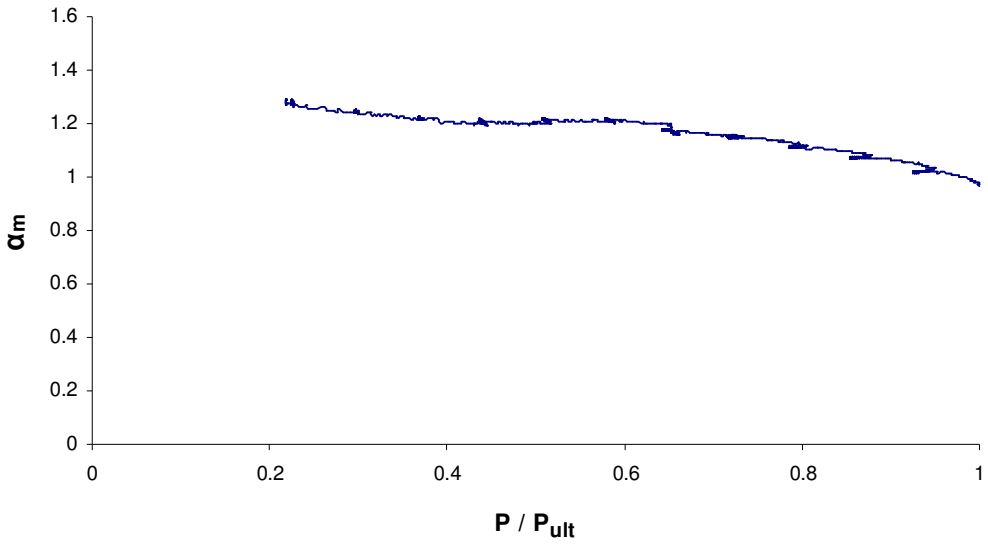

Fig. 6.11: Plot of hogging : sagging moment ratio during loading to failure of AN23

The change in moment balance can be assessed between specimens by comparing values at 55% & 90% of the ultimate load. Table 6.9 shows values of moment ratio for all repaired specimens. Relevant control specimen moment ratios are also included.

Specimen	55%	90%	Difference	% diff
AN21	1.49	1.50	+0.01	+1%
UR21H	1.39	1.70	+0.31	+22%
UR21S	1.55	1.63	+0.08	+5%
AN23	1.21	1.07	-0.14	-12%
PR23H	1.17	1.12	-0.05	-4%
UR23H	0.94	1.13	+0.19	+20%
PR23S	1.02	1.12	+0.10	+10%
UR23S	1.03	1.09	+0.06	+6%
UR34H	0.73	0.88	+0.15	+21%
UR34S	1.01	0.99	-0.02	-2%

Table 6.9: Hogging : sagging moment ratios at 55% & 90% of ultimate load

6.5 Analysis of displacement transducer output

6.5.1 Midspan displacements

Exposure of tension reinforcement within a specimen causes an increase in displacement. Midspan displacements were monitored during testing to ensure service load displacements of specimens with exposed reinforcement were not excessive. It should be noted that the displacement transducers were removed during concrete breakout to prevent damage. They were repositioned immediately after each increment of breakout to give the same displacement reading as the displacement prior to that breakout increment. Thus, the increase in displacement during the breakout process could not be measured. The measurements quoted represent the total displacement (from the datum established for the "fully bonded" specimen before loading began), less the increases in displacement during the concrete breakout process.

Fig. 6.12 shows the change in midspan displacements (relative to the span length) under service load as breakout increased on AB23H and AB23S. Due to the symmetry of the AB23H, both midspan displacements were approximately equal and Fig. 6.12 shows the average of the left and right midspan displacements. An increase of 30% occurred during breakout over the support (to 50% of the span length). The left midspan displacement of AB23S increased by 29% as the breakout length increased within the left span. The change in right midspan displacement was negligible.

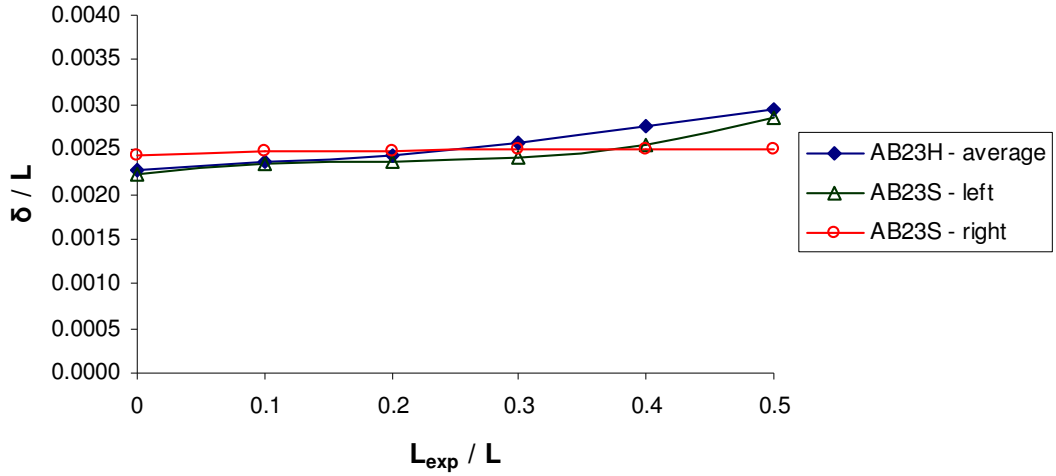

Fig. 6.12: Plot of displacement (relative to span length) as breakout increased on AB23H and AB23S

If a repair is to be carried out without temporary propping, it is desirable that serviceability limit state criteria are not exceeded while the reinforcement is exposed. Thus, service load displacements for the full extent of breakout are of interest. Table 6.10 displays the service load displacements for the progressive breakout specimens for the maximum breakout length. The pre-repair service load displacements of specimens repaired under service load are also included.

Progressive breakout specimens	Left displacement (mm)	Right displacement (mm)	Specimens repaired under load	Left displacement (mm)	Right displacement (mm)
AB21H	5.039	5.457	UR21H	6.342	5.773
AB21S	5.955	4.277	UR21S	6.785	3.898
AB23H	5.581	6.195	UR23H	6.785	6.897
AB23S	5.726	5.015	UR23S	8.334	4.498
AB34H	4.657	6.564	UR34H	6.147	5.974
AB34S	6.456	6.107	UR34S	8.850	5.023

Table 6.10: Midspan displacements under service load for progressive breakout specimens (maximum breakout length) and specimens repaired under service load (pre-repair)

6.5.2 Section rotation

The order of occurrence of plastic hinges (usually associated with a flexural failure) influences the moment redistribution within a member close to ultimate load. Plastic hinge formation can be visually observed but is more readily identified by examining section rotations as moment increases. It is therefore useful to monitor section rotations at locations where plastic hinge formation is likely.

Hinges will form at sections of maximum moment; namely at the central support and at the outer point loads in both spans. Fig. 6.13 shows a diagram of a specimen with hinges at sections of maximum hogging and sagging moments. Some simplifying assumptions were made to relate the measured midspan displacements to the rotations at each of the hinges. The member was assumed undeformed between plastic hinges. Also, rotations were assumed to remain small, so $\theta \approx \text{Sin}\ \theta \approx \text{Tan}\ \theta$.

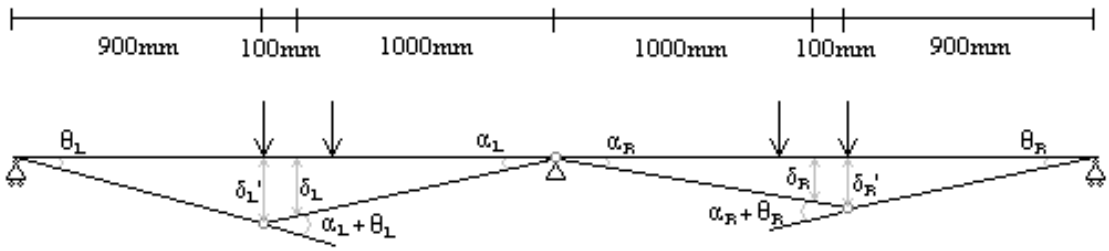

Fig. 6.13: Schematic diagram of specimen after plastic hinge formation

Consider initially section rotation at the central support. The rotation to the left of the central support can be related to the left midspan displacement δ_L by Equation 6.6.

$$\alpha_L = \delta_L / 1000 \qquad 6.6$$

The total hinge rotation at the central support is then given by

$$\alpha_L + \alpha_R = 0.001\ (\delta_L + \delta_R) \qquad 6.7$$

Now consider section rotation at the hinge within the left span. The rotation at the left pinned support is found from

$$\theta_L = \delta_L` / 900 = (1.1\ \delta_L) / 900 \qquad 6.8$$

The rotation at the left hinge is then calculated from

$$\alpha_L + \theta_L = \delta_L / 1000 + (1.1\ \delta_L) / 900 = 0.0022\ \delta_L \qquad 6.9$$

Similarly, the rotation at the hinge within the right span is $0.0022\ \delta_R$.

A plot of moment vs. rotation illustrates plastic hinge formation within a member loaded to failure. Fig. 6.14 plots moment vs. section rotation as UR23H was loaded to failure. Moment vs. rotation graphs were plotted for three likely positions of plastic hinge formation. The plots were continued until the load decreased from the ultimate load by 10% to display significant rotation at the plastic hinges. The plot shows initially similar moment vs. rotation patterns within both spans. Note: For a given applied load, the maximum sagging moment within both spans should be equal due to the symmetry of the loading about the central support. The moment capacity of the section within the spans should be greater than over the central support if the reinforcement remained fully bonded throughout (larger reinforcement area within the spans). However, the effect of load dispersion was much greater at the central support cross-section than within the spans (Section 4.5.1). Also, as the repair was cast under service load, tension stiffening within the patch repair was significant. Consequently, a larger moment is attained at the central support than within the spans for plastic hinge formation. No moment redistribution occurred near ultimate load (moment ratio remained constant) so the plastic hinges at the central support and within the right span formed simultaneously. A reduction in section rotation occurred within the left span due to hinge formation within the right span and at the central support.

Fig. 6.15 shows the moment vs. rotation plot for UR23S. The rotation on initial loading was greater within the left span (than the right span) as the repair was cast under service load in this span. As UR23S was loaded to failure, moment redistribution to the spans occurred at 90% of the ultimate load. After reaching its peak value the support moment reduced, consistent with the observed moment

redistribution to the spans. UR23S experienced a sudden shear failure so significant hinge rotation did not occur. Shear failure was denoted by a significant drop in moment carried by the member in Fig 6.15.

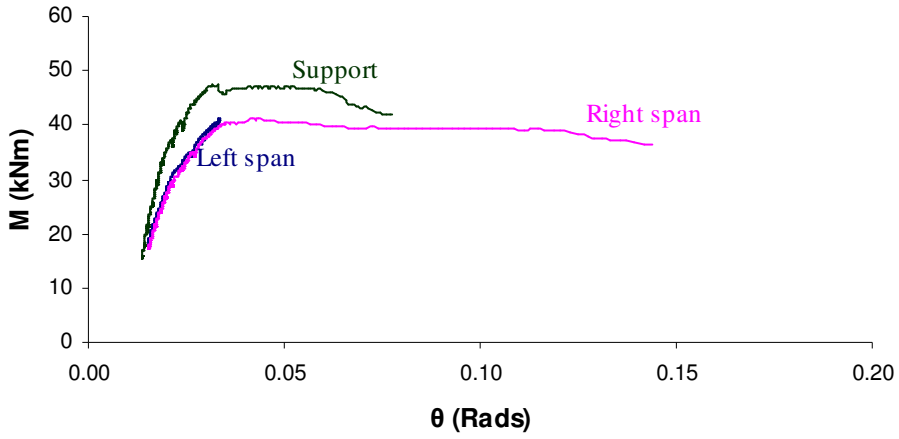

Fig. 6.14: Plot of moment vs. rotation during loading to failure of UR23H

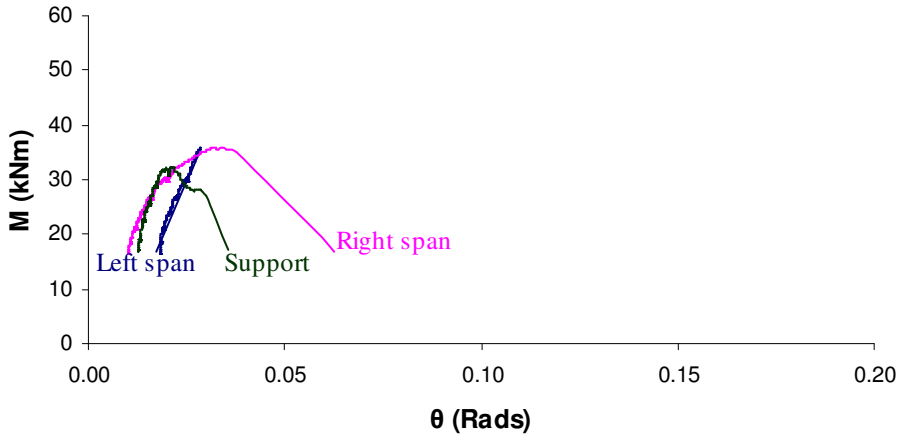

Fig. 6.15: Plot of moment vs. rotation during loading to failure of UR23S

6.5.3 Ductility

Section ductility is the capacity of a cross-section within a member to undergo plastic deformation without a significant loss of strength. Ductility can be quantified by comparing the rotation at ultimate load to that at yield of the reinforcement. θ represents the rotation at the section being considered.

$$\mu = (\theta_{ult} - \theta_y) / \theta_y \qquad 6.10$$

where θ_{ult} = rotation at ultimate load

θ_y = rotation at reinforcement yield

θ_{ult} was measured after a 10% drop in ultimate load as it is difficult to detect a true peak on a near horizontal trace. The section ductility was calculated for sections of maximum hogging and sagging moment (i.e. possible locations of hinge formation). The ductility of the member was then quantified from the hinge that underwent the largest rotation.

The ductility of UR23H can be quantified from its moment vs. rotation plot, Fig. 6.14. Consider initially, section ductility at the central support. The rotation at yield was approximately 0.031 and the final rotation recorded was 0.078. Therefore, the ductility at the central support was $\mu = (0.078 - 0.031) / 0.031 = 1.5$. Similarly, the ductility within the right span was $\mu = (0.144 - 0.035) / 0.035 = 3.1$. The ductility of UR23H was taken as that for the hinge within the right span. Table 6.11 includes the ductility of failure calculated for "as new" and repaired specimens. The location at which the ductility was measured is also included (LS, CS & RS represent the left span, central support and right span respectively).

	AN	UR H	UR S	PR H	PR S
21	1.3 (RS)	6.0 (RS)	7.4 (RS)	-	-
23	0.4 (LS)	3.1 (RS)	0.3 (RS)	0.1 (CS)	1.0 (RS)
34	-	0.2 (CS)	0.2 (LS)	-	-

Table 6.11: Ductility of failure of "as new" and repaired specimens

6.6 Summary

This chapter discussed calculation of useful measures of structural performance from test data. Strain measurements at sections of maximum hogging and sagging moments were used to construct strain distribution graphs, from which, extreme fibre concrete compression strains, tension steel strains and section curvatures were calculated. The applied load and support reactions were continually logged during testing and were used to calculate maximum hogging and sagging moments for a given load. Midspan displacements were also recorded throughout testing and were used to calculate rotations at sections of maximum moment.

Sample test results were also presented in this chapter. Initial observations suggest that significant increases in curvature occurred at the breakout location due to loss of composite action between the steel and the concrete. Appreciable increases in extreme fibre concrete compression strain occurred at the breakout location in conjunction with observed reductions in neutral axis depth. Loss of section stiffness caused significant moment transfer away from the breakout location but the increases in compression strain at non-breakout locations were small. This suggests initial concerns that moment transfer from the breakout location could cause overstressing in other parts of the structure were largely unfounded. Ultimate strength of repaired specimens was generally greater than the equivalent "as new" specimens, although in some cases, the mode of failure changed. Test results are examined in greater detail in Chapter 7 with particular attention paid to the influence of the parameters chosen for investigation on structural behaviour.

Chapter 7: Analysis of test results

7.1 Introduction

Chapter 6 discusses the manipulation of test data to attain useful measures of structural performance and illustrates sample results for reinforcement combination 23. This chapter will analyse these results and examine the influence of the parameters chosen for investigation. Measures of structural performance will be examined at both serviceability limit state (midspan displacements, crack widths) and ultimate limit state (failure load, ductility etc.). For progressive breakout specimens, the change in these measures of performance with increasing breakout length was described in Chapter 6. This chapter will focus on the influence of the other parameters investigated (for the maximum breakout lengths tested), namely; the position of breakout, the hogging : sagging reinforcement ratio and the reinforcement percentages. The same parameters are of interest in the repaired specimens, along with the effect of load relief during casting of the repair.

The analysis of behaviour when concrete is broken out is covered in Section 7.2, while that of beams repaired unloaded and under service load is discussed in Sections 7.3 & 7.4 respectively. The areas of structural performance of specific interest are:

- transfer of moment away from the breakout zone to other parts of the beam, the increase in deformation in these areas and the potential effects on strength and ductility once repair is completed
- loss of capacity while the beam is in the "weakened" condition with reinforcement exposed
- the effect of stresses "locked into" the repair section if the beam carries load when the repair is cast

7.2 Post-breakout behaviour

7.2.1 Serviceability limit state behaviour (entire member)

7.2.1.1 Moment transfer

The parameters that affect moment transfer during concrete breakout were investigated to assess whether breakout caused overstressing in other parts of the beam. Table 6.8 displays the increases in non-breakout moment under service load throughout breakout of concrete. Fig. 7.1 plots the increase in moment at non-breakout locations (that occurred during breakout to the maximum breakout length) against the hogging : sagging reinforcement ratio. Increases in moment ranged between 10% – 18% and the hogging : sagging reinforcement ratio had no apparent influence on the increase in non-breakout moment throughout breakout.

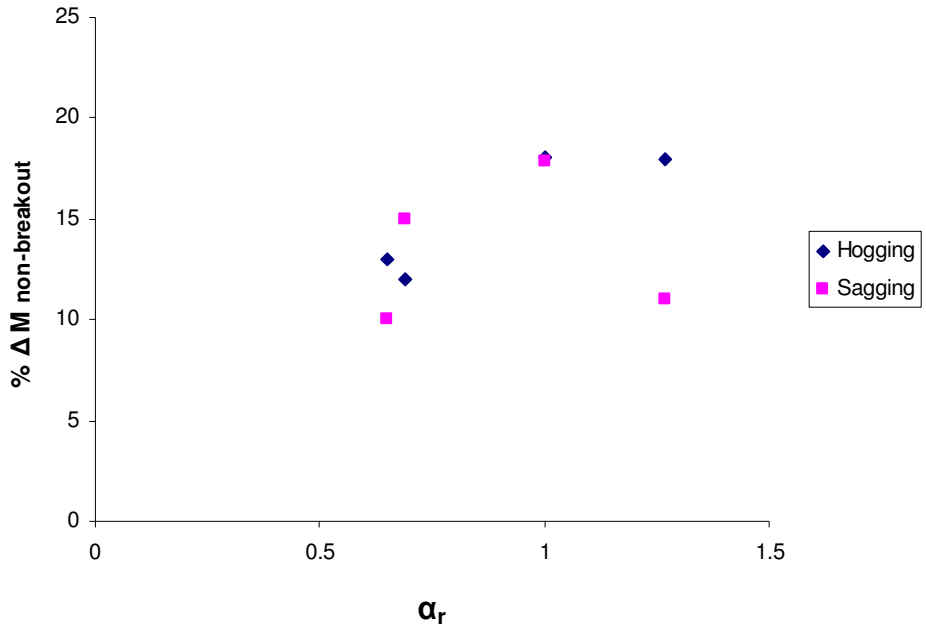

Fig. 7.1: Plot of increase in moment at non-breakout locations throughout breakout vs. reinforcement ratio

Variations in moment at a given location are closely linked to changes in section curvature. The influence of the chosen parameters on section curvature variation during concrete breakout highlights their effect on crack widths. As moment transferred to non-breakout locations during breakout, changes in section curvature at these locations were recorded and are displayed in Table 6.6. Fig. 7.2 plots the change in curvature at non-breakout locations (during breakout to the final breakout length) against hogging : sagging reinforcement ratio. The influence of the reinforcement ratio on the non-breakout curvature increase was insignificant. However, the observed increases in curvature within the spans for hogging breakout were greater than at the central support for sagging breakout.

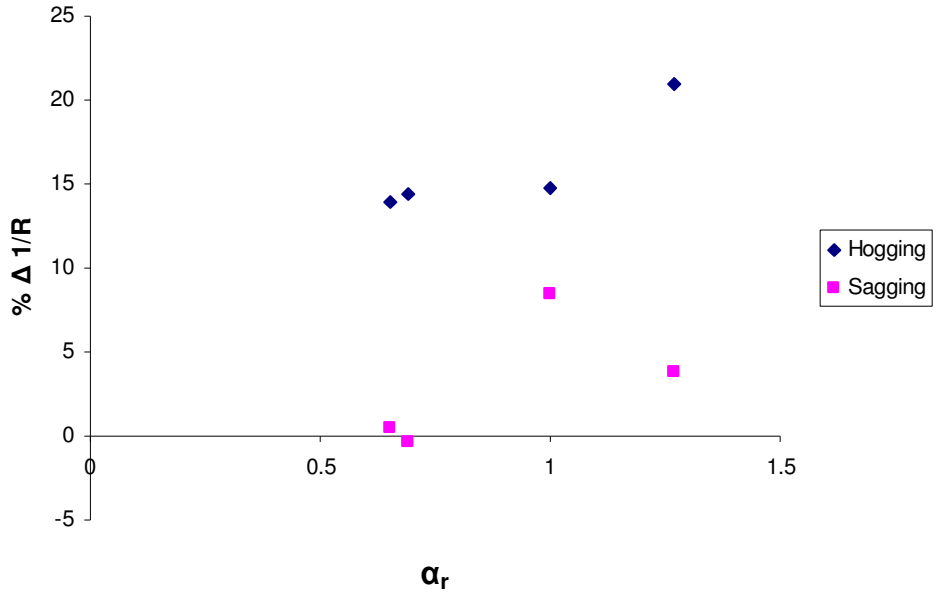

Fig. 7.2: Plot of increase in curvature at non-breakout locations throughout breakout vs. reinforcement ratio

Fig. 7.3 shows sketches of the deflected shapes before and after breakout, for both breakout locations. The dashed blue lines represent the deflected shapes under service load before breakout began on a given specimen. The red lines represent the deflected shapes under service load after breakout of concrete. For breakout over the central support, the section curvature increased over the central support. A curvature increase also occurred within both spans due to the transfer of moment during concrete breakout. An increase in curvature was also observed at the breakout location for

breakout within the left span. However, a reduction in curvature occurred within the right span throughout breakout (midspan displacement under service load reduced slightly with increasing breakout length). This curvature reduction was caused by rotation of the section at the central support. This rotation accommodated the increase in curvature within the left span without the need for a significant curvature increase at the central support. Consequently, the increase in section curvature at the non-breakout location was less significant than for hogging breakout.

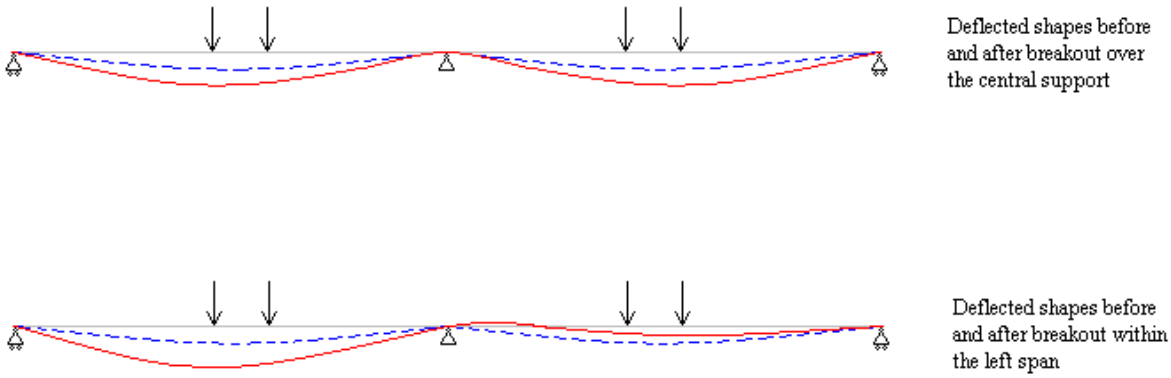

Fig. 7.3: Deflected shapes of specimens before and after breakout at both locations

Although appreciable increases in moment occur at the non-breakout location (Fig. 7.1), Table 6.3 shows the associated increases in compression strain are small in relation to those at the breakout location. Therefore, the effect of moment transfer during concrete breakout on the flexural capacity of the non-breakout cross-section is considered insignificant. However, moment transfer from the breakout location may influence serviceability limit state behaviour and should be examined in greater detail.

7.2.1.2 Midspan displacements

If a repair is to be carried out at service load, midspan displacements of the specimen with exposed reinforcement should satisfy serviceability limit state criteria. Table 6.10 displays the measured midspan displacements under service load for the maximum breakout length in progressive breakout specimens. Note: The displacement that occurred during the actual breakout process was not included in

these measurements. Therefore, service load displacement values measured from progressive breakout specimens may be considered as a lower bound estimate to the "true" displacement.

Pre-repair midspan displacements for specimens to be repaired under service load are also recorded in Table 6.10. Removal of the displacement transducers during pre-repair testing was unnecessary so the total displacement was measured with reference to "zero" displacement, before loading began. However, significant crack widening at the breakout region (due to a portion of the tension reinforcement being exposed before loading began) caused excessive displacement. Pre-repair displacements recorded from the specimens to be repaired under service load are considered as upper bound estimates to the "true" displacements.

According to BS 8110 **[61]**, the maximum deflection in a member under service load should not exceed 0.004 times the span length ($L / \delta \geq 250$). Therefore, the allowable service load deflection was 8mm for the test specimen span length of 2m. All the lower bound estimates of midspan displacement were less than the allowable. In some cases however, the serviceability limit was exceeded by the upper bound estimate, particularly the left midspan displacement for reinforcement exposure within the left span. This may be just cause to reduce allowable breakout length for repair under service load within the span. Unfortunately, it is impossible to establish an acceptable reduced breakout length from test measurements as pre-repair testing of specimens repaired under service load was carried out for the maximum breakout length.

Casting of the repairs during testing took place at either end of the load relief range (i.e. at "zero" load and notional service load for the "fully bonded" specimen). In practice, a reasonable proportion of load relief can be achieved by reducing or completely removing the imposed load on the member during breakout and casting of the repair. Load relief during casting of a repair reduces the subsequent service load displacements of the repaired specimen. By analysing load-displacement logged data, the desirable load reduction during casting (to prevent excessive deflection) can be approximated. For example, to ensure "upper bound" service load displacements were not excessive, load reductions of 9% and 21% were required for UR23S and UR34S respectively. Such load reductions are achievable without the need for temporary propping (by reducing the imposed load on the specimen).

In practice, an "even" crack pattern is established before breakout begins, so deflections less than the "upper bound estimate" are expected. The LUSAS numerical model was used to assess the "true" service load displacements for breakout up to 50% of the span length. This is discussed in greater detail in Section 8.3.4.

7.2.2 Serviceability limit state behaviour (breakout location)

7.2.2.1 Moment transfer

The parameters that influence the reduction in moment at the breakout location are of interest. Table 6.8 displays the reduction in bending moment that occurred at the breakout location due to the loss of section stiffness. Fig. 7.4 plots the reduction in moment at the breakout location against hogging : sagging reinforcement ratio. Note: A 32% decrease in moment occurred for AB11H ($\alpha_r = 1$) due to excessive cracking in the "weak" concrete near the breakout region. Greater moment transfer for sagging breakout occurred for larger values of hogging : sagging reinforcement ratio while for hogging breakout, greater moment transfer occurred for smaller values of reinforcement ratio. Therefore, the relative section stiffness in the "fully bonded" member slightly influenced moment transfer from the breakout location during concrete breakout. However, the influence of the load arrangement at the breakout location was far more significant. Greater moment transfer due to concrete breakout occurred for breakout over the central support than within the left span and this trend was apparent for all reinforcement combinations. This is attributed to the influence of load arrangement on the loss of section stiffness during breakout as described in Section 3.2.

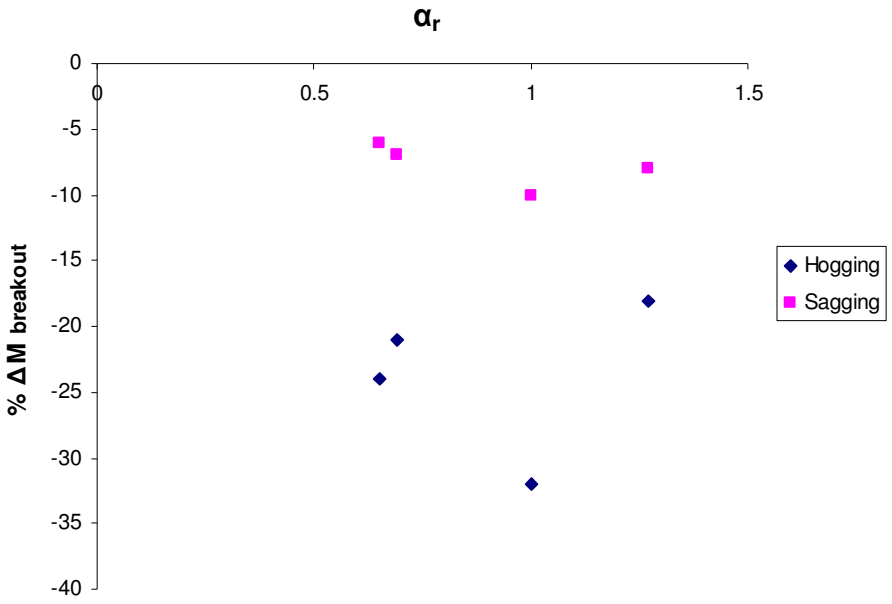

Fig. 7.4: Plot of decrease in moment at breakout locations throughout breakout vs. reinforcement ratio

Significant increases in curvature occurred for both breakout locations due to the loss of bond between the steel and the concrete (Table 6.5). Fig. 7.5 plots the increase in curvature at the breakout location during breakout against the hogging : sagging reinforcement ratio. In general, increases of 300% - 350% occurred for both breakout locations. Note: A 462% increase occurred during hogging breakout on AB11H (α_r = 1) due to extensive crack widening in the "weak" concrete. The percentage increase in curvature (relative to the "fully bonded" curvature) was similar for both breakout locations but the magnitude of the curvature increase at the breakout location was greater for hogging breakout.

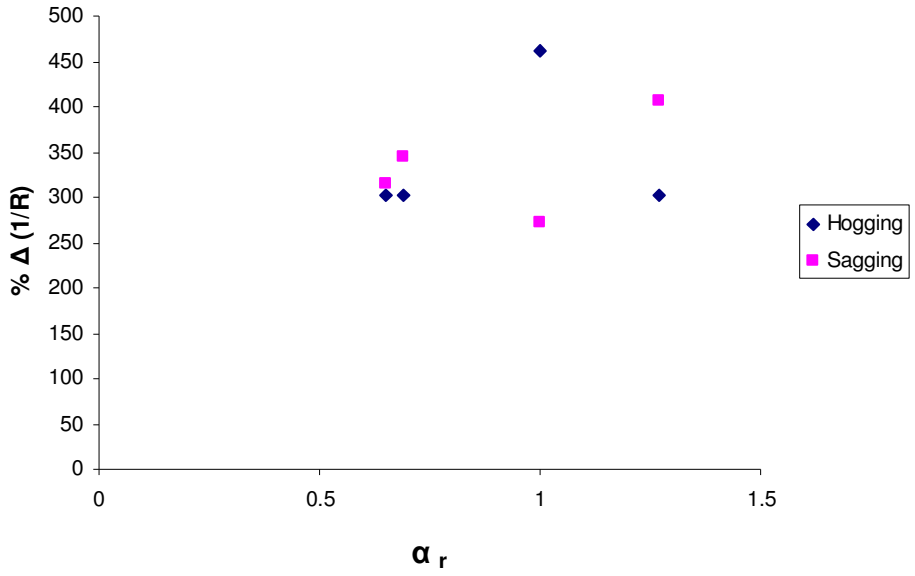

Fig. 7.5: Plot of increase in curvature at breakout locations throughout breakout vs. reinforcement ratio

7.2.2.2 Extreme fibre compression strains

Concrete compression strain is not a criterion used to satisfy the service load performance of a reinforced concrete member. However, the maximum concrete compression strain at ultimate load is limited to 0.0035 (BS 8110 **[61]**). Measurement of compression strains at service load assesses what proportion of the ultimate strain is attained at the serviceability limit state. Previous research found an increase in the compression strain during exposure of reinforcement. If the increase due to concrete breakout occupies a significant portion of the 0.0035 limit, ductility and flexural strength may be reduced. Increases in compression strain at the breakout location are of particular interest (increases in non-breakout compression strains were negligible). Flexural strength is more likely to be reduced in a heavily reinforced section as reinforcement may not reach yield before concrete crushes. Therefore, the influence of the reinforcement area on the increase in service load compression strain during breakout is of particular relevance. As concrete and steel material properties were not consistent in all test specimens, the design x / d ratio (calculated from

Equation 3.3) is used here to represent the reinforcement ratio at the section being considered.

In practice, ultimate load x / d values for bonded sections can be calculated from the section geometry and material properties. Therefore, behaviour during repair of a specimen at a section of known x / d ratio can be postulated. Before the influence of the design x / d ratio on the increase in compression strain can be assessed, calculated x / d ratios for the test specimens must be verified against measured values from strain distribution graphs close to ultimate load. Table 7.1 shows the calculated values of x / d ratio at sections of maximum hogging and sagging moment for "as new" specimens. The x / d ratios were calculated on the assumption of a singly reinforced specimen from Equation 3.3. Material properties from tests were used in the calculation (calculated values for "fully bonded" specimen of reinforcement combination 34 (AN34) used a concrete cube strength of 42.6 N/mm^2).

The inclusion of compression reinforcement reduces the x / d ratio at a given section. Curtailment of reinforcement within compression zones was not carried out in AN11 so the proportion of compression reinforcement in the specimen was significant. Consequently, measured x / d values for AN11 were noticeably less than the values calculated assuming a singly reinforced section.

There is reasonable correlation between the remaining measured and calculated values, except within the span of AN21. The higher measured x / d ratio value is attributed to the observed crack pattern near the section where strains were measured. Cracks formed mainly outside the gauge length and hence measured tension strains underestimated the "true" values. This led to a measured value of x / d appreciably larger than the calculated value.

	Measured x / d	Calculated x / d
AN11 “support”	0.38	0.60
AN11 “span”	0.44	0.60
AN21 “support”	0.26	0.28
AN21 “span”	0.36	0.21
AN23 “support”	0.27	0.28
AN23 “span”	0.50	0.44
AN34 “support”	-	0.44
AN34 “span”	-	0.63

Table 7.1: Comparison between measured and calculated values of design x / d

Fig. 7.6 shows the increase in service load compression strain at the breakout location during breakout (from Table 6.2) vs. the design x / d ratio (calculated value from Table 7.1) at the section being considered. Note: A significant increase in compression strain occurred for AB11H (0.0024, 0.60) due to the specimen’s “weak” grade of concrete. This considerable increase in compression strain was consistent with the observed increase in section curvature (Fig. 7.5) and caused a significant reduction in the flexural strength of the member (failure occurred at approximately 1.3 times the service load of the “fully bonded” specimen). In general, increases in strain of 0.0008 – 0.0013 occurred during breakout and were relatively unaffected by the design x / d ratio at ultimate load. Increases in strain were generally greater for breakout over the central support.

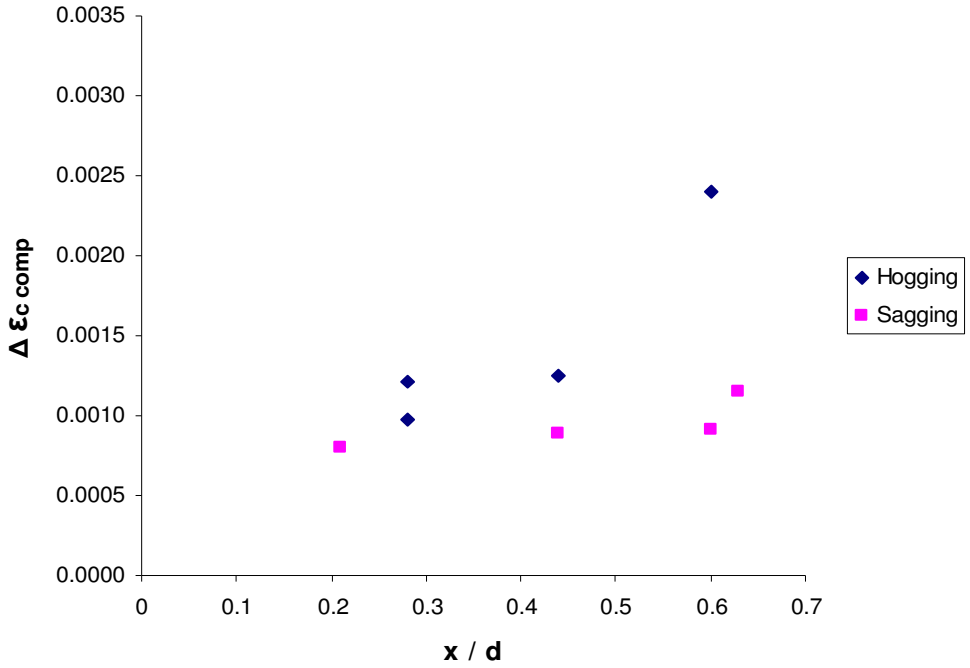

Fig. 7.6: Plot of increase in extreme fibre compression strain at breakout locations vs. design x / d ratio at the section being considered

7.2.3 Ultimate limit state behaviour

To carry out an unpropped repair, an adequate margin of safety against failure must be maintained while the specimen is in the "weakened" condition. The influence of reinforcement exposure on the expected failure modes was also of interest. Loading of specimens with exposed reinforcement continued to failure to examine these issues.

Specimen	Test failure load (kN)	Test failure mode	$P_{exposed}$ / P_{bonded}
AB11H	81.7	Shear	0.64
AB11S	88.9	Flexural	0.69
AB21H	178.8	Flexural	1.10
AB21S	176.1	Shear	1.08
AB23H	212.6	Shear	0.94
AB23S	225.4	Shear	1.00

Table 7.2: Test failure loads of specimens with exposed reinforcement

Test failure loads of specimens with exposed reinforcement are displayed in Table 7.2 and are compared with the test failure loads of the equivalent "as new" specimens. The failure loads of AB11H and AB11S were significantly less than the equivalent "as new" specimen. The lower grade concrete used in these specimens caused relatively high x / d ratios at the breakout locations and increases in compression strain during breakout caused greater loss of flexural strength. The influence of concrete cube strength on the ultimate strength of specimens with exposed reinforcement is well documented **[2, 22]**. Such decreases in ultimate strength would not be expected had these specimens been constructed from a structural grade of concrete.

The measured flexural failure load of AB21H was 10% greater than the shear failure load of AN21. Section 2.3.3 describes the observed increase in shear strength in simply supported beams with exposed reinforcement **[33]**, caused by movement of the neutral axis, changing behaviour to a combination of flexural and tied-arch action. This change in behaviour was identified by a reduction in the compression zone depth at the centre of the breakout (to maintain compatibility between the exposed steel and the substrate), which was confirmed by examining strain distribution graphs as the length of reinforcement exposure increased. Tied-arch action increased the shear strength of AB21H near the central support. Shear failure of the specimen was delayed as the shear force was largest in this region (between the inner point loads). As a result, AB21H experienced a flexural failure (Fig. 7.7).

Fig. 7.7: Flexural failure for breakout over the central support (AB21H)

The measured shear failure load of AB21S was 8% greater than that for AN21. Concrete breakout within the left span caused an increase in shear strength in that region due to the change in the neutral axis profile. The change in strain pattern within the right span was less significant and the observed shear failure occurred within the right span (Fig. 7.8).

Fig. 7.8: Shear failure within right span for breakout within the left span (AB21S)

The shear strengths of AB23H and AB23S were not expected to be less than that for AN23 but both failed in shear at slightly lower loads. The observed reduction in neutral axis depth with breakout on AB23H was slightly less than for AB21H so the observed increase in shear strength was less. Similarly to AB21S, the change in neutral axis profile in the left span of AB23S had a negligible effect on the shear strength within the right span and the observed shear failure occurred in the right span.

The experimental failure loads of AB34H and AB34S were significantly greater than the value calculated for the corresponding "fully bonded" specimen (Table 6.1). This is partly attributed to BS 8110 **[61]** providing a lower bound estimate of the shear strength of a specimen. The increase in shear strength due to breakout of concrete may have also contributed to the discrepancy. Both specimens failed at approximately the same load but AB34S experienced an unusual flexural failure within the left span. One of the flexural cracks within the exposed length opened quite suddenly and caused an instantaneous drop in load.

Exposure of reinforcement over the support of AB12H and AB22H would be expected to reduce the flexural strength of the specimens and as expected, both failed in flexure. However, the measured ultimate loads of AB12H and AB22H were greater than those calculated for equivalent "fully bonded" specimens due to the assumptions made in the "fully bonded" ultimate load calculation.

7.3 Unloaded repair

7.3.1 Serviceability limit state behaviour

Specimens repaired while unloaded would not be expected to exceed serviceability limit state criteria as behaviour should be similar to equivalent "as new" specimens. However, it is impossible to completely relieve the structure of strain for casting of the repair. It is therefore pragmatic to ensure serviceability limit state criteria are not exceeded during subsequent reloading of the repaired specimen.

Crack widths were examined at maximum moment locations at service load. Crack widths in the substrate near the repair interface were greater than the 0.3mm limit but it is common practice to inject these cracks with an epoxy resin before casting of the repair. Cracks at non-repair locations were not excessive and cracks within the patch repair only reached 0.1mm.

Table 7.3 displays the service load displacements for specimens repaired while unloaded and for the corresponding control specimen. For both repaired specimens, both midspan displacements were greater than the equivalent "as new" specimen. This was caused by wedged cracks preventing full relief of strain from the substrate during casting of the repair. However, the repaired specimen displacements were still appreciably less than the 8mm service load limit for a 2m span.

	Left disp (mm)	Right disp (mm)
AN23	4.275	4.277
PR23H	5.162	5.922
PR23S	5.310	5.098

Table 7.3: Service load midspan displacements for "as new" and "propped repaired" specimens

7.3.2 Behaviour during loading to failure

7.3.2.1 Flexural stiffness

The effect of carrying out a repair while unloaded on the flexural stiffness of the member should also be assessed. The stiffness of the control specimens and repaired specimens were calculated for sections of maximum hogging and sagging moment and results are displayed in Table 6.7. Fig. 7.9 compares the flexural stiffness of specimens repaired while unloaded to the stiffness of the corresponding control specimen. Crack re-opening within the substrate during loading to failure tends to reduce the flexural stiffness at the repair location (relative to the "as new" specimen). However, tension stiffening provided by the repair concrete partially restores stiffness. This tension stiffening effect is greater for smaller areas of previously exposed tension reinforcement. The shape of the bending moment diagram at the section being considered also affects the tension stiffening effect (flexural cracking over a greater length for the two-point load arrangement within the spans). Consequently, the reduction in flexural stiffness for repair over the central support was less severe than for repair within the more heavily reinforced left span.

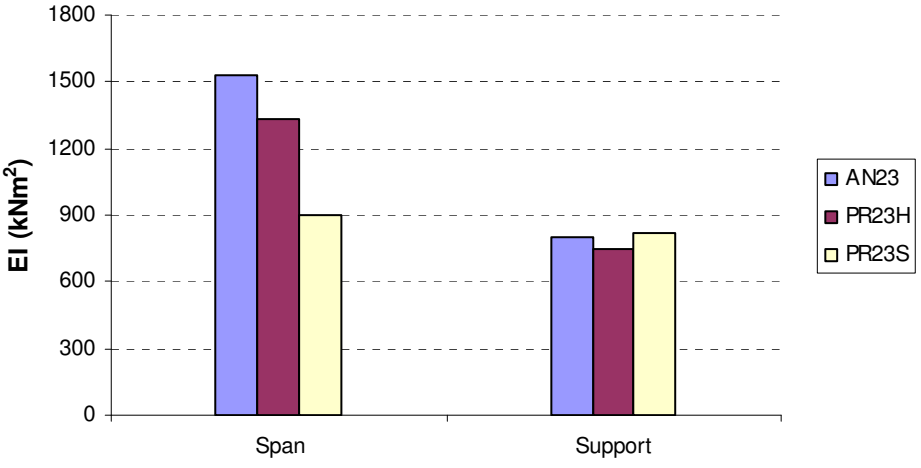

Fig. 7.9: Flexural stiffness of specimens repaired while unloaded and the equivalent "as new" specimen

7.3.2.2 Extreme fibre compression strains

The extreme fibre compression strain at the breakout region under service load has been shown to increase during the exposure of reinforcement (Fig 7.6). Although the compression strains were reduced significantly during unloading before casting of the repair, a residual compression strain may remain "locked into" the repaired member as complete unstraining of the member is difficult to achieve. Table 6.4 displays the values of compression strain at the repair location for unloaded repair specimens at 55% & 90% of the "as new" ultimate load. Compression strains at the repair location were marginally higher than at the same cross-section in the equivalent control specimen. Therefore, the effect of carrying out an unloaded repair on the ductility and flexural strength of the repaired section is small.

7.3.3 Ultimate limit state behaviour

Table 7.4 shows experimental failure loads of specimens repaired while unloaded and compares them to the test failure load of the corresponding "as new" specimen. As discussed previously, arching of the neutral axis occurred near the breakout region during concrete breakout. However, if a specimen is repaired while unloaded, the effect of the "arching" stress pattern is greatly reduced as stresses throughout the member are minimised before the repair is cast. Therefore, it is more likely to behave like the equivalent "as new" specimen (in this case, fail in shear). PR23S had a similar failure load to the "as new" specimen and the observed shear failure occurred within the right span. However, the failure load of PR23H was 21% greater than for the "as new" specimen. This was attributed to the "arched" neutral axis profile (in the region of highest shear within the specimen) which remains "locked into" the member once the repair was cast.

Specimen	Test failure load (kN)	Test failure mode	$P_{repaired}$ / P_{bonded}
PR23H	273.9	Shear	1.21
PR23S	232.5	Shear	1.03

Table 7.4: Test failure loads of specimens repaired while unloaded

Table 6.11 displays the ductility of failure for all repaired specimens and the corresponding control specimens. The influence of a patch repair on member ductility can only be meaningfully compared for flexural failures. As shear failures were observed in AN23, PR23H & PR23S, the effect of an unloaded repair on section ductility cannot be assessed.

Specimens of reinforcement combination 23 did not include sufficient shear reinforcement to ensure a flexural failure. Therefore, full plastic behaviour was not achieved before the observed shear failures. Analysis of strains at the repair cross-section highlights the influence of the patch repair process on the flexural strength of the member. The extreme fibre compression strains at the repair location and previously exposed steel strains at 90% of the "fully bonded" ultimate load can be examined to determine the proximity of the repaired section to a flexural failure.

Section 7.3.2.2 observed that the extreme fibre compression strains in the unloaded repair specimens at 90% of the ultimate load were only slightly greater than for the corresponding "as new" specimen. Table 7.5 shows the previously exposed steel strains at 55% & 90% of the "fully bonded" ultimate load for specimens repaired while unloaded. The tension steel strains at the corresponding cross-sections in AN23 are also included. The tension reinforcement over the support of AN23 was considered to have yielded at 65% of the ultimate load and this was confirmed by the observed moment redistribution to the spans (Fig. 6.11). The observed shear failure in AN23 occurred before the flexural capacity of the spans was reached.

By comparing Fig. 3.1 & 3.2, the reduction in exposed steel strain (relative to the "fully bonded" steel strain at the section of maximum moment) is greater for breakout over the support. Also, as mentioned in Section 7.3.2.1, tension stiffening within the patch repair was greater for PR23H than for PR23S due to flexural cracking over a greater length and the larger area of previously exposed steel in PR23S. Consequently, the steel strain of PR23H was significantly less than for the control

specimen (even though it reached yield near ultimate load) but the steel strain of PR23S was appreciably greater than for the control specimen (so hinge formation within the repaired span would occur at a lower load than for the control specimen).

Specimen	55%	90%	Increase	% incr
AN23 - H	0.0027	0.0044	+0.0017	+63%
PR23H	0.0015	0.0029	+0.0014	+93%
AN23 - S	0.0009	0.0016	+0.0007	+78%
PR23S	0.0014	0.0024	+0.0010	+71%

Table 7.5: Previously exposed steel strains at repair location at 55% & 90% of the ultimate load ("propped" repair specimens)

7.4 Repair under service load

7.4.1 Behaviour during loading to failure

7.4.1.1 Flexural stiffness

When casting a repair, it is desirable that the flexural stiffness of the repaired cross-section is similar to that for the initially "fully bonded" section. The flexural stiffness of specimens repaired under service load and the corresponding "as new" specimens are included in Table 6.7. Fig. 7.10 compares flexural stiffness at sections of maximum hogging and sagging moment. The categories are named according to the specimen reinforcement combination code and the location within the member where flexural stiffness was measured. The three series represent "as new" specimens, hogging repair specimens and sagging repair specimens respectively.

As appreciable flexural cracking had occurred at service load, the flexural stiffness (as defined in Section 6.3.5) at a given section within "as new" specimens was related to the area of tension reinforcement. Therefore, flexural stiffness over the support was greater than that within the spans for specimens of large hogging : sagging reinforcement ratio and vice versa.

For a repair cast under service load, the repair material is only strained by subsequent load increments. This allows considerable tension stiffening to develop within the repair material and is more significant for smaller areas of previously exposed steel **[4]**. Therefore, the area of previously exposed reinforcement influences the flexural stiffness at the repair location.

Consider initially, sagging repair within the left span. A reduction from the "as new" stiffness was observed for UR23S (larger reinforcement area within the span), while an appreciable increase was observed at the same repair location for UR21S. For hogging repair over the central support, increases in stiffness were observed for both UR21H and UR23H as the area of previously exposed steel was relatively small in both specimens.

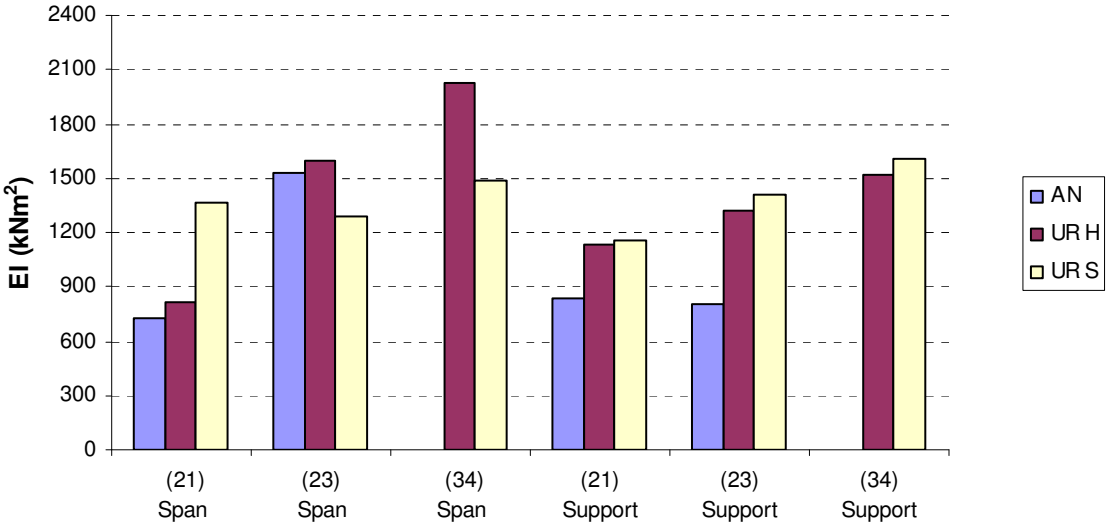

Fig. 7.10: "Measured" flexural stiffness at sections of maximum hogging and sagging moment for specimens repaired under service load

For specimens repaired under service load, the repair material is only strained by the load increase from service load. In unloaded repair specimens however, the repair material is strained by the total load on the specimen. The less highly strained repair material in specimens repaired under service load provides greater tension stiffening within the patch repair. Consequently, the stiffness at both repair and non-repair locations was greater for specimens repaired under service load than for specimens repaired while unloaded.

7.4.1.2 Moment transfer

Once the repair material is cast and section stiffness restored, moment transfer to the repair location may take place. Table 6.9 records the change in hogging : sagging moment ratio between 55% & 90% of the "fully bonded" ultimate load for specimens repaired under service load. Fig. 7.11 plots the change in moment ratio against the hogging : sagging reinforcement ratio. Noticeable increases in moment ratio occurred for hogging repair as moment transferred back to the repair location. This was consistent with the observed increases in flexural stiffness (relative to the "as new" flexural stiffness) for repair at the central support (Fig. 7.10). However, changes in

the moment pattern for sagging repair were insignificant as tension stiffening within the span patch repairs was less effective (due to the larger number of cracks that occurred within the span repair).

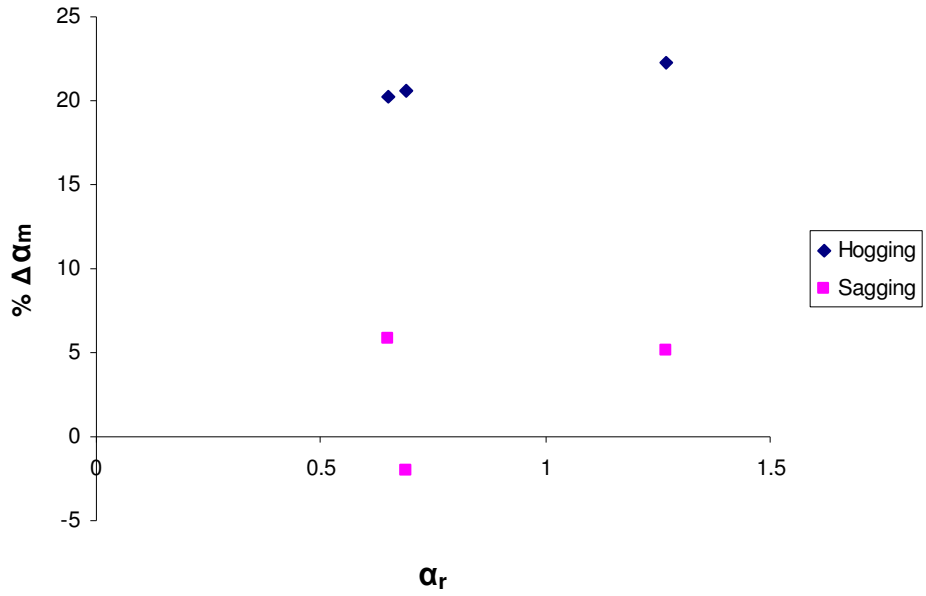

Fig. 7.11: Plot of change in moment ratio between 55% – 90% of ultimate load vs. reinforcement ratio

7.4.1.3 Extreme fibre compression strains

Fig. 7.6 plots the increase in extreme fibre compression strain at the breakout location during concrete breakout. If the repair material is cast while the specimen is under load, this increase in compression strain remains "locked into" the member. To assess the overall effect of the repair process on the flexural strength of the member, the parameters that affect the subsequent increase in compression strain during loading to failure of the repaired specimen also require investigation.

Table 6.4 shows the increases in extreme fibre compression strain at the repair location during loading between 55% & 90% of the ultimate load. Fig. 7.12 plots the increase in the extreme fibre compression strain at the repair location against the design x / d ratio at the section being considered. The increase in compression strain

during loading to failure of the repaired specimens was greater for larger values of design x / d, irrespective of the repair location being considered.

Assuming a linear strain distribution, a given increase in tension reinforcement strain causes a greater increase in extreme fibre concrete compression strain for larger x / d. Also, as the repair material was placed at 55% of the ultimate load, it was initially unstrained so its contribution to tension stiffening during subsequent loading was significant. This effect was greater for smaller tension reinforcement areas and thus, smaller x / d. Consequently, the increase in concrete compression strain was much greater for larger values of design x / d.

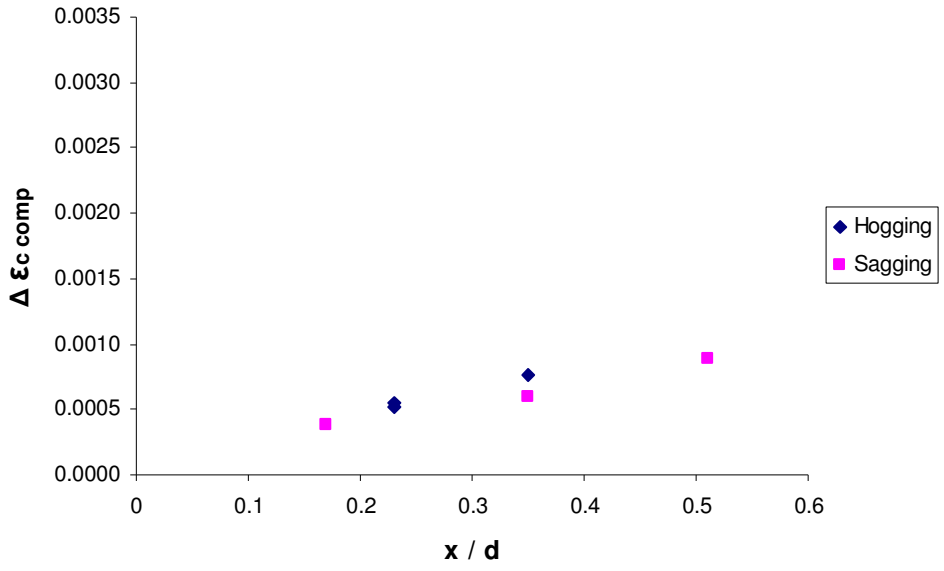

Fig. 7.12: Plot of increase in extreme fibre compression strain at repair locations between 55% –90% of the ultimate load vs. design x / d ratio at section being considered

Table 6.4 also includes the extreme fibre compression strains at 55% & 90% of the ultimate load for unloaded repair specimens. The compression strains at service load were greater for specimens repaired under load due to the increase in strain that occurred during reinforcement exposure. Note: This strain was reduced during pre-repair unloading of the "propped" repair specimens and the subsequent increase during loading to service load of the repaired specimen was less severe. The observed increases in strain between 55% – 90% of the ultimate load were slightly larger for the unloaded repair specimens. As tension stiffening within the repair material was

greater for specimens repaired under load, the increase in section curvature and therefore compression strain was less severe.

7.4.2 Ultimate limit state behaviour

The effect of carrying out a repair under service load on ultimate limit state behaviour can be evaluated by comparing repaired specimens with equivalent "as new" specimens. The failure load and the ductility of failure are of particular interest. Table 7.6 displays measured failure loads of specimens repaired under service load and compares them with the corresponding "as new" test failure loads. The ultimate load of repaired specimens was in general, appreciably greater than for the equivalent "as new" specimen (a slight reduction in ultimate strength occurred in UR23S).

Specimen	Test failure load (kN)	Test failure mode	$P_{repaired}$ / P_{bonded}
UR21H	198.5	Flexural	1.22
UR21S	199.4	Flexural	1.23
UR23H	279.6	Flexural	1.24
UR23S	219.2	Shear	0.97
UR34H	279.4	Shear	-
UR34S	316.2	Flexural	-

Table 7.6: Test failure loads of specimens repaired under service load

Observed increases in ultimate strength of the repaired specimens were primarily caused by the change in failure mode from shear to flexural. An increase in the shear strength of the specimens occurs during breakout due to arching of the neutral axis near the region of breakout. This trend delayed a shear failure in UR21H and UR21S and appreciable plastic behaviour developed in these specimens as their elastic and plastic bending moment diagrams were similar. Flexural failures at significantly higher loads than the equivalent "as new" specimen were observed in UR21H and UR21S (Fig. 7.13).

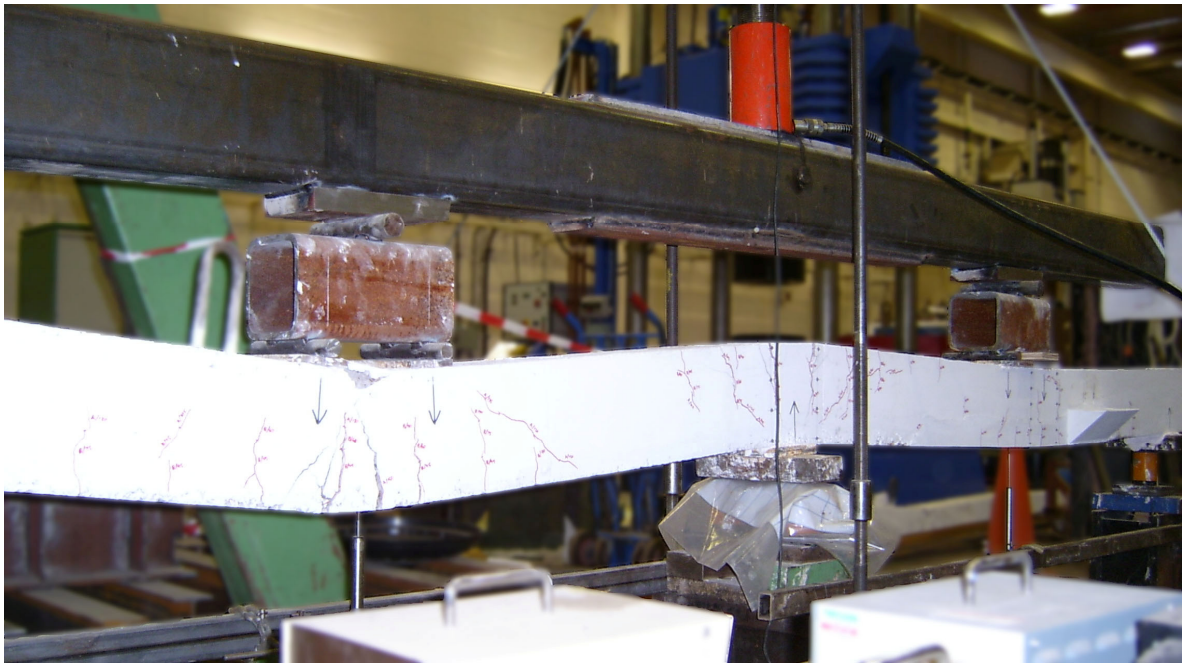

Fig. 7.13: Flexural failure of UR21S (hinge formation within "non-repaired" span and at central support)

For specimens with hogging : sagging reinforcement ratios less than 1, moment transfer from the central support to the spans was desirable. For UR23H, moment transfer from the central support to the spans occurred while the reinforcement was exposed and moment transfer back to the central support during loading to failure of the repaired specimen was less significant. Therefore, the repair process brought the moment balance closer to the plastic bending moment diagram. Thus, full plastic capacity was more likely to be reached simultaneously at both the central support and within the spans.

For UR23S however, moment transferred to the central support while the reinforcement was exposed and moment transfer back to the repair location during loading to failure was negligible. Therefore, the moment in the region of highest shear (between the inner point loads) increased during the repair process. While reinforcement was exposed in UR23S, arching of the neutral axis occurred near the breakout region within the left span but the neutral axis profile within the right span was not affected. As the repair was cast under service load, the altered neutral axis profile remained "locked into" the member. This caused an increase in shear strength within the left span and the observed shear failure occurred within the right span (Fig. 7.14).

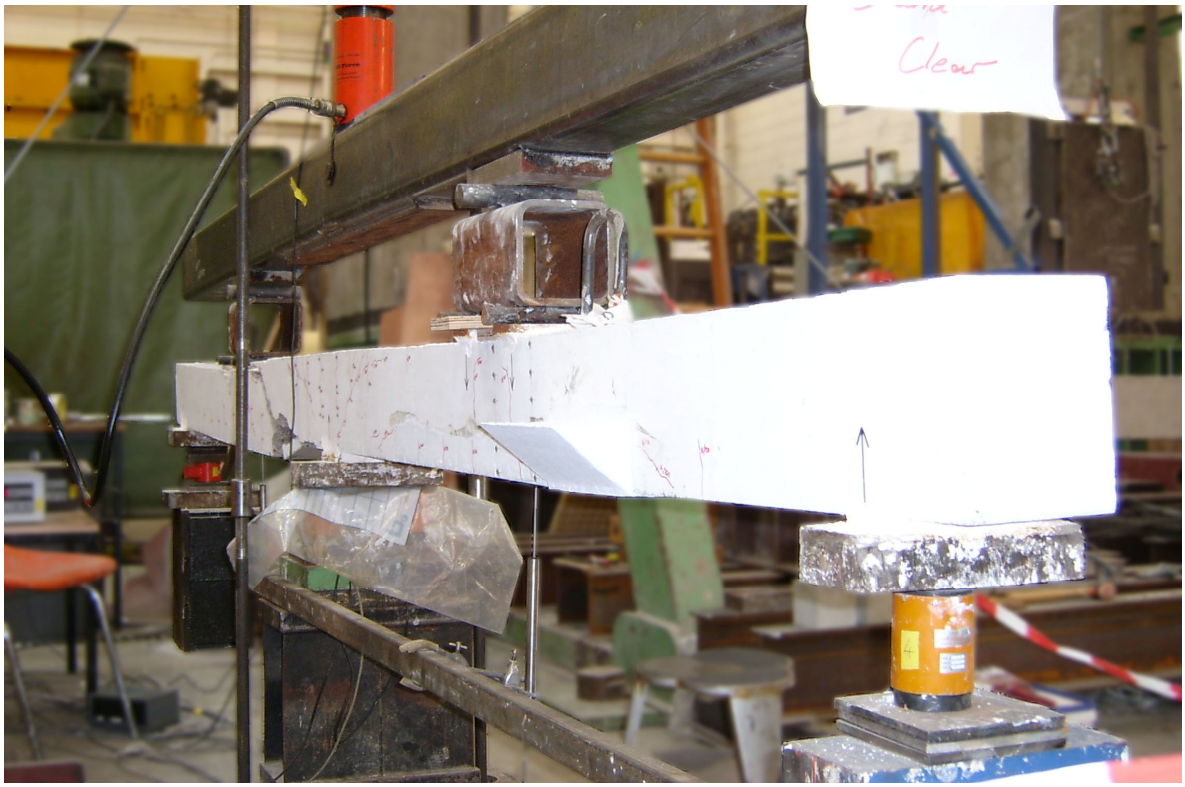

Fig. 7.14: Shear failure of UR23S (within non-repaired span)

Table 6.11 shows the ductility of failures for “as new” and repaired specimens. Fig. 7.15 compares the ductility of the “as new” specimens to specimens repaired under service load. Note: The ductility of UR34S was low as sudden opening of a flexural crack within the left span caused an abrupt flexural failure. The ductility of the “as new” specimens was generally much lower than the equivalent repaired specimens as both control specimens suffered shear failures. The ductility was greater in more lightly reinforced repaired specimens as they were more likely to achieve the plastic bending moment diagram. As the failure modes of the repaired specimens differed to those of the control specimens, the effect of the repair process on the ductility of the member was difficult to evaluate.

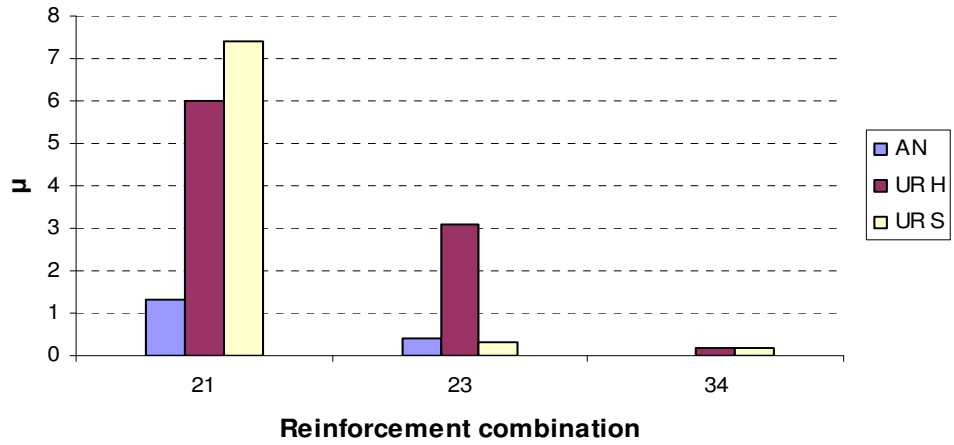

Fig. 7.15: Ductility of "as new" specimens and specimens repaired under service load

Insufficient shear reinforcement was provided in AN21 and AN23 to ensure a flexural failure. However, the extreme fibre compression strains and tension steel strains close to ultimate load can be compared to those in the repaired specimens to assess the effect of the patch repair on the flexural strength of the section. The extreme fibre compression strains at the repair location at 55% & 90% of the "fully bonded" ultimate load are displayed in Table 6.4. The compression strains at the repair location at 90% of the ultimate load are appreciably larger than the corresponding strains in the control specimens as the increase in compression strain that occurred during concrete breakout remained "locked into" the member.

Table 7.7 displays the previously exposed steel strains and corresponding steel strains from the "as new" specimens at 55% & 90% of the ultimate load. The rate of increase of steel strain was less in the repaired specimens due to the greater contribution to tension stiffening of the less highly strained repair concrete.

For repair over the central support, reinforcement strains at 90% of the ultimate load were significantly less than in the control specimens (yielding of reinforcement occurred over the central support in the "as new" specimens). As mentioned previously, the concrete compression strains at the same cross-sections were greater in the repaired specimens. Therefore, the repair process brought the central support cross-section closer to a balanced failure.

For span repairs however, a greater number of flexural cracks occurred within the patch repair so tension stiffening was less effective (particularly for the more heavily reinforced section UR23S). Previously exposed steel strains at 90% of the ultimate

load were similar to the corresponding strains in the "as new" specimens. As the concrete compression strains in the repaired specimens were appreciably larger, the patch repair reduced the flexural capacity of the member.

Specimen	55%	90%	Increase	% incr
AN21 - H	0.0031	0.0051	+0.0020	+65%
UR21H	0.0014	0.0020	+0.0006	+43%
AN21 - S	0.0014	0.0026	+0.0012	+85%
UR21S	0.0017	0.0024	+0.0007	+41%
AN23 - H	0.0027	0.0044	+0.0017	+63%
UR23H	0.0019	0.0028	+0.0009	+47%
AN23 - S	0.0009	0.0016	+0.0007	+78%
UR23S	0.0013	0.0020	+0.0007	+54%

Table 7.7: Previously exposed steel strains at repair location at 55% & 90% of the ultimate load ("unpropped" repair specimens)

Strains at the repair cross-section can also be compared between specimens repaired while unloaded and specimens repaired under service load. The unloaded repair specimens exhibited greater increases in previously exposed steel strain between 55% – 90% of the ultimate load due to the greater contribution to tension stiffening of the less highly strained repair concrete in the specimens repaired under service load (Tables 7.5 & 7.7). Consequently, the previously exposed steel strains at 90% of the ultimate load were slightly greater in the unloaded repair specimens. However, appreciably larger concrete compression strains occurred in specimens repaired under service load (due to the increase in compression strain during concrete breakout remaining "locked into" the member) so their flexural capacity was less than for specimens repaired while unloaded.

7.5 Summary of test results

In this chapter, test results were analysed with respect to the parameters chosen for investigation. The transfer of moment from the breakout location increased with the length of breakout. The reinforcement layout influenced the moment balance within the "fully bonded" member but had little effect on the transfer of moment due to concrete breakout. The reduction in moment at the breakout location was greater for hogging breakout and this was attributed to the shape of the bending moment diagram within the breakout region (Section 3.2). Increases in extreme fibre compression strains of approximately 100% occurred at the breakout location during reinforcement exposure to 50% of the span length. However, increases in compression strain at non-breakout locations were small in comparison. Therefore, the ultimate flexural strength of a member with exposed reinforcement is primarily influenced by the increase in compression strain at the breakout location.

Reductions in ultimate strength due to reinforcement exposure were generally small (Note: The appreciable reductions in strength in AB11H & AB11S were attributed to the weak concrete grade) and in some cases, increases in strength occurred. Increases in shear strength occurred due to the change in neutral axis profile near the breakout region and this effect was more prevalent when the reinforcement was exposed over the central support (in the region of highest shear within the member). Ultimate flexural strength was relatively unaffected if the exposed reinforcement yielded at ultimate load.

For repairs cast under service load, the flexural stiffness during loading to failure of the repaired member was generally greater than for the equivalent specimen with the repair cast while unloaded (although accumulated deformations were significantly greater). The flexural stiffness of specimens repaired under service load was also generally greater than for the equivalent "as new" specimen. This enhanced stiffness is attributed to significant tension stiffening within the less highly strained repair material.

Repair over the central support was more influential in increasing the shear strength throughout the member. This trend was more pronounced for specimens repaired under service load as the "tied-arch" effect was reduced during unloading for specimens repaired under zero load. Reductions in flexural strength were more likely for repair under service load (than for unloaded repair specimens) as the increase in

extreme fibre compression strain that occurred during reinforcement exposure remained “locked into” the member. Even if the reinforcement at the repaired cross-section attained yield at ultimate load, the ductility of failure would be reduced (as the strain in the steel when concrete crushing occurs would be lower than in a member repaired while unloaded).

Chapter 8: Results from numerical analysis

8.1 Introduction

In parallel with physical testing, numerical analyses were carried out using LUSAS finite element software. The numerical analysis procedure is described in Chapter 4. The initial numerical analysis for specimen design was carried out using assumed material properties. The analysis was subsequently re-run with properties determined from material testing as detailed in Table 5.5. Numerical results presented in this chapter are from the "corrected" analysis. Note: Results for AN11, AB11H and AB11S were unreliable due to the weak concrete grade, so comparison between test and numerical results has been excluded.

This chapter aims to compare numerical and experimental results to verify the numerical model. The numerical results should help to reinforce conclusions being drawn from test results. They are also used to clarify ambiguity about certain aspects of test specimen behaviour.

Numerical results can be used to estimate values that could not be measured during experimental work. For example, the total midspan displacement could not be measured during testing because the displacement transducers had to be removed during breakout / repair to prevent damage. LUSAS provided a means of estimating displacements that occurred throughout the breakout / repair process. The measured change in reinforcement strain during the breakout process was limited to changes after the initial breakout segment was completed. The numerical analysis can be used to estimate the change in reinforcement strain on initial exposure and subsequent changes in strain (from LUSAS) for increased breakout lengths should be comparable to test measurements.

8.2 "As new" model behaviour

The LUSAS software was first verified against test results from "as new" specimens. Moment transfer during the breakout and repair processes was of particular interest in this study. Parameters chosen for investigation influenced the moment balance between support and span within "fully bonded" specimens. Fig. 8.1 shows a plot of the moment ratio for AN23 throughout loading to failure. The test specimen plot begins just below 50% of the service load and was taken to ultimate load. The numerical plot begins at the initial load interval and continues until model failure.

Before flexural cracking began, the "LUSAS" hogging : sagging moment ratio was approximately equal to the elastic value of 1.32 (from Fig. 3.5). As flexural cracking developed, flexural stiffness was increasingly influenced by the cracked section properties, which were primarily dependent on reinforcement areas in this study. Reductions in the moment ratio occurred for both the test specimen and the numerical model as AN23 had appreciably larger reinforcement areas within the spans than over the support ($\alpha_r = 0.65$). The noticeable reduction in "LUSAS" moment ratio occurred at 93% of the test ultimate load consistent with reinforcement yielding in the most highly strained area over the central support.

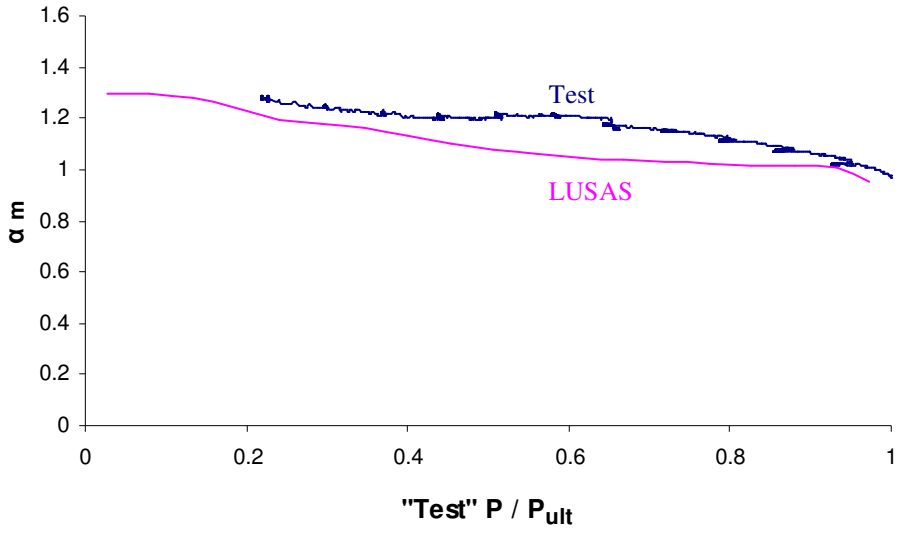

Fig. 8.1: Sample plot of hogging : sagging moment ratio vs. proportion of test ultimate load (AN23)

Fig. 8.2 shows a plot of applied load vs. midspan displacement for AN23 from both LUSAS analysis and test measurements. The "test" plot used displacement measurements from the left midspan of AN23. The "LUSAS" plot included an unload – reload cycle below service load to represent the loading of the test specimen (previous test load cycles continued to service load). LUSAS midspan displacements up to service load were slightly less than those measured during testing. However, as loading increased from service load, the model displacement was similar to that of the test specimen.

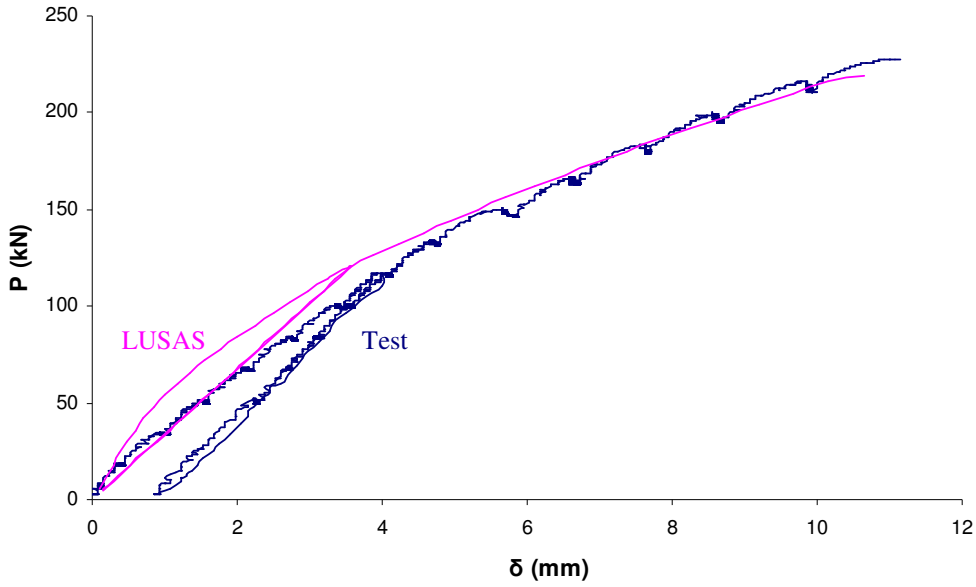

Fig. 8.2: Sample plot of load vs. midspan displacement (AN23)

Unload – reload behaviour of the test specimens was not well represented by LUSAS. The permanent displacement (i.e. displacement for zero load after unloading specimen) predicted by LUSAS was significantly less than that observed during testing. CEB-FIP Model Code 90 **[63]** describes unload – reload behaviour as shown in Fig. 8.3. The "permanent curvature" is influenced by the flexural stiffness of the uncracked and cracked sections, the moment at which cracking occurs and the moment attained before unloading begins.

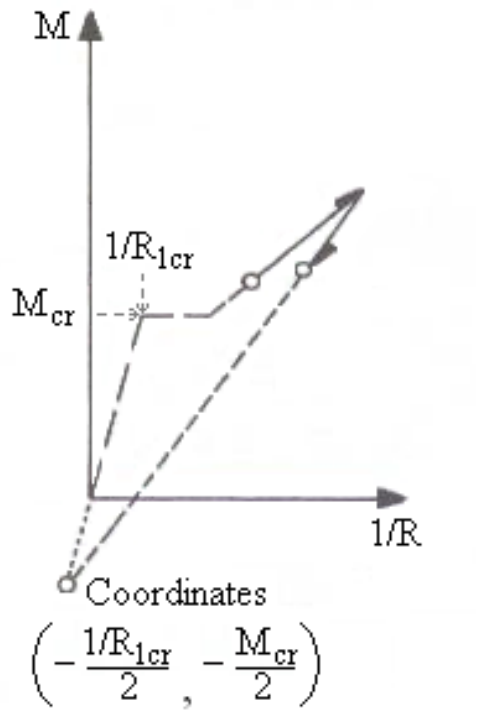

Fig. 8.3: Unload – reload behaviour from CEB-FIP Model Code 90 **[63]**

Fig. 8.4 shows a sample plot of moment vs. curvature from LUSAS (over the central support of AN23). Note: Moments were calculated from the applied loads and support reactions and curvatures were calculated from a linear regression analysis of strain measurements. The moment at which the flexural stiffness reduces due to cracking was estimated from the plot and the "permanent curvature" was determined graphically using the CEB-FIP Model Code 90 **[63]** approach. The "permanent curvature" from LUSAS is slightly less than that estimated using the Model Code approach but this value is significantly influenced by the choice of moment at which flexural cracking occurs. Comparing the stiffness during initial loading of the model with that of the test specimen (Fig. 8.2), the reduction in stiffness due to cracking appears to occur at a greater load in the model. Consequently, the permanent displacement was appreciably greater in the test specimen.

Post-service load model behaviour is similar to that observed in the test specimens. Therefore, inaccurate modelling of unload – reload behaviour only affects ultimate load performance of specimens repaired while unloaded. LUSAS results from unloaded repair specimens are used with caution in deriving conclusions.

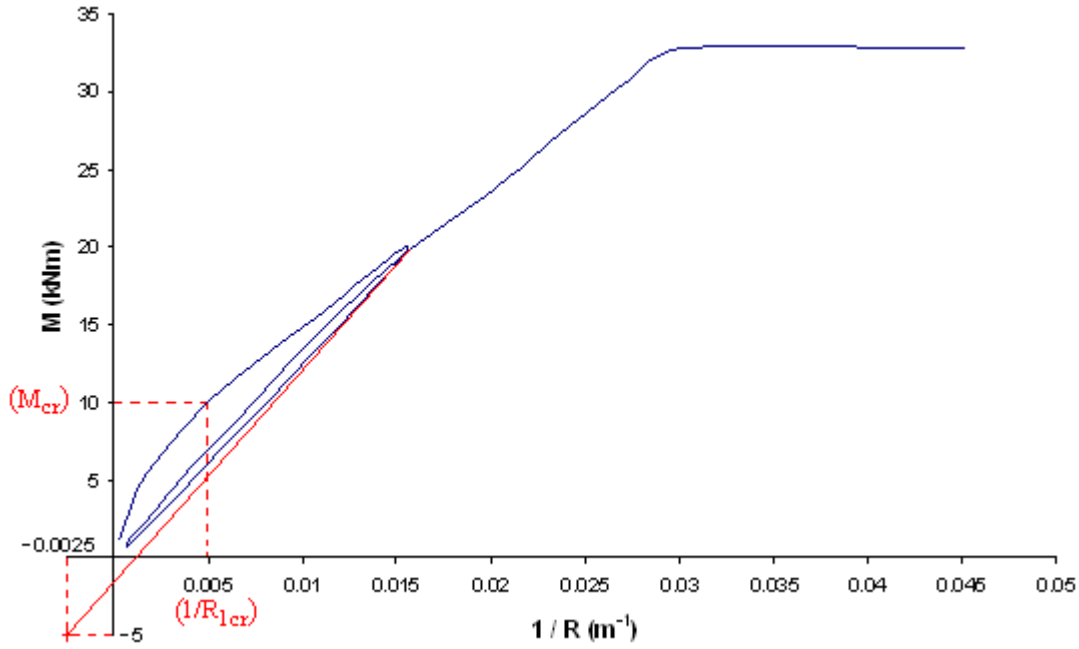

Fig. 8.4: Sample plot of moment vs. curvature from LUSAS (over the support of AN23)

Table 8.1 shows the failure loads and failure modes of "as new" models. The failure loads calculated in accordance with BS 8110 **[61]** and the test failure loads (from Table 6.1) are also included for comparison. The model failure mode was assessed by analysing strains at sections of maximum hogging and sagging moment to determine whether concrete crushing or reinforcement yielding occurred. If a flexural failure was not considered to have occurred, a shear failure was assumed. As the LUSAS failure modes were consistent with those calculated from BS 8110 **[61]**, this assumption was deemed valid.

The LUSAS failure loads were consistently greater than the calculated values as the effect of load dispersion (Section 4.5.1) was accounted for by the model but not the BS 8110 **[61]** calculations. The distribution of strain within individual elements reduced peak strains near concentrated loads below those predicted from the bending moment diagram.

Differences between the test failure loads and the ultimate loads predicted by LUSAS can be attributed to a number of factors. The primary cause of "inaccurate" ultimate load predictions is due to discrepancies in the bending moment diagrams near ultimate load. As the shear force at a given location is related to the bending moment, the balance of bending moments near ultimate load also affects the shear failure load. For

example, the proportion of moment over the central support in AN21 was appreciably greater in the test specimen than in the model (see Section 8.3.1). As the shear force was largest near the central support, test specimen AN21 failed in shear at a lower load than the predicted flexural failure load from LUSAS. Other contributory factors for discrepancies in ultimate load include the effects of strain hardening and load dispersion. The beneficial effect of strain hardening was neglected by the model. Also, although LUSAS accounts for a certain amount of load dispersion, the effect of load dispersion was greater during testing as steel plates were used to transmit the "concentrated" loads to the test specimens.

Specimen	Calc failure load (kN)	Calc failure mode	Test failure load (kN)	Test failure mode	LUSAS failure load (kN)	LUSAS failure mode
AN21	149.7	Flexural	162.4	Shear	175.0	Flexural
AN23	206.2	Shear	225.8	Shear	219.1	Shear
AN34	210.7	Shear	-	-	241.1	Shear
AN12	163.8	Flexural	-	-	188.4	Flexural
AN22	177.5	Flexural	-	-	203.9	Flexural

Table 8.1: "As new" model failure loads

8.3 Exposed reinforcement model behaviour

8.3.1 Bending moment transfer

The procedure for modelling concrete breakout is described in Section 4.4.1. Moment transfer away from the breakout location during concrete breakout was of particular interest in this study. Table 8.2 displays the maximum hogging and sagging moments under service load from LUSAS analysis for the "fully bonded" specimen and for the maximum breakout length. Values may be compared with the corresponding test measurements from Table 6.8.

Specimen	Initial M_{hog}	Final M_{hog}	% diff M_{hog}	Initial M_{sag}	Final M_{sag}	% diff M_{sag}	Initial α_m	Final α_m	% diff α_m
AB21H	16.59	12.27	-26%	12.78	14.73	+15%	1.30	0.83	-36%
AB23H	19.44	13.96	-28%	18.25	20.72	+14%	1.07	0.67	-37%
AB34H	23.88	18.14	-24%	21.65	24.24	+12%	1.10	0.75	-32%
AB21S	16.59	18.73	+13%	12.78	11.82	-8%	1.30	1.58	+22%
AB23S	19.44	20.64	+6%	18.25	17.71	-3%	1.07	1.17	+9%
AB34S	23.88	24.79	+4%	21.65	21.24	-2%	1.10	1.17	+6%

Table 8.2: Maximum hogging and sagging moments at service load before and after breakout

Fig. 8.5 graphs the increase in service load moment at the non-breakout location during breakout and Fig. 8.6 graphs the corresponding decrease in moment at the breakout location. Moment transfer during concrete breakout was greater for AB23S and AB34S during testing than predicted by the numerical model. Before breakout began, tension stiffening within the proposed breakout region of AB23S and AB34S was less significant than for the other specimens due to the larger areas of reinforcement to be exposed. The loss of stiffness due to concrete breakout was greater in the test specimens (as greater moment transfer was observed). Loss of tension stiffening during reinforcement exposure contributes to the loss of section stiffness. This suggests tension stiffening was underestimated by LUSAS for larger

reinforcement areas as loss of tension stiffening was more severe in the test specimens.

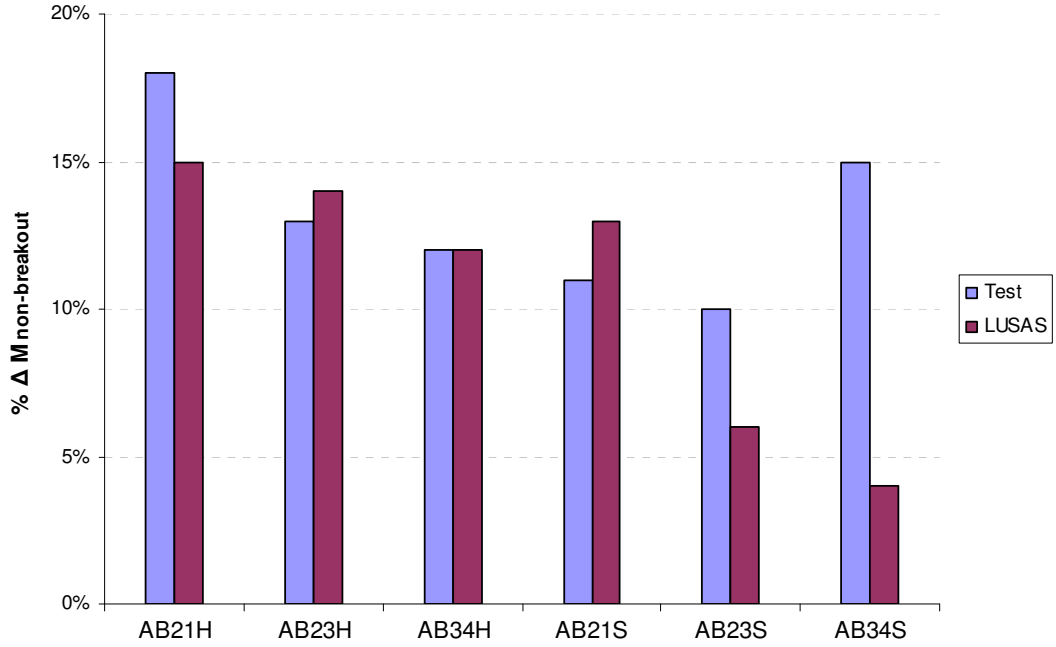

Fig. 8.5: Graph of change in moment at non-breakout location during concrete breakout

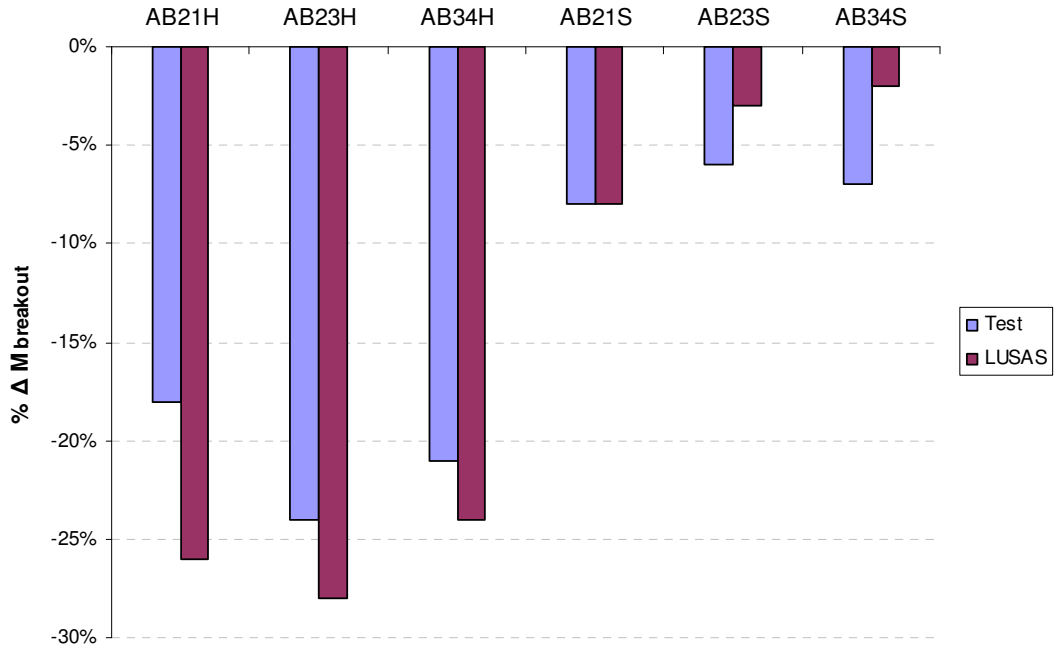

Fig. 8.6: Graph of change in moment at breakout location during concrete breakout

Before breakout began, the proportion of moment at the central support was greater in the test specimens than in the corresponding numerical models for all reinforcement combinations (by comparing initial α_m values from Table 6.8 & Table 8.2). Note: Initial moment balance within the specimens affected values of $\%\Delta M_{non\text{-}breakout}$ and $\%\Delta M_{breakout}$ in Fig. 8.5 & 8.6. For example, a smaller reduction in "breakout moment" but a larger increase in "non-breakout moment" occurred in test specimen AB21H than in the corresponding numerical model. This is due to the pre-breakout moment ratio for AB21H being significantly greater in the test specimen.

Fig. 8.7 graphs both test and LUSAS values of hogging : sagging moment ratio under service load before breakout began on all progressive breakout specimens. The reinforcement areas at relevant sections influenced the difference in moment ratios (greater difference for larger hogging : sagging reinforcement ratios). However, the hogging : sagging reinforcement ratio is not the sole influence as "fully bonded" moment ratios were generally greater in the test specimens for the full range of hogging : sagging reinforcement ratios. Therefore, the load arrangement also contributes to the difference in moment ratios.

Section 4.5.2 describes a numerical investigation of the influence of load arrangement on moment balance within a propped cantilever up to service load. Larger service load hogging : sagging moment ratios were observed for two-point load arrangements due to the greater extent of flexural cracking caused by the load being dispersed over a larger distance. This reduced the effect of tension stiffening within the spans relative to the support. This effect was more evident in the test specimens than predicted by the model and is attributed to LUSAS overestimating the extent of cracking over the central support relative to that within the spans.

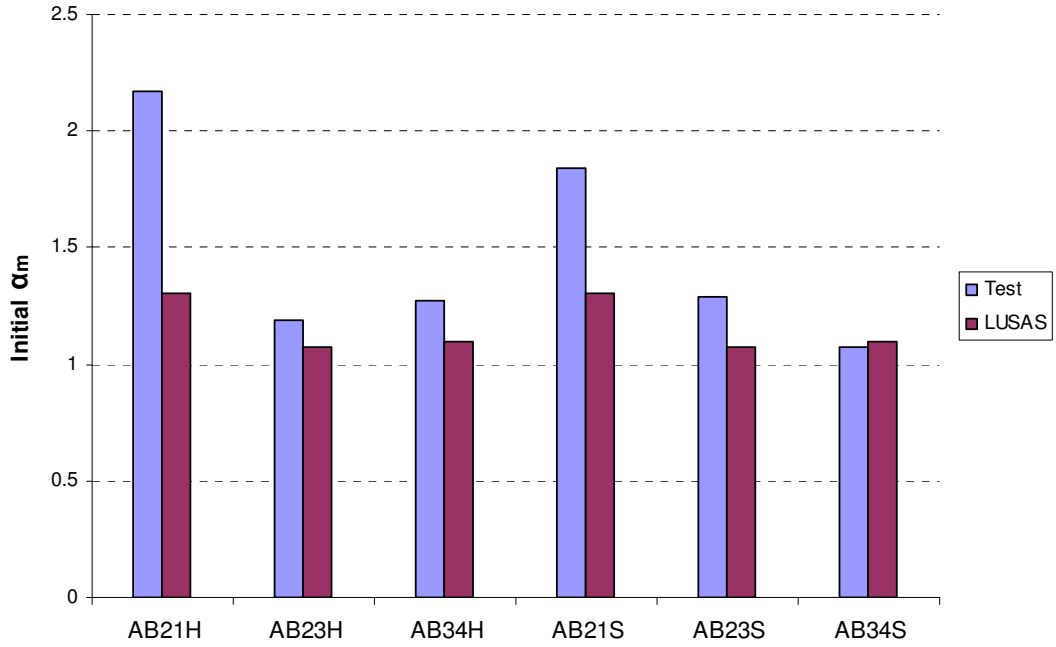

Fig. 8.7: Graph of hogging : sagging moment ratio under service load before breakout began on progressive breakout specimens

8.3.2 Extreme fibre compression strains

Increases in extreme fibre compression strains during breakout mean that reinforcement strains will be lower when concrete reaches its limiting compression strain. If concrete starts to crush before reinforcement reaches yield, the bending capacity of the section will be reduced. Even if reinforcement reaches yield, rotation capacity is expected to reduce. Compression strains at breakout and non-breakout locations were monitored throughout breakout to assess the influence on the flexural capacity of the member. Fig. 8.8 shows strain contour diagrams for AN23 and for the maximum breakout lengths for AB23H & AB23S at service load. Extreme fibre compression strains at sections of maximum hogging and sagging moment are noted on the diagrams. Compression strains at both breakout locations were approximately 100% greater than the equivalent strains in the "as new" specimen. However, increases in compression strain at non-breakout locations during breakout were small.

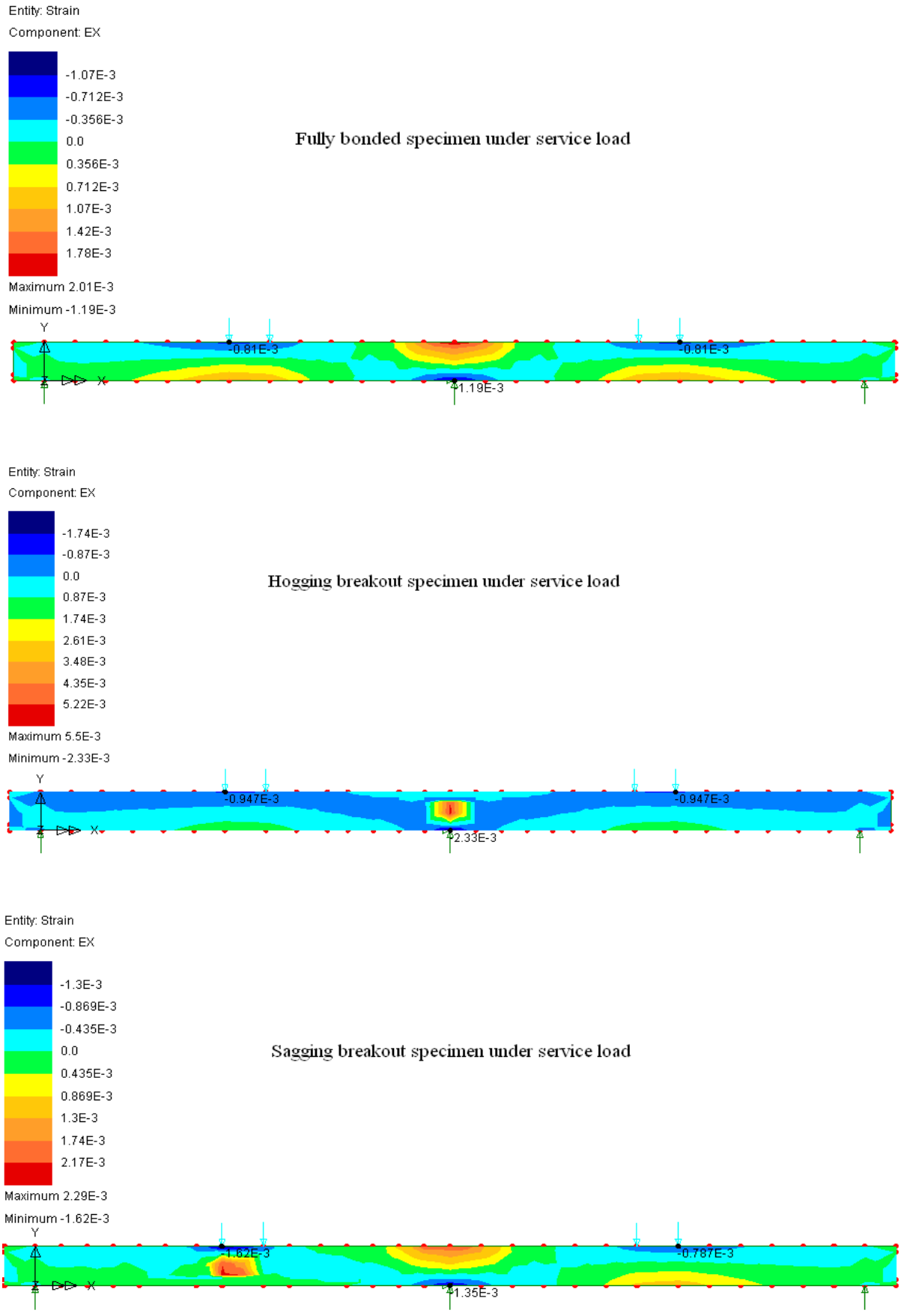

Fig. 8.8: Strain contours for AN23, AB23H & AB23S models

Fig. 8.9 graphs the pre-breakout and post-breakout compression strains at the breakout location under service load. Values of pre-breakout and post-breakout compression strain from the LUSAS analysis were similar to corresponding test measurements (from Table 6.2). Increases in compression strain at the breakout location occur in conjunction with the observed increases in curvature due to loss of bond between the steel and the concrete. Both sets of results predict increases in the compression strain at the breakout location of approximately 100% for an exposed length of reinforcement of 50% of the span length. Also, the magnitude of the compression strain increase was greater for breakout over the central support for both data sets.

Fig. 8.10 graphs the pre-breakout and post-breakout compression strains at non-breakout locations. Note: Measured reductions in non-breakout compression strain during breakout were not graphed. Increases in the non-breakout compression strain were originally expected to occur due to moment transfer to the non-breakout location during concrete breakout. The LUSAS analysis confirms that the increases in non-breakout compression strain were negligible, relative to the observed increases in compression strain at the breakout location.

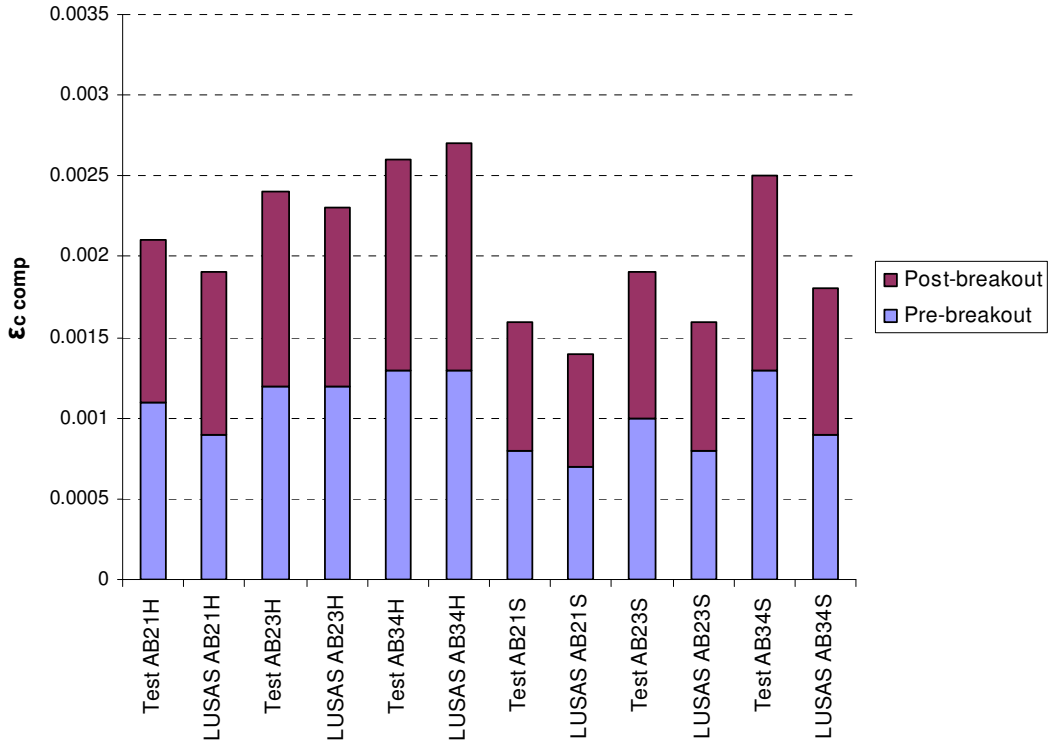

Fig. 8.9: Service load compression strains at breakout location before and after breakout

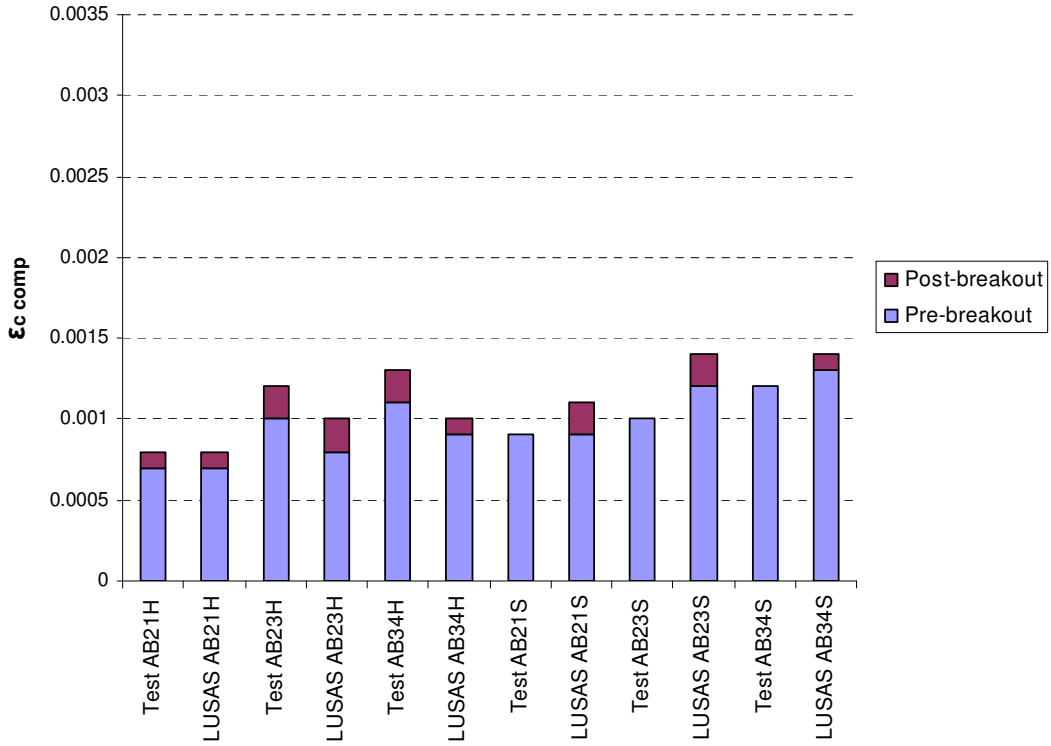

Fig. 8.10: Service load compression strains at non-breakout location before and after breakout

8.3.3 Exposed steel strain

As discussed in Section 6.3.3, the change in strain in the steel upon initial exposure could not reliably be measured during testing. LUSAS results may be used to track this strain variation so the overall change in steel strain throughout breakout can be estimated. Fig. 8.11 plots the exposed steel strain as the length of breakout increases on AB23H and AB23S. The magnitudes of the LUSAS steel strains were appreciably lower than the test measurements. The "fully bonded" steel strain measured during testing was dependent on the precise location of cracks in relation to the gauge length. "Measured" steel strains in Fig. 8.11 were considered excessive due to a greater number of cracks occurring between the Demecs, which significantly reduced the apparent influence of tension stiffening. This effect is discussed in Section 6.3.3.

Section 3.2 discussed the variation in steel strain with increasing breakout length. LUSAS predicted an increase in strain upon initial exposure of the steel for both breakout locations as tension stiffening was lost when the reinforcement was exposed. After initial exposure, the exposed steel strain decreased with increasing length of breakout, confirming the reductions observed during testing. This reduction occurred due to moment transfer away from the breakout location. The increase in the lever arm (to maintain compatibility between the exposed steel and the substrate) may have also contributed to the decrease in steel strain. LUSAS results showed the subsequent decrease in strain was more significant for breakout over the central support. This was attributed to the more severe decrease in moment for breakout at the central support than for breakout within the left span (Fig. 8.6). As significant increases in steel strain do not occur during concrete breakout, the moment capacity of the exposed steel section is not reduced unless increases in concrete strain cause an over-reinforced failure.

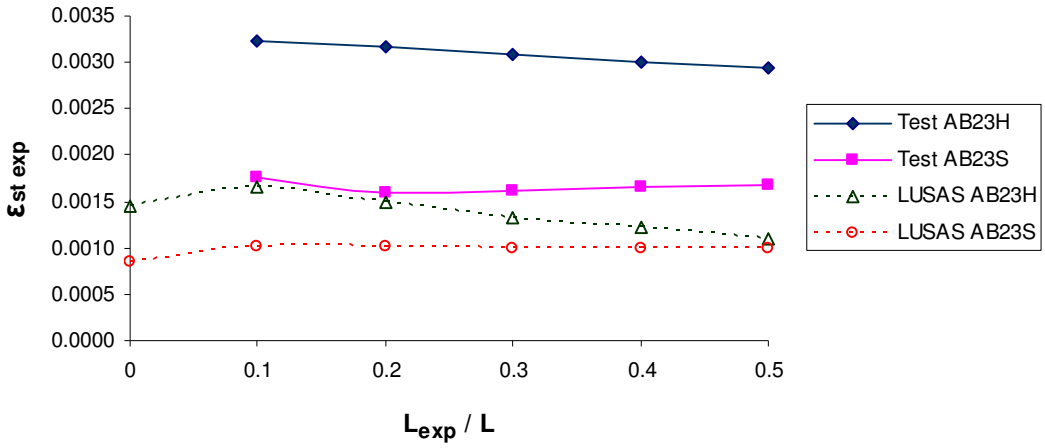

Fig. 8.11: Plot of exposed steel strain as breakout length increased on AB23H and AB23S

8.3.4 Midspan displacements

The total midspan displacements could not be recorded during testing as the displacement transducers had to be removed during concrete breakout. LUSAS results can be used to predict the overall increase in displacement during concrete breakout. Fig. 8.12 graphs the pre-breakout and post-breakout left midspan displacements under service load from both test measurements and LUSAS results. Changes in the right midspan displacement for breakout within the left span were small so changes in left midspan displacement during breakout were of primary concern. Note: The left and right midspan displacements were approximately equal for breakout over the central support. Although the displacements calculated by LUSAS are less than measured, increases in displacement during concrete breakout were consistent for both data sets. The larger pre-breakout displacements measured during testing may be attributed to the repeated load cycles and sustained loading to which the test specimens were subjected to. Increases in displacement were slightly greater for breakout within the left span (for both data sets).

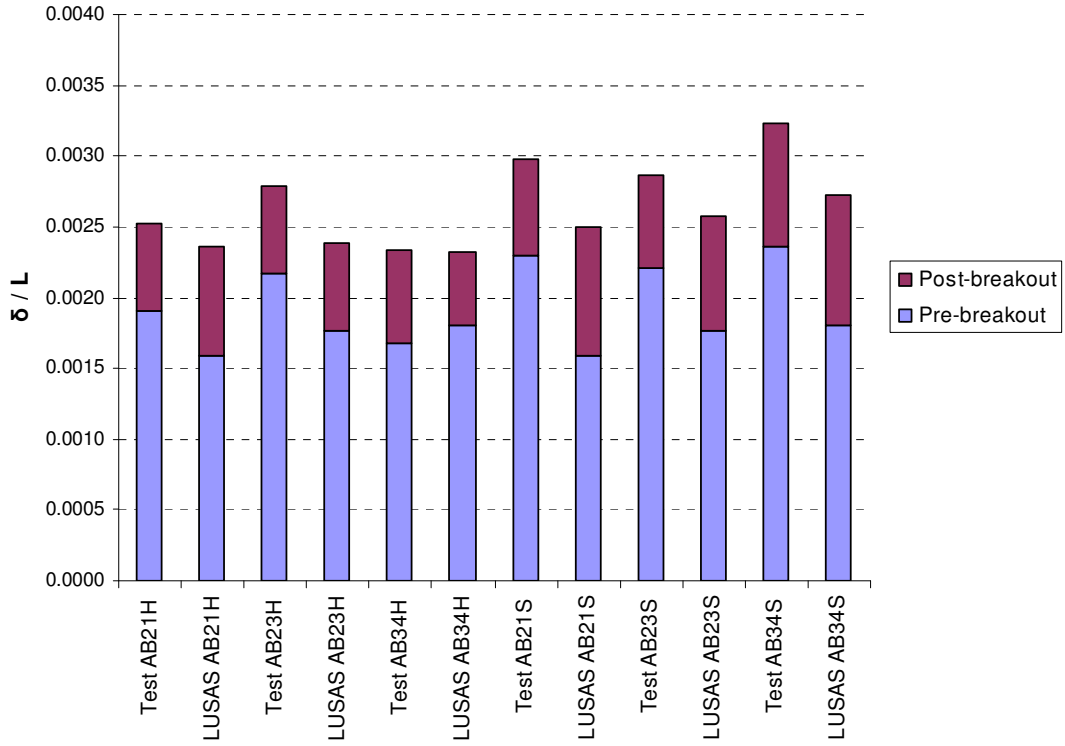

Fig. 8.12: Left midspan displacements under service load before and after breakout

8.3.5 Ultimate limit state behaviour

Table 8.3 shows the ultimate loads recorded from LUSAS for specimens with exposed reinforcement and the corresponding test failure loads. In general, LUSAS gave reasonable estimates of the measured strength. The final column in Table 8.3 describes the change in LUSAS ultimate load due to breakout (relative to the "as new" model ultimate load, Table 8.1) and thus, highlights the effect of breakout on ultimate limit state behaviour.

Slight reductions in flexural strength were observed due to breakout on AB21H & AB21S. A shear failure was observed for AN23 but a flexural failure occurred for AB23H at a greater ultimate load. Arching of the neutral axis near the breakout region increased the shear strength of AB23H. A flexural failure was also observed for AB23S but occurred at a slightly lower ultimate load than the "as new" specimen. Moment transfer due to concrete breakout on AB23H brought the bending moment diagram closer to the fully plastic bending moment diagram but had the opposite effect for breakout on AB23S. Also, the area of exposed reinforcement was greater

for AB23S so the reduction in flexural strength due to concrete breakout was greater. The increase in shear strength due to concrete breakout on AB34H & AB34S was not sufficient to ensure flexural failures. The largest shear force within the member occurred near the central support (Fig. 3.9) and breakout over the central support increased the shear strength in that region. However, breakout within the span caused moment transfer to the central support and increased the shear to the right of the central support. Consequently, the shear failure load of AB34H was appreciably higher than for AB34S. Slight reductions in flexural strength were also observed for breakout on AB12H & AB22H.

Specimen	Test failure load (kN)	Test failure mode	LUSAS failure load (kN)	LUSAS failure mode	$P_{exposed}$ / P_{bonded} (LUSAS)
AB21H	178.8	Flexural	171.4	Flexural	0.98
AB21S	176.1	Shear	172.5	Flexural	0.99
AB23H	212.6	Shear	258.2	Flexural	1.18
AB23S	225.4	Shear	216.0	Flexural	0.99
AB34H	256.3	Shear	267.9	Shear	1.11
AB34S	256.6	Flexural	232.2	Shear	0.96
AB12H	200.3	Flexural	187.1	Flexural	0.99
AB22H	193.0	Flexural	202.5	Flexural	0.99

Table 8.3: Failure loads of models with exposed reinforcement

8.4 Unloaded repair model behaviour

Repair specimen models were analysed with activation of the repair material while they were under virtually no load. This analysis procedure is described in Section 4.4.3. To examine the effect of the repair process on the flexural performance of the member, the extreme fibre compression strains at the repair locations are compared to corresponding strains in the "as new" model. Fig. 8.13 graphs the extreme fibre compression strains at the repair location (after completion of the repair) at 55% & 90% of the "fully bonded" ultimate load from both LUSAS analysis and test measurements. The corresponding strains in the "as new" models and test specimens are also included.

LUSAS compression strains at the central support at 90% of the ultimate load were noticeably greater than the corresponding test measurements. The proportion of moment at the support was less in the "fully bonded" model than observed in the test specimens (Section 8.3.1) and this was attributed to LUSAS overestimating cracking over the central support. Consequently, increases in curvature and thus, compression strain during loading to failure were greater in the model. In general, the post-repair compression strain at the repair location at 90% of the ultimate load was slightly greater than the corresponding strain in the "as new" specimen in both test and LUSAS results.

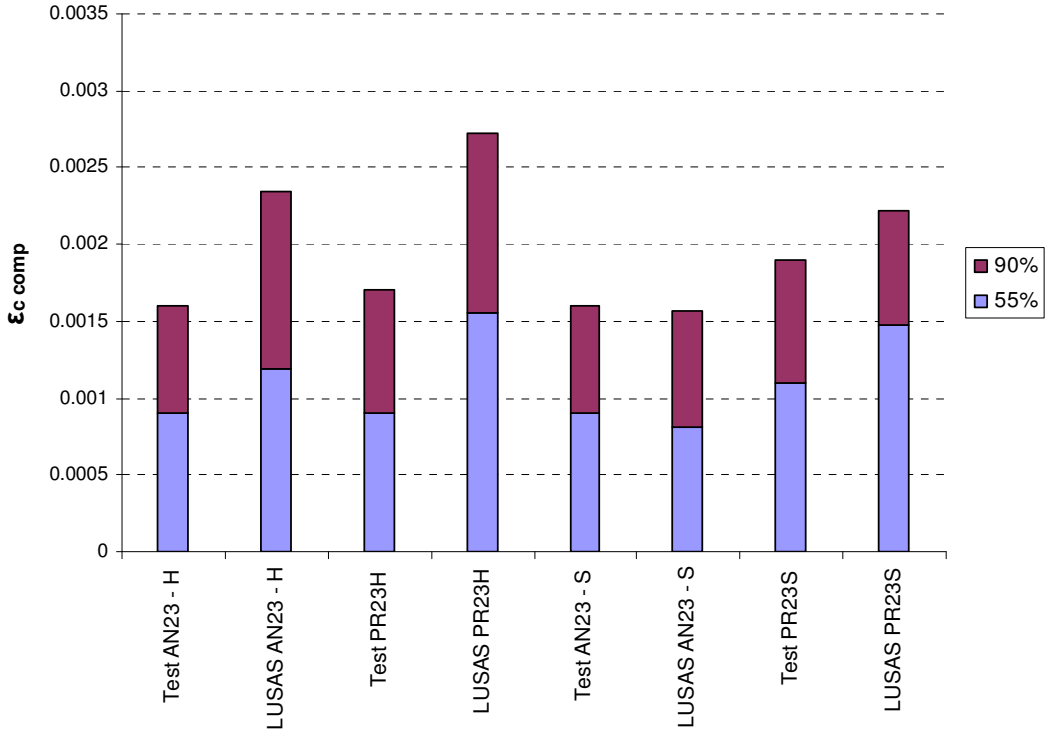

Fig. 8.13: Extreme fibre compression strains at repair locations and corresponding "as new" strains at 55% & 90% of the ultimate load ("propped" repair)

Table 8.4 displays the LUSAS failure loads for the unloaded repair specimens. The final column represents the difference between the LUSAS failure loads and the failure load of the corresponding "as new" model (Table 8.1). Both unloaded repair models failed in shear at greater loads than the equivalent "as new" model. Arching of the neutral axis near the breakout region increases the shear strength of specimens with exposed reinforcement. This arching effect was reduced during unloading before casting of the repair but was sufficient to cause the observed increases in shear strength (relative to the "as new" model). Increases in shear strength were greater for repair over the central support and this trend was apparent from both data sets. Arching of the neutral axis for repair over the support caused a greater increase in shear strength as the shear in the member was largest in this region (between the inner point loads) while arching of the neutral axis for repair within the left span had a negligible effect on shear strength within the right span.

Specimen	Test failure load (kN)	Test failure mode	LUSAS failure load (kN)	LUSAS failure mode	$P_{repaired}$ / P_{bonded} (LUSAS)
PR23H	273.9	Shear	237.3	Shear	1.08
PR23S	232.5	Shear	221.5	Shear	1.01

Table 8.4: Failure loads of models repaired while unloaded

8.5 Service load repair model behaviour

Repair specimen models were subsequently reanalysed with activation of the repair material while under a sustained load equal to the service load of the equivalent "fully bonded" specimen. Modelling of the repair procedure is described in Section 4.4.3. Again, the effect of the repair process on the flexural performance of the member can be assessed analysing the extreme fibre compression strains at the repair location close to ultimate load and comparing with the corresponding strains in the "as new" models.

Fig. 8.14 shows sample strain contours at 90% of the "fully bonded" ultimate load for AN23, UR23H and UR23S. Extreme fibre compression strains at sections of maximum hogging and sagging moment are noted. Strains at the repair cross-sections were appreciably larger than the corresponding strains in the "as new" model as the increase in compression strain during concrete breakout remained "locked into" the member. Increases in extreme fibre compression strains at non-repair locations (relative to the "as new" model) were negligible.

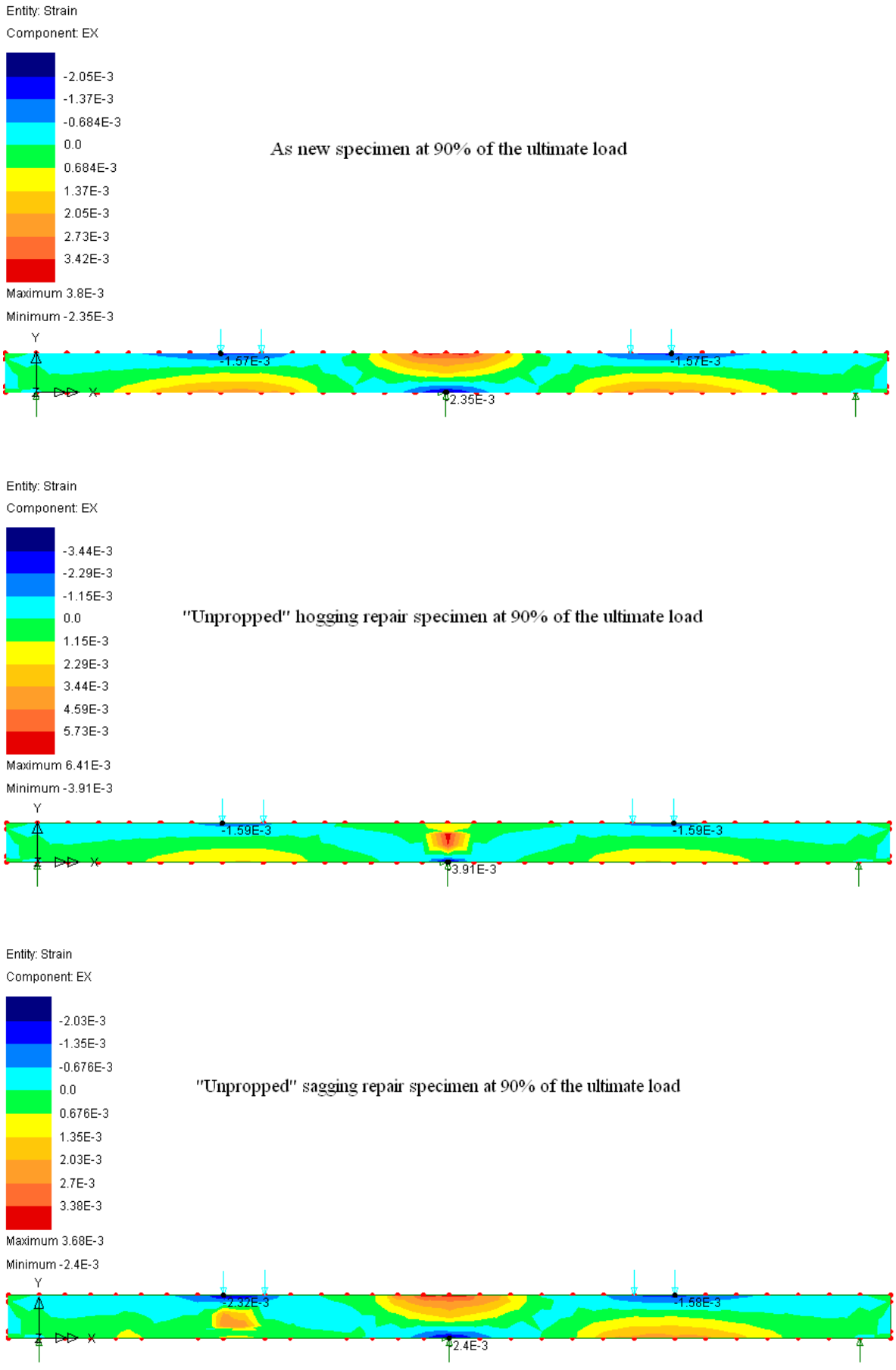

Fig. 8.14: Strain contours for AN23, UR23H & UR23S models

Fig. 8.15 shows the extreme fibre compression strains (at 55% & 90% of the "fully bonded" ultimate load) at the repair location for specimens repaired while unloaded. LUSAS showed larger increases in compression strain during loading to failure for repair over the central support when compared with the corresponding test measurements. In some cases, LUSAS compression strains at 90% of the ultimate load were in excess of 0.0035. However, for span repair, the LUSAS compression strains at 90% of the test ultimate load were less than the measured strains.

Section 8.3.1 has shown that the proportion of moment at the central support within "fully bonded" test specimens was greater than predicted by the numerical analysis. This was attributed to LUSAS overestimating cracking at the central support while underestimating cracking within the spans. Consequently, LUSAS overestimates the increase in curvature and therefore extreme fibre compression strain at the central support at 90% of the ultimate load. This trend was also apparent for the "as new" and unloaded repair models (Fig. 8.13).

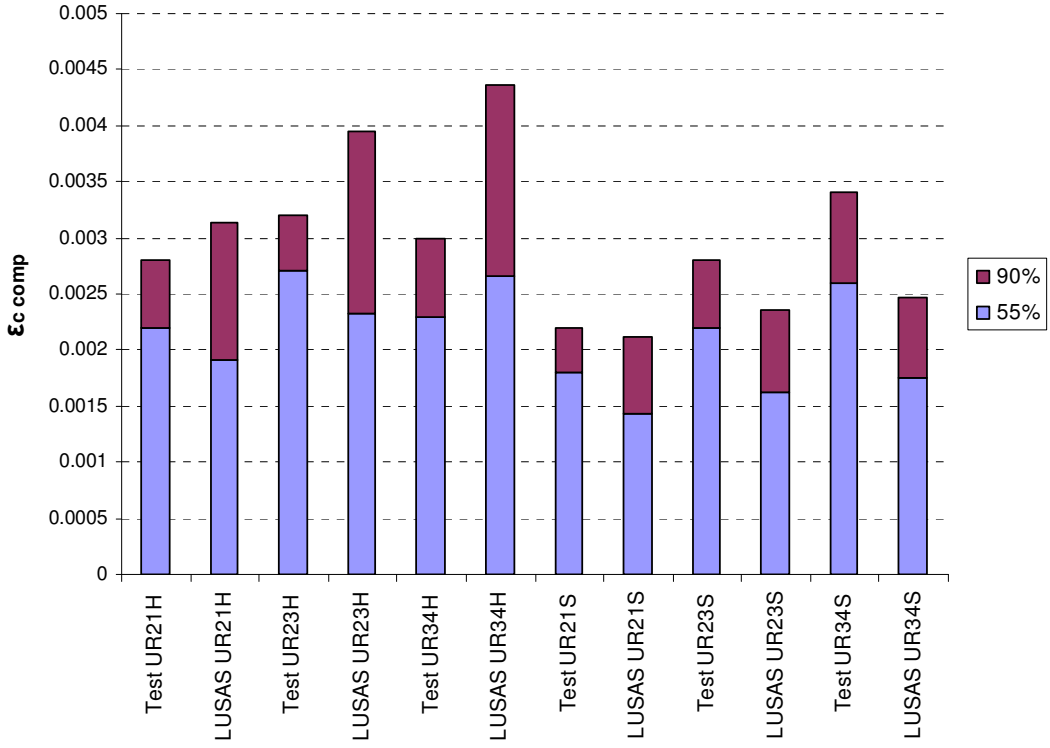

Fig. 8.15: Extreme fibre compression strains at repair locations at 55% & 90% of the ultimate load ("unpropped" repair)

Table 8.5 displays the LUSAS failure loads of specimens repaired while under service load. The final column represents the difference between the LUSAS failure loads and the failure loads from the corresponding "as new" models. The flexural strength of the UR21H model was similar to that for the "as new" model. The ultimate load of UR21S was also similar to the "as new" model but the repair process changed the failure mode from flexural to shear. Moment transfer to the central support during concrete breakout within the left span causes an increase in shear near the central support (region of highest shear within the specimen, Fig. 3.9). Consequently, the repair process reduced the shear strength of UR21S. UR23H failed in flexure at an appreciably higher load than the "as new" model. The increase in shear strength due to arching of the neutral axis near the central support delayed a shear failure in UR23H. UR23S failed in shear at a similar load to the "as new" model. Arching of the neutral axis within the left span had a negligible effect on the shear strength to the right of the central support. Similarly to UR23H, an increase in shear strength due to arching of the neutral axis near the central support occurred for UR34H but it was not sufficient to cause a flexural failure. Also, UR34S failed in shear at a similar load to the corresponding "as new" model (similar behaviour to UR23S).

Specimen	Test failure load (kN)	Test failure mode	LUSAS failure load (kN)	LUSAS failure mode	$P_{repaired}$ / P_{bonded} (LUSAS)
UR21H	198.5	Flexural	177.3	Flexural	1.01
UR21S	199.4	Flexural	174.1	Shear	0.99
UR23H	279.6	Flexural	261.2	Flexural	1.19
UR23S	219.2	Shear	221.2	Shear	1.01
UR34H	279.4	Shear	283.3	Shear	1.18
UR34S	316.2	Flexural	239.0	Shear	0.99

Table 8.5: Failure loads of models repaired at service load

8.6 Summary of numerical analysis results

Overall, general trends from numerical modelling appear consistent with experimental results. For specimens with exposed reinforcement, the moment transfer due to concrete breakout was of similar scale for both data sets. LUSAS confirms that moment transfer from the breakout location was greater for hogging breakout. Increases in extreme fibre compression strains at the breakout location during reinforcement exposure to 50% of the span length were similar to those measured during testing. Also, negligible increases in compression strain occurred at non-breakout locations for both data sets.

The effect of breakout on serviceability limit state behaviour and ultimate limit state behaviour was examined. LUSAS midspan displacements increased by approximately 30% - 55% during concrete breakout to 50% of the span length and observed increases were generally greater for breakout within the span. At the ultimate limit state, slight reductions in flexural strength ($\leq 2\%$) were observed due to reinforcement exposure. Note: It is difficult the quantify the change in flexural strength in AB23H and AB23S as the failure mode changed from shear to flexural but larger reductions in flexural strength were anticipated for greater areas of exposed reinforcement. Exposure of reinforcement over the central support caused increases in the shear strength of the member due to arching of the neutral axis in the region of highest shear. However, for breakout within the left span, arching of the neutral axis within that span had a negligible effect on shear capacity to the right of the central support. Also, moment transfer to the central support during concrete breakout within the span increased shear near the support. Consequently, appreciable increases in shear strength due to reinforcement exposure were observed for breakout over the support but the changes in shear strength for span breakout were negligible.

Ultimate limit state behaviour of repaired models was similar to the test specimens. LUSAS failure loads for “hogging” repair were consistently greater than the corresponding failure loads for “sagging” repair. Repair over the central support was more influential in increasing the shear strength throughout the member. This trend was more pronounced for specimens repaired under service load as the “tied-arch” effect was reduced during unloading for specimens repaired under zero load. Also, reductions in flexural strength were less likely for repair over the central support, particularly for specimens of lower hogging : sagging reinforcement ratio as the

"unpropped" repair process brought the bending moment diagram closer to the fully plastic moment diagram.

Some minor discrepancies were apparent between test measurements and numerical results. Differences in behaviour at the ultimate limit state are discussed in Section 8.2. Unload – reload behaviour in the model did not accurately represent behaviour in the test specimens as the reduction in stiffness (due to flexural cracking) occurred earlier in the test specimens (than predicted by the model). Disagreement between the service load hogging : sagging moment ratio for "fully bonded" specimens was also apparent. Values of α_m in "fully bonded" test specimens were consistently larger than in the corresponding models. This was attributed to LUSAS overestimating the extent of cracking occurring over the central support. This reduced the tension stiffening effect at the support and consequently, extreme fibre compression strains at the central support were greater than the corresponding test measurements.

Chapter 9: Discussion of results

9.1 Introduction

Chapters 6 & 7 present and analyse results from the experimental investigation on the patch repair of two-span reinforced concrete beams. The influence of the parameters chosen for investigation on critical measures of structural performance is assessed. Chapter 8 compares the experimental results with results from a finite element analysis of the specimens. Reasonable correlation exists between numerical and experimental results and general trends appear to coincide. The numerical analysis was also used to monitor changes in behaviour that could not be measured during testing (e.g. exposed steel strains and midspan displacements).

The current chapter gives an overview of the results. The influences of the chosen parameters are quantified and assessed in terms of their advisable limits. This allows a series of guidelines to be formulated to ensure the behaviour of a member both during and after completion of a patch repair is acceptable. The relative merits of propped and unpropped repair are also debated. From this, a desirable proportion of load relief during casting of the repair can be chosen by the contractor depending on the design of the existing member and the requirements of the repaired structure.

9.2 Behaviour of members with exposed tension reinforcement

9.2.1 Influence of load arrangement on moment balance

An extensive experimental investigation of the influence of load arrangement on specimen behaviour during repairs was deemed beyond to scope of this study. However, a two-point load arrangement was chosen within the spans to highlight the difference between behaviour within the relatively constant moment zone within the spans and at the peak moment above the "one-point" central support reaction. Two positions of breakout (over the central support and within one of the spans) were chosen for investigation during testing. Much of the difference in behaviour between breakout locations can be attributed to the shape of the bending moment diagram and therefore the load arrangement within the breakout region.

The bending moment at relevant sections within a "fully bonded" specimen at service load provides a baseline against which, moment transfer that occurs during reinforcement exposure can be evaluated. As appreciable flexural cracking occurs up to service load, the moment balance (i.e. the ratio of maximum hogging : sagging moments) in a "fully bonded" specimen is primarily dictated by the reinforcement areas. However, the load arrangement has also been shown to influence the service load moment balance **[59]**.

A numerical investigation of the influence of load arrangement on the moment balance at service load was carried out (Section 4.5.2). The load arrangement influenced the length of the flexurally cracked zones and therefore moment balance within the member. A single concentrated load at the midspan of a continuous beam caused a lower hogging : sagging moment ratio than a two-point load arrangement or a distributed load. Consequently, the two-point load arrangement used during testing caused the "fully bonded" hogging : sagging moment ratios at service load to be larger than initially expected (initial α_m values, Table 6.8).

While the hogging : sagging reinforcement area ratio dictated the moment balance within the "fully bonded" specimen, it had little influence on the moment transfer that took place during concrete breakout. Moment transfer was primarily influenced by the position of breakout (i.e. essentially the load arrangement within the breakout region). Previous research **[2]** on beams with exposed reinforcement under a two-

point load arrangement have shown that for a given value of maximum moment, the elongation of the exposed steel and therefore the loss of section stiffness was greater when the point loads were positioned closer together, as discussed in Section 3.2. This trend was apparent from test measurements and numerical results as greater moment transfer from the breakout location occurred for breakout over the "one-point" central support reaction than for the two-point load arrangement within the spans (Fig. 8.6).

9.2.2 Influence of breakout length on flexural strength

Moment transfer during concrete breakout was monitored during testing to assess whether concrete breakout at one location causes overstressing at other locations within the member. Experimental and numerical results showed that increases in extreme fibre compression strains at non-breakout locations during concrete breakout were negligible (Fig. 8.10). Therefore, the effect of concrete breakout on the flexural strength of the member was primarily influenced by the increase in compression strain at the breakout location.

As the length of breakout increases, departure from "as new" specimen behaviour is more severe. The increase in extreme fibre compression strain at the breakout location to maintain compatibility between the exposed steel and the substrate causes a reduction in flexural capacity if reinforcement is unable to reach yield before concrete crushes. Even if reinforcement reaches yield, exposure will reduce strain hardening before concrete starts to crush. The loss of flexural strength mainly depends on the length of breakout and the area of tension reinforcement at the breakout location. If a section is initially designed for a balanced failure, it essentially becomes over-reinforced when the reinforcement is exposed, due to the increase in concrete compression strain. Therefore, loss of flexural strength is less severe in more lightly reinforced sections as the reinforcement is more likely to reach yield before concrete crushing begins.

Section 2.3.2 describes a simplified analysis to quantify the maximum "allowable" breakout length to ensure reinforcement reaches yield before concrete crushes. As LUSAS analysis of specimens with exposed reinforcement was verified against experimental results, LUSAS may be used to explore the validity of Equation 2.11.

Fig. 9.1 shows the simplified model used to verify Equation 2.11. As the increase in compression strain at the breakout location was of primary concern, a simply supported model was sufficient to assess the effect of the breakout length on ultimate flexural strength.

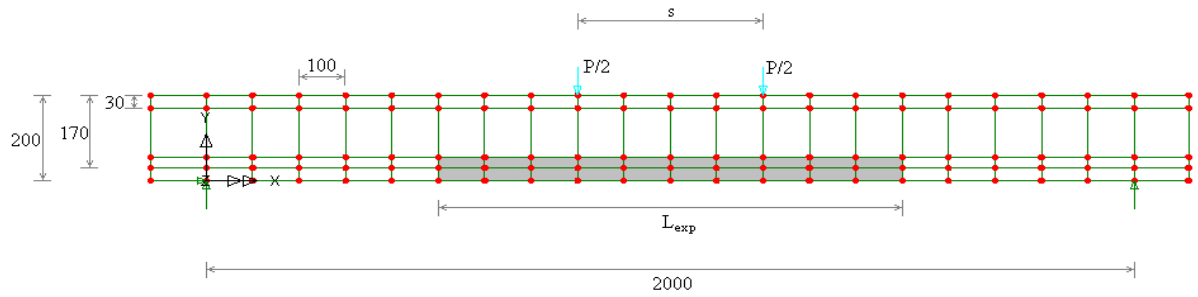

Fig. 9.1: Simplified model for breakout length investigation

Relevant model information is as follows: b = 150mm, d = 170mm, L = 2000mm, $A_{s\ top}$ = 100mm^2, $A_{s\ bottom}$ = 100mm^2 – 600mm^2, A_{sv} = 60mm^2, s_v = 100mm, s = 0m – 1m, f_{cu} = 35N/mm^2, E_c = 32.5kN/mm^2, f_y = 520N/mm^2, E_{st} = 200kN/mm^2.

Fig. 9.2 shows a sample plot of ultimate load of a specimen with exposed reinforcement (relative to the ultimate load for the "fully bonded" specimen) vs. breakout length (relative to span length) for $A_{s\ bottom}$ = 300mm^2 and s = 0.4m. Note: Sufficient shear reinforcement was included in the model to ensure a flexural failure so Fig. 9.2 represents the reduction in flexural strength. Fig. 9.3 shows the corresponding plot of the reduction in exposed steel strain at ultimate load as the breakout length increased ($\varepsilon_y = f_y / E_{st}$ = 0.0026). Note: If reinforcement reached yield, steel strain values at ultimate load were plotted as 0.0026 for clarity, as subsequent increases in strain before the model failed to converge were quite random.

The correlation between Fig. 9.2 & 9.3 is evident. Where $L_{exp} \leq s$ (i.e. reinforcement exposure within the constant moment zone), the change in ultimate flexural strength was negligible. For $L_{exp} / L \leq 0.3$, the steel strain still reached yield at ultimate load and the moment capacity was scarcely affected. For $0.3 < L_{exp} / L < 0.6$, the steel strain at ultimate load was slightly less than yield but the extreme fibre compression strain was also below its limit (due to premature failure to converge). For $L_{exp} / L \geq 0.6$, significant reductions in flexural strength occurred due to a shift towards over-reinforced behaviour.

From the model results, the "allowable" L_{exp} was calculated for $\varepsilon_{st} = 0.9\ \varepsilon_y$, to account for the "ultimate load" strain being slightly less than yield due to premature failure to converge. In this case, the "allowable" $L_{exp} = 0.54L$, which coincides with a reduction in ultimate flexural strength of 11%.

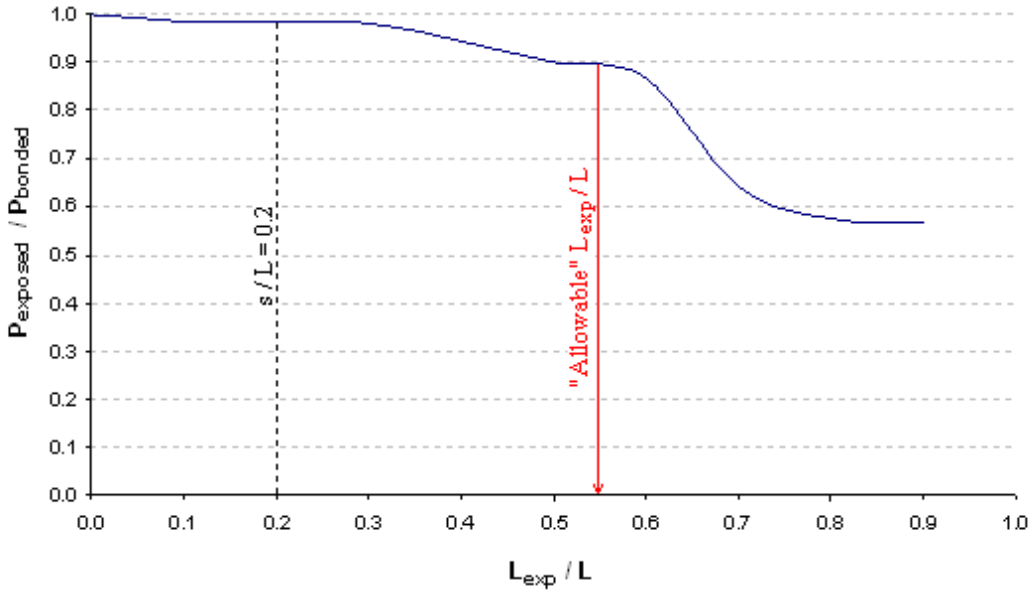

Fig. 9.2: Reduction in ultimate strength with increasing breakout length

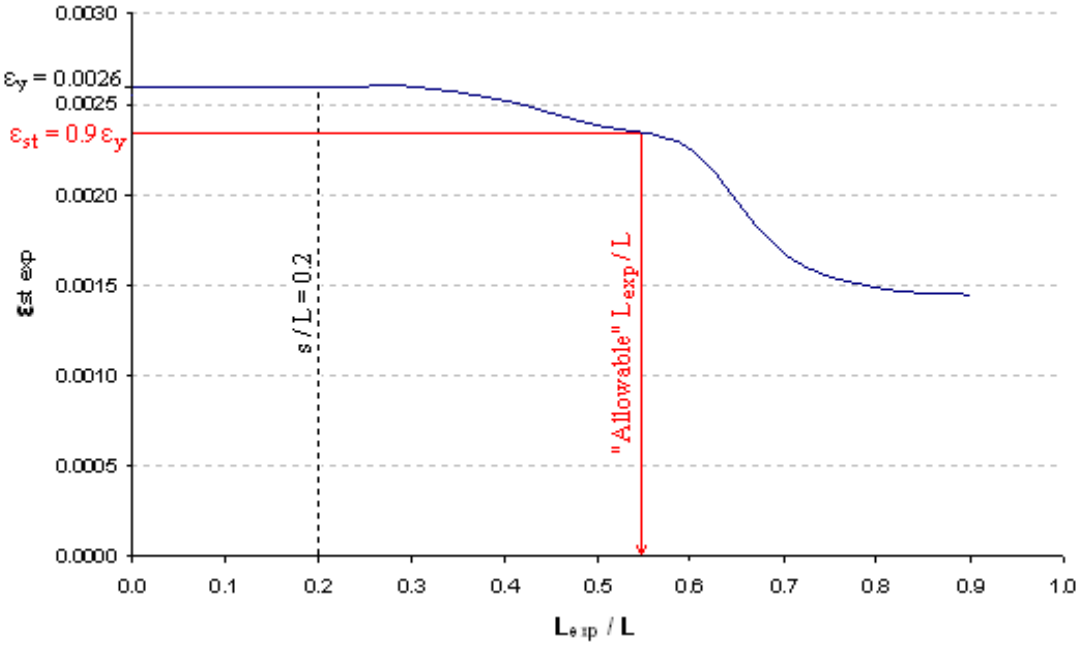

Fig. 9.3: Reduction in exposed steel strain at ultimate load with increasing breakout length

The validity of Equation 2.11 was checked by calculating the "allowable" exposed length and comparing with the value estimated from Fig. 9.3. The length over which the limiting compression strain is reached, L_{crush}, was initially taken as 0.4m (the spacing of the point loads). The compression zone depth (x) was calculated from Equation 2.5. The "allowable" breakout length from Equation 2.11 (for the example chosen here) is then

$$L_{exp} = (0.4)\ (200000 / 520)\ (0.0035)\ ((170 - 49.3) / 49.3) = 1.318m = 0.66\ L \qquad 9.1$$

To cover a range of sections, the x / d ratio was varied by varying the area of tension reinforcement between $100mm^2$ – $600mm^2$. This range of reinforcement areas covered the typical range of x / d values (0.10 – 0.58, from Equation 3.3). The LUSAS analysis was repeated for the range of x / d ratios and breakout lengths while maintaining all other parameters constant. The "allowable" L_{exp} was determined for each value of x / d and was taken as the exposed length corresponding to a steel strain at ultimate load of $\varepsilon_{st} = 0.9\ \varepsilon_y$.

Fig. 9.4 plots the "allowable L_{exp}" vs. the x / d ratio from both the LUSAS analysis and from Equation 2.11. In general, Equation 2.11 gives a reasonable approximation of the "allowable L_{exp}" derived from LUSAS (generally conservative for larger x / d). For x / d < 0.21, breakout can essentially extend to the support points without loss of flexural strength if sufficient anchorage is provided. For greater x / d, the "allowable" exposed length reduces as loss of flexural strength is more likely in heavily reinforced sections.

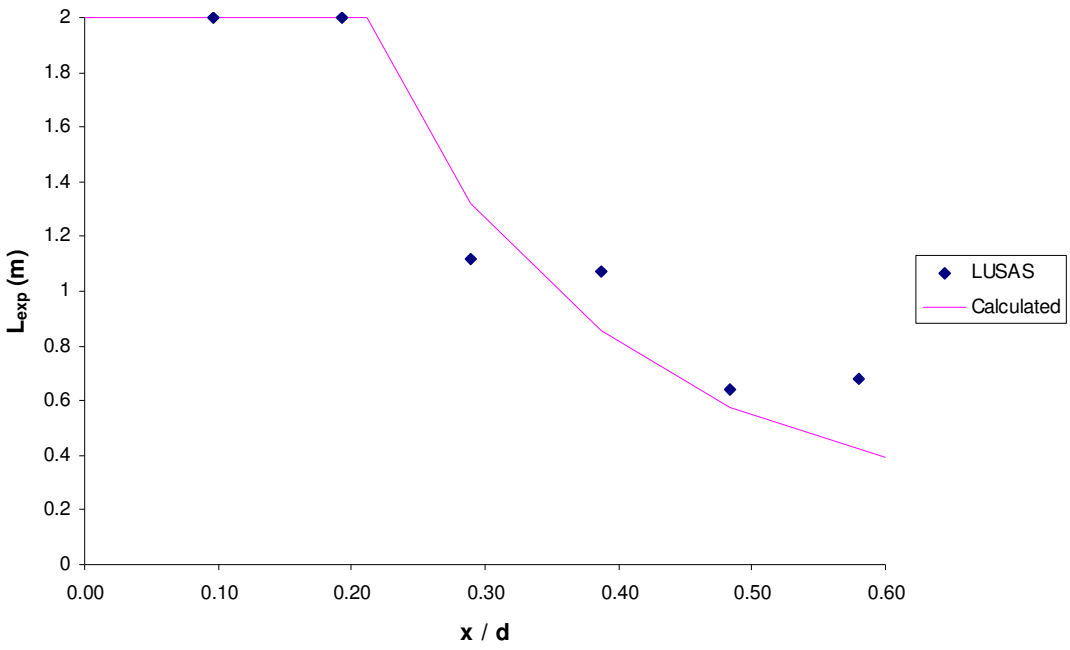

Fig. 9.4: "Allowable L_{exp}" vs. x /d ratio (L_{crush} = s = 0.4m)

From Equation 2.11, the "allowable" breakout length is directly proportional to the length over which the limiting compression strain is reached (L_{crush}) at ultimate load in the "fully bonded" section, so the assumed value of L_{crush} has a significant effect on the "allowable L_{exp}". Cairns **[25]** suggests that if the load arrangement does not produce a constant moment zone (e.g. a single point load arrangement), L_{crush} may be calculated using an expression derived by Phipps **[26]** (Equation 2.7). Pannell **[73]** carried out tests on unbonded prestressed concrete beams under a central point load and found the length over which crushing occurs at ultimate load as L_{crush} = 10x. This expression would allow a significantly longer breakout length than that calculated using the expression derived by Phipps **[26]**. Cairns also suggests that for a two-point load arrangement, L_{crush} should be taken as the spacing between the point loads. The LUSAS model was further analysed to investigate the influence of the "L_{crush}" parameter on the "allowable L_{exp}".

For this analysis, the area of tension reinforcement was initially maintained constant ($A_{s\ bottom}$ = 300mm^2 → x / d = 0.29). The spacing between the point loads was varied between 0m – 1.0m. The length over which crushing occurs, L_{crush} was taken as the spacing between the point loads for calculation of the "allowable L_{exp}" from Equation 2.11. Fig. 9.5 shows the resulting plot of "allowable L_{exp}" vs. s. Equation 2.11

assumes that the "allowable breakout length" is directly proportional to L_{crush}. This assumption is conservative for values of $s = L_{crush} < 0.31m$. For distances between the point loads greater than 0.31m, the assumption that the limiting compression strain is reached throughout the constant moment zone is flawed and Equation 2.11 is unconservative.

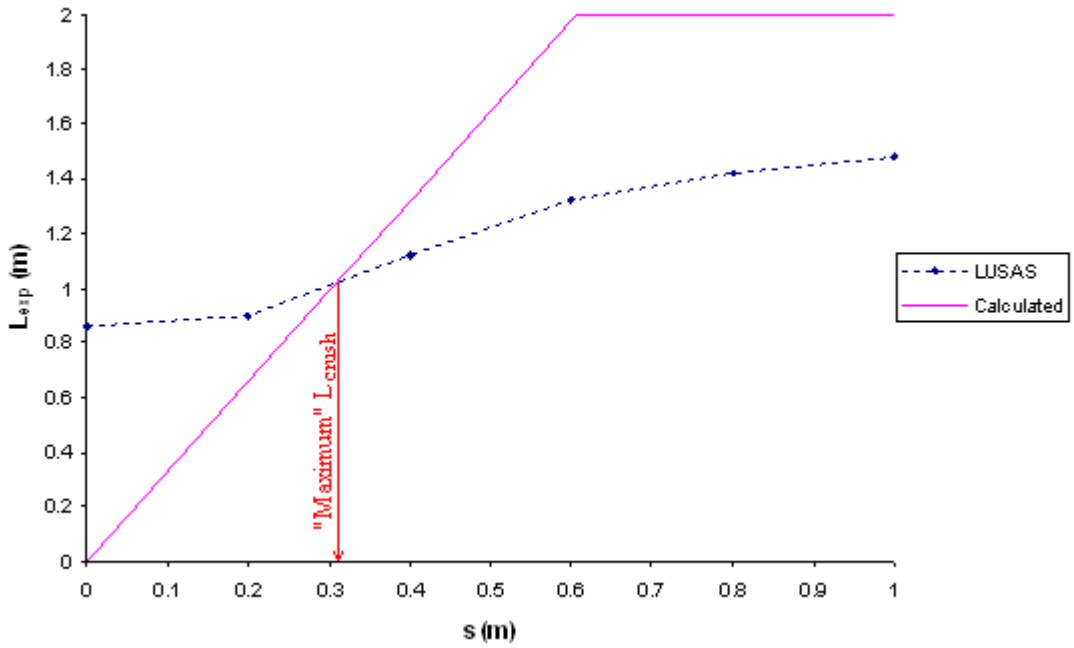

Fig. 9.5: "Allowable L_{exp}" vs. s (x / d = 0.29)

The "maximum L_{crush}" value of 0.31 (Fig. 9.5) represents the maximum point load spacing for which, L_{crush} can be assumed equal to s (for an x / d ratio of 0.29). The analysis was re-run for the full range of x / d and limiting L_{crush} values (for which L_{exp} from Equation 2.11 becomes unconservative) were established. Note: A 5m long model (with identical properties to that in Fig. 9.1) was used to establish the "maximum L_{crush}" value for $x / d \leq 0.19$, as reinforcement yielded before concrete crushing, even when breakout continued to the supports in the 2m long model (for this range of x / d). "Maximum L_{crush}" values for $x / d > 0.19$ from the 2m long model were verified using the 5m long model. Fig. 9.6 shows a plot of the "maximum L_{crush}" value for the full range of x / d. The best-fit polynomial equation to the data points describes the maximum L_{crush} value in terms of the x / d ratio.

$$L_{crush} = 2.263(x/d)^2 - 0.286(x/d) + 0.239 \qquad 9.2$$

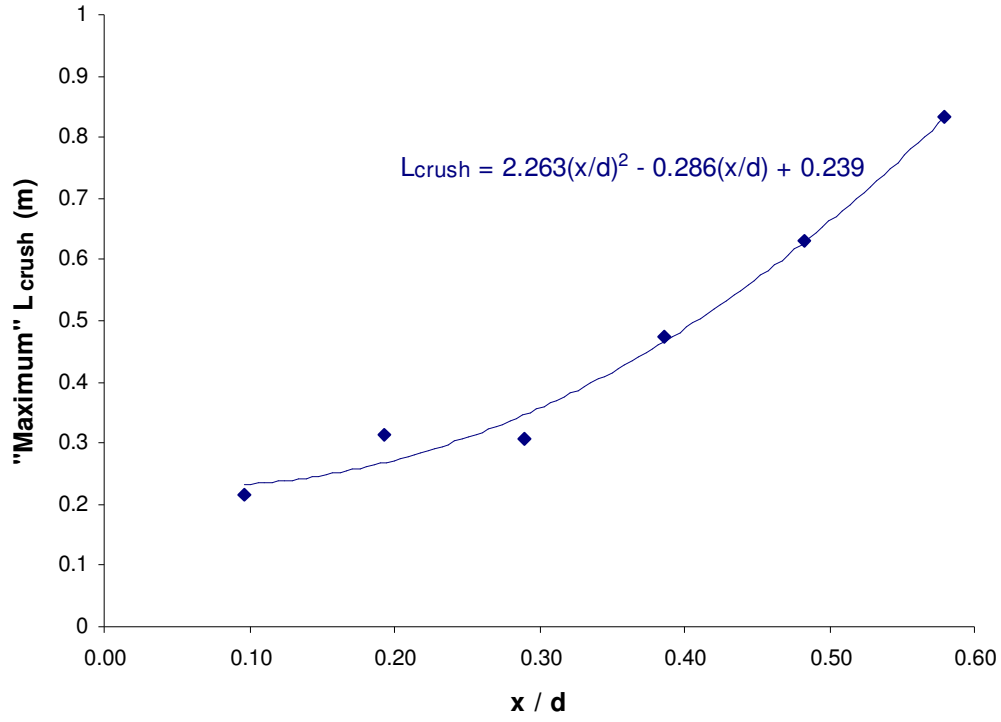

Fig. 9.6: Plot of "maximum" L_{crush} vs. x / d ratio

9.2.3 Serviceability limit state behaviour

It is desirable that the service load behaviour of the repaired specimen is acceptable. If serviceability limit state criteria are exceeded, remedial measures should be taken (e.g. epoxy resin injection of cracks). If a repair is to be carried out under service load, the service load behaviour of the repaired specimen will be similar to that of the specimen with exposed reinforcement. It is therefore desirable that serviceability limit state criteria are not exceeded by the specimen with exposed reinforcement.

Crack widths at service load should not exceed 0.3mm. Excessive crack widths may facilitate moisture ingress and cause subsequent corrosion within the repaired structure. As stated in Section 6.2, cracks at the breakout location exceeded the allowable serviceability limit but substrate cracks are generally injected with an epoxy resin during the repair process. Cracks at non-breakout locations approached the 0.3mm serviceability limit due to moment transfer from the breakout location. Fig. 9.7 illustrates the increases in displacement due to breakout (to the left of the supports shown) for "pinned" and "encastre" supports. Section rotation was permitted at the

"pinned" supports in the test apparatus so increases in non-breakout curvatures during concrete breakout were less than for a specimen that prevented rotation at the supports. Consider a continuous beam monolithically cast into a reinforced concrete structure. In-situ cast columns at the internal supports would severely reduce the amount of rotation allowed to occur. This rotational restraint would increase the curvature and therefore crack widths at non-breakout locations. Therefore, further investigation of other structural arrangements is necessary.

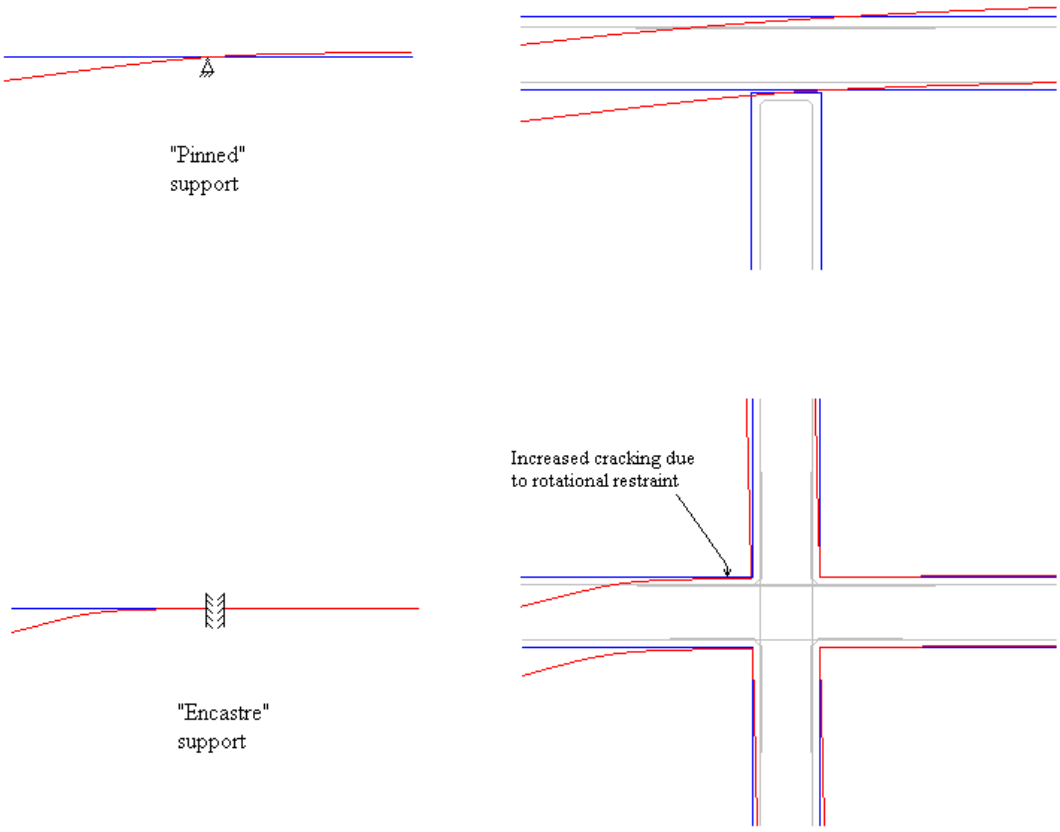

Fig. 9.7: Increase in displacement due to breakout for "pinned" and "encastre" supports

Upper and lower bound estimates of the service load displacements of specimens with reinforcement exposed over 50% of the span length are displayed in Table 6.10. In some cases, the upper bound estimates exceeded the maximum allowable displacement of 8mm, for a 2m span. These upper bound displacements were considered excessive as a portion of the tension reinforcement was exposed before loading began. It should also be noted that structural continuity at the supports would

considerably reduce the service load displacements of a member with exposed reinforcement.

The tolerable increase in displacement due to concrete breakout depends on the span / effective depth ratio (L / d) of the specimen. As stated in Section 3.3, the L / d ratio chosen for all test specimens was 11.9 (average effective depth of 168mm). The basic L / d ratio (excluding modification factors for tension and compression reinforcement) for the test load arrangement was 23 (BS 8110 **[61]**). Therefore, an appreciable increase in displacement due to concrete breakout was permitted. The observed increases in displacement (relative to the average "fully bonded" service load displacement) ranged between 21% – 49% for the "lower bound" estimates and 48% – 87% for the "upper bound" estimates. For a given L / d ratio, the tolerable increase in displacement can be established. Where the tolerable increase in displacement is small (L / d close to the limiting value), the soffit of the repaired beam may be recast near the supports to reduce the visual impact of the excessive displacement.

9.3 Unpropped vs. propped repair

9.3.1 Behaviour during loading to failure

The effect of the repair process on ultimate strength and flexural stiffness during loading to failure is of particular interest. Service load section curvatures at the repair location were significantly greater for specimens repaired under service load than for unloaded repair specimens as the curvature increase during "unpropped" concrete breakout remains "locked into" the member. However, the flexural stiffness at both repair and non-repair locations during subsequent loading to failure was consistently greater for specimens repaired under service load than for unloaded repair specimens (Table 6.7). In most cases, the flexural stiffness of the specimens repaired under service load was also greater than the corresponding "as new" specimens. Casting a repair under service load meant that the repair material was only strained by subsequent increase in load. Consequently, cracking within the patch repair during loading to failure was less severe in specimens repaired under service load so the contribution of the repair material to tension stiffening was significant. This is consistent with earlier work on simply supported beams **[4]**.

Increases in extreme fibre compression strain at the breakout location reduce the flexural strength of a member with exposed reinforcement. If the repair material is cast under load, the altered strain pattern remains "locked into" the member. Therefore, subsequent increases in compression strain during loading to failure of the repaired specimen are of interest, particularly for "unpropped" repair. The increase in compression strain was greater for larger values of ultimate load x / d as tension stiffening within the patch repair was less significant for larger reinforcement areas and thus, larger values of x / d. Caution is urged when choosing an acceptable repair length or required proportion of load relief during casting of a repair for specimens with large x / d ratios.

9.3.2 Ultimate limit state behaviour

It is desirable that the patch repair process does not reduce the load carrying capacity of the structure. Also, significant loss of section ductility at the repair location is undesirable. It is difficult to assess the effect of the patch repair process on section ductility from tests conducted here as the mode of failure was not consistent throughout. Evaluation of ultimate limit state behaviour is more reliable by considering the shear strength and flexural strength of the members separately.

Increases in shear strength occur near the breakout region due to arching of the neutral axis where bars are exposed. As shear within the member was greatest near the central support, appreciable increases in shear strength were observed for hogging repair specimens. As the strains throughout the member reduced significantly during unloading for casting of an unloaded repair, the arching effect was less significant than for a repair under load. Therefore, a greater increase in shear strength was expected for a specimen repaired under service load. From both test results and numerical modelling, UR23H suffered a flexural failure at a higher load than the shear failure load of PR23H. For repair within the left span, the change in neutral axis profile and therefore shear strength within the "undamaged" right span was insignificant. Changes in ultimate load for both UR23S and PR23S (relative to the corresponding "as new" specimen) were small and the observed shear failures in the test specimens occurred within the "undamaged" right span.

The proximity of a repaired section to a flexural failure was assessed by comparing the extreme fibre compression strains and "previously exposed" steel strains at 90% of the "fully bonded" ultimate load. The compression strains at the repair cross-section in the "unpropped" repair specimens (at 90% of the ultimate load) were appreciably greater than those for the "propped" repaired specimens (and also the corresponding strains in the equivalent "as new" specimens) due to the increase in extreme fibre compression strain during the breakout process that remained "locked into" the member once the repair was cast. The previously exposed steel strains (at 90% of the ultimate load) for "unpropped" repair specimens were only slightly less than for "propped" repair specimens. This suggests a flexural failure was closer for the specimens repaired under load and if the repaired specimens possessed sufficient section rotation capacity, flexural failure loads would be greater for the unloaded repair specimens. The strain patterns therefore suggest that a greater proportion of

load relief during casting of the repair increases the flexural strength of a repaired member. However, provided reinforcement reaches yield, a reduction in strength (as a result of the member carrying load during the repair) would not be expected. As the extreme fibre compression strain is greater for repair under load, the limiting compression strain of 0.0035 is reached at a lower deformation. Consequently, a reduction in member ductility (i.e. the deformation between reinforcement yield and concrete crushing) is also expected.

Chapter 10: Conclusions and recommendations for further research

10.1 Conclusions

1. Moment balance within "fully bonded" members at service load primarily depends on reinforcement areas at relevant sections within the member. However, the load arrangement also influences the service load moment balance.

2. Moment transfer away from the breakout location (to elsewhere within the member) increases with the length of breakout. The rate of transfer is greater for a concentrated load than for a distributed load within the breakout length.

3. Increases in compression strains at non-breakout locations due to moment transfer from the breakout region are small in relation to increases in strain within the breakout region, and are deemed insignificant. Initial concerns that moment transfer during concrete breakout may cause overstressing elsewhere within the structure are largely unfounded.

4. For "unpropped" repair, crack widths at the repair location were excessive but epoxy resin injection before casting of the repair material may be used to restore the member. Service load crack widths at the non-repair locations were not excessive but curvature patterns suggest rotational restraint from columns in a framed structure could increase crack widths near internal supports.

5. The tolerable increase in service load displacement during the breakout process depends on the L / d ratio of the "fully bonded" member. Displacement increase is directly proportional to the breakout length with increases of 30% – 55% expected for breakout to 50% of the span. If predicted displacements are considered excessive, partial or complete removal of the imposed load before casting of the repair can reduce service load displacements of the repaired member.

6. The increase in the extreme fibre compression strain at the breakout location is the main criterion for limiting the advisable exposed length. The acceptable breakout length to ensure yielding of reinforcement at ultimate load is given from

$$L_{exp} \leq (L_{crush} E_{st} / f_y) \, 0.0035 \, ((d - x) / x)$$

where L_{exp} = the length of exposed reinforcement

E_{st} = the elastic modulus of the reinforcement

f_y = the yield capacity of the reinforcement

d = the effective depth of the reinforcement

x = the neutral axis depth at ultimate load

$$L_{crush} \, (m) = 2.263(x/d)^2 - 0.286(x/d) + 0.239$$

for specimens of a similar scale to those tested in this study ($d \approx 170mm$).

7. The flexural stiffness of an "unpropped" repaired member on reloading after repair is greater than for a "propped" repaired member due to the greater contribution to tension stiffening of the less highly strained repair concrete. The stiffness is also generally greater than that of an equivalent "as new" specimen.

8. An over-reinforced failure is more likely to occur in "unpropped" repaired specimens (than in "propped" repaired specimens) due to the increase in compression strain at the breakout location that remains "locked into" the member. Even if the reinforcement yields, the ductility of the "unpropped" repaired section would be less.

9. The shear strength of a member is not significantly reduced by the patch repair process. Increases in shear strength occur if the patch repair is in a region of high shear, particularly if the repair is cast while the specimen is under load. This is attributed to tied-arch action caused by arching of the neutral axis where the reinforcement was exposed.

10.2 Recommendations for further research

1. Structural continuity affects the curvatures and therefore crack widths during the breakout process (Section 9.2.3). The effect of rotational restraint should be examined through other structural arrangements.

2. Numerical simulations investigating the influence of load arrangement on the service load moment pattern of "fully bonded" continuous members was carried out (Section 4.5.2). An experimental study of the influence of load arrangement would prove insightful. This study could be extended to include specimens after concrete breakout and after completion of a patch repair.

3. The expression in Conclusion 6 for the length over which, the limiting compression strain is reached at ultimate load is applicable to the scale of specimens tested in this study. Further experimental and numerical investigation is required to modify the expression to make it generally applicable.

4. Where severe corrosion has taken place, specimens may require replacement of existing bars or lapping with supplementary reinforcement. The effect of lapped reinforcement within patch repairs requires investigation.

References

[1] Swiss Bank Corporation (Stockbrokers). Quarterly building bulletin, London, January 1989, 5-7.

[2] Cairns J. and Zhao Z. Behaviour of concrete beams with exposed reinforcement. Procs ICE Structures and Buildings, May 1993, **99**, 141-154.

[3] Raoof M. and Lin Z. Structural characteristics of R.C. beams with exposed main steel. Procs ICE Structures and Buildings, February 1997, **122**, 35-51.

[4] Cairns J. Load relief during structural repairs to reinforced concrete beams. Procs ICE Structures and Buildings, November 1993, **99**, 417-427.

[5] Mangat P.S. and O'Flaherty F.J. Factors affecting the efficiency of repair to propped and unpropped bridge beams. Magazine of Concrete Research, August 2000, **52**, 303-319.

[6] Canisius T.D.G. and Waleed N. The behaviour of concrete repair patches under propped and unpropped conditions: Critical review of current knowledge and practices. FBE Report 3, March 2002.

[7] Mangat P.S. and Molloy B.T. Prediction of free chloride concentration in concrete using routine inspection data. Magazine of Concrete Research, December 1994, **46**, 279-287.

[8] Al-Sulaimani G.J., Kaleemullah M., Basunbul A. and Rasheeduzzafar. Influence of corrosion and cracking on bond behaviour and strength of reinforced concrete members. ACI Structural Journal, March 1990, **87**, 220-231.

[9] Cairns J., Du Y. and Law D. Structural performance of corrosion-damaged concrete beams. Magazine of Concrete Research, June 2008, **60**, 359-370.

[10] Mangat P.S. and Elgarf M.S. Flexural strength of concrete beams with corroding reinforcement. ACI Structural Journal, January 1999, **96**, 149-158.

[11] Eyre J.R. and Nokhasteh M.A. Strength assessment of corrosion damaged reinforced concrete slabs and beams. Procs ICE Structures and Buildings, May 1992, **94**, 197-203.

[12] Collins F. and Roper H. Laboratory investigation of shear repair of reinforced concrete beams loaded in flexure. ACI Materials Journal, March 1990, **97,** 149-159.

[13] Abu-Tair A., Rigden S. and Burley L. The effectiveness of the resin injection repair method for cracked RC beams. The Structural Engineer, October 1991, **69,** 335-341.

[14] Tabor L.J. The evaluation of resin systems for concrete repair. Magazine of Concrete Research, 1978, **30**, 221-225.

[15] Chung H.W. Epoxy-repaired reinforced concrete beams. ACI Journal, May 1975, 233-234.

[16] Emmons P.H., Vaysburd A.M. and McDonald J.E. A rational approach to durable concrete repairs. Concrete International 1993, **15**, 40-45.

[17] Emmons P.H., Vaysburd A.M. and McDonald J.E. Concrete repair in the future turn of the century – any problems? Concrete International 1994, **16**, 42-49.

[18] Davison N., Roberts A., Taylor J., Glass G. and Aldridge, D. Innovative approaches to electrochemical remediation of concrete. Technical Report: Fosroc International Ltd.

[19] Haboubi L. Extending the boundaries of concrete repair – an electrochemical approach to cost-effective durability. Concrete, January 2001.

[20] Garbacz A., Gorka M. and Courard L. Effect of concrete surface treatment on adhesion in repair systems. Magazine of Concrete Research, February 2005, **57**, 49-60.

[21] Austin S.A. and Robins P.J. Development of patch test to study behaviour of shallow concrete patch repairs. Magazine of Concrete Research, September 1993, **45,** 221-229.

[22] Zhang S. and Raoof M. Prediction of the behaviour of R.C. beams with exposed reinforcement. Magazine of Concrete Research, December 1995, **47**, 335-344.

[23] Raoof M. and Lin Z. Implications of exposure of main steel during patch repairs. International Association for Bridge and Structural Engineering, 1995, **73/1**, 499-504.

[24] Raoof M. and Lin Z. Loss of strength in reinforced concrete beams due to exposure of reinforcement: Synopsis. The Structural Engineer, July 1994, **72,** 229.

[25] Cairns J. Strength of concrete beams during concrete breakout. International Association for Bridge and Structural Engineering, 1995, **73/1**, 499-504.

[26] Phipps M.E. The strain capacity of compression-zone concrete subjected to short term loading. Magazine of Concrete Research, June 1976, **28.**

[27] Cairns J. and Rafeeqi S.F.A. Analysis of reinforced concrete beams strengthened by external unbonded bars. Magazine of Concrete Research, April 2002, **54**, 141-153.

[28] Cairns J., Carpi R. and Plizzari G.A. Strengthening of reinforced concrete beams using external reinforcement: Effect of load at installation. Procs International Conference on Structural Faults and Repair 2003.

[29] Cairns J. and Rafeeqi S.F.A. Strengthening reinforced concrete beams with external unbonded bars: experimental investigation. Procs ICE Structures and Buildings, February 2003, **156**, 27-37.

[30] Cairns J. and Rafeeqi S.F.A. Strengthening reinforced concrete beams with external unbonded bars: theoretical investigation. Procs ICE Structures and Buildings, February 2003, **156**, 39-48.

[31] Cairns J. Minelli F. and Plizzari G.A. Strengthening RC beams by external reinforcement. Technical Report: Heriot Watt University.

[32] Kong F. and Evans R.H. Reinforced and prestressed concrete. Van Nostrand Reinhold, London, 1987, 3rd Edition.

[33] Cairns J. Strength in shear of concrete beams with exposed reinforcement. Procs ICE Structures and Buildings, May 1995, **110**, 176-185.

[34] Jeppsson J. Shear behaviour of beams with reduced bond on longitudinal reinforcement. Technical Report: Lund Institute of Technology.

[35] Canisius T.D.G. and Waleed N. Concrete patch repairs under propped and unpropped implementation. Procs ICE Structures and Buildings, April 2004, **157**, 149-156.

[36] Cairns J. Alternative strategies for temporary support during structural repair of reinforced concrete beams. Journal of Structural Engineering, March 1996, **122,** 238-246.

[37] Ali Y. A.-Z. and Ambalavanan R. Flexural behaviour of reinforced concrete beams repaired with styrene-butadiene rubber latex, silica fume and methycellulose repair formulations. Magazine of Concrete Research, April 1999, **51,** 113-120.

[38] Emberson N.K. and Mays G.C. Significance of property mismatch in the patch repair of structural concrete. Part 1: Properties of repair systems. Magazine of Concrete Research, September 1990, **42,** 147-160.

[39] Mai Y.-W. and Cotterell B. Porosity and mechanical properties of epoxy resin modified cement mortar. Cement and Concrete Research 1986, **16**, 646-652.

[40] Emberson N.K. and Mays G.C. Significance of property mismatch in the patch repair of structural concrete. Part 2: Axially loaded reinforced concrete members. Magazine of Concrete Research, September 1990, **42,** 161-170.

[41] Plum D.R. The behaviour of polymer materials in concrete repair, and factors influencing selection. The Structural Engineer, September 1990, **68,** 337-345.

[42] Mangat P.S. and Limbachiya M.C. Repair material properties for effective structural application. Cement and Concrete Research 1997, **27**, 601-617.

[43] Mangat P.S. and Elgarf M.S. Strength and serviceability of repaired reinforced concrete beams undergoing reinforcement corrosion. Magazine of Concrete Research, April 1999, **51,** 97-112.

[44] Rizzo E.M. and Sobelman M.B. Selection criteria for concrete repair materials. Concrete International, September 1989, 46-49.

[45] Emmons P.H., Vaysburd A.M. and McDonald J.E. The total system concept – necessary for improving the performance of repaired structures. Concrete International 1995, **17**, 31-36.

[46] Xiong G., Liu J. and Xie H. Flexural behaviour of reinforced concrete beams with unbonded repair patch. ACI Structural Journal, September 2000, **97,** 783-786.

[47] Cleland D.J. and Long A.E. The pull-off test for concrete patch repairs. Procs ICE Structures and Buildings, November 1997, **122**, 451-460.

[48] Cleland D.J. and Basheer L. Pull-off adhesion testing for concrete repairs. Magazine of Concrete Research, December 2007, **59**, 771-776.

[49] Mays G.C. and Barnes R.A. The structural effectiveness of large volume patch repairs to concrete structures. Procs ICE Structures and Buildings, November 1995, **110**, 351-360.

[50] Mangat P.S. and O'Flaherty F.J. Influence of elastic modulus on stress redistribution and cracking in repair patches. Cement and Concrete Research 2000, **30**, 125-136.

[51] Emberson N.K. and Mays G.C. Significance of property mismatch in the patch repair of structural concrete. Part 3: Reinforced concrete members in flexure. Magazine of Concrete Research, March 1996, **48,** 45-57.

[52] Mangat P.S. and O'Flaherty F.J. Long term performance of high-stiffness repairs in highway structures. Magazine of Concrete Research, October 1999, **51,** 325-339.

[53] Asad M., Baluch M.H. and Al-Gadhib A.H. Drying shrinkage stresses in concrete patch repair systems. Magazine of Concrete Research, December 1997, **49,** 283-293.

[54] O'Flaherty F.J. and Mangat P.S. A simplified design approach to prevent shrinkage cracking in patch repairs. Magazine of Concrete Research, February 2006, **58,** 31-42.

[55] Mangat P.S. and O'Flaherty F.J. Analysis of interfacial shrinkage stresses in patch repairs. Magazine of Concrete Research, September 2004, **56,** 375-386.

[56] Scott R.H. and Whittle R.T. Serviceability influences on moment redistribution in beams. Structural Concrete 2005, **6,** 135-140.

[57] do Carmo R.N.F. and Lopes S.M.R. Ductility and linear analysis with moment redistribution in reinforced high strength concrete beams. Canadian Journal of Civil Engineering 2005, **32,** 194-203.

[58] Beeby A.W. Ductility in reinforced concrete: why it is needed and how is it achieved? The Structural Engineer, September 1997, **75,** 311-318.

[59] Scott R.H. and Whittle R.T. Moment redistribution effects in beams. Magazine of Concrete Research, February 2005, **57,** 9-20.

[60] Blight G.E., Alexander M.G. and Lampacher B.J. Structural repair of reinforced concrete portal frame. Magazine of Concrete Research, 1993, **45,** 97-101.

[61] British Standards Institution. Structural use of concrete – Design and Construction. BSI London, 1997, BS 8110-1:1997

[62] LUSAS Theory Manual 1: Version 14.1.

[63] Comité Euro-International du Béton-Fédération International de la Précontrainte. CEB-FIP Model Code 1990. Thomas Telford, London 1993.

[64] British Standards Institution. Measurement of bending dimensions. BS4466:1989.

[65] British Standards Institution. Testing Concrete – Part 116 Method of determination of compressive strength of concrete cubes. BS 1881-116:1983.

[66] Fosroc Ltd. Renderoc LA: Shrinkage compensated micro-concrete.

[67] British Standards Institution. Testing Concrete – Part 117 Method for determination of tensile splitting strength. BS 1881-117:1983.

[68] British Standards Institution. Testing Concrete – Part 121 Method of determination of static modulus of elasticity in compression. BS 1881-121:1983.

[69] Croney D. and Croney P. Design and performance of road pavements 3rd Edition, 1994, 223-224.

[70] Lange D. Long term strength development of pavement concretes. Journal of Materials in Civil Engineering, February 1994, **6,** 78-87.

[71] Al-Khaiat H. and Fattuhi N. Long-term strength development of concrete in arid conditions. Cement and Concrete Composites 2001, **23,** 363-373.

[72] Alexander M.G. An experimental critique of the BS8110 method of estimating concrete elastic modulus. Magazine of Concrete Research, December 1991, **43,** 291-304.

[73] Pannell F. N. The ultimate moment of resistance of unbonded prestressed concrete beams. Magazine of Concrete Research, March 1969, **21,** 43-54.

Appendix A

The load arrangement used during testing was analysed using the stiffness matrix method to acquire the elastic bending moment diagram. Due to the symmetry of the load arrangement about the internal support, the structure may be analysed as a propped cantilever shown in Fig. A.1.

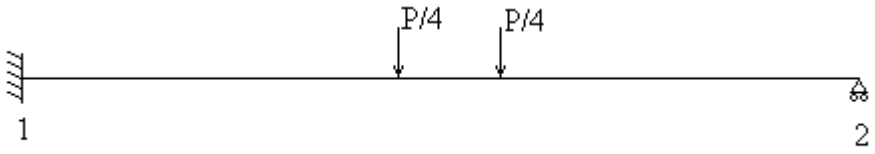

Fig. A.1: Propped cantilever representing test load arrangement

To analyse the structure, it was initially rendered kinematically indeterminate. This was achieved by imagining the joints clamped to prevent displacement. The resulting solution is the particular solution of the structure. Fig. A.2 shows the structure for the particular solution. From the symmetry of the structure, the vertical reactions $R_L = R_R = P/4$. The moment at the fixed supports is found from

$$M = P/4 \{((0.9)(1.1^2) / 2^2) + ((1.1)(0.9^2) / 2^2)\} = 0.1238P \quad \text{A.1}$$

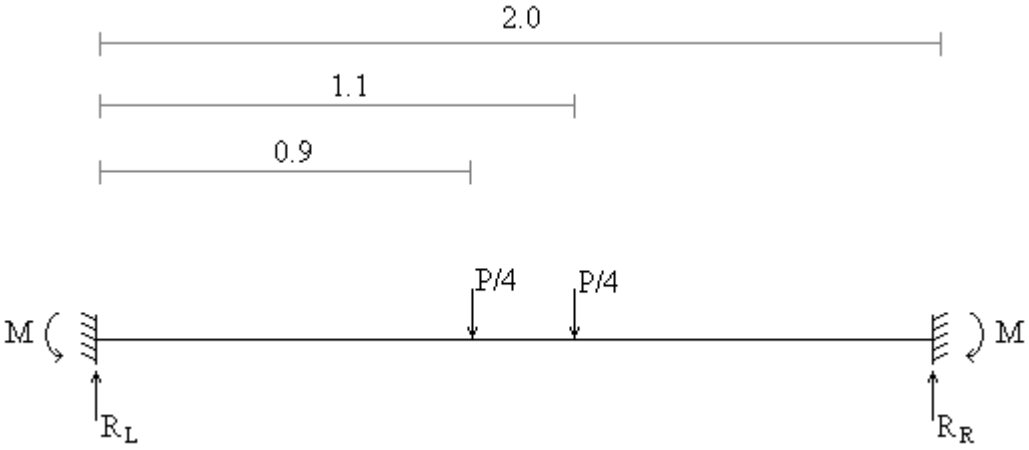

Fig. A.2: Structure for particular solution

The particular solution for the structure was then

$$p_1^{part} = \begin{Bmatrix} 0.25P \\ -0.1238P \end{Bmatrix} \qquad p_2^{part} = \begin{Bmatrix} 0.25P \\ 0.1238P \end{Bmatrix}$$

A complementary analysis was then carried out by applying a set of joint loads equal to those exerted by the clamps in the particular solution. Since node 2 is the only node which undergoes a displacement, the stiffness equation for the structure may be written as $K_{22}\, u_2 = p_2$ where $p_2 = -p_2^{part}$. The following is the full form of the stiffness equation (Note: Axial displacements were considered negligible).

$$\begin{Bmatrix} 12EI/L^3 & 6EI/L^2 \\ 6EI/L^2 & 4EI/L \end{Bmatrix} \begin{Bmatrix} \delta_2 \\ \theta_2 \end{Bmatrix} = \begin{Bmatrix} q_2 \\ m_2 \end{Bmatrix}$$

The value of EI was taken as constant throughout the member. The span length, L = 2m. Also, the vertical displacement at node 2, $\delta_2 = 0$.

$$EI \begin{Bmatrix} 1.5 & 1.5 \\ 1.5 & 2.0 \end{Bmatrix} \begin{Bmatrix} 0 \\ \theta_2 \end{Bmatrix} = \begin{Bmatrix} -0.25P \\ -0.1238P \end{Bmatrix}$$

Solving this matrix gave the rotation at node 2.

$2\theta_2 = -0.1238P / EI \rightarrow \theta_2 = -0.0619\, P / EI$ A.2

The complementary solutions were found from $p_1^{comp} = K_{12}\, u_2$ and $p_2^{comp} = K_{22}\, u_2$

$$p_1^{comp} = EI \begin{Bmatrix} -1.5 & -1.5 \\ 1.5 & 1.0 \end{Bmatrix} \begin{Bmatrix} 0 \\ -0.0619P / EI \end{Bmatrix} = \begin{Bmatrix} 0.0929P \\ -0.0619P \end{Bmatrix}$$

$$p_2^{comp} = EI \begin{Bmatrix} 1.5 & 1.5 \\ 1.5 & 2.0 \end{Bmatrix} \begin{Bmatrix} 0 \\ -0.0619P / EI \end{Bmatrix} = \begin{Bmatrix} -0.0929P \\ -0.1238P \end{Bmatrix}$$

Superimposing both the particular and complementary solutions gave

$$p_1 = p_1^{part} + p_1^{comp} = \begin{Bmatrix} 0.25P + 0.0929P \\ -0.1238P - 0.0619P \end{Bmatrix} = \begin{Bmatrix} 0.3429P \\ -0.1857P \end{Bmatrix}$$

$$p_2 = p_2^{part} + p_2^{comp} = \begin{Bmatrix} 0.25P - 0.0929P \\ 0.1238P - 0.1238P \end{Bmatrix} = \begin{Bmatrix} 0.1571P \\ 0 \end{Bmatrix}$$

Therefore, the moment at the internal support was -0.1857P.

$M_{hog} = 0.186P$ A.3

The maximum sagging moment in the span was calculated from the roller support reaction.

$M_{sag} = 0.9\ (0.1571P) = 0.141P$ A.4

Appendix B

Sample failure load calculation for AN23 to BS 8110 **[61]**

Geometric properties of AN23 (from Table 5.3)

b = 150mm

d = 168mm

$A_{s\ hog}$ = 326mm^2

$A_{s\ sag}$ = 502mm^2

s_v = 125mm

A_{sv} = 57mm^2

Material properties of AN23 (from Table 5.5)

$f_{y\ hog}$ = 570N/mm^2

$f_{y\ sag}$ = 559N/mm^2

f_{yv} = 439N/mm^2

f_{cu} = 42.6N/mm^2

The moment capacity at sections of maximum hogging and sagging moment was calculated from

$$M_{cap} = A_s f_y z \quad \text{B.1}$$

The x / d ratio at a given cross-section was calculated from

$$x / d = (A_s f_y) / (0.9\ (0.67)\ f_{cu}\ b\ d) \quad \text{B.2}$$

Over the central support, $x / d = (326\times570) / (0.9\ (0.67)\times42.6\times150\times168) = 0.29$ B.3

Within the spans, $x / d = (502\times559) / (0.9\ (0.67)\times42.6\times150\times168) = 0.43$ B.4

The lever arm at a given section was calculated from the x / d ratio

$$z = d\ (1 - 0.45\ x / d) \quad \text{B.5}$$

The lever arm of the section of maximum hogging moment was given by

$$z_{hog} = 168\ (1 - 0.45\ (0.29)) = 146\text{mm} \quad \text{B.6}$$

Similarly, the lever arm of the section of maximum sagging moment was given by

$$z_{sag} = 168\ (1 - 0.45\ (0.43)) = 135\text{mm} \quad \text{B.7}$$

At the central support, $M_{cap} = 326\times570\times146\times10^{-6} = 27.13\text{kNm}$ B.8

Within the spans, $M_{cap} = 502\times559\times135\times10^{-6} = 37.88\text{kNm}$ B.9

All specimens were designed for varying amounts of moment redistribution from the central support. To calculate the allowable redistribution from the support, the value of β_b must first be calculated from

$$\beta_b = x / d + 0.4 \quad \text{B.10}$$

For redistribution from the central support

$$\beta_b = 0.29 + 0.40 = 0.69 \quad \text{B.11}$$

The allowable redistribution was then given from

$$\text{Allowable redistribution} = (1 - \beta_b) \times 100\% \quad \text{B.12}$$

$$\text{Allowable redistribution from support} = (1 - 0.69) \times 100\% = 31\% \quad \text{B.13}$$

Note: Value exceeds BS 8110 **[61]** limit of 30% imposed for serviceability reasons.

The next step was to calculate the shear capacity of the section. The design concrete shear stress was calculated from

$$v_c = 0.79 \{100A_s / (b\,d)\}^{1/3} (400/d)^{1/4} (40/25)^{1/3} \quad \text{B.14}$$

A smaller area of tension reinforcement gives a smaller design concrete shear stress. As a constant shear reinforcement spacing was used throughout the test specimens, the most critical section shear capacity was calculated for a section with the smallest area of tension reinforcement. For AN23, the design concrete shear stress was calculated using the area of tension reinforcement over the central support.

$$v_c = 0.79 \{100 \times 326 / (150 \times 168)\}^{1/3} (400/168)^{1/4} (40/25)^{1/3} = 1.25 \text{ N/mm}^2 \quad \text{B.15}$$

The design shear stress was then calculated from

$$v = \{(A_{sv} f_{yv})/(b\, s_v)\} + v_c \quad \text{B.16}$$

$$v = \{(57 \times 439)/(150 \times 125)\} + 1.25 = 2.57 \text{ N/mm}^2 \quad \text{B.17}$$

The shear force capacity was then calculated from

$$V_{cap} = v\, b\, d = 2.57 \times 150 \times 168 \times 10^{-3} = 64.76\text{kN} \quad \text{B.18}$$

The test load arrangement and elastic bending moment diagram are shown in Fig. 3.5. The stiffness method used to acquire the elastic bending moment diagram is described in Appendix A. The required redistribution (relative to the elastic bending moment diagram) to achieve the fully plastic bending moment diagram was calculated by setting the hogging : sagging moment ratio (α_m) equal to the reinforcement area ratio (α_r). The reinforcement ratio was calculated as

$$\alpha_r = A_{s\,hog} / A_{s\,sag} = 326 / 502 = 0.65 \qquad \text{B.19}$$

If the fully plastic bending moment diagram is achieved, the hogging and sagging moments are related by

$$\alpha_m = M_{P\,hog} / M_{P\,sag} = 0.65 \rightarrow M_{P\,hog} = 0.65\, M_{P\,sag} \qquad \text{B.20}$$

From the fully plastic bending moment diagram (Fig. 3.6), the maximum hogging and sagging moments can be related to the applied load.

$$M_{P\,sag} + (0.9/2)\, M_{P\,hog} = (0.9)\, P/4 \qquad \text{B.21}$$

By substituting from Equation B.20 into Equation B.21, the "fully plastic" hogging and sagging moments can be calculated

$$M_{P\,sag} = 0.225\, P / (1 + 0.45\, (0.65)) = 0.174P \qquad \text{B.22}$$

$$M_{P\,hog} = 0.65\, (0.174P) = 0.113P \qquad \text{B.23}$$

The required redistribution from the central support to achieve the plastic bending moment diagram was calculated from

$$\text{Required redistribution} = (M_{E\,hog} - M_{P\,hog}) / M_{E\,hog} \times 100\% \qquad \text{B.24}$$

$$\text{Required redistribution} = ((0.186P - 0.113P) / 0.186P) \times 100\% = 39\% \qquad \text{B.25}$$

As the allowable redistribution was less than the required redistribution from the central support, the predicted failure bending moment diagram was calculated according to the allowable redistribution.

The predicted bending moment at the central support was calculated from

$$M_{hog\ (predicted)} = 0.186P - (0.186P \times 31\%) = 0.128P \qquad B.26$$

A modified form Equation B.21 is used to calculate the corresponding predicted bending moment beneath the outer point loads.

$$M_{sag\ (predicted)} = (0.9)\ P/4 - (0.9/2)\ M_{hog\ (predicted)} = 0.225P - 0.058P = 0.167P \qquad B.27$$

By setting the predicted bending moment equal to the moment capacity of the section being considered, the flexural failure load of the section can be established.

For a flexural failure over the central support,

$$M_{hog\ (predicted)} = 0.128P = 27.13 \rightarrow P = 211.95kN \qquad B.28$$

For a flexural failure within the spans,

$$M_{sag\ (predicted)} = 0.167P = 37.88 \rightarrow P = 226.83kN \qquad B.29$$

The lower of these failure loads was taken as the flexural failure load for AN23.

To calculate the shear failure load of the specimen, the maximum shear force in the member must be determined. The shear force within the member was calculated according to the predicted failure bending moment diagram (Fig. 3.9). The left support reaction was calculated from

$$0.9\ R_L = M_{sag\ (predicted)} = 0.167P \rightarrow R_L = 0.186P \qquad B.30$$

The maximum shear force in the member was then calculated in terms of the applied load.

$$V_{max} = P/2 - R_L = (0.5 - 0.186)P = 0.314P \quad \text{B.31}$$

The shear failure load was then calculated by setting the maximum shear force in the member equal to the shear force capacity of the section.

$$V_{max} = 0.314P = 64.76 \rightarrow P = 206.24\text{kN} \quad \text{B.32}$$

In this case, the shear failure load was slightly lower than the flexural failure load for AN23. Therefore, a shear failure was expected.

Appendix C

Section 4.5.2 investigates the influence of load arrangement on the moment transfer in a "fully bonded" specimen up to service load. Fig. 4.15 shows the three sample load arrangements investigated. The method of acquiring the magnitudes of the point loads for load arrangements B & C is presently discussed.

Certain criteria had to be fulfilled to ensure the bending moment diagrams for the two-point load arrangements were comparable to the moment diagram for the single point load arrangement. Firstly, a constant "elastic" moment zone between the point loads was desirable. The ratio of the left load to the right load was chosen accordingly. Secondly, the same magnitude of fixed support (elastic) moment was required for the three specimens. The magnitudes of the point loads were chosen to give the same fixed support moment for all load arrangements (for a given load factor). A fixed support moment of 375Nm was chosen for the moment transfer investigation (compatible with the fixed support moment of a central point load of 1000N on a 2m long propped cantilever (M = 3PL / 16)).

Fig. C.1 shows a diagram of a propped cantilever with two-point loads (P_L & P_R), each at a distance of s / 2 from the midspan. Note: P_L must be greater than P_R for a constant moment zone to exist between the point loads. Consider a free body diagram of the right side of the structure (Fig. C.1). Taking clockwise moments about point "a" (at a variable distance "a" from the right support) gives the equation

$$-M_a + P_R (a - r) - R_R(a) = 0 \qquad \text{C.1}$$

Rearranging Equation C.1 gives

$$M_a = (P_R - R_R)(a) - P_R (r) \qquad \text{C.2}$$

This equation describes the moment between the point loads at a given distance "a" from the right support. To maintain a constant value of moment between point loads P_L & P_R,

$$P_R - R_R = 0 \rightarrow R_R = P_R \qquad \text{C.3}$$

To maintain vertical equilibrium for the whole structure,

$$R_L + R_R - P_L - P_R = 0 \rightarrow R_L = P_L \qquad \text{C.4}$$

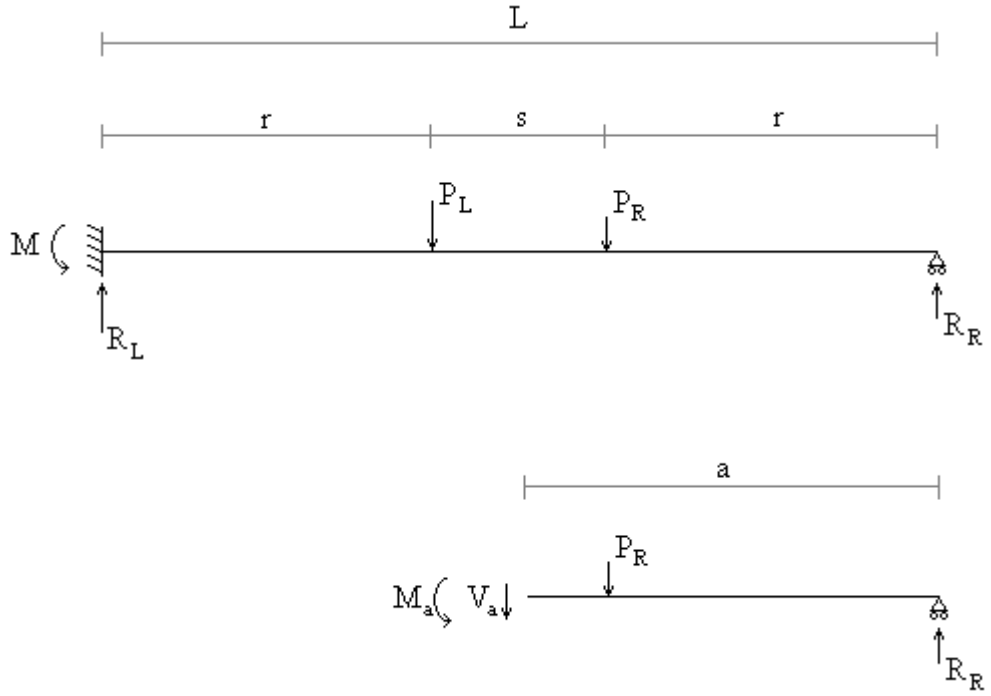

Fig. C.1 Propped cantilever with general two-point load arrangement and free body diagram of right side of structure

The moment at the fixed support can now be related to the applied point loads. Taking clockwise moments about the fixed support,

$$-M + P_L(r) + P_R(r + s) - P_R(2r + s) = 0 \qquad \text{C.5}$$

Rearranging Equation C.5 gives

$$M = P_L(r) - P_R(r) \qquad \text{C.6}$$

A virtual work method was then used to provide another equation relating the support moment to the applied loads. Fig. C.2 shows the primary structure used for the initial analysis. The secondary structure with a virtual applied moment (to determine the rotation at the left support) is also shown. A static analysis of the primary structure

was carried out to determine the magnitudes of the reactions in terms of the applied loads. Taking moments about the left support,

$$P_L(r) + P_R(r + s) - R_R(L) = 0 \rightarrow R_R = P_L(r) / L + P_R(r + s) / L \qquad C.7$$

Similarly, taking moments about the right support

$$R_L(L) - P_L(r + s) - P_R(r) = 0 \rightarrow R_L = P_L(r + s) / L + P_R(r) / L \qquad C.8$$

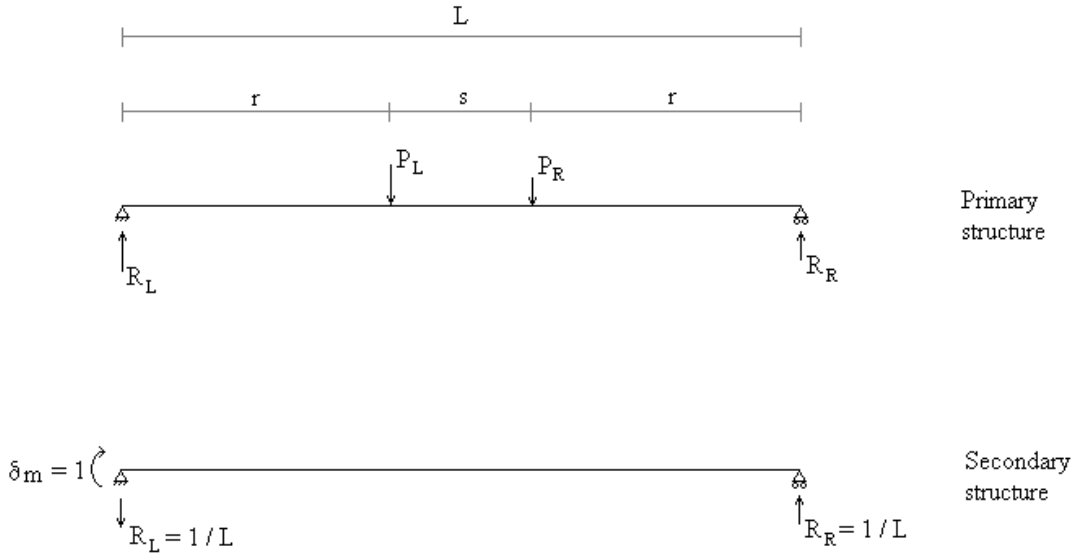

Fig. C.2: Primary and secondary structures for initial analysis

Fig. C.3 shows the bending moment diagrams for both the primary and secondary structures. The values of the bending moment within the primary structure were initially expressed in terms of the reactions to simplify the analysis. The rotation at the left support was given by

$$\delta m\, \theta = \int m\, M/EI \qquad C.9$$

Note: $\delta m = 1$

The product integral was determined by multiplying the area under the bending moment diagram for the primary structure, by the value of the bending moment in the secondary structure, at the centroid of the area of the primary bending moment

diagram. For simplicity, the primary bending moment diagram was split into triangles and rectangles as the positions of their centroids were more readily identified.

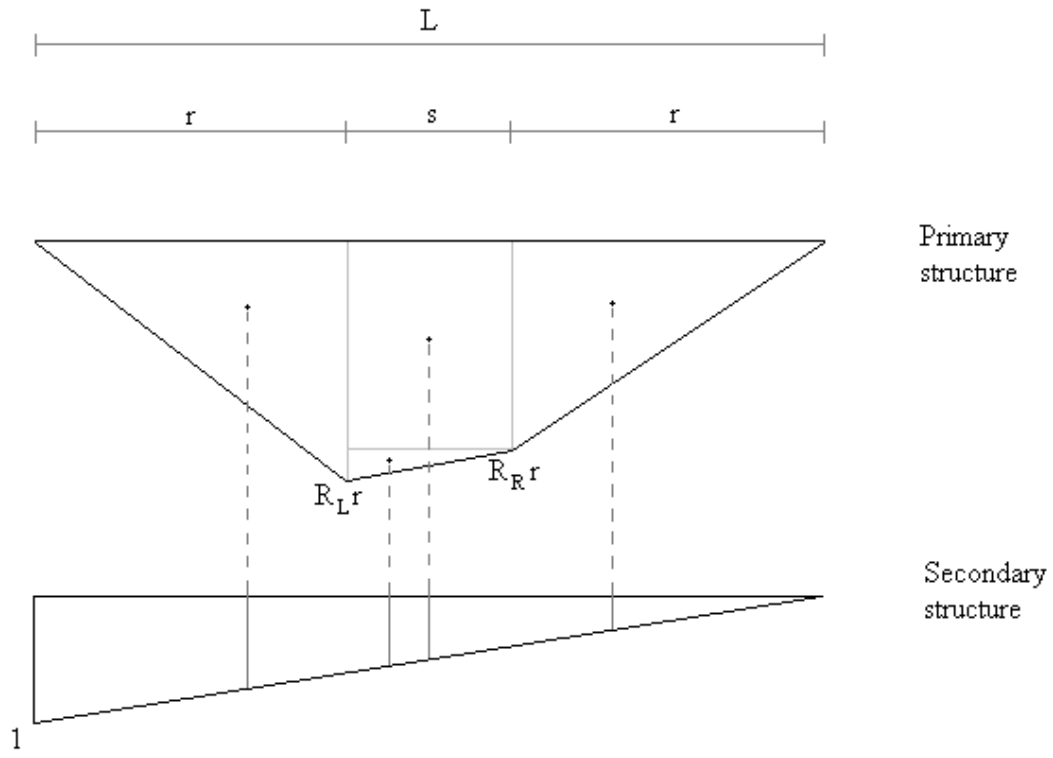

Fig. C.3: Bending moment diagrams for primary and secondary structures (initial analysis)

The rotation at the left support was calculated from

$$\theta = 1/EI \{\{(R_L r^2 / 2)\,(1 - (1 / L)(2r / 3))\} + \{(s\,r / 2)(R_L - R_R)(1 - (1 / L)(r + s / 3)\} + \{(R_R\,s\,r)\,(1/2)\} + \{(R_R\,r^2 / 2)(2r / 3L)\}\} \quad \text{C.10}$$

When simplified, this equation becomes

$$\theta = R_L / EI \{(-r^3 / 3L) + (r^2 / 2) + (s\,r / 2) - (s\,r^2 / 2L) - (s^2\,r / 6L)\} + R_R / EI \{(r^3 / 3L) + (s\,r^2 / 2L) + (s^2\,r / 6L)\} \quad \text{C.11}$$

Equations C.7 & C.8 express the reactions in terms of the applied loads. By substituting into Equation C.11, the rotation at the left support can be expressed in terms of the magnitudes and positions of the applied loads.

$$\theta = 1 / EI \{ \{P_L(r + s) / L + P_R(r) / L\}\{(-r^3 / 3L) + (r^2 / 2) + (s\, r / 2) - (s\, r^2 / 2L) - (s^2\, r / 6L)\} + \{P_L(r) / L + P_R(r + s) / L\}\{(r^3 / 3L) + (s\, r^2 / 2L) + (s^2\, r / 6L)\}\} \quad \text{C.12}$$

A second structure was then analysed to determine the rotation at the left support for a given positive applied moment (M) at the left support. Diagrams of the primary and secondary structures for this analysis are illustrated in Fig. C.4.

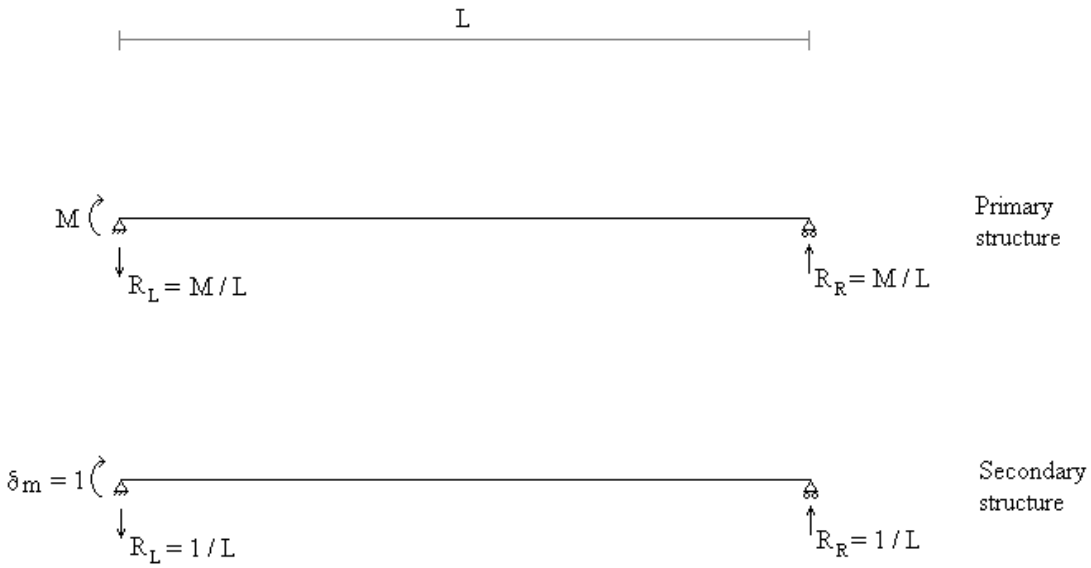

Fig. C.4: Primary and secondary structures for second analysis

The method of determining the rotation at the left support was similar to the previous analysis. The bending moment diagrams for the primary and secondary structures are shown in Fig. C.5. The rotation at the left support was given by

$$\theta = 1 / EI \{(M\, L / 2)(2/3)\} = 1 / EI\, (M\, L / 3) \quad \text{C.13}$$

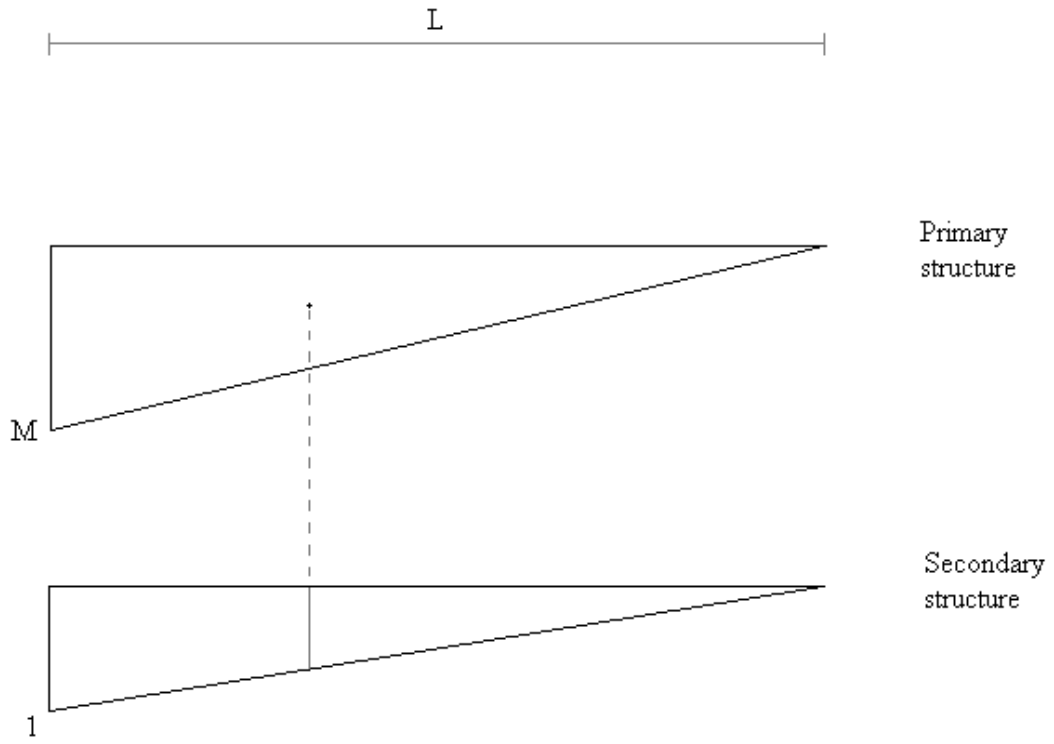

Fig. C.5: Bending moment diagrams for primary and secondary structures (second analysis)

The rotation due to the moment M applied at the left support was then subtracted from the rotation from the primary analysis. If the resulting rotation was set equal to zero, M represents the moment at an encastre support for the actual load arrangement.

$$\{P_L(r + s) / L + P_R(r) / L\}\{(-r^3 / 3L) + (r^2 / 2) + (s\ r / 2) - (s\ r^2 / 2L) - (s^2\ r / 6L)\} +$$
$$\{P_L(r) / L + P_R(r + s) / L\}\{(r^3 / 3L) + (s\ r^2 / 2L) + (s^2\ r / 6L)\} - (M\ L / 3) = 0 \qquad \text{C.14}$$

For a given load arrangement, the values of s, r and L are known. As stated previously, a support moment value of 375Nm was desirable. Solving simultaneous Equations C.6 & C.14 gave the desirable magnitudes of the applied loads for a given load arrangement. For Specimen B, Equation C.6 and C.14 simplified to Equations C.15 and C.16 respectively.

$$375 = 4/5\ P_L - 4/5\ P_R \qquad \text{C.15}$$

$$250 = 32/125\ P_L + 28/125\ P_R \qquad \text{C.16}$$

These equations were solved to give $P_L = 739.58N$ and $P_R = 270.83N$.

Similarly for Specimen C, Equation C.6 and C.14 simplified to Equations C.17 and C.18 respectively.

$$375 = 3/5\ P_L - 3/5\ P_R \qquad C.17$$

$$250 = 119/500\ P_L + 91/500 P_R \qquad C.18$$

These equations were solved to give $P_L = 866.07N$ and $P_R = 241.07N$. These answers were verified with LUSAS by carrying out a simple linear analysis on a propped cantilever model and examining the resulting bending moment diagrams.

During the moment transfer investigation, the design moment redistribution was varied by altering the hogging : sagging reinforcement ratio. If specimens were designed for 0% redistribution, the plastic bending moment diagram should be similar to the elastic bending moment diagram (from Fig. 4.15). Consider Specimen B designed for 0% redistribution from the central support. The hogging : sagging moment ratio is given by

$$\alpha_m = 375.00 / 216.67 = 1.731 \qquad C.19$$

For 0% redistribution, the hogging : sagging reinforcement area ratio (α_r) should equal 1.731. The area of "hogging" reinforcement was $300mm^2$ throughout the analysis. The required area of "sagging" reinforcement was then calculated from

$$A_{s\ sag} = 300 / 1.731 = 173.31mm^2 \qquad C.20$$

Now consider Specimen B designed for 30% redistribution from the central support. This required a 30% reduction in the moment at the fixed support from the elastic bending moment. Fig. C.6 illustrates the change in bending moment diagram for 30% redistribution. The redistributed hogging moment was 70% of 375Nm = 262.5Nm. The change in moment at the midspan may then be calculated from

$$\Delta M = (375.00 - 262.50) / 2 = 56.25\text{Nm} \quad \text{C.21}$$

The redistributed sagging moment at the midspan was then given by

$$M_{sag} = 216.67 + 56.25 = 272.92\text{Nm} \quad \text{C.22}$$

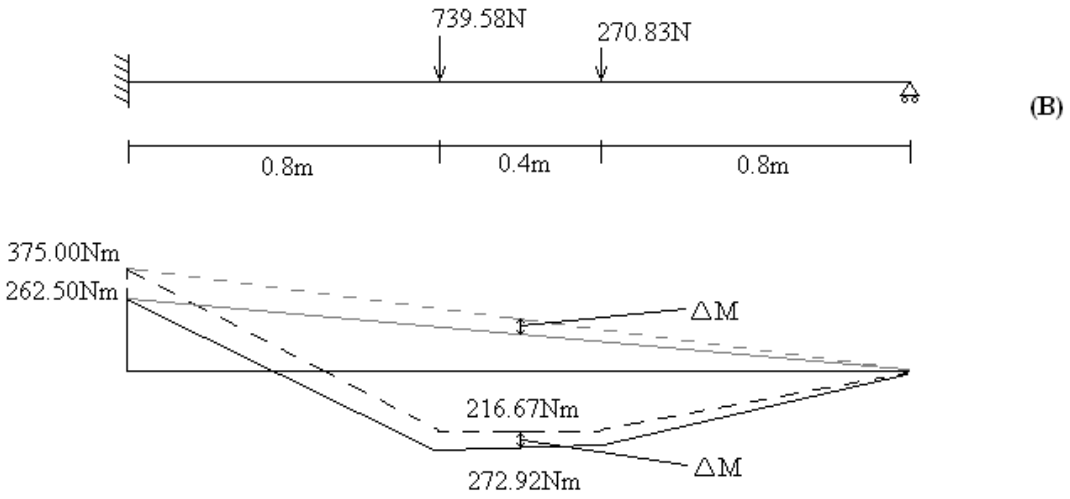

Fig. C.6: 30% redistribution for load arrangement B

The hogging : sagging moment ratio for 30% redistribution was calculated as

$$\alpha_m = 262.50 / 272.92 = 0.962 \quad \text{C.23}$$

Since the area of reinforcement over the support was constant and the required hogging : sagging reinforcement ratio was known, the required area of tension reinforcement within the spans was calculated as before.

Appendix D

Member reinforcement combinations	Bar mark	Type	Size	No. of members	No. of bars in each	Total No.	Length	Shape Code	A	B	C	D	h
All	6	R	6	21	34	714	700	61	162	112			
All except 11's	8	T	8	18	4	72	4250	20	4250				
11's	12	T	12	3	4	12	4250	20	4250				
12	T10	T	10	1	2	2	1720	33	1500				110
21's	B10	T	10	5	4	20	2085	32	1975				110
21's, 22, 23's	T12	T	12	13	2	26	1780	33	1500				140
12, 22	B12	T	12	2	4	8	2115	32	1975				140
34's	T16	T	16	4	2	8	1860	33	1500				180
23's	B16	T	16	7	4	28	2155	32	1975				180
34's	B20	T	20	4	4	16	2195	32	1975				220

Table D.1: Reinforcement schedule for all test specimens

Beam	Top reinforcement	Bottom reinforcement
AN11	12	12
AN21	T12	B10
AN23	T12	B16
AB11H	12	12
AB11S	12	12
AB21H	T12	B10
AB21S	T12	B10
AB23H	T12	B16
AB23S	T12	B16
AB34H	T16	B20
AB34S	T16	B20
AB12H	T10	B12
AB22H	T12	B12
UR21H	T12	B10
UR21S	T12	B10
UR23H	T12	B16
UR23S	T12	B16
UR34H	T16	B20
UR34S	T16	B20
PR23H	T12	B16
PR23S	T12	B16

Table D.2: Main tension reinforcement bar marks for all test specimens